THE DISTRIBUTION AND BEHAVIOUR OF PLATINUM IN SOILS OF THE TULAMEEN ULTRAMAFIC COMPLEX, SOUTHERN BRITISH COLUMBIA: APPLICATIONS TO GEOCHEMICAL EXPLORATION FOR CHROMITITE-ASSOCIATED PLATINUM DEPOSITS

by

STEPHEN JOHN COOK

B.Sc. (Hons) Carleton University, 1984

A THESIS SUBMITTED IN PARTIAL FULFILMENT OF

THE REQUIREMENTS FOR THE DEGREE OF

MASTER OF SCIENCE

in

THE FACULTY OF GRADUATE STUDIES

Department of Geological Sciences

We accept this thesis as conforming

to the required standard

THE UNIVERSITY OF BRITISH COLUMBIA

June, 1991

In presenting this thesis in partial fulfilment of the requirements for an advanced degree at the University of British Columbia, I agree that the Library shall make it freely available for reference and study. I further agree that permission for extensive copying of this thesis for scholarly purposes may be granted by the head of my department or by his or her representatives. It is understood that copying or publication of this thesis for financial gain shall not be allowed without my written permission.

Department of Geological Sciences

The University of British Columbia
Vancouver, Canada

Date July 23, 1991

DE-6 (2/88)

ABSTRACT

Exploration for chromitite-associated Pt deposits is hampered by a poor understanding of the distribution and behaviour of Pt in the surficial environment. This study investigates Pt content, residence sites and PGE mineralogy of soils developed on till and colluvium above the Tulameen ultramafic complex in southern British Columbia.

Seventy-six soil profiles, as well as sediments, bogs and waters were sampled above the dunite core of the Tulameen complex, within which Pt occcurrences consist of massive-to-discontinuous segregations of platinic chromitite. Pt content of the -212 um fraction of soils and sediments was determined by fire assay-inductively coupled plasma spectroscopy. Samples from fourteen selected profiles were then examined in detail to determine Pt mineralogy and its distribution between different size, density and magnetic fractions.

Pt concentrations in the -212 um fraction of C horizon soils range from 2 to 885 ppb and are closely related to soil dunite content, as estimated from MgO content and verified by XRD mineralogy. Dunite colluvium (mean: 24.2% MgO), locally-derived dunitic till (mean: 16.5% MgO) and exotic non-dunitic till (mean: 5.7% MgO) have median Pt concentrations of 88 ppb, 36 ppb and 8 ppb, respectively.

This trend is evident in all size and density fractions. Pt content of heavy mineral (SG > 3.3) fractions is 10-20x greater than in light mineral fractions. Pt is most abundant in the heavy magnetic fraction from non-dunitic tills and dunitic tills remote from known mineralization, but the proportion of Pt in the heavy non-magnetic fraction increases with increasing proximity to mineralization.

SEM and microprobe studies of heavy fractions from C horizons identified Pt-Fe-Cu alloys as free grains, and as inclusions in Mg-silicates and chromites. Chromite occurs as Mg-Cr-rich anhedral fragments and as Fe-rich euhedral to subhedral crystals. The latter, relatively more important in the magnetic fraction, are interpreted as Pt-poor grains disseminated throughout the dunite whereas fragments are relatively more important in the non-magnetic fraction and are interpreted as remnants of Pt-bearing massive chromitite segregations. The abundance of chromite fragments in soils near chromitite segregations accounts for the high Pt content of the non-magnetic heavy fractions of these soils.

The -270 mesh fraction or the magnetic heavy fraction of C horizon soils would be the most suitable sample media for reconnaissance geochemical sampling. However, the greater contrast, more limited dispersion and Mg-Cr-rich chromite association of the non-magnetic heavy fraction make it a more suitable media for detailed geochemical sampling.

TABLE OF CONTENTS

LIST OF TABLES

LIST OF FIGURES

ACKNOWLEDGEMENTS

The author is grateful for the assistance of numerous individuals during thesis research and preparation. The author would like to thank Pasakorn Paopongsawan for his able assistance in the field, and Joni Borges and Deb Feduik for their help with sample preparation. Several individuals provided helpful support, discussion and advice, especially Drs. P.W. Friske, C.E. Dunn, G.T. Nixon, J.K. Russell, A.J. Macdonald and W.B. Coker, and S.B. Ballantyne, J.J. Lynch, C. Bulmer and J. Knight. Drs. A.J. Sinclair and K.W. Savigny read and commented upon the manuscript. In addition, G.E.M. Hall of the Geological Survey of Canada and P.F. Matysek of the British Columbia Geological Survey Branch are thanked for providing various chemical analyses. The author is indebted to Stanya Horsky for electron microprobe and x-ray diffraction determinations, Joni Borges for her skillful analytical work, and Yvonne Douma for her careful preparation of polished grain mounts. Steve Sibbick, Pasakorn Paopongsawan, and Tracy Delaney offered inspirational discussions on exploration geochemistry.

The author also wishes to thank Dr. W.K. Fletcher of the University of British Columbia for guiding the progress of the project. The author is grateful to Newmont Exploration of Canada for providing valuable information, and to Irene and Karl Strom of Tulameen for their neighbourly assistance during the summers of 1988 and 1989.

The study was supported by funding from the Science and Technology Development Fund of the Province of British Columbia through the Science Council of British Columbia; the British Columbia Ministry of Energy, Mines and Petroleum Resources; the Geological Survey of Canada; and Placer Dome Inc.

Chapter One

INTRODUCTION

CHAPTER ONE. INTRODUCTION

1.1 Introduction

Platinum is valuable both as a precious metal and for its industrial usage in a variety of high-technology applications. Production of platinum is dominated by South Africa and the Soviet Union, which in 1989 produced 77% and 16%, respectively, of the 3,375,000 ounces supplied to the western world (Coombes, 1990). Rising platinum prices during 1986, fueled by both concern for the long-term stability of current producers, and rapidly-increasing demand in the automotive, investment and jewelry markets, led to a worldwide rush to explore and develop new deposits. The presence of transported overburden in the Canadian Cordillera has traditionally been viewed as an obstacle to mineral exploration. Platinum targets may be obscured by Pleistocene till, fluvioglacial and glaciolacustrine deposits. The landscape may be further modified by Recent colluvial and pedogenic processes. Platinum exploration is also hampered by three additional factors: the particle sparcity effect arising from the low abundance and erratic distribution of many platinum-group minerals (PGM), a poor knowledge of their distribution and behaviour in the surficial environment, and the consequent lack of any effective geochemical exploration techniques and guidelines appropriate for the efficient and reliable detection of

platinum-group element mineralization.

1.2 Properties of the Platinum-Group Elements

Platinum is a soft, malleable and ductile metal with a whitish steel-grey colour. It occurs in Group VIII of the periodic table together with the other five platinum-group elements (PGE) iridium, osmium, ruthenium, rhodium and palladium. The PGE comprise two subgroups based on atomic weight. The former three, including Pt, comprise the heavy platinum-group elements whereas the latter three comprise the light platinum-group elements (Wright and Fleischer, 1965). The PGE are catalysts, have high melting temperatures and are relatively unreactive over a wide temperature range (Westland, 1981; Cabri, 1982). They are also siderophilic and chalcophilic, forming solid solution alloys with each other and with Fe, Cu and Ni as a result of their similar atomic radii. Pt density of 21.45 is reduced by alloying, as pure end member PGE are not found in nature. "Native platinum" is an alloy of Pt and Fe containing > 80 at.% platinum (Cabri, 1981).

1.3 Platinum-Group Element Mineralogy

PGE form metallic alloys and also combine with Fe, Cu, S, Se, Te, As, Sb, Bi, Sn, Pb and Hg to form discrete platinum-group minerals (PGM). Eighty-four PGM are currently recognized (Hulbert et al, 1988), the majority of which are Pd-rich. PGE also occur in variable amounts within sulfides, rock-forming silicates and hydrous iron oxides (Wright and Fleischer, 1965; Razin, 1965, 1971; Makovicky et al, 1986; Paktunc et al, 1990). Pt itself forms 22 minerals (Cabri, 1981) comprising the native metal, Fe and Cu alloys, and various arsenides, antimonides, sulfides, tellurides, bismides and stannides. Pt also substitutes within other PGM.

1.4 Platinum-Group Element Deposits

1.4.1 Classification

Several classification schemes have been proposed for PGE deposits and occurrences (Mertie, 1969; Naldrett, 1981; Macdonald, 1987; Hulbert et al, 1988), but they can be divided roughly into three genetic varieties: magmatic, hydrothermal, and surficial.

Magmatic deposits comprise stratabound, discordant, marginal and unclassified varieties (Hulbert et al, 1988). Stratabound deposits, occurring in stratiform ultramafic complexes formed in cratonic environments (Naldrett and Cabri, 1986), are by far the most important sources of PGE. They include deposits of the Bushveld Complex, South Africa, the Great Dyke, Zimbabwe, and the Stillwater Complex, U.S.A. (Macdonald, 1987; Hulbert et al, 1988). The other varieties of magmatic PGE deposits (Hulbert et al, 1988) comprise discordant dunite pipes of the Bushveld Complex, Cu-Ni-PGE sulfide deposits in marginal zones of mafic/ultramafic intrusions such as at Sudbury and Noril'sk, and unclassified deposits in primarily concentric Alaskan-type mafic/ultramafic intrusions emplaced in the latter stages of orogenesis (Naldrett and Cabri, 1976) such as those of British Columbia and the Soviet Urals.

Hydrothermal PGE deposits have been recognized as a deposit type since the 1920's (Wagner, 1929; Mihalik et al, 1974; Stumpfl, 1974, 1986; Stumpfl and Tarkian, 1976). Examples include the Pt-Pd-Cu New Rambler deposit, Wyoming; occurrences at Messina and in the Waterberg district, South Africa; and the Nicholson Bay U-Au-Pt-Pd occurrence in Saskatchewan (Hulbert et al, 1988). PGE enrichment in Polish Kupferschiefer black shales has been attributed to diagnetic fluids (Kucha, 1982).

Surficial, or placer, PGE deposits were the only world source of platinum prior to 1919, when production began from the Sudbury Ni-Cu deposits (Mertie, 1969). Platinum placers are predominantly of alluvial origin, although eluvial, beach, marine, paleoplacer and other varieties are also known (Mertie, 1969; Owen, 1978; Macdonald, 1987; Hulbert et al, 1988). Alluvial placers, which constitute only a small proportion of current PGE production, are formed by hydraulic concentration of mechanically-liberated PGM, although there is evidence supporting a chemical origin for some alluvial PGE (Cousins and Kinloch, 1976; Bowles, 1986, 1988; Burgath, 1988). Larger deposits, such as those of the Soviet Urals, Alaska, Columbia, Ethiopia and British Columbia are associated with Alaskan-type intrusions.

Chromite-PGE occurrences are also known in Alpine-type ultramafic bodies contained within ophiolite complexes.

1.4.2 Platinum-Group Element Occurrences in British Columbia

Lode and placer PGE occurrences in British Columbia and the Cordillera have been reviewed by O'Neill and Gunning (1934), Boyle (1982) and Rublee (1986), and favourable host rocks by Evenchick et al (1987). No primary lode platinum production has been recorded. PGE occur primarily in

Alaskan-type and Alpine-type complexes and in their associated placers, with minor occurrences in alkaline intrusions and other mafic-ultramafic bodies (Rublee, 1986; Evenchick et al, 1987). Alaskan-type complexes, several of which occur in the accreted Quesnel and Stikine terranes, offer good targets for chromitite-associated PGE deposits (Nixon, 1990). Placers associated with the most important, the Tulameen ultramafic complex, produced 20,000 ounces of PGE between 1887 and 1936 (Rice, 1947; Mertie, 1969). PGE are also associated with chromitite in Alpine-type bodies within oceanic terranes, particularly the Cache Creek terrane (Whittaker and Watkinson, 1985; Rublee, 1986).

1.5 Problems and Objectives

Several factors influencing the design and interpretation of geochemical surveys for platinum in the Cordillera are poorly understood. These problems include:

1) irregular geographic distribution and varying background platinum contents of various Cordilleran surficial deposits.

2) vertical distribution and residence sites of platinum within surficial deposits.

3) physical and chemical behaviour of platinum and its host grains within surficial deposits during pedogenesis and other processes.

4) mineralogy and morphology of the PGM and their host grains within the soil profile

Objectives of this study are twofold. The first is to determine the distribution and behaviour of platinum in the surficial environment in the vicinity of a known occurrence, the Tulameen ultramafic complex of southwestern British Columbia. *Distribution* relates to the determination of the background and anomalous platinum contents of ultramafic dispersion trains and other surficial deposits, the vertical distribution and residence sites of platinum within the soil profile, and the mineralogy and morphology of the soil PGM. *Behaviour* relates to the physical and chemical dispersion of platinum in the surficial environment in response to post-glacial and pedogenic processes.

The second objective is to apply an understanding of platinum dispersion to development of practical guidelines for geochemical exploration in the Cordillera. This study provides data and recommendations for the following criteria:

1) Background and anomalous platinum contents of a variety of types of Cordilleran surficial deposits.
2) Associated pathfinder elements.
3) Optimum soil horizon.
4) Optimum size fraction.
5) Optimum density and magnetic fractions.

Chapter Two

DESCRIPTION OF THE STUDY AREA

CHAPTER TWO. DESCRIPTION OF THE STUDY AREA

2.1 Location and Access

The field area is located within NTS map area 92 H/10 on Grasshopper Mountain on the north side of the Tulameen River, approximately 25 km west of Princeton in southwestern British Columbia. It comprises the main study area on the southern slope of the mountain, and a second, smaller area near the summit (Figure 2-1).

The lower part of the study area is approximately 152 m (500') in elevation above the Tulameen River road, and is accessible by an old pack trail originating on the north side of the road approximately 12 km west of Tulameen. Vehicle access into the study area is via two logging roads on the north and west sides of Grasshopper Mountain; these connect with several kilometres of recently-constructed drill roads on the mountain itself. The drill roads are not passable in all areas however, particularly in the early part of the summer. The logging roads connect with the Lawless Creek forestry road and provide vehicle access from both Tulameen and the nearby Coquihalla Highway.

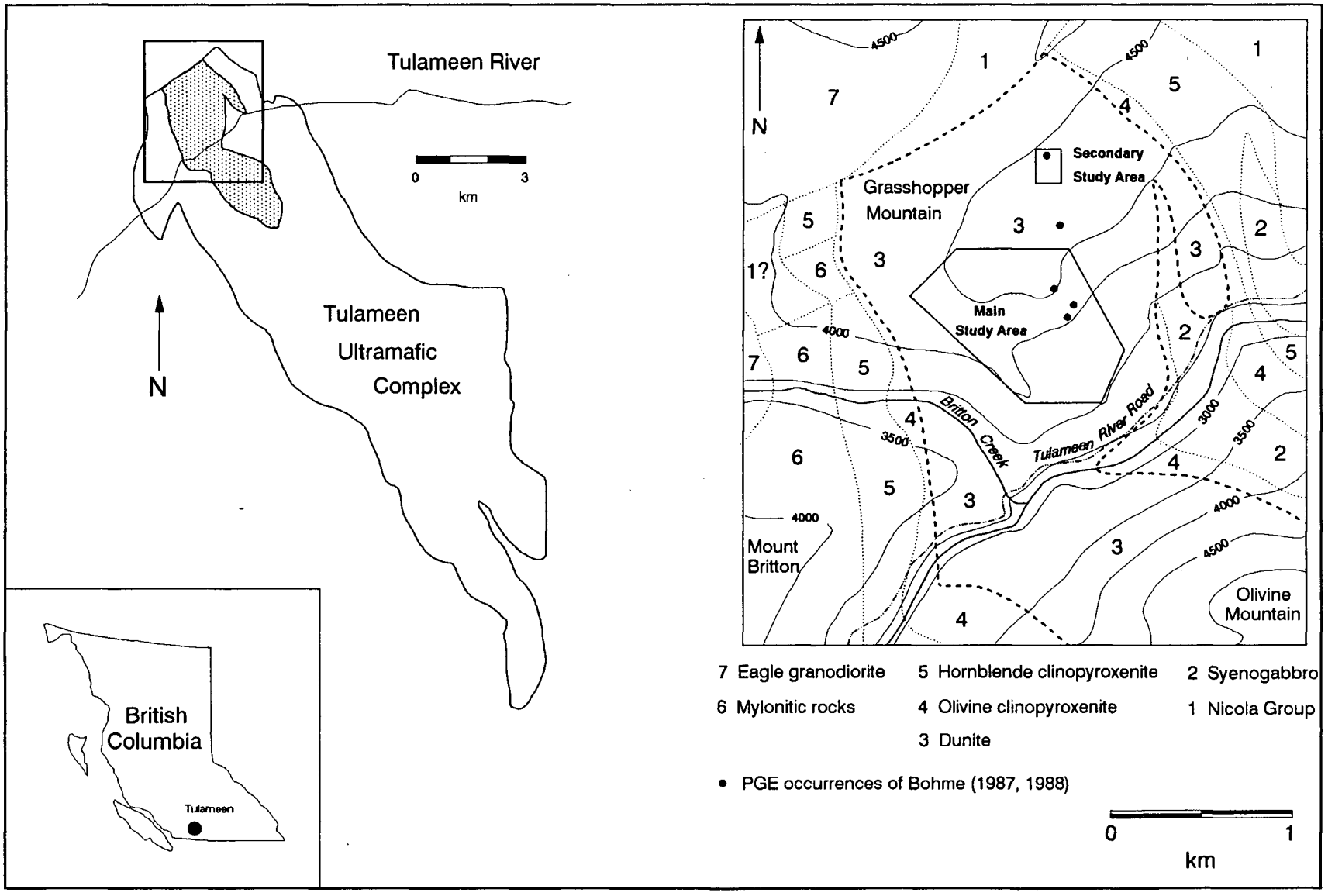

Figure 2-1. Location and generalized geology of the study areas within the dunite core of the Tulameen ultramafic complex in southwestern British Columbia (modified after Nixon and Rublee, 1988)

2.2 Exploration History

2.2.1 Tulameen District

The Tulameen district was a prominent producer of placer gold and platinum in the late nineteenth century. Placer gold was first discovered near the mouth of the Tulameen River in 1860, but the area was bypassed by prospectors travelling to the Cariboo district. A prospecting rush did not begin until the discovery of coarse gold in Granite Creek, a Tulameen River tributary, in 1885 (Camsell, 1913). Platinum recovered with the gold was initially discarded by the miners during the first few years (Kemp, 1902), but by 1891 the district had become the largest platinum producer in North America (Camsell, 1913). The Tulameen River (Figure 2-2) and its tributaries ultimately yielded approximately 20,000 ounces of platinum between 1887 and 1936 (Rice, 1947; Mertie, 1969). Production declined at about the turn of the century (Rice, 1947), but intermittent placer exploitation has continued on a small scale up to the present day.

Figure 2-2. View from the summit of Grasshopper Mountain, looking southwest up the Tulameen River valley into the Hozameen Range of the Cascade Mountains.

2.2.2 Grasshopper Mountain

Exploration for the primary sources of the gold and platinum commenced about 1898 (Camsell, 1913). Ultramafic rocks, particulary dunite exposed on Grasshopper and Olivine Mountains on the upper Tulameen River, were soon determined to be the primary source of the platinum placers (Kemp, 1902; MacAulay, 1919). These were noted to be geologically similar to those associated with rich platinum placers in the Ural Mountains of Russia (Poitevin, 1923).

Lode platinum exploration has been sporadic, and economic lode deposits have not been discovered. Platinic chromite occurrences on the southern slopes of Grasshopper Mountain were staked during the late 1930's and early 1940's as the Girl claims. Assays as high as 40% chromium and 0.35 oz/t platinum were reported at the time (Rice, 1947; Canmindex, 1986). The more recent exploration history of the Grasshopper Mountain area is given by Bohme (1987, 1988). Most of the field area of this study lies within the westernmost 12 units of the Grasshopper 1 and 2 claims. These were optioned to Monica Resources and subsequently to Newmont Exploration of Canada Limited, which undertook a prospecting, chip sampling, and trenching program during 1986 and 1987. The claims were then optioned to Longreach Resources which in 1988 built roads and undertook a program of mainly percussion drilling before ceasing operations.

The extent of placer mining on Grasshopper Mountain is not known. However, the pack trail from the Tulameen River Road leads to the remains of two abandoned cabins on upper Grasshopper Creek, and appears on the map of Camsell (1913). More recent excavations were observed in perched bogs and drainage channels on the plateau of the mountain.

2.3 Bedrock Geology

2.3.1 General Geology and Regional Setting

Grasshopper Mountain comprises the northern end of the Tulameen ultramafic complex, a zoned Alaskan-type ultramafic-gabbroic intrusion within metasedimentary and metavolcanic rocks of the Upper Triassic Nicola Group. The 20 km-long southeast-trending complex covers an area of 60 square kilometres in the marginal region of the Quesnellia tectonostratigraphic terrane, and is the largest and most southerly of several Alaskan-type complexes within the Intermontane Belt (Nixon and Rublee, 1988; Nixon, 1990). Recent U-Pb zircon dating (204-212 Ma) suggests a Late Triassic to Early Jurassic age of emplacement (Rublee and Parrish, 1990).

The geology of the complex was first described by Camsell (1913) and Rice (1947), and more recently by Findlay (1963, 1969) and Nixon and Rublee (1988). It comprises a dunite core surrounded by crudely-concentric shells of olivine clinopyroxenite, hornblende clinopyroxenite and gabbroic rocks (Figure 2-1). Metasedimentary and intermediate to felsic metavolcanic country rocks of the Nicola Group near Tulameen have been regionally metamorphosed to greenschist grade and comprise primarily argillite, tuffaceous siltstone and lapilli tuff, pyroxene andesite and hornblende dacite flows. Subordinate lithologies include rhyolite, chert, chert breccia and limestone (Nixon and Rublee, 1988). The Eagle plutonic complex, comprising granodiorite and granite, occurs to the west of the Tulameen complex. The Tulameen complex is unconformably overlain by terriginous sedimentary and volcanic rocks of the Eocene Princeton Group (Nixon and Rublee, 1988).

Mafic-ultramafic complexes are divided into three classes: stratiform, alpine, and concentric complexes (Jackson and Thayer, 1972). Concentric complexes, also known as zoned, Alaskan-type or Uralian-type intrusions, are most common in southeastern Alaska and in the Ural Mountains of the U.S.S.R. They are characterized by a concentric arrangement of mafic and ultramafic rock units, the absence of orthopyroxene and plagioclase, silica undersaturation,

iron-rich chromite and abundant magnetite (Findlay, 1969; Naldrett and Cabri, 1976; Nixon and Rublee, 1988). The Tulameen complex differs, however, in that the gabbroic rocks are alkalic rather than tholeiitic.

Alaskan-type complexes are thought to be emplaced in later-stage orogenic settings (Naldrett and Cabri, 1976). Nicola Group rocks represent a volcanic arc formed by late Triassic subduction to the west (Mortimer, 1987). The Tulameen complex is one of three alkaline plutons which intrude the Nicola Group, and which have been interpreted as being comagmatic with the Nicola volcanics (Findlay, 1969; Mortimer, 1987). Findlay (1969) suggested that the gabbroic and ultramafic rocks of the Tulameen complex represent separate but genetically-related intrusions. The intrusion of alkaline gabbroic rocks, and their subsequent intrusion by later partially-consolidated ultramafic rocks, was contemporaneous with regional deformation of the Nicola rocks. The ultramafic rocks reflect an original fractional crystallization of an ultramafic magma, forming a sill-like stratiform body in the order dunite, olivine clinopyroxenite and hornblende clinopyroxenite (Findlay, 1969). Emplacement of dunite as either a crystal mush (Findlay, 1969) or as possibly solid state thrusting (Nixon and Rublee, 1988) into pyroxenite deformed the overlying gabbroic rocks and created the present concentric distribution of rock units.

2.3.2 Geology of the Dunite Core

The dunite core crops out over about 6 square kilometres on Olivine and Grasshopper Mountains at the northern end of the Tulameen complex (Figure 2-1). The dunite is typically fine-grained, green to black, and weathers buff brown on exposed surfaces. The primary mineralogy comprises forsteritic olivine (Fo_{88}-Fo_{91}), with accessory chromite and rare augite. Secondary alteration minerals include serpentine, carbonate, magnetite, talc, chlorite and antigorite (Nixon and Rublee, 1988; Bohme, 1988)). Serpentine is the most common alteration mineral. Primary cumulate textures are not preserved. Serpentinization of primary olivine is widespread and variable, and is structurally controlled by contacts and faults (Findlay, 1969); large zones of serpentinization were mapped by Bohme (1987, 1988) as inferred fault or shear zones. These areas of almost total serpentinite are fine-grained, light green to white, and contain fine magnetite (Bohme, 1988). They weather to a distinctive rusty orange on exposed surfaces. The zonation of serpentinization within the dunite core is shown in Figure 2-3. The dunite on Grasshopper Mountain is more extensively serpentinized than on Olivine Mountain (Findlay, 1969), but decreases westward from 80% serpentine in the east to 20% serpentine on Mount Britton in the west. Isolated occurrences of fresh olivine dunite are restricted to the western margin of the

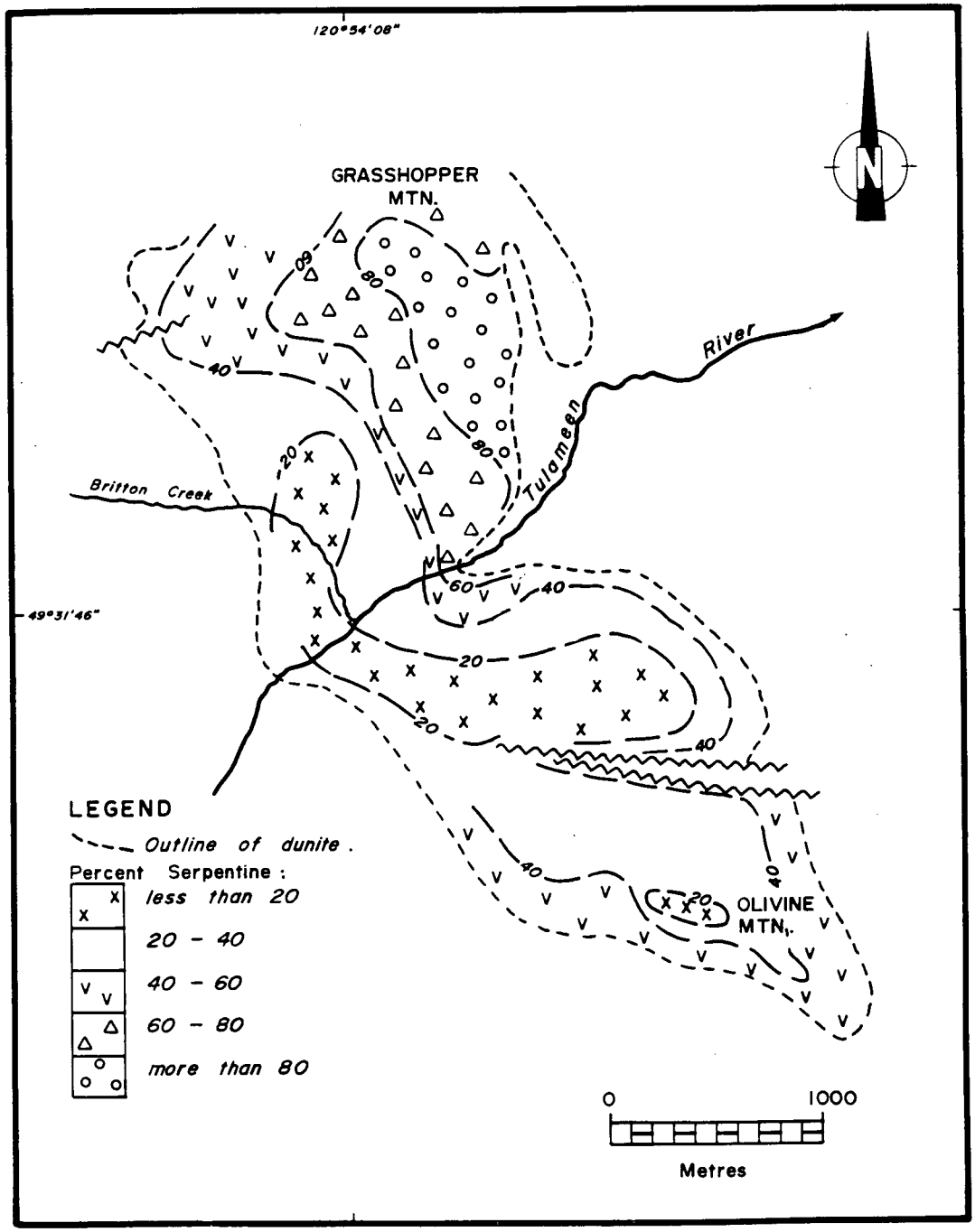

Figure 2-3. Serpentinization within the dunite core of the Tulameen ultramafic complex (White, 1987 after Findlay, 1963).

core (White, 1987) and are not observed within the study area.

Chromite occurs as randomly distributed massive to discontinuous pods, segregations, schlieren and disseminated grains (Figures 2-4 and 2-5). Schlieren typically range from 5 to 25 cm in length and 1 to 4 cm in width, with maximum lengths of about 4 m. They are randomly distributed throughout the dunite, are concordant with the regional foliation, and may exhibit fracturing, boudinaging and isoclinal folding (Nixon and Rublee, 1988). Circular ring structures, or condom folds, of chromite occurring at one of the occurrences have been interpreted as erosional expressions of domical folds (Nixon and Rublee, 1988). Nixon et al (1990) stated that chromitite segregations are bordered by 1-2 mm chromite crystals which grade sharply into much smaller disseminated grains (<20 um) within the surrounding dunite. Olivine inclusions within chromitites are more forsteritic (Fo_{92}-Fo_{95}) than those in dunite (Nixon et al, 1990). The segregations are thought to represent remnants of former cumulate layers which were deposited, disrupted by slumping and redeposited in a crystal mush prior to magmatic consolidation (Rice, 1947; Nixon and Rublee, 1988; Nixon et al, 1990). Chromite segregations are usually associated with a pale green alteration halo of primarily serpentine, with subordinate carbonate and chlorite (Bohme, 1988). The halo weathers to a paler colour

Figure 2-4. Discontinuous and massive chromitite segregations in dunite showing associated serpentine alteration. Sample is from active colluvium in the main study area.

Figure 2-5. Thin discontinuous chromitite segregations in dunite from the A-Zone PGE occurrence, secondary study area.

than the surrounding dunite, and is particularly well-developed around discontinuous chromite segregations (Figure 2-4). Tulameen chromite has an unusually high Fe^{3+} content, containing 15-25% Fe_2O_3, and is moderately to strongly magnetic (Findlay, 1969).

2.3.3 Platinum-Group Element Occurrences

Platinum-group element (PGE) mineralization is preferentially associated with massive chromitite segregations in Tulameen dunite, as opposed to disseminated chromite grains in dunite or with other lithologies (Findlay, 1965; St. Louis et al, 1986). Mean Pt content of unmineralized dunite and serpentinized dunite is in the range 60-85 ppb (Findlay, 1965; St. Louis, 1984). Massive chromitite segregations, however, have maximum Pt contents of between 8000 and 16000 ppb (Findlay, 1965; Bohme, 1987; Nixon et al, 1990). Chromitite segregations are most common on southern Grasshopper Mountain in the central region of the dunite core; PGE are somewhat erratically distributed within them. Five zones of chromitite-associated PGE mineralization were identified in this region by Bohme (1987, 1988) within a well-exposed 800 m x 300 m area (Figure 2-1). The subvertical Cliff Zone area (Figure 2-6) measures about 250m x 150m and contains two zones (C and D) about 6m x 6m each containing 2915 ppb and 2340 ppb of Pt,

Figure 2-6. The Cliff Zone PGE occurrence in dunite on the southeast face of Grasshopper Mountain.

Figure 2-7. Massive chromitite segregation in dunite at the Cliff Zone PGE occurrence.

respectively (Bohme, 1987, 1988). One of the largest known chromite segregations, 1m in length, occurs in this area (Figure 2-7). The A-Zone area, near the summit of Grasshopper Mountain, contains more wispy and disseminated chromite than does the Cliff Zone, with a much more uniform Pt content of 0.025 oz/ton over 26m (Bohme, 1987, 1988). Bohme (1988) noted that chromite is rarely found within 200 m of the dunite-pyroxenite contact. Exposures, however, are less common in this area.

2.3.4 Platinum-Group Mineralogy

PGE mineralogy of Grasshopper Mountain chromitite has been studied by St. Louis et al (1986) and Nixon et al (1989, 1990), and is summarized in Table 2-1 along with that of associated placers. Nixon et al (1989, 1990) observed ten platinum-group minerals (PGM), the most common of which are the three Pt-Fe alloys tetraferroplatinum (Pt_2Fe_2), isoferroplatinum (Pt_3Fe) and tulameenite (Pt_2FeCu). Geversite ($PtSb_2$), hollingworthite-irarsite [Rh-Ir(AsS)], sperrylite ($PtAs_2$), platinian copper (Cu, Pt), platinum oxide (Pt,O)?, erlichmanite (OsS_2) and laurite (RuS_2), in decreasing order of abundance, were also observed (Nixon et al, 1989, 1990). St. Louis et al (1986) reported eight discrete PGM, but did not distinguish between the Pt-Fe alloys. However, stumpflite (PtSb) and genkinite

[$(Pt,Pd)_4Sb_3$] were also observed. Pt-Fe alloys, sperrylite and irarsite were considered the most abundant PGM.

PGM occur as both discrete minerals and as complex polymetallic grains (Nixon et al, 1990). St. Louis et al (1986) recognized two types of PGM. Type 1 PGM occur as discrete euhedral to subhedral inclusions within chromite grains, while Type 2 PGM occur as anhedral grains interstitial to chromite grains. Type 1 grains are dominantly Pt-Fe alloys, geversite, stumpflite and irarsite, and have been interpreted as being of primary magmatic origin. Sperrylite ($PtAs_2$) is the most common Type 2 grain; it, with the hollingworthite-irarsite series and platinian copper, replaces the rims of Pt-Fe alloys in fractured chromite grains (St. Louis et al, 1986; Nixon et al, 1990). St. Louis et al (1986) reported that these grains are rarely in direct contact with chromite, however, and are usually associated with serpentine and base metal sulfides. They were interpreted as having been remobilized hydrothermally from platinum originally present in sulfides.

Some additional PGM associations were reported by Newmont Metallurgical Services (Bohme, 1988). Platinum was observed as fine Pt-Fe alloy inclusions in olivine as well as, more commonly, in chromite. It was also observed as submicroscopic disseminations in sparse sulfide phases.

Base metal sulfides, native metals and oxides, and base metal arsenides and antimonides are a minor interstitial to and fracture-filling constituent of chromitite segregations (St. Louis et al, 1986; Nixon et al, 1990). The most common sulfide minerals in chromitite are disseminated pyrite (Nixon et al, 1990) and pentlandite (St. Louis et al, 1986). Other nickel and nickel-cobalt-iron sulfides include violarite and bravoite (St. Louis et al, 1986) and millerite/heazlewoodite (Nixon et al; 1989, 1990). Other fracture-filling minerals include serpentine, chlorite, magnetite, carbonate, nickel antimonides, nickel arsenides, native copper, native silver, and copper and nickel oxides (Nixon et al; 1989, 1990).

Discrete PGM usually range in size from less than 2 um to about 30 um, although a platinum oxide grain of 150 um was reported by Nixon et al (1990). Large free PGM grains of up to 115 um are also reported in this study, but observations of macroscopic primary PGM are limited to those of early workers. "...Small grains of platinum..." were observed in Grasshopper Mountain chromitite (Rice, 1947), and "...several particles of native platinum..." were reported from Olivine Mountain dunite (Johnston, 1911), but no data is available on their exact composition or size.

Mineral	Ideal Formula	Minor Constituents	Chromitites[1]	Placers[1]
cooperite	PtS	Pd,Ni	-	x
Cu-Pt alloy	(Cu,Pt)	Pd,Rh,Fe,Ni,Sb	xx	x
erlichmanite	OsS_2	Pt,Pd,Rh,Ir	x	x
genkinite	$(Pt,Pd)_4Sb_3$	Rh,S	x	x
geversite	$PtSb_2$	Rh,Ir,Fe,Cu,Ni,As	xx	x
hollingworthite-irarsite series	Rh-Ir(AsS)	Pt,Pd,Rh,Os,Ru,Sb,Cu,Ni,Co	xx	x
iridium	Ir	Pd,Rh,Os,Ru,Fe,Cu,Ni	-	x
iridosmine	(Os,Ir)	Pt,Pd,Rh,Ru,Fe,Cu,Ni	-	xx
isoferroplatinum	Pt_3Fe	Pd,Rh,Ir,Os,Cu,Ni,Sb	(xxx)	xxx
kotulskite*	PdTe	Pt,Sb,Bi	-	x
laurite	RuS_2	Rh,Ir,Os	x	x
osmiridium	(Ir,Os)	Pd,Rh,Ru,Fe,Cu,Ni	-	x
osmium	Os	Pt,Pd,Rh,Ir,Ru,Fe,Cu,Ni	-	xx
platiniridium	(Ir,Pt)	Os,Ru,Fe,Cu,Ni	-	x
platinum, ferroan	(Pt,Fe) > 20 at.% Fe	Ir,Cu,Ni	-	xxx
platinum, native	(Pt,Fe) > 80 at.% Pt	Pd,Ir,Fe,Cu,Ni	x	xxx
platinum oxide	(Pt,O)?	Rh,Ir,Fe,Cu,Ni,Sb	x	-
Pt-Fe-Cu-Ni alloys	(Pt,Fe,Cu,Ni)	Pd,Rh,Ir,Sb	xxx	x
rutheniridosmine	(Ru,Os,Ir)	Pt,Pd,Rh,Fe,Cu,Ni	-	x
sperrylite	$PtAs_2$	Pd,Ni,Ru,Fe,Sb,S	xx	x
stumpflite	PtSb	Pd,Ru	x	-
tetraferroplatinum	PtFe	Pd,Rh,Ir,Cu,Ni,Sb	(xxx)	x
tolovkite**	IrSbS	Rh,As	-	x
tulameenite	Pt_2FeCu	Pd,Rh,Ir,Os,Ni,Sb	xx	xx
unnamed RhSbS	RhSbS	Pt,Ir,As	-	x

* only found as inclusions in one grain of gold; not derived from the Tulameen ultramafic complex.

** Originally reported as unnamed IrSbS

[1] Frequency: xxx = most common; xx = common; x = infrequent to rare; (xxx) = probably present in Pt-Fe-Cu-Ni alloys but not confirmed by XRD.

Table 2-1. Platinum-group mineralogy of Tulameen chromitites and placers (modified after Nixon et al, 1990).

2.4 Topography and Physiography

2.4.1 Regional Physiography

Grasshopper Mountain lies on the western margin of the Thompson Plateau in a transitional zone with the Hozameen Range of the Cascade Mountains (Holland, 1976). This region of the the Interior Plateau is characterized by a rolling upland topography of broadly rounded summits and low relief lying between 1220 and 1525 m (4000 and 5000 feet) above sea level (Holland, 1976). Grasshopper Mountain is very near the Cascade-Thompson boundary (Figure 2-2); plateau features are not completely developed and the topography assumes a more rugged appearance (Camsell, 1913).

The summit region of Grasshopper Mountain exhibits a rolling plateau-like topography with a maximum elevation of 1507 m (4940'). The slope steepens below about 1400 m (4600') beneath the plateau region, and prominent cliffs and scree slopes are exposed on the steep southeast face of the mountain (Figure 2-8). Relatively flat-lying ledge and bench areas at about 1220 m (4000') and 1068 m (3500') provide isolated topographic breaks in steep plunges to the Tulameen River and Britton Creek on the southeast and southwest faces of the mountain. The Tulameen River occupies a narrow channel between Grasshopper and Olivine Mountains at an elevation of 885 to 900 m (2900' to 2950').

2.4.2 Physiographic Zones of Grasshopper Mountain

Four major physiographic zones occur within the study area on Grasshopper Mountain (Figures 2-1 and 3-1), each exhibiting characteristic relief, forest cover, and soil development. The zones are: the cliffs and colluvial slopes, the rolling plateau and western forested slopes, the southern forested slopes, and the flat lying bench area.

The cliffs and colluvial slopes (Figure 2-8A and 2-9) are characterized by steep dunite cliffs and extensive accumulations of talus and colluvium. The rolling plateau (Figure 2-8B) and western forested slopes exhibit thin till cover and discontinuous outcrop. The steep southern forested slopes are characterized by the presence of stabilized colluvium in the western portion, and its absence in the east. Finally, the bench area (Figure 2-9B) is characterized by low relief, the presence of bogs and seepage zones, and the occurrence of a prominent northeast-southwest-trending clay-rich knoll.

2.5 Quaternary and Surficial Geology

2.5.1 Quaternary History of the Southern Interior

Evidence of at least four Quaternary glaciations and

Figure 2-8. Different physiographic zones on Grasshopper Mountain; A. Recent colluvium beneath steep cliffs on southeast face of Grasshopper Mountain. Cliff Zone PGE occurrence is at far right; B. Rolling plateau area adjacent to soil site 73 showing thin till cover and discontinuous outcrop.

Figure 2-9. Different physiographic zones on Grasshopper Mountain; A. Talus cone extending into the forest at the base of active colluvium beneath the Cliff Zone PGE occurrence; B. flat-lying seepage zone area below active colluvium. Tulameen River valley and Olivine Mountain in background.

two main nonglacial periods has been uncovered in the Canadian Cordillera (Fulton, 1984). The Late Wisconsin Fraser Glaciation was the last of the Cordilleran Ice Sheets (Blaise et al, 1990) to occupy southern British Columbia. All of the southern Cordillera, including the Tulameen area (Rice, 1947) was completely ice-covered. Cold conditions leading to ice-sheet development began about 25,000 years ago and glaciation commenced about 19,000 years ago (Fulton, 1975). The Tulameen valley would probably have been the local channel for the eastward advance of alpine glaciers originating in the higher Cascade mountains to the west (Camsell, 1913). Coalescence of valley glaciers resulted in the southern interior being covered by a continental ice sheet by about 17,240 years ago (Fulton, 1984). One of the Quaternary ice sheets was sufficiently thick to erode mountaintops of 2623 m (8600') elevation (Rice, 1947).

Striae reported by Rice (1947) indicate that the continental ice-sheet moved in a roughly southerly direction north of the Tulameen district, but began to move in a more southwesterly direction in the area north of Grasshopper Mountain. Striae mapped by Camsell (1913) on nearby Rabbit, Britton, and Olivine Mountains range from 205^{o} to 240^{o}, whereas those reported by Findlay (1963) from Lodestone Mountain average 220^{o} to 230^{o}. Rare striae near the summit of Grasshopper Mountain itself also indicate a south-southwesterly direction of ice movement.

The Fraser ice-sheet reached its maximum extent in northern Washington about 15000 to 14500 years ago prior to retreating through the southern Interior about 10500 years ago (Fulton, 1975; Blaise et al, 1990). The Tulameen valley was probably occupied by valley glaciers retreating westward (Camsell, 1913) at this time. Mathews (1944) and Hills (1962) have described the deglaciation history of the Princeton-Tulameen area. Mathews (1944) stated that ice damming created glacial lakes near Princeton in the Upper Similkameen valley while the glaciers retreated north or northwestward. Hills (1962) extended this to the Tulameen River drainage and suggested that glacial lakes existed in the Whipsaw Creek and Granite Creek valleys and at the headwaters of the Tulameen River near Jim Kelly Creek. During initial ice retreat, water drained southwards through the Skaist River and then successively westward through Snass Creek, the Podunk Valley, and Vuich Creek at a series of elevations ranging from 1510 to 1388 m (4950 to 4550 feet). Existence of the glacial lakes is marked by strand lines on the east slope of the Tulameen River opposite Jim Kelly Creek at about 1280 m (4200′), and by terraces on the Tulameen River at 1205 m (3950′). The Tulameen River subsequently drained north and east along the retreating ice front (Hills, 1962). The two Murphy Lakes, located just north of Grasshopper Mountain, are the only remaining glacial lakes in the vicinity of the study area. They are dammed by morainal material in a valley interpreted by

Camsell (1913) as a possible former drainage channel of the Tulameen River.

Fulton (1984) suggested that most of the southern interior was ice-free by 9510 years ago, and that the prevailing climate was warmer and drier than present.

2.5.2 Surficial Geology

Till, fluvioglacial and glaciolacustrine sediments deposited by the Wisconsin Fraser glaciation comprise the Kamloops Lake Drift (Fulton, 1984). It consists of (Fulton, 1975):

a) a lower stratified unit of silt and fine sand which cannot be distinguished from older unconsolidated units

b) nonstratified morainal deposits, predominantly basal till

c) an upper stratified drift deposited by water during the retreat of the Fraser ice-sheet

The surficial geology of Grasshopper Mountain and the surrounding area is a composite of the products of the

Fraser glaciation, particularly the Kamloops Lake Drift, and the subsequent modification of these deposits and creation of new ones by post-glacial processes. Colluvial, alluvial, bog and minor volcanic ash deposits have accumulated on Grasshopper Mountain since the deposition of the Kamloops Lake Drift and glacial retreat.

Basal till of unit b of the Kamloops Lake Drift is the surface cover over much of south-central British Columbia (Fulton and Smith, 1978). Grasshopper Mountain is mantled with a basal till of variable thickness. It is yellow-brown to brown and consists of subrounded to subangular lithic fragments in an oxidized silt-clay matrix. Clasts do not usually exceed cobble-size, and large boulder-sized examples are rare. Till cover in the plateau region of the mountain is thin and discontinuous, however, particularly near the summit where till and disintegrating bedrock locally form a rubbly residual-like soil. The contribution of till to the parent material seems to be minimal in some ridge and plateau areas. A thick post-glacial apron of active colluvium blankets the till beneath steep cliffs on the southeast face of the mountain. Boulder accumulations, locally stabilized by vegetation, form the lower margin of the colluvium in some parts of the western forested area, but are absent from the eastern part. A prominent talus cone, stabilized at lower levels, occurs on the margin of the boulder field and extends from the colluvium into the

forest (Figure 2-9B). Multiple parent materials are common, and generally take the form of till overriden by stabilized dunitic colluvium (Figure 2-10). This is particularly widespread in the western part of the main study area, but also occurs on flanks of the summit in the secondary study area.

Fluvioglacial sediments similar to unit c of the Kamloops Lake Drift dominate lower levels of the area, particularly the valleys of the Tulameen River, its tributaries and former drainage channels north of Grasshopper Mountain. Only minor buried channel or glaciolacustrine deposits occur within the study area however. These were observed in recent roadcuts at two high-elevation localities at 1159 m (3800′) and 1281 m (4200′). Neither was identifiable from the surface. Three parent materials were observed at the higher site (Figure 2-10B) - till, a fining-upward sequence of well-sorted sandy sediments, and a final blanket of colluvium. The lateral extent of these or other buried paleochannels on the slopes of Grasshopper Mountain is not known.

Active alluvial deposits are restricted to a small intermittent stream, Grasshopper Creek. On the plateau it comprises a series of interconnected bogs which occupy bedrock depressions. The creek disappears during the plunge down a steep slope, and reappears to flow through the lower

Figure 2-10. Composite soil profiles; A. stabilized colluvium (C) above non-dunitic till (BC, IIC) at soil site 31 on gentle slope; B. stabilized colluvium (C) and outwash (IIC) above dunitic till (BC, IIIC) at soil site 71 on steep slope.

levels of the study area prior to entering the Tulameen River as a hanging valley. A second, smaller, intermittent stream serves as the eastern boundary of the study area. Both drain through the flat bench at 1068 m (3500'). This area appears to collect much subsurface drainage; small seepage-zone bogs and gleysolic soils occur in this area, and groundwater remains close to the surface well into June when the remainder of the mountain is dry.

A small area of the bench at the base of the main study area is underlain by clay containing relatively few coarse fragments. Most, but not all, of this area is occupied by a prominent knoll which rises several metres above the bench. It may be some form of glaciolacustrine deposit.

A thin layer of volcanic ash was encountered in the top 30 cm of a perched bog near the summit of Grasshopper Mountain. Organic soils of the Coley series, which occur as small isolated units within the Tulameen district, commonly contain a thin layer of volcanic ash 30 to 45 cm (12 to 18 inches) below the surface (Lord and Green, 1974). The occurrence and sources of ash layers in southern British Columbia has been discussed by Nasmith et al (1967). Although the Mazama ash (6,600 years), originating in Oregon, is the most widespread in south-central British Columbia (Nasmith et al, 1967), the Grasshopper Mountain area also lies within the plume of the St. Helens Y ash

(3,200 years). It is not known which ashfall is represented in the bog.

Soils are developed in what appears to be reworked till overlying lodgement till on the east side of the sparsely-forested ridge facing Britton Creek (Figure 2-1). The profile is unique among those studied in that the two uppermost horizons are poorly consolidated, contain few coarse fragments, and have a remarkably uniform grain size distribution among five fractions of the <2 mm component (Appendix 11.1). Proportions of both the coarsest and finest fractions are much lower relative to those of most tills, suggesting local reworking and sorting by water. XRD results (Appendix 6) show that the two upper and the two lower horizons are mineralogically distinct (section 4.6), although the boundary between the two groups in the soil profile is gradational.

2.6 Climate

The climate is transitional between that of the dry southern interior and the much moister Cascade and Coast Mountains to the west. Summers are hot and dry, and winters are cold with heavy snowfall at high elevations. Temperatures at Princeton airport (elev. 696 m/2283') ranged from a summer high of 41.7^{o}C to a winter low of -42.8^{o}C

during the years 1941-1970 (Atmospheric Environment Service, 1974). Temperatures at Allison Pass (elev. 1342 m/4400'), located in the Cascades southwest of Grasshopper Mountain, ranged from 31.7°C to -42.8°C during the same period. Total annual precipitation over this period averaged 1452mm at Allison Pass (snowfall: 9652mm), but only 359mm at Princeton (snowfall: 1570mm). Patches of snow may remain on the plateau of Grasshopper Mountain until late May. The mountain is well drained however, and dries rapidly during the summer.

2.7 Soil Development

Soil development, limited by high relief and active colluvial processes, is generally juvenile. The thicknesses of surficial LFH horizons seldom exceed a few centimetres and are particularly thin on steep slopes. The four physiographic zones of Grasshopper Mountain correspond roughly to different types and stages of soil development.

Active colluvium is characterized by orthic regosols (Figures 2-11 and 2-12). Genetic horizons are absent, although sites in the western part of the colluvial slope exhibit a distinctive orange-brown surface colouration and an increasing fines content with depth. These appear to correspond to upslope serpentinite outcrop. LFH horizons

are generally absent on active colluvium, and those that do exist usually have a high content of upslope-derived rock fragments.

Eutric brunisols (Figures 2-13 and 2-14A) are the dominant soil on the rolling plateau area of Grasshopper Mountain, and on ridges and the gentle western slope where colluvial activity is absent or minimal. Surficial Bm horizons are well developed, and may be gradational to underlying C horizons. The soils are almost residual in origin on high plateau areas of thin discontinuous till cover over the dunite bedrock, such as directly above the trench at the A-Zone PGE occurrence (Figure 2-14B)

The steep forested southern slopes of Grasshopper Mountain exhibit the most diverse range of soil types. Humo ferric podzols (Figure 2-15A) and minor orthic regosols characterize the eastern portion, whereas the western portion has eutric brunisols in places covered and modified by later colluvium. The eastern portion of the study area has more mature soil development than the western portion, where sites are marked by a greater degree of colluvial soil disruption and are devoid of genetic horizons. Younger stands of douglas fir and large boulders of dunite scattered through the lower reaches of the eastern portion also attest to this.

Figure 2-11. Unhorizonated orthic regosol soil profiles in active colluvium; A. soil site 9 on the margin of a steep colluvial gully beneath Cliff Zone PGE occurrences; B. soil site 37 in relatively fine-grained colluvium within a talus field near the base of slope.

Figure 2-12. Unhorizonated orthic regosol soil profile (soil site 16) in active colluvium immediately beneath one of the Cliff Zone PGE occurrences (D Zone); A. general view of site; B. close-up of pit face showing absence of horizon development. Free PGM grains were observed in heavy mineral concentrates from this site (Figure 4-52).

Figure 2-13. Eutric brunisol soil profiles developed on dunitic till, showing Bm, BC and C mineral horizons; A. profile on gentle south slope (soil site 66); B. profile on flat, sparsely-vegetated ridgetop (soil site 65). The latter is atypical due to the absence of an LFH horizon.

Figure 2-14. Soil profiles above and adjacent to A-Zone PGE occurrence, secondary study area; A. Unhorizonated orthic regosol (soil site 56) in dunitic rubble above trenched occurrence; B. eutric brunisol (soil site 57), with thin colluvial Bm above BC and C horizons, in dunitic till.

Figure 2-15. Soil profiles developed on non-dunitic till; A. humo-ferric podzol (LFH, Aej, Bf, C) at soil site 19 on steep forested southeast slope of Grasshopper Mountain; B. gleyed melanic brunisol (LFH, Ah, Cg) at soil site 6 in flat seepage area.

Soil development on the flat-lying bench area is dominated by seepage zones, a relatively high degree of organic production, and the local occurrence of a clay parent material. The area is characterized by relatively thick LFH horizons, organic-rich mull Ah horizons, and both gleyed Cg till and clay parent materials (Figure 2-15B) at the lower levels, and by an upslope gradation to drier and more juvenile regosols at the base of the steep forested slope.

2.8 Vegetation

Tree cover on Grasshopper Mountain is diverse in both species and intensity, and related to the physiographic zones of the mountain. Flanks and slopes are moderately to well-wooded, with sparsely-forested areas common in the plateau and summit areas, and open vegetation dominating active colluvium.

The plateau and western flank region of the mountain are characterized by mature stands of Douglas fir, the largest of which are fire-scarred and exceed two feet in diameter. The secondary study area near the summit has a more ragged assortment of trees dominated by sub-alpine fir, with minor Douglas fir, lodgepole pine and whitebark pine. The southern forested slope of the mountain is thickly-

forested and dominated with much younger Douglas fir. The flat forested bench area is populated primarily by mature Douglas fir, with subordinate cedar, sub-alpine fir and englemann spruce. The knoll is occupied by young lodgepole pine. The dry and well-drained colluvial slope and cliffs are open and populated by scattered Douglas fir, Ponderosa pine, and juniper. Trees commonly exhibit curved trunks indicative of colluvial creep, as well as upslope scars resulting from being struck by boulders bouncing downhill. Ponderosa pine is relatively more common at higher elevations on the cliff, and has a much more gnarled appearance than those growing at lower elevations in the Tulameen River valley.

The understory over much of the mountain comprises only thin grasses and groundflowers. The understory is much more diverse in the forested bench area, probably because of the greater moisture content of the soil and the presence of a more nutrient-rich exotic till. Grasses are sparse on active colluvium. The ultramafic plant *Eriogonum heracliodes* was identified in this area (R. Scagel, personal communication, 1988).

Chapter Three

FIELD AND LABORATORY PROCEDURES

CHAPTER THREE. FIELD AND LABORATORY PROCEDURES

3.1 Selection of the Field Area

Selection of the Tulameen ultramafic complex as a site to investigate the surficial dispersion of platinum was based on orientation surveys during 1987 (Fletcher, 1989) and on fieldwork by Newmont Exploration of Canada during 1986 and 1987 (Bohme; 1987, 1988). Grasshopper Mountain was selected as the study area because it hosts the most extensive known occurrences of chromite-hosted PGM in the Tulameen complex.

3.2 Sample Collection Methods

3.2.1 Introduction

Soils, stream sediments and associated banks, bogs, and waters were sampled (Figure 3-1). Soils constitute the main focus of the study. Distribution of samples is shown in Table 3-1.

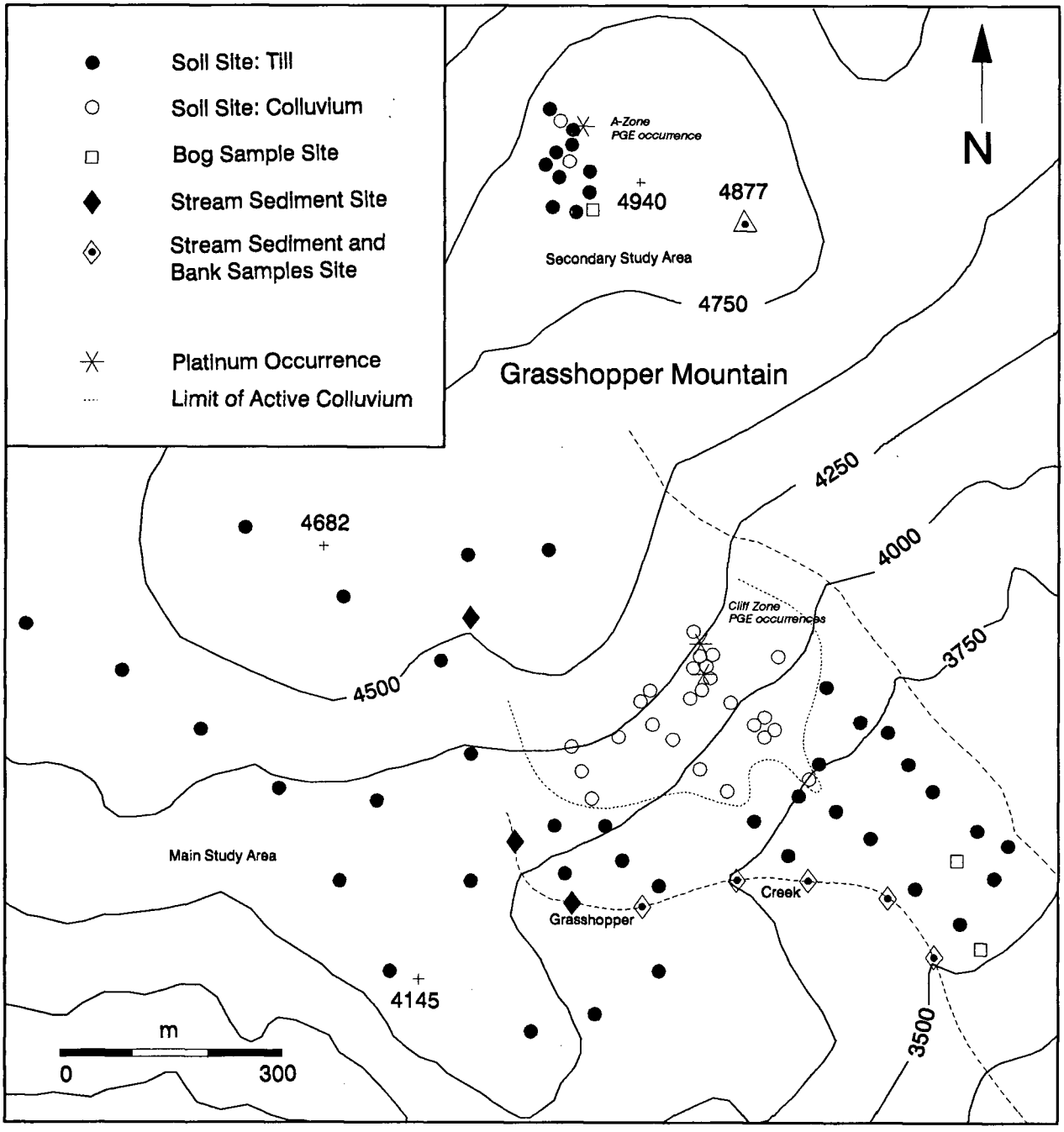

Figure 3-1. Sample location map showing soil, stream, bank and bog sample sites within the dunite core of the Tulameen ultramafic complex, Grasshopper Mountain, B.C. Site numbers are shown in Appendix 1 (basemap adapted from Bohme, 1987).

	Main Study Area	Secondary Study Area	Total
Mineral horizons	149	31	180
LFH horizons	40	7	47
Stream sediments	8	-	8
Moss mats	5	-	5
Bank samples	10	-	10
Bog samples	4	2	6
Water samples	16	1	17
Background soils	-	-	5

Table 3-1. Distribution of sample media according to study area, Grasshopper Mountain, B.C. See Figure 3-1 for locations.

	Main Study Area	Secondary Study Area	Total
Till	38	11	49
Colluvium	25	2	27
Total Soil Profiles	63	13	76

Table 3-2. Distribution of soil profiles according to study area and parent material, Grasshopper Mountain, B.C.

3.2.2 Soils

Soils were profiled and sampled in 76 pits in two study areas (Figure 3-1) during 1988 and 1989. A total of 227 horizons were sampled: 180 mineral soils and 47 surficial LFH samples (Tables 3-1 and 3-2). Site locations and numbers are given in Appendix 1.

Sampling within the main study area was carried out along lines crossing both till and colluvium in order to detect both downslope and downice dispersion of the Cliff Zone Pt occurrences and from the plateau area of the mountain. The lines comprise two to twelve sites each, with the longest transecting all major landscape environments of the study area. Strict grid spacing was avoided; individual sample sites were selected to reflect local variations in the landscape. Sample sites in the eastern part of the main study area are approximately 50 m apart, while a much wider spacing was allowed in the western part of the main study area (Figure 3-1). Several closely-spaced pits were situated above and below the Cliff Zone occurrences to allow both the distance and the manner of downslope PGE dispersion in colluvium to be determined.

The secondary study area was situated around the A-Zone occurrence to assess the effect of reportedly more widespread disseminated chromite (Bohme, 1987, 1988) on the

platinum content of overlying soil horizons. Pits were dug above and downslope of the showing, and along three lines radiating from it at 180 to 210 degrees.

Organic LFH horizons were collected, where possible, prior to the digging of the pit to prevent contamination of the sample with mineral matter. The turf was turned over with a shovel or mattock and the LFH material carefully separated from the underlying mineral matter and transferred to a large paper grocery bag. LFH horizons were sampled at all but one of the main study area till sites and at 7 of the 13 secondary study area sites. Only 3 were collected on active colluvium.

Most soil sites were located on undisturbed ground. Several sites were excavated from roadcut exposures however, and one was located directly above the trenched showing at the secondary study area. Soil pits were generally dug to a depth of slightly less than 1 m. In till, pits bottomed out in C horizon till representing oxidized parent material. The depth of pits on steep colluvial slopes was limited by constant collapse of the pit face. Individual genetic horizons were identified on the basis of colour, compaction and root penetration, measured, and sampled with a trowel from the bottom up. Duplicate samples, A and B, of 10-15 kg generally were collected from mineral horizons. Samples from upper horizons were generally smaller than those from C

horizons because of their thinner size. Cobbles greater than 10 cm were avoided during sampling. Soil pedons were classified according to the Canadian System of Soil Classification (Agriculture Canada Expert Committee on Soil Survey, 1987). Colour, presence or absence of mottles, percentage of coarse fragments, fragment shape and soil texture were recorded for each horizon. Among the site parameters recorded were topography, drainage, parent material, proximity to bedrock, intensity and type of vegetation, and possible sources of contamination. Samples were removed from the field area both on foot and on horseback.

In order to assess the direction of glacial dispersion, background C horizon till samples were also collected from 5 sites on the northern margin and to the west of the dunite core on Grasshopper Mountain and Mount Britton (Figure 4-18).

3.2.3 Stream Sediment, Moss mat and Bank samples

Stream sediments were collected from seven sites along Grasshopper Creek at approximately 100 m intervals, and from an additional site within a drainage trough in the summit area of the mountain (Figure 3-1). Moss mat samples were also collected, if present, and bank samples were taken at

five of the sites.

Stream sediments were generally collected from small gravel-filled pools in the active stream channel. Individual samples were composites of sediment from several such pools, which rarely exceeded 1 m in width or 1-2 dm in depth over a distance of several metres. Three samples were wet-sieved with a plastic 10-mesh sieve and only the -10 mesh fraction collected; there was insufficient stream water available to wet-sieve at other sites. The creek was completely dry at sites 6 and 7.

Moss mat samples were collected at five of the stream sediment sites to compare the Pt contents of the two alluvial media. They were mostly collected from above the water level on rocks and logs over a distance of several metres.

Bank samples were collected from both banks adjacent to five of the stream sediment sites. The banks were relatively low with the exception of those at sites 3-5, where the creek is deeply incised. Those at site 1 are alluvial, while the remainder are till.

3.2.4 Bogs

Centre and margin samples were collected from three bogs within the study areas. Two of the bogs are on unconsolidated material in the seepage zone area, whereas the third is a perched bog occurring in bedrock near the A-Zone occurrence. Samples comprised the uppermost 20-35 cm of organic material, excluding only the top few centimetres. Underlying clay mineral matter was collected from the smallest of the three bogs.

3.2.5 Waters

Water samples were collected from 17 sites during the period May 17-20, 1989 following the spring snowmelt when only scattered patches of snow remained on the plateau area of Grasshopper Mountain. The period available for water collection is very short because early collection may dilute samples with transient snowmelt, but bogs and creeks on Grasshopper Mountain dry up by mid-June.

Samples were collected in three general areas: Grasshopper Creek, the seepage zone in the main study area, and the mountain plateau. Stream waters were collected at sediment locations along Grasshopper Creek. A sample was also collected from the intermittent stream on the eastern

boundary of the study area. Seepage zone samples were collected from bogs and from soil pits that temporarily filled with water. Plateau samples were collected from interconnected perched bogs and ponds in a drainage trough and from the bog adjacent to A-Zone mineralization.

One litre polypropylene bottles used for collecting water samples were pre-treated in the laboratory using the method outlined by Fletcher (1981). Each bottle was rinsed with distilled water, filled with 6N hydrochloric acid, and allowed to soak for 24 hours. Each bottle was then rinsed three times and refilled with distilled water until the field sample was taken. Water bottles were kept tightly sealed in plastic sample bags during transport to and from the field to prevent potential contamination from dirt and dust.

Samples were collected from several centimetres beneath the water surface to avoid surface scum and debris. Water pH was measured at the site with a DSPH-3 portable pH meter, and water colour categorized as either colourless, light brown, or brown. Preparation procedures for water samples were performed in the field immediately following sample collection. Waters were filtered to < 0.45 um with a portable compressed nitrogen pressure filtration aparatus (Figure 3-2) and millipore filters to remove suspended organic and inorganic particles. One litre samples were

Figure 3-2. Portable pressure apparatus for field filtration of water samples.

acidified with 20 ml of 6N hydrochloric acid within a few hours of collection to keep elements in solution and prevent their adsorption onto the walls of the bottle (Chao et al, 1968). Hall (1988) has stated that 10 ml of concentrated (12N) HCL per litre is the minimum required to maintain 50 ppt Pt and Pd in solution for at least two months.

Three duplicate water samples were collected in the field, including a pair in which one sample was filtered and acidified in the usual manner but the second was not.

3.3 Sample Preparation Methods

3.3.1 Overview Soil Samples

A representative split of each C horizon soil, stream sediment, moss mat and bank sample was wet-sieved to obtain a -70 mesh (<212 microns) fraction. The preparation procedure, described below, is summarized in Figure 3-3.

One of the two duplicate C horizon soil samples from each site was weighed, spread on a clean 6'x6' plastic tarpaulin and rolled from end to end several times to homogenize it. The sample was then quartered with a trowel,

and two 1/8 slices from diagonally-opposite quarters removed. The 1/4 split was placed in a pail, reweighed, and rehomogenized on the tarpaulin. The split was again quartered, and two diagonally-opposite quarters, each representing 1/8 of the original sample, were removed. One split was kept in reserve for determination of miscellaneous soil properties. The second 1/8 split was weighed and sieved. The tarpaulin was cleaned with a sponge before and after each use.

Each sample split was wet-sieved to obtain a -70 mesh (<212 microns) fraction. The sieving apparatus, consisting of two stainless steel ASTM sieves (10-mesh, 70-mesh), a large plastic bucket, a modified bucket lid and a recirculating pump is shown in Figure 3-4. A portion of the sample was placed into the upper 10-mesh sieve and washed through the sieves with a combination of finger action and water recirculated from the bucket. Care must be taken that the lower sieve does not clog up with fine material. Fresh tap water was used in the latter part of each sieving cycle to ensure that the fractions were properly washed. The two coarse fractions (+10 mesh, -10+70 mesh) were emptied onto kraft paper, air-dried, weighed and stored. Recirculating pump hoses were rinsed out between samples, and sieves and buckets cleaned with soap and water. A toothbrush was used to clean the sieves once they had dried.

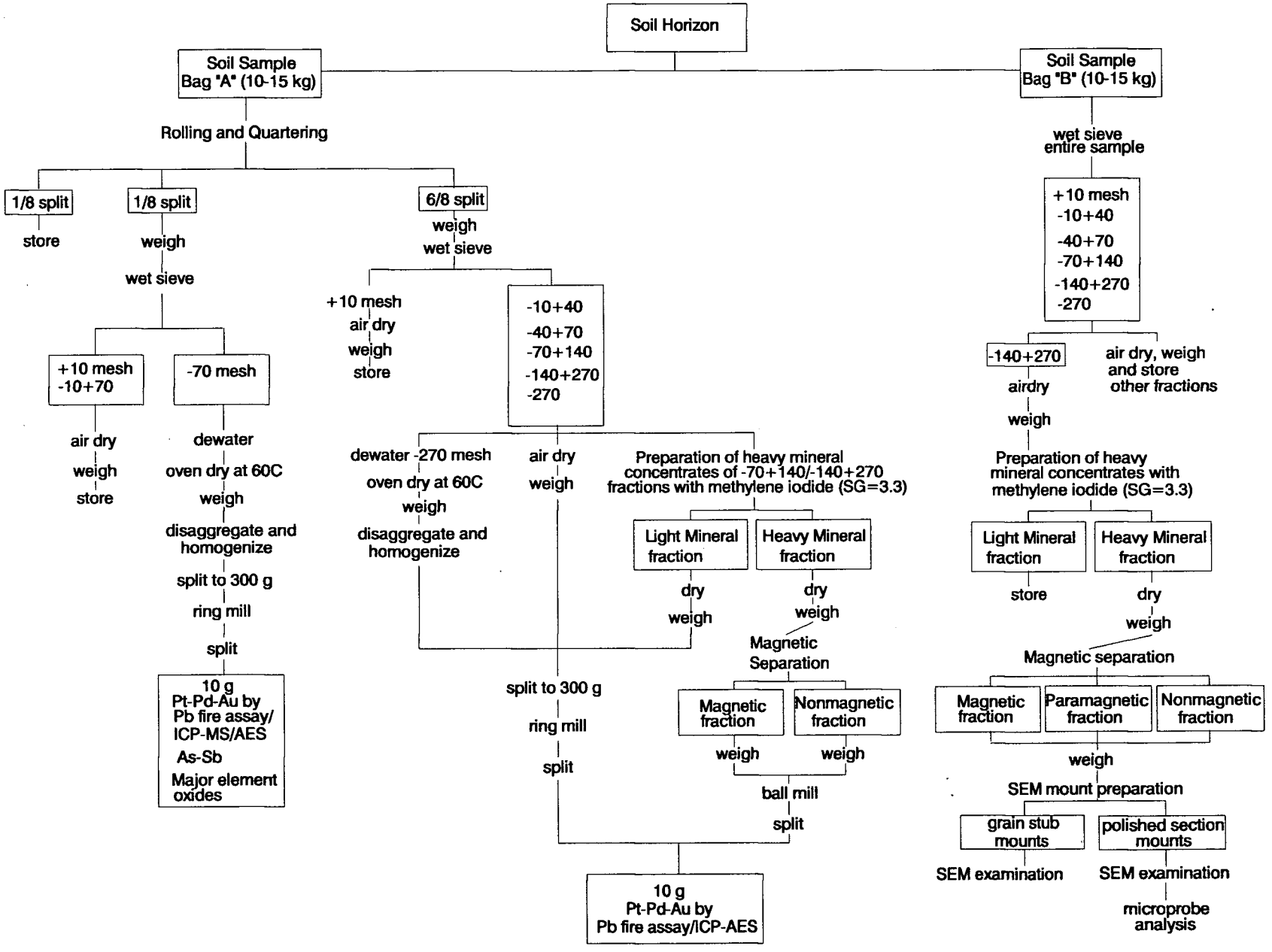

Figure 3-3. Flowchart for soil sample preparation and analysis.

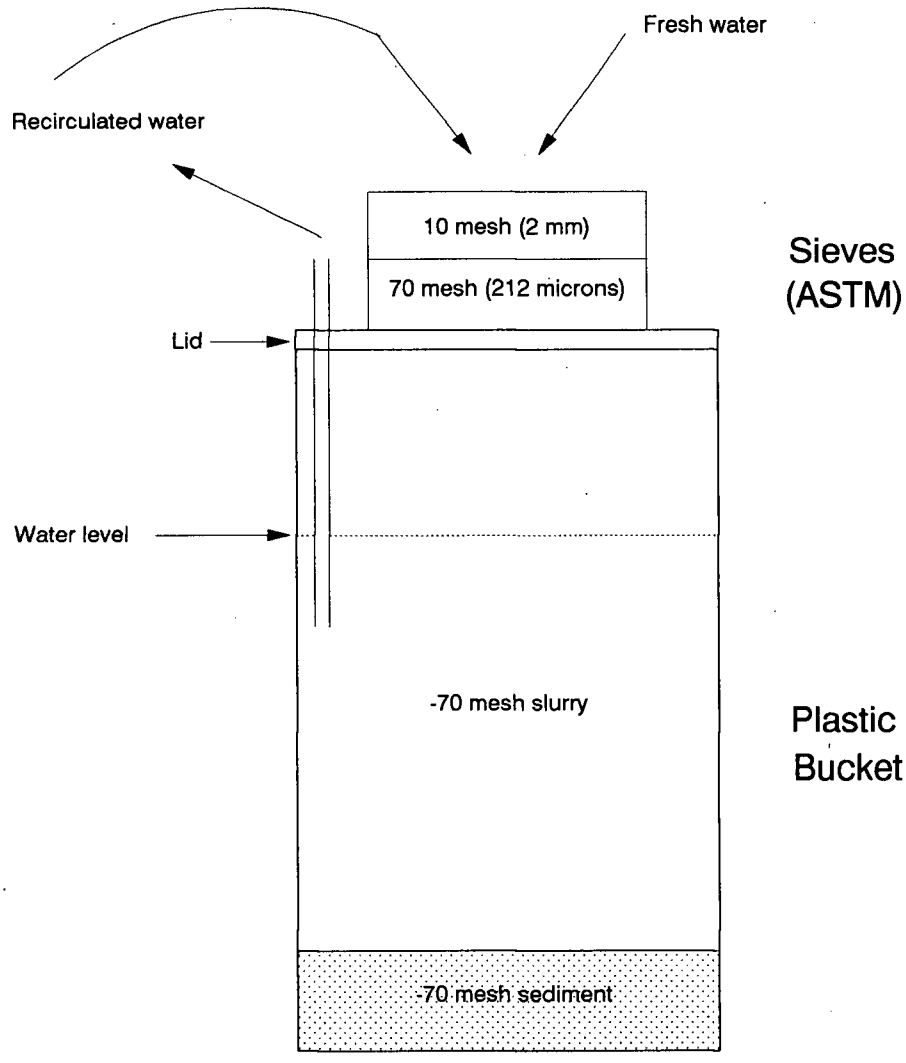

Figure 3-4. Wet sieving apparatus for overview sample preparation.

The -70 mesh slurry was allowed to settle in the bucket for a few weeks. That portion already settled on the bucket bottom was scooped directly into drying trays and oven-dried at 60°C. The remainder was dewatered with a pressure filtration apparatus constructed in the Department of Geological Sciences at U.B.C. The apparatus consists of an aluminum base with a spigot, a large plastic cylinder, and an aluminium cover linked to compressed air line. Heavy white paper was placed on the base to serve as a filter to trap the sediment. The -70 mesh slurry was poured into the apparatus. A black heavy mineral segregation which commonly collected at the bottom of each bucket was, however, washed with a wash bottle into the drying tray rather than into the filtration apparatus to prevent possible entrappment and loss of fine heavy minerals in the filter paper.

The top of the filtration apparatus was bolted on, and air pressure increased to 25-50 psi until all water was discharged. The sediment-laden filter was then removed and oven-dried. Finally, the sample was scraped from both the filter and drying tray with a plastic scraper, weighed, and placed in a small pastic pail to be hand-mixed and -ground with a porcelein pestle. This step is neccessary both to homogenize sediment which may have been density-stratified within the drying tray, and to reduce the size of the dry aggregates so they will pass a riffle splitter.

Splits of 200-300 g were taken with a stainless steel Jones riffle splitter and pulverized for three minutes in a tungsten carbide ring mill to approximately -200 mesh. Several charges of about 50 g each were required for each sample. A tungsten-carbide ring mill, rather than chrome steel, was used to prevent possible chromium and iron contamination of the sample (Hickson and Juras, 1986). Splitter and splitting pans were cleaned with compressed air between samples, and the ring mill sponge-cleaned with soap and water. The final stage of overview sample preparation involved the further splitting of the 200-300 g splits down to 10 g subsamples for analysis. A number of duplicate samples (Table 3-3) were also prepared at this stage.

3.3.2 LFH Samples

LFH samples were air-dried, mixed within the bag, and weighed. One-half of the sample, or more if the weight was less than 100 g, was ground in a Wiley mill at the Department of Soil Science, U.B.C. The mill was cleaned with compressed air between samples. Samples were transferred to numbered Coors crucibles, weighed, and ignited in a muffle furnace at 700^{o}C until a white ash was obtained. This typically required about 12 hours. The relatively high ashing temperature is desireable to achieve a complete recovery of Pd (Dunn et al, 1989). After cooling

for a further 12 hours, the ash was transferred to a pre-weighed vial or bag and weighed. Ten grams of ash was obtained in most instances; samples larger than 20 g were further split in a stainless steel splitter and the splits used as duplicates.

3.3.3 Stream Sediment, Moss mat and Bank Samples

Minus 70 mesh fractions of stream sediment and bank samples were prepared using the same procedures as overview soils (Figure 3-3). Stream sediments were dried and weighed prior to wet-sieving, however, and because of their coarser grain size both duplicate bags were combined, homogenized and split.

Moss mats were prepared differently because of their high proportion of organic material, the small proportion of coarse clasts, and their relatively small size. Samples were weighed, oven-dried, and disaggregated in their plastic bags by gently pounding with a rubber mallet (Gravel and Matysek, 1989). They were then reweighed and homogenized on the plastic tarpaulin. The homogenized sample was quartered with a trowel and two diagonally-opposite quarters removed. This split, representing one-half of the original sample, was then wet-sieved in the standard manner to obtain a -70 mesh fraction.

3.3.4 Bog Samples

Bog samples were dried, weighed, and disaggregated by pounding with a rubber mallet. As this did not sufficiently reduce the hard dry substance in size, samples were then transferred to a small bucket and further pulverized with a porcelein pestle. The sample was then split into duplicate 150-250 g portions with a Jones riffle splitter. One duplicate was pulverized in a tungsten carbide ring mill for 1-2 minutes. The second was hand-ground with a porcelein mortar and pestle to further reduce the size of the aggregates and then ashed in a muffle furnace at 700^{o}C.

3.3.5 Detailed Soil Profiles

The second major sample preparation stage involved wet-sieving horizons from each of fourteen selected soil profiles and one stream sediment into six ASTM size fractions. The sites (Figure 3-5) were chosen as being representative of the wide variety of surficial material and soil types, landscapes, and Pt contents occurring on Grasshopper Mountain. Two size fractions (-70+140 and -140+270 mesh) were then separated into light and heavy mineral fractions and the latter further separated into magnetic and nonmagnetic fractions. Five size fractions (-10+40, -40+70, -70+140 Lights, -140+270 Lights, -270) and

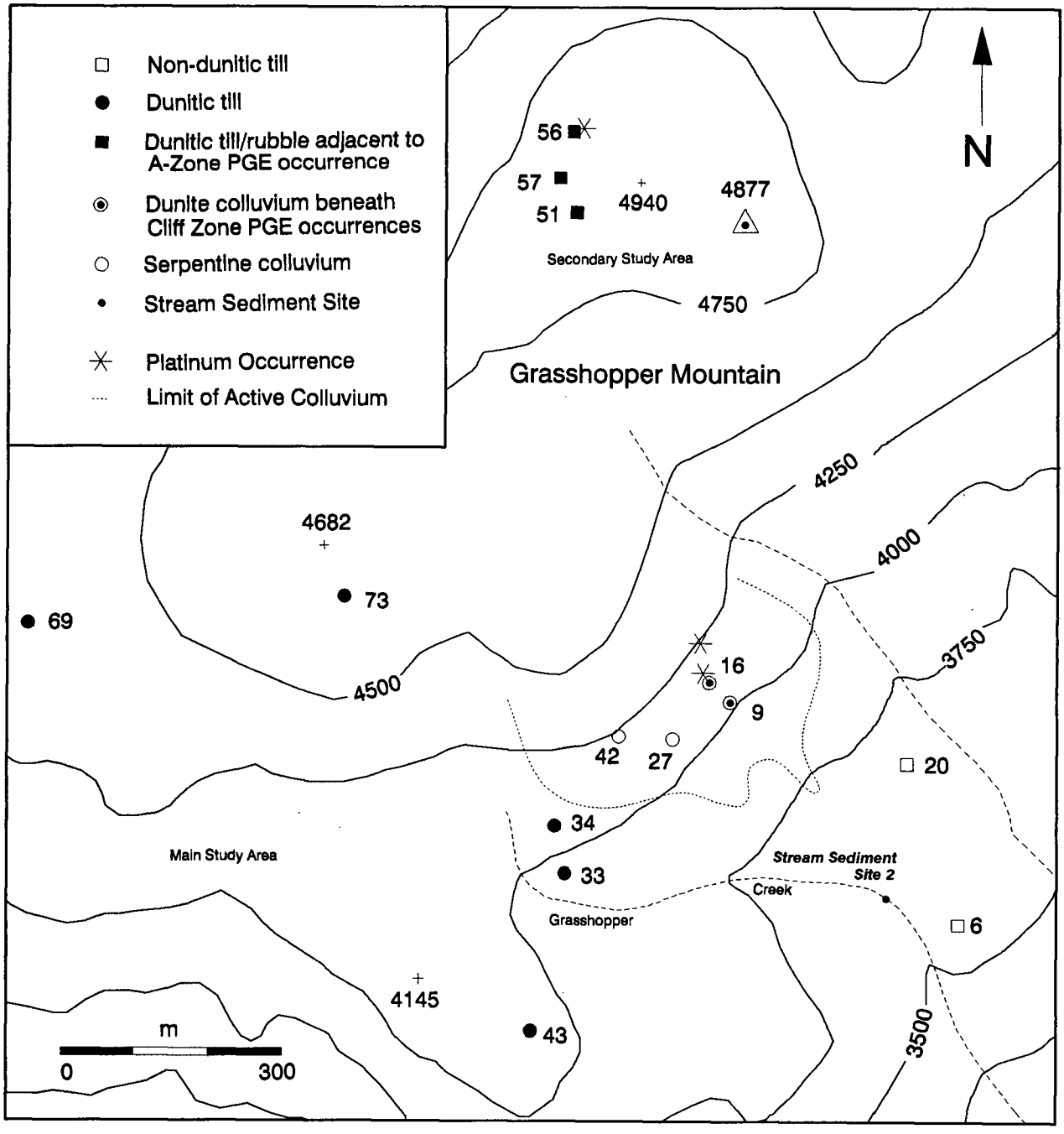

Figure 3-5. Location map of detailed soil profiles (n=14) and stream sediment site (n=1), showing surficial material type and soil site number, Grasshopper Mountain, B.C.

four density/magnetic fractions (-70+140 Magnetic Heavies, -70+140 Non-magnetic Heavies, -140+270 Magnetic Heavies, -140+270 Non-magnetic Heavies) were produced from each of 34 horizons/sediments for a total of 306 samples.

3.3.5.1 Size Fractions

Samples from previously-processed C-horizons were retrieved and sieved in their entirety. Previously unprocessed samples from A and B horizons were first homogenized on the plastic tarpaulin, quartered, and a 1/8 split removed for determination of miscellaneous soil properties. The remaining 7/8 of the sample was wet-sieved as previously described, but using additional sieves to produce six size fractions (+10, -10+40, -40+70, -70+140, -140+270, and -270). Wet-sieving of soil into multiple size fractions is a lengthy and labour-intensive process. An experienced person typically requires 2-3 working days to sieve a 10 kg till sample; an inexperienced person requires considerably longer. The advantage of wet-sieving over dry-sieving is the much greater amount of fine material recovered. Day (1988) reported 76% to 676% increases in the recovery of -270 mesh stream sediment when dry-sieving was followed by wet-sieving.

Size fractions were air-dried and weighed. The coarse

+10 mesh fraction was stored, while the -270 mesh fraction was allowed to settle for several weeks before recovery from the water-sediment slurry as previously-described. Several buckets were typically required to contain the -270 mesh slurry because of the large sample size. The drying process, using both glass trays and the pressure filtration apparatus, often required several days per sample. The dry sample was then hand-pulverized and homogenized.

After separation of a heavy mineral fraction for the -70+140 and -140+270 mesh fractions (section 3.3.5.2), two light (S.G.<3.3) and three whole size fractions were split to 200-300 g and pulverized to -200 mesh in a tungsten-carbide ringmill. A fine powder of at least -150 to -200 mesh is necessary to ensure a proper fusion during the Pb fire assay (Beamish and Van Loon, 1977). Grinding times varied from 1.5 to 3.5 minutes per charge depending on the grain size of the fraction. Pulverized splits were further split to 10 g subsamples in the Jones riffle splitter.

3.3.5.2 Density and Magnetic Fractions

Heavy mineral separations of the -70+140 and -140+270 mesh fractions were performed with the heavy liquid methylene iodide (S.G.=3.3). Sixty-nine separations were performed on samples from 34 horizons and sediments. The

entire unsplit fraction was used in nearly all cases. Because these were large, typically in the 200-400 g range, a 1000 ml separatory funnel was usually used. Separations involved manual stirring for several hours with a glass stirring rod. The abundance of spinel-bearing Mg-silicate grains with a specific gravity only slightly above that of the heavy liquid resulted in extremely slow separations requiring 12-15 hours to complete. Whatman 1 filters were used to recover the heavy concentrates, which mostly weighed less than 50 g. Methylene iodide was removed from the samples by vigourous washing with acetone. The resulting acetone-methylene iodide mixture was then mixed with bubbling water in a separatory tube to separate and recover the methylene iodide, the specific gravity of which was checked with a standard (S.G.= 3.27) each morning prior to beginning a new sample. Heavy and light mineral concentrates were left to dry overnight in the fumehood; they were then transferred to bags and vials in a separate fumehood and allowed to dry for several more days before weighing.

Dry heavy mineral concentrates were weighed and then further separated into magnetic and non-magnetic fractions by the repeated passing of a hand magnet over the sample. The face of the magnet was covered with a piece of paper to prevent magnetic grains from becoming attached to it. Both fractions were weighed.

Magnetic and non-magnetic heavy mineral concentrates were pulverized in a Spex ceramic ball mill. The entire sample was pulverized to minimize the nugget effect resulting from the splitting of such a heterogeneous medium (Coker and DiLabio, 1989). Samples weighing less than 15 g were pulverized with 3 balls, as recommended by Lavergne (1988), for approximately 12 minutes. Those weighing greater than 15 g were ground with 4 ceramic balls for up to 20 minutes. Longer grinding times resulted in the sample being smeared onto the inside of the ball mill. Samples larger than about 20 g were pulverized in two charges. The mill and balls were cleaned betweem samples with one, and often two, charges of quartz because of the smearing in the mill.

A few, particularly the non-magnetic, fractions were very small and 10 g of sample was not obtained. The whole of these samples was submitted for analysis. The remainder were split to the required weight in a stainless steel microsplitter. This has been shown by Otto (1933) to be the most satisfactory method of obtaining a representative split of heavy mineral concentrates. Its use was confined to the splitting of pulverized rather than unpulverized samples.

3.4 Analytical Techniques

A summary of the total number of samples of each type analyzed, including duplicates, standards and quartz blanks, is shown in Table 3-3.

3.4.1 Overview Mineral Soils, Sediments, Banks and Bogs

Overview soils, stream sediments, moss mats, bank samples and bogs were analyzed for three groups of elements and major element oxides at Acme Analytical Laboratories, Vancouver. Samples were submitted in two separate batches containing duplicates and reference standards:

(1) Pt-Pd-Au-Rh were determined using lead-fire assay on a 10.0 g subsample, following the procedure of Bugbee (1933) (C. Leong, personal communication, 1990). An inductively coupled plasma-mass spectrometry (ICP-MS) finish in 1988 and an inductively coupled plasma-atomic emission spectroscopy (ICP-AES) finish in 1989 were used for all but Rh, which was determined by graphite furnace-atomic absorption spectrophotometry (GF-AAS). Stated detection limits are 1 ppb for Pt and Au, and 2 ppb for Pd and Rh.

Sample Type	Routine Samples	Duplicate Samples	Standards	Quartz Blanks	Other	Total
Overview Suite I	81	8	8	2	-	99
Overview Suite II	32	4	6	1	-	43
Detailed Suite I	216	27	22	3	2	270
Detailed Suite II	106	20	14	3	9	152
Total	**435**	**59**	**50**	**9**	**11**	**564**
LFH I	34	8	2	-	-	44
LFH II	20	2	2	-	-	24
Total	**54**	**10**	**4**	**-**	**-**	**68**
Waters	**17**	**3**	**-**	**-**	**-**	**20**
All	**506**	**72**	**54**	**9**	**11**	**652**

Table 3-3. Sample suite summary for Pt-Pd-Au analyses of overview mineral soils, sediments, banks and bogs; detailed soil profiles; LFH and ashed bog samples; and waters. Waters were analyzed for Pt only.

(2) As-Sb-Bi-Ge-Se-Te by hydride generation. A 0.5 g subsample was digested with 3 ml of 3:1:2 $HCl-HNO_3-H_2O$ at 95°C for one hour and diluted to 10 ml with water. Hydrides are then determined by ICP-AES. Stated detection limits for As, Sb and Bi are 0.1 ppm. Detection limits for Ge and Se, and for Te, are 0.2 ppm and 0.3 ppm, respectively, in 1988 and 0.1 ppm for all in 1989. Eight samples, including two standards, were subsequently re-analyzed for As by hydride generation at the British Columbia Geological Survey Branch laboratory, Victoria. Samples underwent a total HF digestion and hydrides were determined by atomic absorption spectrophotometry (R. Lett, personal communication, 1990).

(3) Major Element Oxides. A 0.2 g subsample was fused with $LiBO_2$, dissolved in 100 ml nitric acid, and analyzed for Si, Al, Fe, Mg, Ca, Na, K, Mn, Ti, P, Cr and Ba by ICP-AES. Loss on ignition was also determined.

3.4.2 LFH and Ashed Bog Samples

Ashed LFH and bog samples were submitted in two additional batches and analyzed for Pt-Pd-Au by ICP-AES and for Rh by GF-AAS following lead-fire assay. Ashed subsamples from thirty-eight LFH horizons were subsequently analyzed for Fe by flame-atomic absorption spectrophotometry (F-AAS) in the Department of Geological Sciences in order to

determine whether or not they had been subject to lithic contamination by underlying dunite. Analyses were performed on a Techtron AA4 atomic absorption spectrophotometer with a Canlab Fe hollow cathode lamp following a hot acid digestion of the ash. Digestions, performed in four daily batches, included both blanks and duplicate samples. Standard solutions of 10, 20 and 50 ppm Fe were prepared from stock solutions, and Fe concentrations calculated (Weberling and Cosgrove, 1965) from a standard solution calibration graph.

A brief description of the digestion procedure is given below:

1) Ten drops of distilled water were added to a teflon dish.

2) A 0.50 g subsample of well-mixed ash was added to the water in the dish and thoroughly moistened.

3) 6 ml of 4:1 nitric:perchloric acid and 2 ml of hydrofluoric acid were added to the dish, in a fumehood, and thoroughly mixed.

4) The dish was placed on a hotplate, allowed to evaporate to dryness or until fuming ceased, and removed from the hotplate to cool.

5) 5 ml of 6M hydrochloric acid was added to the residue. The dish was returned to a warm hotplate for approximately five minutes.

6) The liquid was transfered to a 25 ml volumetric flask, made up to volume with distilled water, and then further

diluted either 10x or 100x with distilled water prior to analysis

Insoluble residue remaining after each digestion was retrieved, dried, weighed and visually examined.

3.4.3 Waters

Pt content of water samples was determined at the Geological Survey of Canada, Ottawa, Ontario. The method has been described by Hall (1988) and Hall and Bonham-Carter (1988). Pt and Pd in the acidified and filtered one-litre sample is absorbed onto 300 mg of activated charcoal. The charcoal is filtered off, ashed at 650^{o}C, and the analytes solubilized in 1.5 ml of aqua regia (Hall, 1988). The sample is evaporated, cooled, and increased in volume to 5 ml prior to analysis by ICP-MS.

3.4.4 Detailed Soil Profile Samples

Detailed soil profile samples were submitted to Acme Analytical Laboratories, Vancouver, in two separate batches and analyzed for Pt-Pd-Au by lead-fire assay on a 10.0 g subsample with an ICP-AES finish. Stated detection limits are 1 ppb for Pt and Au, and 2 ppb for Pd.

3.4.5 Subsample Size Experiment

Incomplete dissolution of chromite during fire assay is a common problem in Pt analyses (section 3.6). Various pretreatment methods, (Grimaldi and Schnepfe, 1969; Moloughney, 1986; Buchanan, 1988; Hall and Bonham-Carter, 1988), commonly involve modifying the composition and quantity of the flux and decreasing the subsample weight in order to dissolve the chromite. Use of the latter to facilitate dissolution negates, however, the advantage of a larger and more representative subsample size in minimizing the nugget effect. Laboratories may further reduce the size of 10 g chromite-rich heavy mineral concentrates, most likely in an arbitrary manner than with a riffle splitter, unless specifically directed otherwise.

Analysis of subsamples larger than 10 g is considered superior in achieving a more representative number of rare particles in gold exploration (Harris, 1982). However, concerns about complete chromite dissolution and subsample size reduction, particularly when heavy mineral concentrates are involved, warranted a test of Pt recovery with 10 g and 30 g subsamples. Seven 10 g and seven 30 g splits of the control monitors RK-05 and PT-5 were prepared, randomized within their weight suite, and submitted for analysis. PT-5 is chromitiferous whereas RK-05 is not; the two are described more fully in Section 3.6.1.

Analytical results (Appendix 2.1) are summarized in Table 3-4 and Figure 3-6. RK-05 shows only a negligible difference in Pt content between the two size ranges. The median Pt content of the 30 g subsamples (325 ppb) of chromitiferous standard PT-5, however, is only 73% that of the 10 g samples (448 ppb). Furthermore, boxplots (Kurzl, 1988) show reproducibility to be poorer with increasing subsample size (Figure 3-6). A t-test shows that mean Pt concentrations of 10 g and 30 g subsamples are significantly different ($p = .05$). The procedure was repeated for PT-5 (Table 3-4). However, due to an error by the laboratory, only 10-20 g of the 30 g subsamples were used. Both median Pt concentrations are higher than those of the first group but a t-test shows that mean Pt content of the larger subsamples remains significantly different ($p = .05$) than that of the 10 g subsamples. Ten gram subsamples of Certified Reference Standard PTA-1 were also analyzed (Table 3-5).

Additional 10 g splits of PT-5 and PTA-1 were analyzed by Chemex Labs using an ICP-AFS rather than an ICP-AES finish. The mean Pt content of PT-5 is greater than that reported by Acme (Table 3-4), whereas Acme's values are higher for PTA-1 (Table 3-5; Appendix 2.2). The cause of these differences is not known although in the case of PTA-1, which is relatively coarse-grained, it may result from a nugget effect.

Standard	Batch		10 g	30g
RK-05	1	A	32.7 ± 1.7[1] 33[2] (31 - 35)[3]	31.7 ± 0.5 32 (31 - 32)
PT-5	1	A	442.1 ± 23.4 448 (396 - 465)	352.3 ± 58.1 325 (274 - 438)
PT-5	2	A	511.9 ± 29.4 501 (488 - 567)	450.6 ± 42.8* 447 (385 - 522)
PT-5	3	B	635.7 ± 24.4 650 (600 - 650)	-

Mean ± 1s[1]
Median[2]
Range (Minimum to Maximum)[3]

Table 3-4. Subsample size experiment: mean ± 1s, median and range of Pt (ppb) concentrations of 10 g versus 30 g subsamples of control reference standards RK-05 and PT-5. N=7 for each grouping. Samples marked with an asterix (*) indicate that subsample sizes of 10-20 g, rather than 30 g, were used by the lab. A = Acme Labs; B = Chemex Labs.

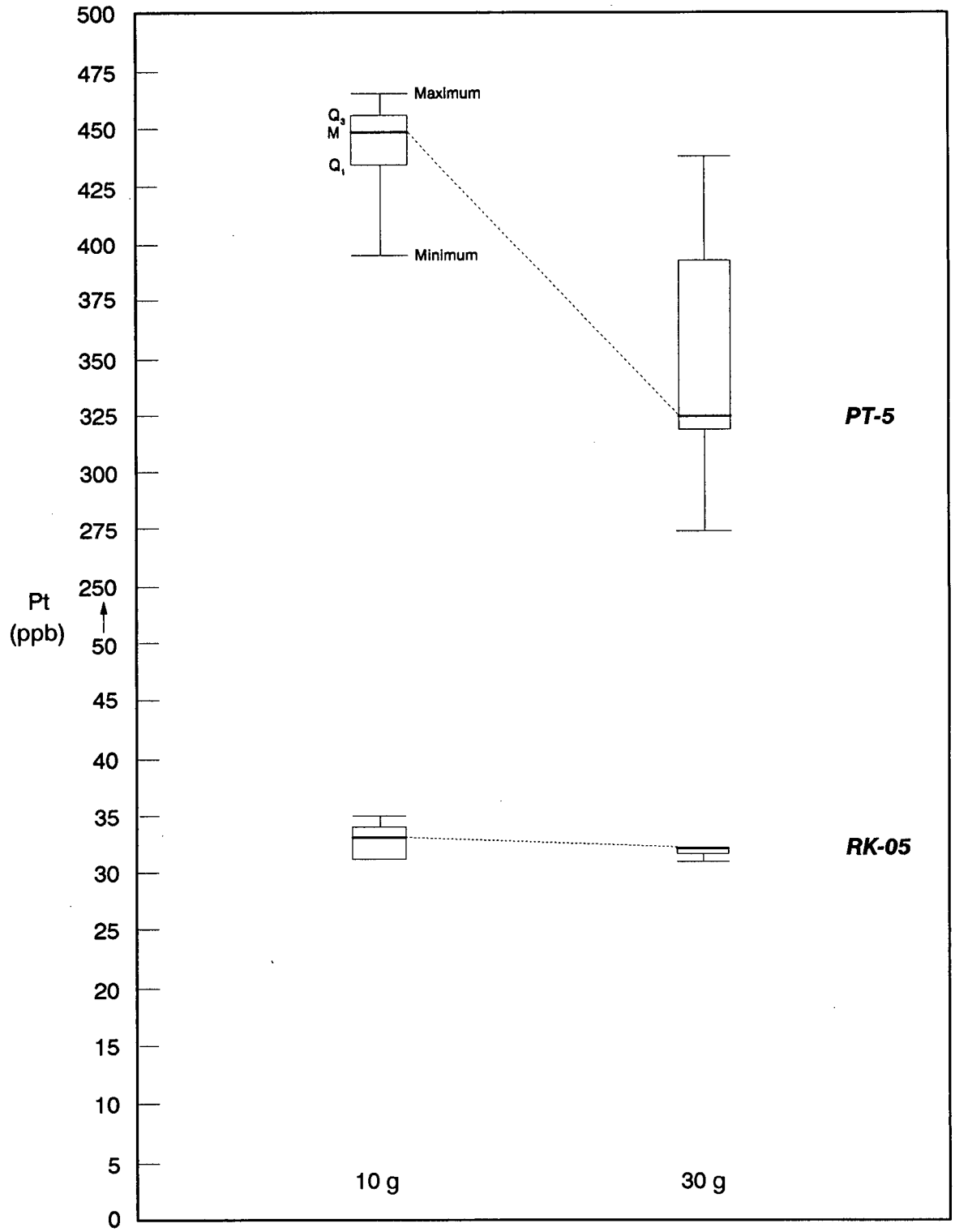

Figure 3-6. Boxplots showing variation in Pt concentrations (ppb) of control standards RK-05 and PT-5 with increasing size of the analytical subsample. N=7 for each grouping. Boxplots show median (M), minimum and maximum concentrations for each grouping; fifty percent of the data for each grouping lies within the box between the first quartile (Q_1) and the third quartile (Q_3).

Standard	Lab	Batch	n	10 g
PTA-1	A	2	7	4367.3 ± 1635.3[1] 3657[2] (2618 - 7078)[3]
PTA-1	B	3	7	3485.7 ± 839.5 3400 (2100 - 4700)
Certified Value				3050 ± 140

Mean ± 1s[1]
Median[2]
Range (Minimum to Maximum)[3]

Table 3-5. Mean ± 1s, median and range of Pt (ppb) concentrations of certified reference standard PTA-1 subsamples determined by two commercial laboratories. Certified value of PTA-1 from Steger (1986). A = Acme Labs; B = Chemex Labs.

The reduction in Pt recovery and analytical precision as subsample size of chromitiferous samples increases (Figure 3-6) has important exploration implications insofar as it negates the advantage of using 30 g analytical subsamples. Use of 10 g subsamples is recommended on this basis.

3.5 Evaluation of Analytical Precision

3.5.1 Overview C Horizons

Precision is a measure of data reproducibility, and was estimated for the overview Pt results with 12 sets of duplicate samples (Appendix 3.1) from a range of soil, sediment and bog sites. Duplicates were prepared during the final splitting of 10 g subsamples from the pulverized subsample and inserted randomly in the two overview analytical suites. Eight duplicates were inserted in the first suite of 81 routine samples, and a further four in the second suite of 32 routine samples (Table 3-3).

Analytical reproducibility was assessed with scatterplots and with a precision control graph. A log scatterplot of routine versus duplicate Pt analyses is shown in Figure 3-7A. The linear correlation coefficient (r) is 0.9975. Precision of the Pt analyses was estimated with a

Thompson and Howarth precision control graph (Figure 3-8). This method, outlined by Thompson and Howarth (1978) and Fletcher (1981), is applicable to data sets containing from 10 to 50 duplicate pairs. Plots of the mean concentration of the duplicates versus the absolute value of their difference are shown for each duplicate pair, and precision control lines for 90th and 99th percentiles of the absolute difference are plotted for the appropriate levels of precision. Results indicate an overall precision of +- 84% at the 95% confidence level, with 1 out of 12 points falling above the 90th percentile. However, it is apparent from the graph that the worst precision is shown by duplicate pairs with low Pt concentrations near the detection limit (1 ppb). If duplicates with mean Pt concentrations less than 13 ppb are disregarded, precision is better than +-20% at the 95% confidence level.

Overview samples were analyzed for As by Acme Analytical Laboratories (section 3.4.1); eight samples were reanalyzed (Appendix 3.2) by the B.C. Geological Survey as a check of the relatively high As concentrations in Grasshopper Mountain soils. Resulting duplicate analyses (Figure 3-7B) are in good agreement. Slightly higher As concentrations reported by the B.C. Geological Survey are attributed to the total digestion method employed (section 3.4.1).

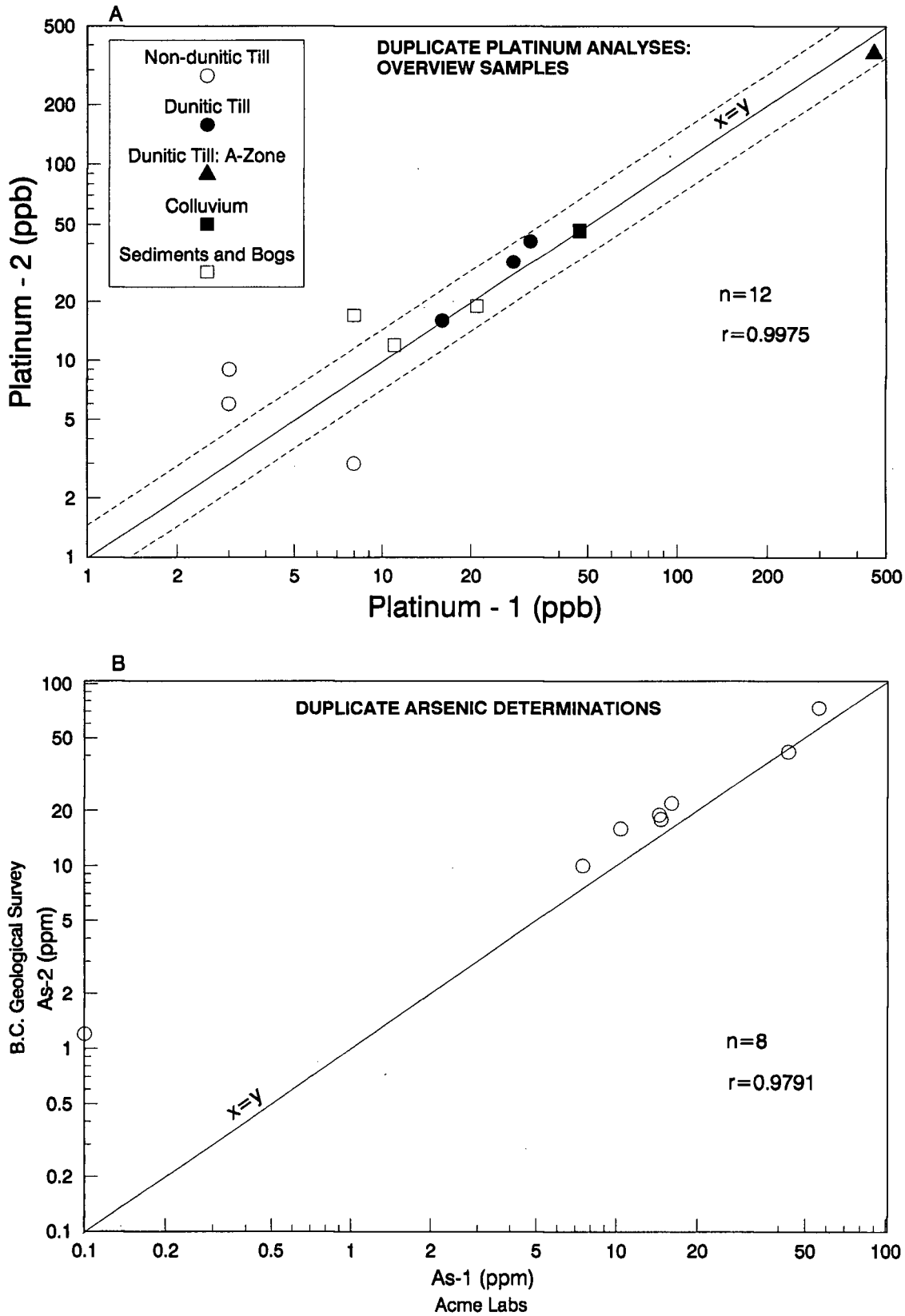

Figure 3-7. Scatterplots of duplicate analyses of -70 mesh overview samples for A. Platinum (n=12) and B. Arsenic (n=8)

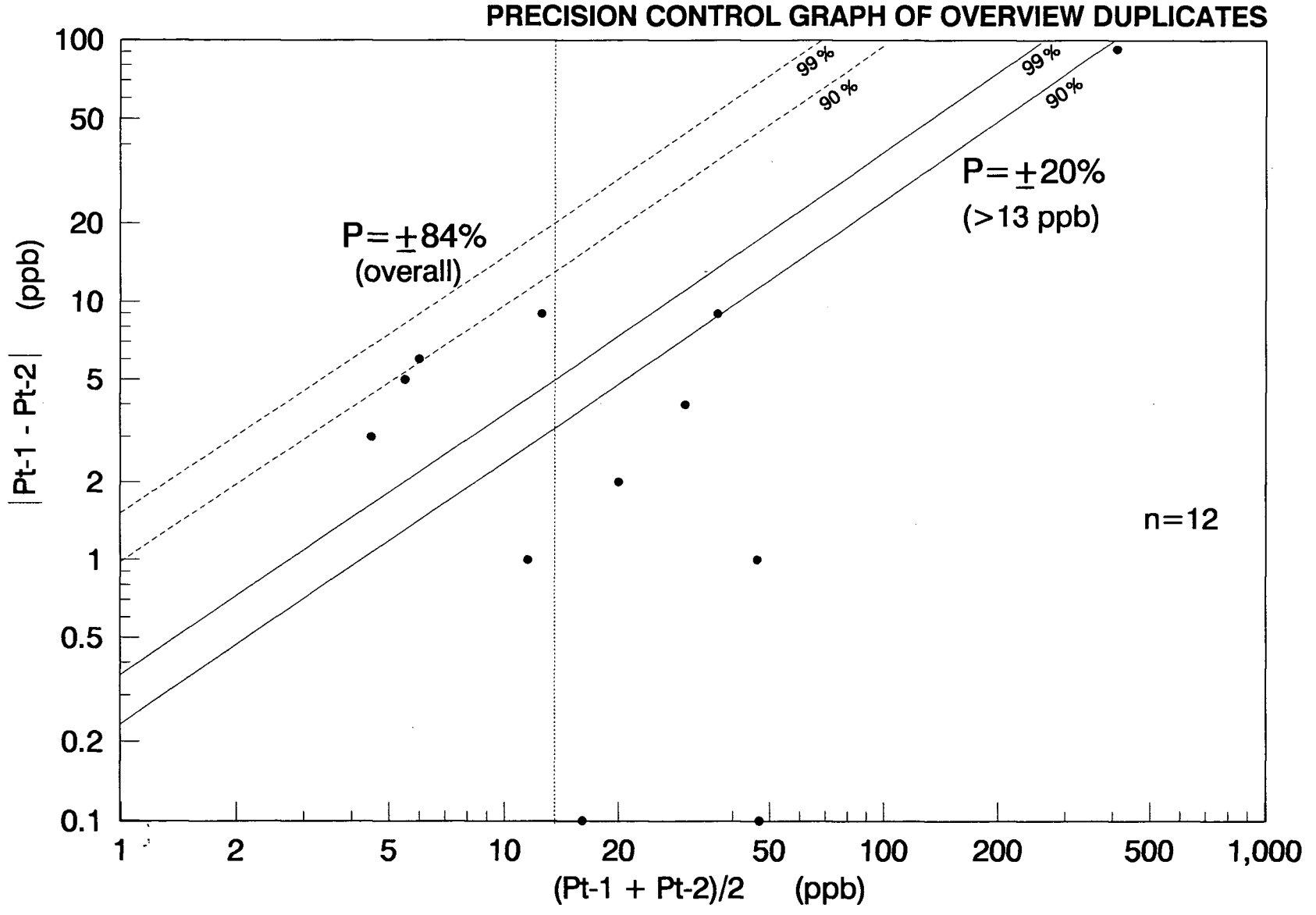

Figure 3-8. Precision control graph of -70 mesh overview duplicate Pt analyses. Dashed lines indicate overall precision of P=+-84% at the 95% confidence level, while solid lines indicate precision of P=+-20% at the 95% confidence level for concentrations > 13 ppb Pt.

3.5.2 LFH Horizons

Ten duplicate pairs, comprising nine LFH and one bog sample duplicate, were used to monitor analytical precision in the two batches (Table 3-3) of ashed organic samples. Analytical data for Pt, Pd and Au are given in Appendix 3.3. In the second batch, an additional (third) insertion of one of the earlier duplicate pairs was made to monitor between-batch as well as within-batch precision. Precision of Pt analyses was evaluated with a scatterplot of duplicate pairs and a Thompson and Howarth precision control graph (Figure 3-9).

It is apparent from both graphs (Figure 3-9) that reproducibility of Pt concentrations is poorer in LFH horizon ash than in mineral C horizons. Precision is about +-60% at the 95% confidence level. A major difference between ashed LFH and overview C-horizon samples is that C horizon samples exhibit poor precision only near the detection limit, whereas ashed LFH samples exhibit it over the entire concentration range. The poorer precision is attributed to the much smaller field size of LFH than mineral soil samples and to the erratic distribution of particulate Pt-hosting grains within the organic matrix of the horizon (section 4.2.2).

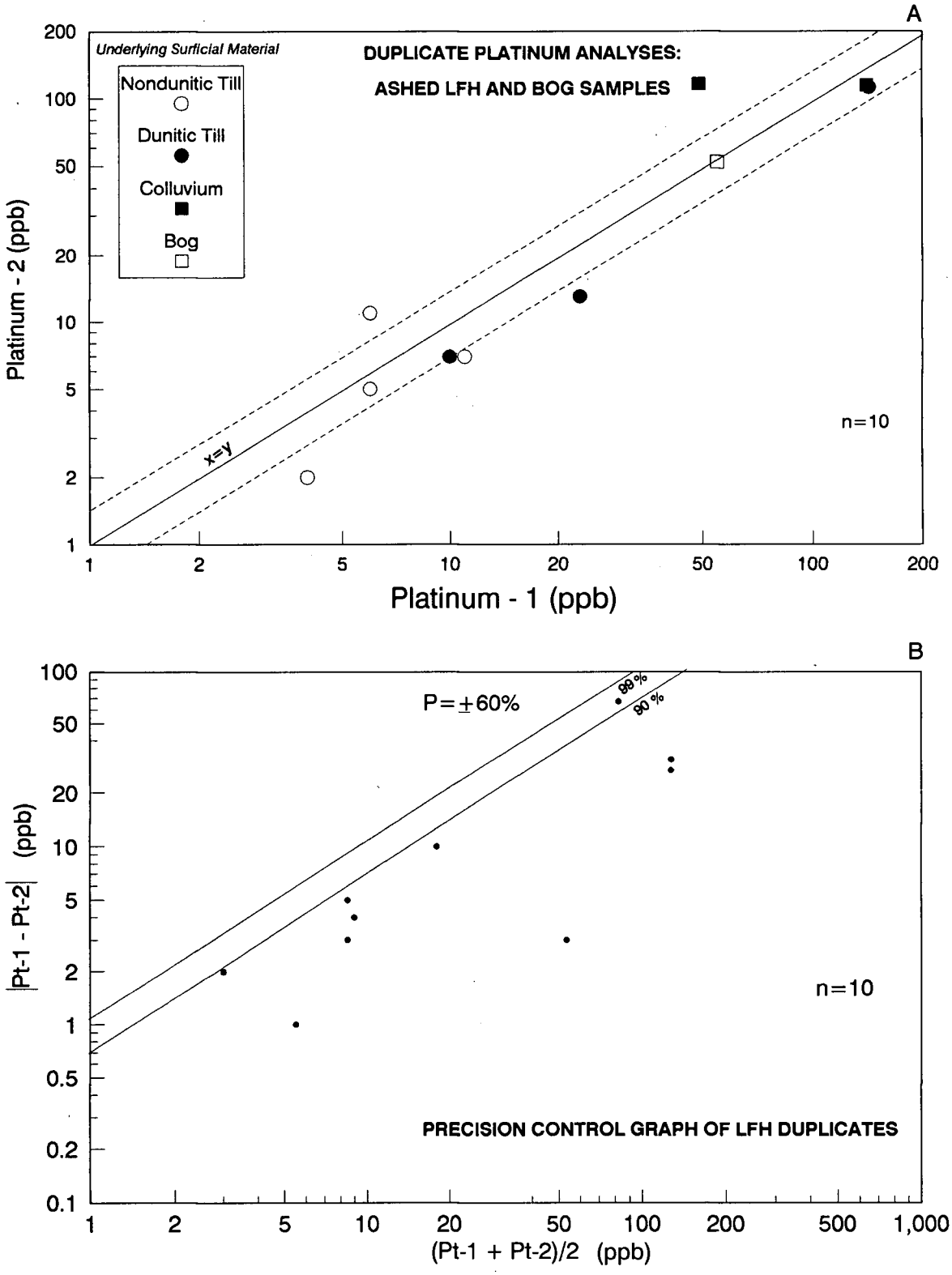

Figure 3-9. Duplicate Pt (ppb) analyses (n=10). A. Scatterplot of duplicate Pt analyses of ashed LFH and bog samples; B. Precision control graph of duplicate LFH Pt analyses, showing P=+-60% at the 95% confidence level.

3.5.3 Detailed Soil Profiles

Precision of Pt analyses in detailed soil horizons was evaluated at two levels. At one level, 47 pairs of standard duplicate samples (Appendix 3.4) from each of the nine different size/density/magnetic fractions were prepared during final splitting of 10 g subsamples from the pulverized subsample. Twenty-seven duplicates were inserted into suite 3 of 216 routine samples; the remaining 20 duplicates were inserted into suite 4 of 106 routine samples (Table 3-3). Duplicates were not inserted randomly over the entire analytical suite, but within blocks of 10-24 samples of the same size/density/magnetic fraction.

At a second level, an additional set of "splitter" duplicates were prepared from original fractions of ten -10+40 mesh and six -40+70 mesh samples (Appendices 3.5 and 3.6) from detailed soil horizons. Splitter duplicates, typically 250-350 g, represent initial splitting as well as analytical precision. Only the coarsest size fractions were chosen as these, with relatively fewer particles than finer fractions, were considered to be most subseptible to sample splitting variability. Duplicates were processed as individual samples, following identical but separate pulverizing and final splitting paths.

Analytical precision was evaluated with scatterplots

and Thompson-Howarth precision control graphs. Scatterplots of standard duplicates (Figure 3-10) show that there are no systematic variations in reproducibility with either analytical batch or overburden type. Scatterplots of splitter duplicates (Figure 3-12A) show somewhat better reproducibility for -10+40 mesh as opposed to -40+70 mesh samples.

Overall precision of standard duplicate analyses as estimated from the Thompson-Howarth control graph (Figure 3-11) is +-60% at the 95% confidence level. The poorest precision is obtained near the detection limit (1 ppb), as with the overview Pt analyses (section 3.5.1), and at the highest mean concentration (Site 16: 3730.5 ppb). There is little variation in precision along the entire concentration range, however, and exclusion of the three lowest and one highest-concentration samples improves it to +-40% at the 95% confidence level in the range 4-1800 ppb. It is apparent from Figure 3-11 that analytical precision is as good with heavy mineral concentrates as it is with standard size fractions.

As might be expected from the splitting of samples comprising coarse particles, precision of splitter duplicates (Figure 3-12B) is much poorer. Precision of the entire data set (n=16) is worse than +-95% at the 95% confidence level, with 3 or 4 out of 16 points plotting

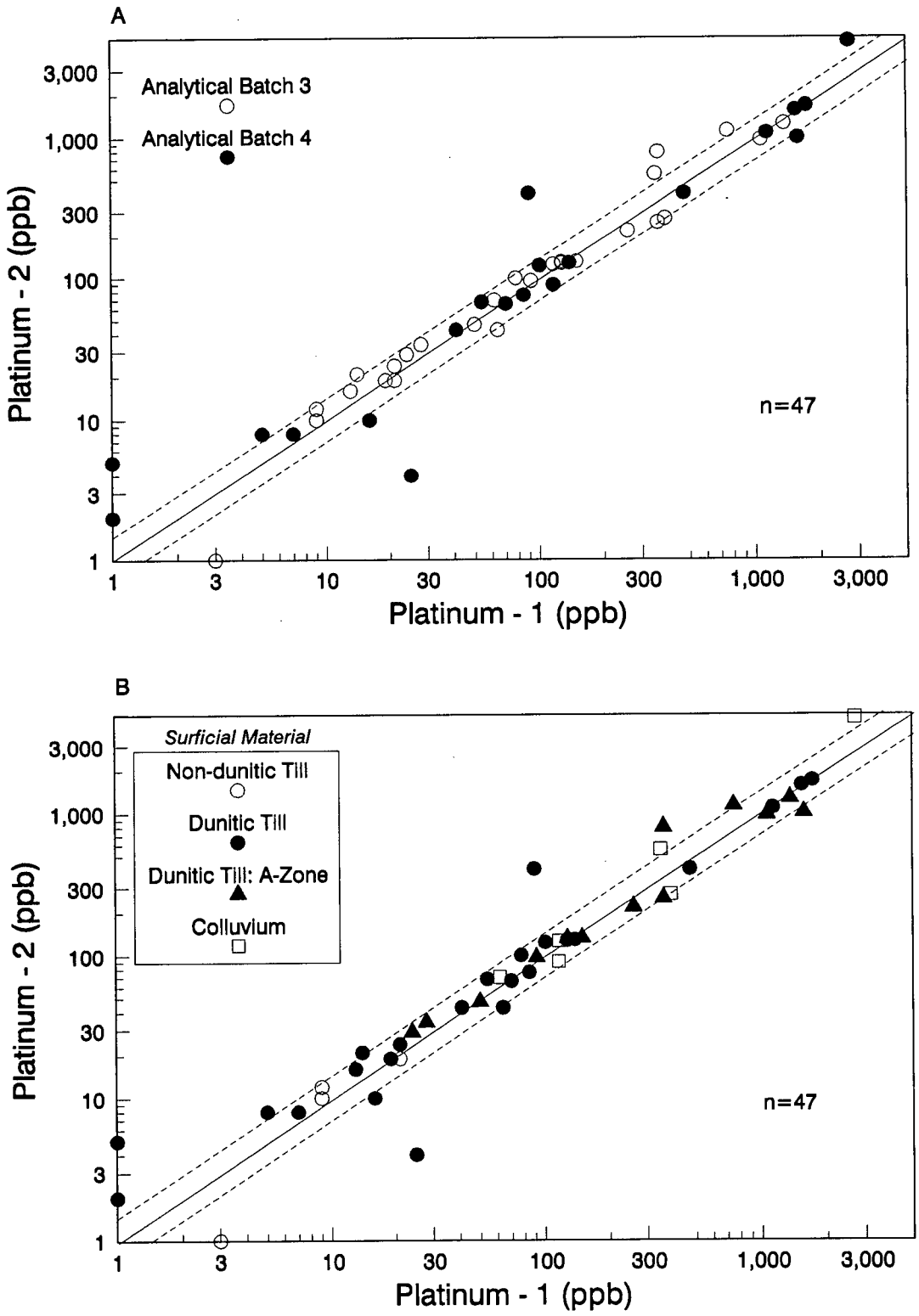

Figure 3-10. Duplicate Pt analyses of detailed soil profile size, density, and magnetic fractions: A. Subdivided by analytical batch; and B. Subdivided by type of surficial material.

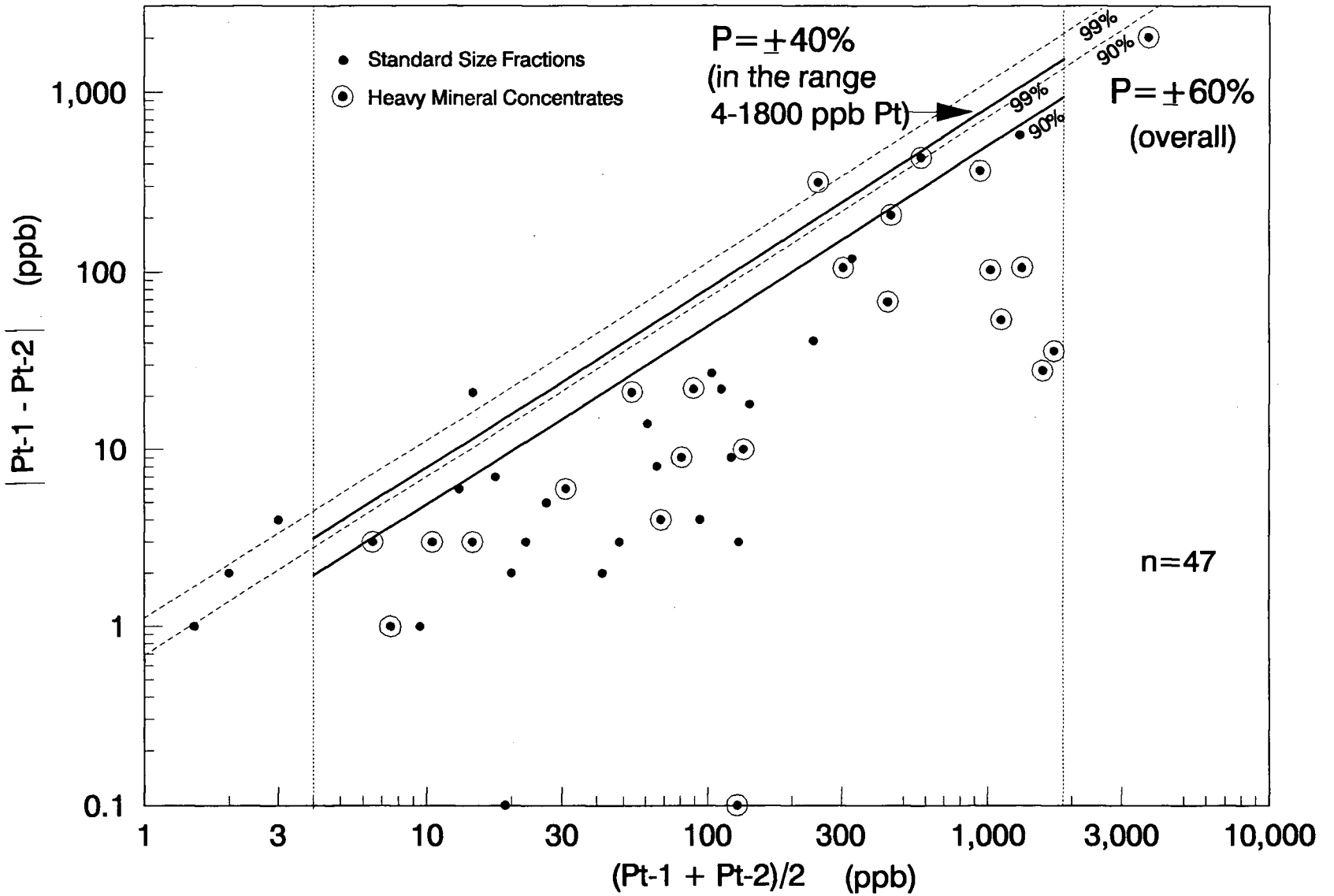

Figure 3-11. Precision control graph of Pt analyses for duplicate samples from detailed soil profiles. Dashed lines indicate overall precision of P=+-60% at the 95% confidence level, while solid lines indicate precision of P=+-40% at the 95% confidence level for both standard size fractions and heavy mineral concentrates in the range 4-1800 ppb Pt.

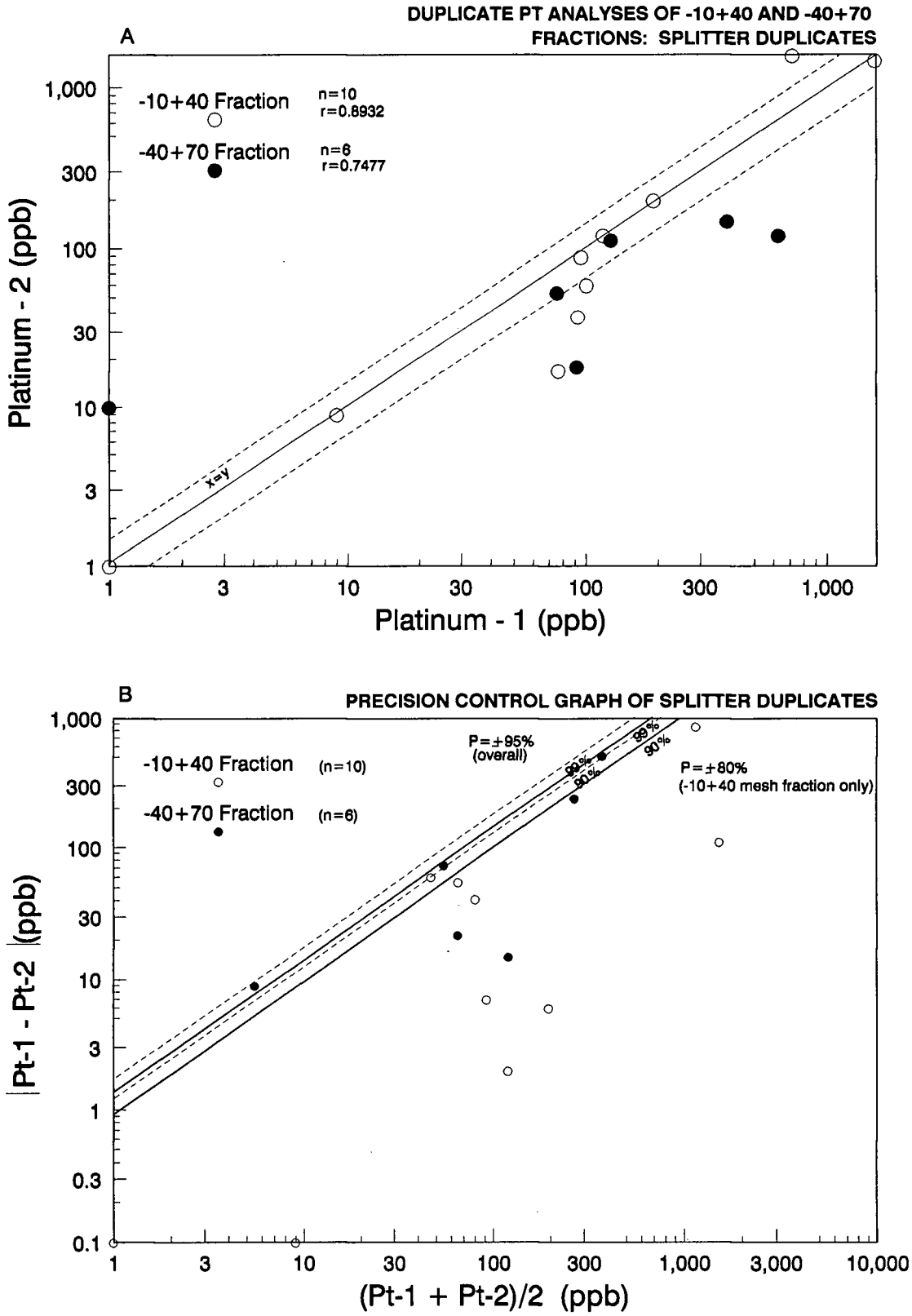

Figure 3-12. Splitter duplicates: A. Scatterplot of duplicate Pt analyses (ppb) of -10+40 and -40+70 mesh fractions; B. precision control graph. Dashed lines indicate overall precision of P=+-95% at the 95% confidence level, while solid lines indicate precision of P=+-80% at the 95% confidence level for -10+40 mesh fraction duplicates only.

above the 90th percentile. Precision for the -10+40 fraction only (n=10) is marginally better, measuring +-80% at the 95% confidence level; only 1 of 10 points plots above the 90th percentile. Splitter duplicates were not always analyzed in the same batch (Appendices 3.5 and 3.6), but this seems to have had little effect on reproducibility. It must be stressed that the two coarse size fractions used represent a "worst case" scenario. Splitter duplicates from finer fractions with a relatively greater number of particles would be expected to exhibit much better precision.

3.6 Monitoring of Analytical Accuracy and Drift

Systematic analytical errors may result from contamination, drift, and physical and chemical interferences (Fletcher, 1981), giving rise to inaccurate results. Control reference standards, drift monitors, and silica blanks were therefore included in all four sample suites to monitor analytical accuracy, as reliable Pt fire-assay analyses are difficult to obtain, particularly from samples with a significant chromite content (Bugbee, 1933; Borthwick and Naldrett, 1984; Bloom, 1986; Moloughney, 1986; Hall and Bonham-Carter, 1988). The incomplete dissolution of refractory chromite grains during the fire-assay flux,

and the heterogeneous distribution of particulate chromite grains within the sample are among the factors responsible. The former results in both incomplete Pt recovery and physical analytical interferences, as PGE remain as inclusions and in solid solution within undissolved chromite rather than entering the flux (Borthwick and Naldrett, 1984), while the latter causes poor analytical precision (section 3.5).

3.6.1 Control Reference Standards and Drift Monitors

One control reference standard (PTA-1) and two drift monitors (RK-05, PT-5) were used to monitor for systematic errors in mineral soil suites, each corresponding to a differing order of magnitude of Pt concentration and varying chromite content. Platiniferous Black Sand PTA-1 is the only certified reference material of the three. It has a Pt content of 3050 $\pm$ 140 ppb at the 95% confidence interval (Steger, 1986). Drift monitors PT-5 and RK-05 are secondary standards containing approximately 500 ppb and 30 ppb Pt, respectively. Certified reference standards containing similar low to mid-level Pt concentrations appropriate for geochemical exploration are not available (Hall and Bonham-Carter, 1988). RK-05 was prepared by the Geological Survey of Canada from pyroxenite from Pyroxene Mountain, Yukon Territory (B. Ballantyne, personal communication, 1988).

PT-5 was prepared by W.K. Fletcher of the University of British Columbia from dunite from Grasshopper Mountain, B.C., and is the only chromitiferous standard of the three.

Forty-eight standards insertions were made into the four mineral soil suites (Table 3-3). PTA-1 was used only in the final two suites which contained heavy mineral concentrates expected to have significant Pt concentrations. Mean, median and ranges of Pt, Pd and Au analyses for each of the three standards are shown in Table 3-6. Analytical data for each of the standards and drift monitors are shown in Appendices 4.1 to 4.3 and individual Pt concentrations for each are plotted on a control graph (Figure 3-13). Mean and median Pt concentrations were calculated for standards and drift monitors in each of the four batches (Table 3-7).

A vegetation standard, composite ash V-3, was used to evaluate the accuracy of the LFH analyses. V-3 was prepared by the Geological Survey of Canada from vegetation from the Rottenstone PGE deposit in Saskatchewan (Hall et al, 1990). Three insertions were made over two batches. Pt results (Appendix 4.4) range from 72-75 ppb and are relatively constant with varying subsample weights from 2.86 to 10 g, although Hall et al (1990) reported poor reproducibility (155 $\pm$ 109 ppb) with 2 g subsamples.

	Pt (ppb)	Pd (ppb)	Au (ppb)
RK-05	30.8 ± 3.3[1]	3.4 ± 1.9	1.6 ± 0.9
	30[2]	2.5	1
(n=20)	(25 - 37)[3]	(2 - 9)	(1 - 4)
PT-5	529.0 ± 73.7	4.0 ± 1.9	2.6 ± 1.8
	505	3	2
(n=21)	(435 - 746)	(2 - 8)	(1 - 7)
PTA-1	2981.0 ± 1116.9	29.7 ± 5.8	61.7 ± 19.6
	2959	29	59
(n=7)	(1626 - 4941)	(21 - 37)	(38 - 89)

Mean ± 1s[1]
Median[2]
Range (Minimum to Maximum)[3]

Table 3-6. Mean ± 1s, median, and range of Pt, Pd, and Au concentrations (ppb) for drift monitors RK-05 and PT-5, and for control standard PTA-1. Certified value for PTA-1 is 3050 ± 140 ppb (Steger, 1986).

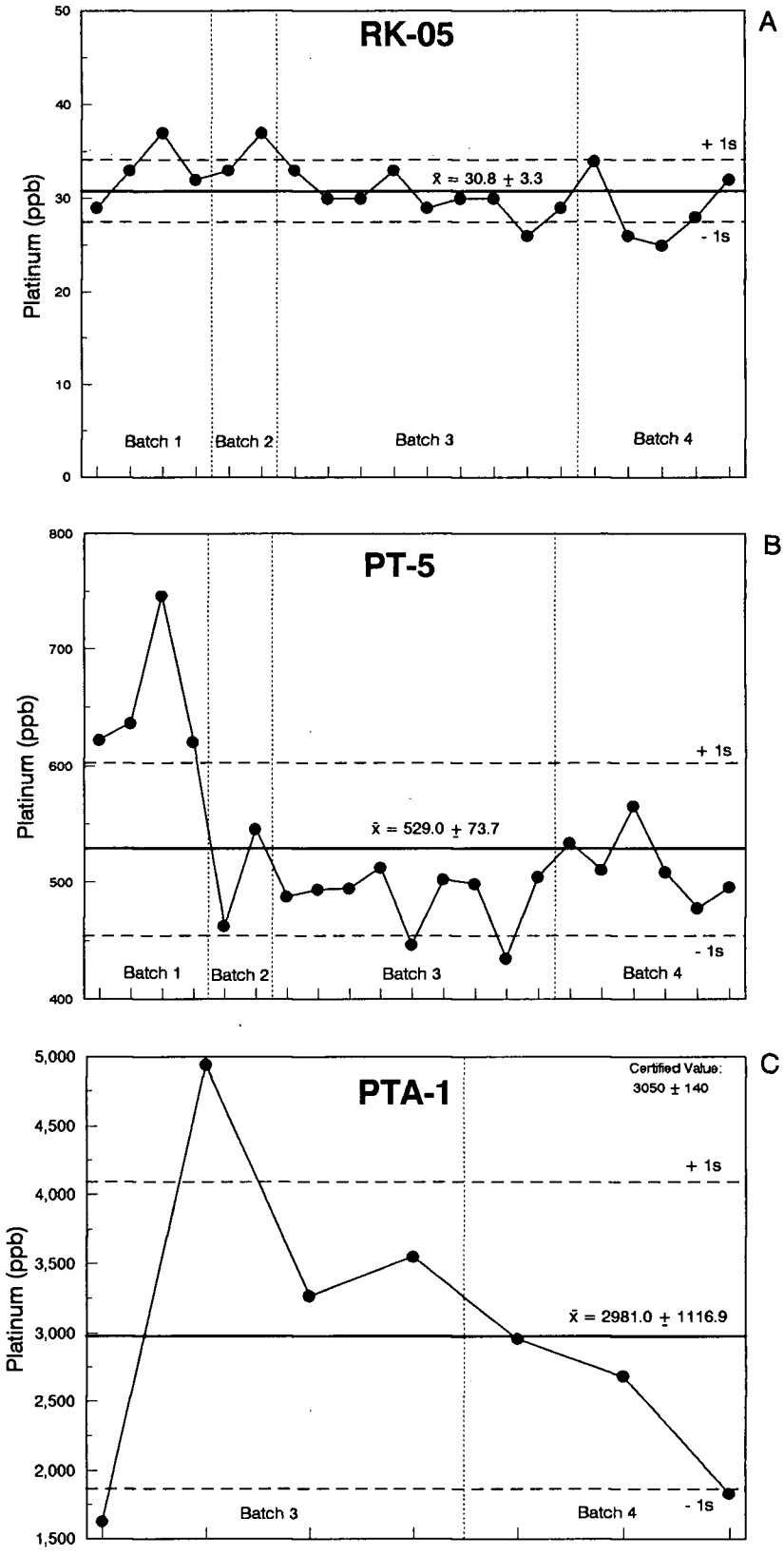

Figure 3-13. Standard control graphs for Pt standards A. RK-05; B. PT-5; and C. PTA-1, showing values in relation to 1s about the mean. All values in ppb.

	RK-05	PT-5	PTA-1
Batch 1	32.8 ± 3.3[1] 32.5[2] (n_1 = 4)[3]	656.8 ± 59.9 630 (n_1 = 4)	-
Batch 2	35.0 ± 2.8 35 (n_2 = 2)	504.5 ± 58.7 504.5 (n_2 = 2)	-
Batch 3	30.0 ± 2.1 30 (n_3 = 9)	486.6 ± 27.0 495 (n_3 = 9)	3346.8 ± 1360.2 3410 (n_3 = 4)
Batch 4	29.0 ± 3.9 28 (n_4 = 5)	515.7 ± 30.8 510 (n_4 = 6)	2493.3 ± 585.5 2685 (n_4 = 3)

Mean ± 1s[1]
Median[2]
Insertions per batch[3]

Table 3-7. Mean ± 1s and median Pt concentrations (ppb) of drift monitors RK-05 and PT-5, and of control standard PTA-1, in each of four analytical batches. Certified value for PTA-1 is 3050 ± 140 ppb (Steger, 1986).

3.6.2 Silica Blanks

Nine silica blanks were inserted in the four sample suites to assess laboratory carryover contamination. Pt, Pd and Au analyses of each of the blanks are shown in Appendix 4.5. Two varieties of silica were used. BDH Fine Laboratory Sand (about -40+100 mesh) was used in the two blanks of the first batch. One was pulverized to approximately -200 mesh to evaluate carryover contamination at the grinding stage while the second was inserted unpulverized. Fisher Scientific SiO_2 floated powder (about -240 mesh) was used for the remaining seven blanks and was inserted without any additional grinding.

Blanks were not randomly placed but were inserted either at the tail ends of the batch or immediately after certified reference standard PTA-1 (3050 ppb). Pt content of blanks in the first three of the four batches (Figure 3-14) is very low, indicating that analytical carryover contamination and, in the case of the first batch carryover from grinding, is negligible. Blanks in batch four, however, returned considerably higher Pt concentrations (range: 19-24 ppb). As all three blanks in this batch were placed immediately after certified reference standard PTA-1, their high Pt content is most probably the result of systematic analytical carryover contamination, either during fire assay preparation or from instrumentation memory. Mean

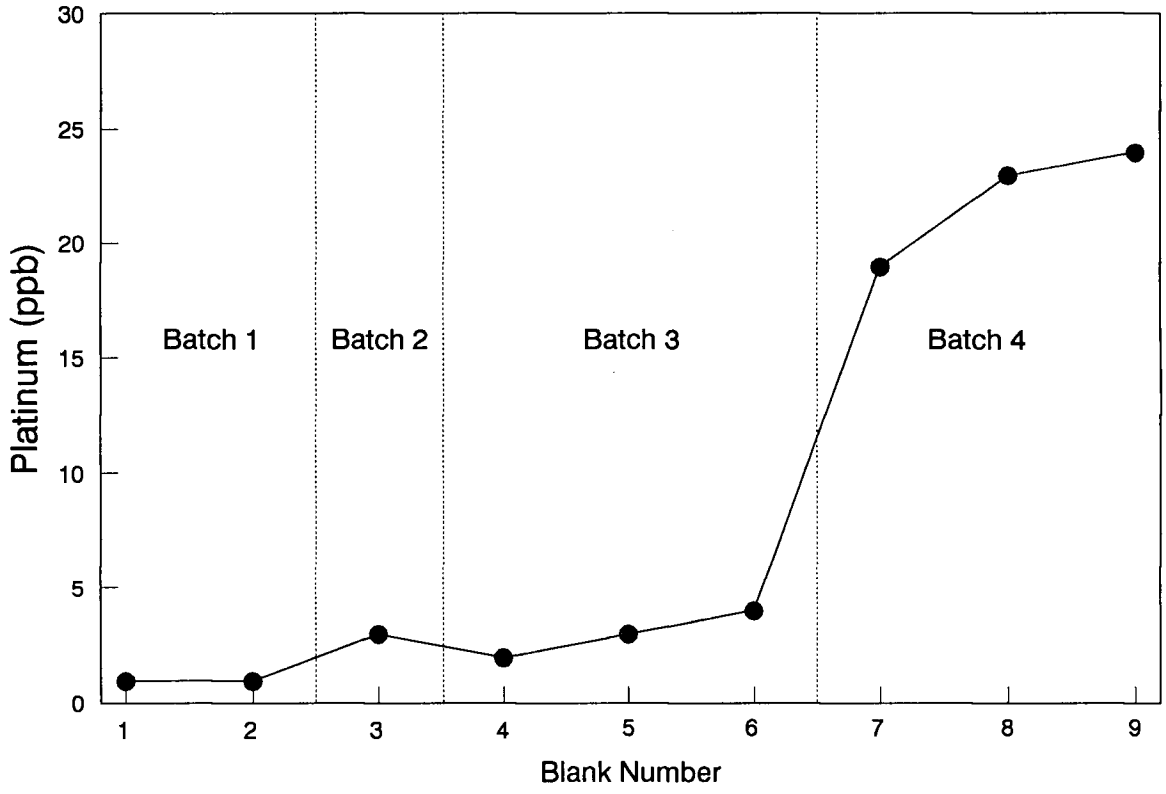

Figure 3-14. Variation in Pt content (ppb) of silica blanks with analytical batch. Blanks in batch 4 were placed immediately after certified reference standard PTA-1 (3050 ppb Pt) only.

Pt content of the three pertinent PTA-1 subsamples (Appendix 4.3) is 2493 ppb and that of the three corresponding blanks (Appendix 4.5) is 22 ppb. Assuming a 10 g subsample size and a silica Pt concentration of 1 ppb, 0.085 g (85 mg) of PTA-1 remaining on a poorly-cleaned spatula would cause a concentration of 22 ppb Pt in the blank. It is apparent that extremely small quantities of high-Pt material can cause these Pt concentration variations if introduced by sloppy subsampling prior to fire assay.

3.7 Scanning Electron Microscopy and Electron Microprobe Analysis of Heavy Mineral Concentrates

3.7.1 Sample Selection and Preparation

C horizon samples from eight soil profiles representative of non-dunitic till, dunitic till, dunitic till near A-Zone Pt mineralization, and both serpentinitic and Cliff Zone colluvium (Tables 4-15 and 4-16) were selected from the detailed sample suite for mineralogical study using scanning electron microscopy (SEM). These span a range of soil types and development, and cover a spectrum of Pt contents. Profile locations are among those shown in Figure 3-5.

As the entire heavy concentrate of each detailed sample

was pulverized in the interests of reproducibility prior to Pt analysis, it was necessary to prepare a new suite of heavy concentrates (Figure 3-3). The duplicate C horizon sample from each of the eight selected sites was wet-sieved to six size fractions as previously described (see section 3.3.5.1) and new heavy mineral concentrates of the -140+270 mesh (106 to 53 um) fraction prepared. This fraction was chosen for mineralogical study because the heavy concentrates generally contain more Pt (Table 4-14) than those from the -70+140 mesh (212 to 106 um) fraction. The concentrates were then separated into magnetic, non-magnetic and paramagnetic fractions using a hand magnet. The paramagnetic grains were incorporated into the magnetic fraction during the initial separation for Pt analysis, but were separated for these samples in case any weakly-magnetic Pt-Fe alloy minerals might be preferentially associated with it. Twenty-three soil concentrates were prepared, as well as two each of stream sediment 503 and paleochannel sediment 207.

Two types of sample were prepared for SEM examination: grain mount stubs and polished grain mounts. To prepare grain mounts the concentrate was emptied onto a piece of glossy paper, and rolled and tumbled back and forth to homogenize the sample prior to subsampling. Adhesive was fixed to a standard circular SEM stub which was then dipped into the sample to pick up a thin layer of grains.

Polished grain mounts were prepared using a method described by Douma and Knight (in preparation). Samples were rolled and tumbled prior to subsampling and insertion into a transoptic powder (methacrylate) mount. The mount was then placed in a mounting press with additional methacrylate and encapsulated. Hand grinding and polishing on a polisher with carbimet paper discs produced a cross-section through the collection of grains. Plucking of fine PGM from the sample, as discussed by Laflamme (1990), is minimized by the use of methacrylate rather than epoxy as a mounting medium (Y. Douma, personal communication, 1990). Both stub and polished grain mounts were carbon coated in a Denton Vacuum DV-515 prior to SEM observation.

3.7.2 Scanning Electron Microscopy Techniques

Samples were examined in the Department of Geological Sciences at U.B.C. using a SEMCO Nanolab 7 scanning electron microscope (SEM), operating at 30 kV, with energy dispersive spectrometry (EDS) qualitative analytical capabilities. The SEM is capable of magnifications of up to 100,000x. Photographic records were made with an attached Polaroid camera.

Twenty-seven grain mount stubs were examined initially under the binocular microscope and the SEM. Backscatter

electron imaging, in which higher atomic number grains appear brighter than lower atomic number grains, was used to determine the presence of PGM and to discern between heavy and light minerals. Generally, high atomic number grains were defined as those in which dominant elements have atomic numbers of at least 22 (Ti).

EDS provided qualitative analyses of the surfaces of PGM and other heavy minerals; mineral identifications in Tables 4-15 and 4-16 are based on relative intensities of characteristic peaks. Secondary electron imaging was used to investigate the external morphology of the heavy minerals. Primary attention was paid to metallic oxide and sulfide phases thought likely to host PGE; silicate phases were not investigated. Twenty-three polished section mounts were similarly examined under the reflecting microscope and SEM in an attempt to discover PGM grains and to obtain qualitative EDS analysis from the interiors of chromite grains.

Binocular and reflected light microscopes proved to be of little use in locating PGM grains due to the very small size of both the PGM and the sieved fraction as a whole. The procedure for locating PGM grains under the SEM involved first scanning the entire mount at low power (50x) to locate any large free PGM or other obvious features, and then methodically searching the mount on an almost grain-by-grain

basis at a much higher power (500-1000x) to locate small PGM inclusions within chromite. PGM, discernible only by backscatter imaging brightness contrast, generally appeared as only tiny points even at high power.

3.7.3 Electron Microprobe Techniques

Electron microprobe analyses of 120 chromite grains in selected polished grain mounts were performed on a Cameca SX-50 electron microprobe in the Department of Geological Sciences. The objectives included:

a) to measure the major-element chemistry of chromite grains, and to determine if any systematic compositional differences exist between spinels associated with high-platinum versus low-platinum samples

b) to determine if there are systematic compositional differences between edges and cores of chromite grains

Electron microprobe analyses were performed on 63 euhedral-subhedral chromite crystals and 57 anhedral chromite fragments from ten polished grain mounts. These, comprising the magnetic and non-magnetic sections from five C horizon soils, cover a wide spectrum of soil types and platinum contents, and include colluvium and dunitic till

sites adjacent to known PGE mineralization as well as both dunitic and non-dunitic till sites distal from known mineralization. Chromites were analyzed for seven elements using an operating potential of 15 kV, a beam current of 30 nA, and a beam size of 1-2 um. The following x-ray lines and standards were used: Si Kα (fayalite S-104), Al Kα (garnet S-007), Ti Kα (rutile S-013), Cr Kα (chromite S-222), Fe Kα (fayalite S-104), Mn Kα (pyroxmangite S-245), and Mg Kα (forsterite S-022).

Analytical procedure consisted of analyzing both the cores and edges of up to 15 randomly-selected chromite grains: crystals in the magnetic fractions and fragments in the non-magnetic and paramagnetic fractions. The paramagnetic fraction was used in place of the non-magnetic fraction in three cases (samples 19, 200, 156) because these contained relatively few chromite grains. Chromites were identified on the basis of their characteristic scratched smooth polished surface and their Cr-rich EDS signature; crystals were discerned from fragments by their shape. A sketch was made of the shape of each analyzed grain for subsequent reference.

Oxide weight percent analyses were converted to mineral formula units on the basis of a spinel unit cell of 24 cations and 32 oxygens. Fe was distributed as Fe^{2+} and Fe^{3+} using FORMULA (Ercit, 1987), a program for formula and

valence calculation. Compositions are plotted on the spinel prism (Stevens, 1944; Irvine, 1965) in Figures 4-58 and 4-59.

3.8 X-Ray Diffraction Analysis of Selected Soil Horizons

The mineralogy of individual horizons from detailed soil profiles was determined with a fully-automated Siemens D-5000 X-Ray diffraction system in order to see if any systematic relation existed between soil mineralogy, major element composition, and platinum content. Forty-eight samples were investigated, comprising two disparate size fractions (-10+40 and -270 mesh) from eleven detailed soil profiles. The locations of the profiles are among those shown in Figure 3-5.

Pulverized sample, prepared earlier for Pt analysis, was applied to a glass slide in water suspension and allowed to dry. Operating conditions were 40 kV and 30 mA using Cu Kα radiation. The angle of scan was 5^{o} to 60^{o} at the rate of 100 seconds per degree. Peak identification was made with DIFFRAC/AT software.

Chapter Four

RESULTS

CHAPTER FOUR: RESULTS

4.1 Introduction

Results are presented for:

A) Overview studies of -70 mesh soils throughout the study area, as well as those of associated LFH samples, banks, stream sediments, moss mats and waters, and X-ray diffraction mineralogy of selected profiles

B) Downprofile size/density/magnetic fraction results for selected soil profiles

C) Scanning electron microscopy and electron microprobe studies of PGM and their host mineral grains

4.2 Part A - Overview Results

4.2.1 Soils

Analytical results for -70 mesh C horizon soils on various parent material types are summarized in Appendices 5.1 and 5.2. Data were evaluated in the manner described by Sinclair (1986): subdivision into till and colluvium parent materials, followed by calculation of basic statistics, correlation analysis and partitioning of populations with probability graphs (Sinclair, 1976) constructed with the program PROBPLOT (Stanley, 1987). Soil mineralogy of representative profiles of each parent material is shown in section 4.2.1.3.

4.2.1.1 Grain Size Distribution

Overview samples were wet-sieved to +10, -10+70, and -70 mesh size fractions (see section 3.3.1). Sample weight data for till and colluvium are shown in Appendices 5.3 and 5.4; weight percent data in Appendices 5.7 and 5.8.

Summary data of mean, median and range of the grain size distribution in various parent materials for the -10

Fraction		Till (n=49)	Colluvium (n=27)	Clay (n=2)
-10+70 mesh	x:	**37.42** ± 8.24	**49.04** ± 8.63	**16.98** ± 1.27
	M:	36.39	46.53	16.98
	R:	(22.75-54.80)	(31.98-67.93)	(16.08-17.87)
-70 mesh		**62.58** ± 8.24	**50.96** ± 8.63	**83.03** ± 1.27
		63.60	53.47	83.03
		(45.20-77.25)	(32.07-68.01)	(82.13-83.92)

Table 4-1. Mean ± 1s (x), median (M) and range (R) of grain size distribution in till (including background samples) and colluvium as weight percent of the -10 mesh (< 2 mm) soil component.

Fraction		Till (n=49)	Colluvium (n=27)	Clay (n=2)
+10 mesh	x:	**45.85** ± 11.24	**71.65** ± 9.82	**17.66** ± 22.43
	M:	46.03	73.51	17.66
	R:	(25.07-70.68)	(53.39-93.94)	(1.80-33.52)
-10+70 mesh		**19.98** ± 5.06	**13.71** ± 5.34	**14.12** ± 4.85
		19.78	12.79	14.12
		(9.37-33.03)	(3.84-31.66)	(10.69-17.55)
-70 mesh		**34.17** ± 9.51	**14.63** ± 6.12	**68.22** ± 17.58
		34.22	12.90	68.22
		(16.21-54.72)	(2.22-31.05)	(55.79-80.65)

Table 4-2. Mean ± 1s (x), median (M) and range (R) of grain size distribution in till (including background samples) and colluvium as weight percent of the total dry weight of the three fractions (dry field weight).

mesh component (Table 4-1) shows that C horizon tills are predominantly composed of -70 mesh (<212 um) particles, whereas colluvial soils are coarser and contain subequal proportions of both -70 mesh (<212 um) and -10+70 mesh (2 mm-212 um) material. In contrast, samples from clay parent material consist almost entirely of -70 mesh particles. With regard to the entire sample (Table 4-2), colluvium is predominantly composed of +10 mesh fragments, and contains a much lower proportion of -70 mesh particles than either till or clay. The absence of any upper size limit for the +10 mesh fraction introduces a sampling bias, as the absence or presence of large cobbles will skew the results. The +10 mesh data cannot be used to characterize the overburden itself, as large cobbles were avoided during sampling. It does, however, highlight relative differences between the three parent materials.

4.2.1.2 Results: Platinum and Other Elements

a) Major Element Till Composition and Grouping of Surficial Materials

Mean, median, and range of major elements, subdivided on the basis of parent material groupings, are shown in Table 4-3. Distribution of MgO, which appears to be most diagnostic of different parent material grouping, in till

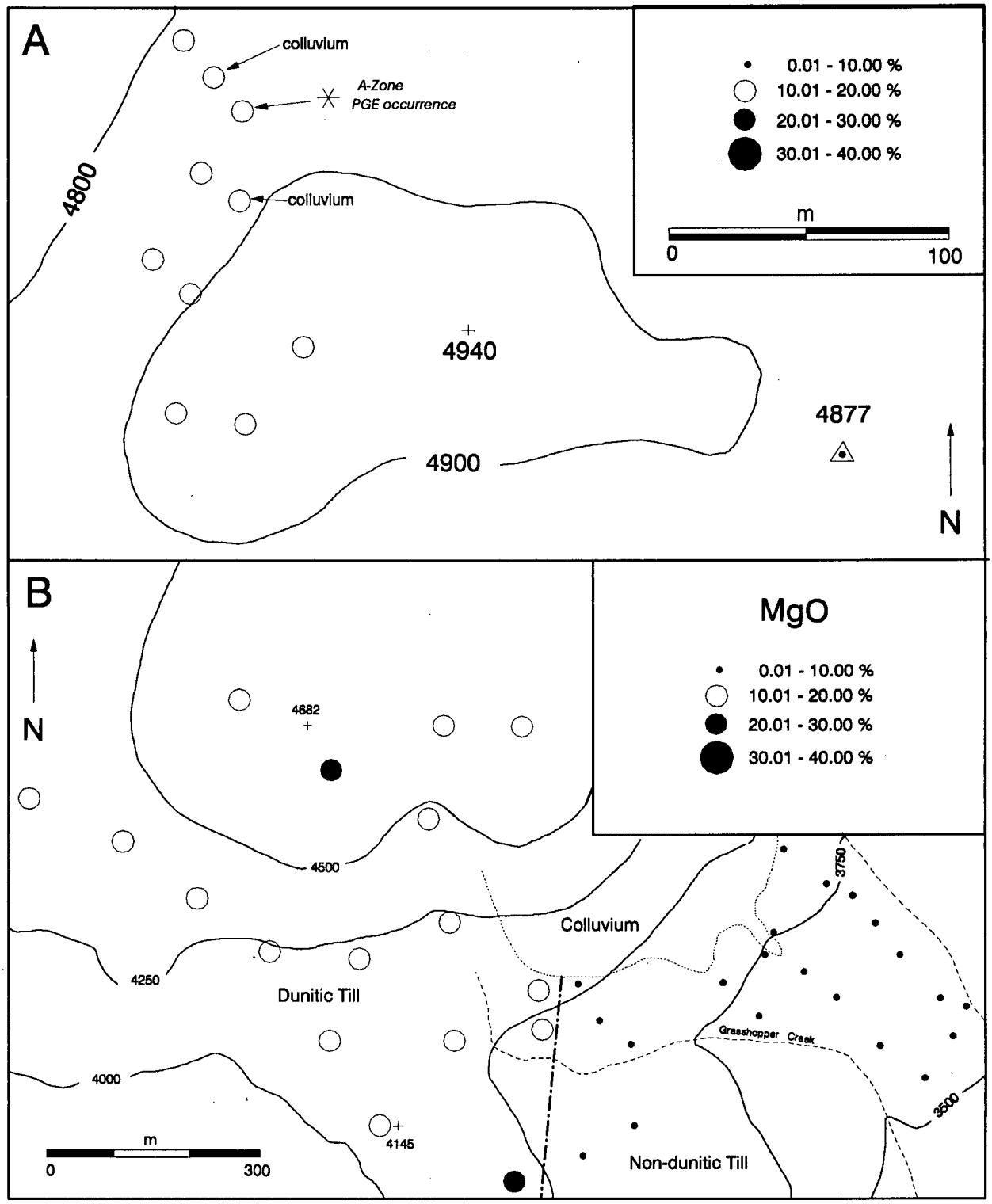

Figure 4-1. MgO content (%) of overview -70 mesh C horizon soils in A. dunitic till, rubble and colluvium adjacent to PGE mineralization in the secondary study area; and B. in dunitic and non-dunitic till in the main study area; Grasshopper Mountain, B.C. Dashed line at lower centre represents the boundary between dunitic and non-dunitic tills (basemap adapted from Bohme, 1987).

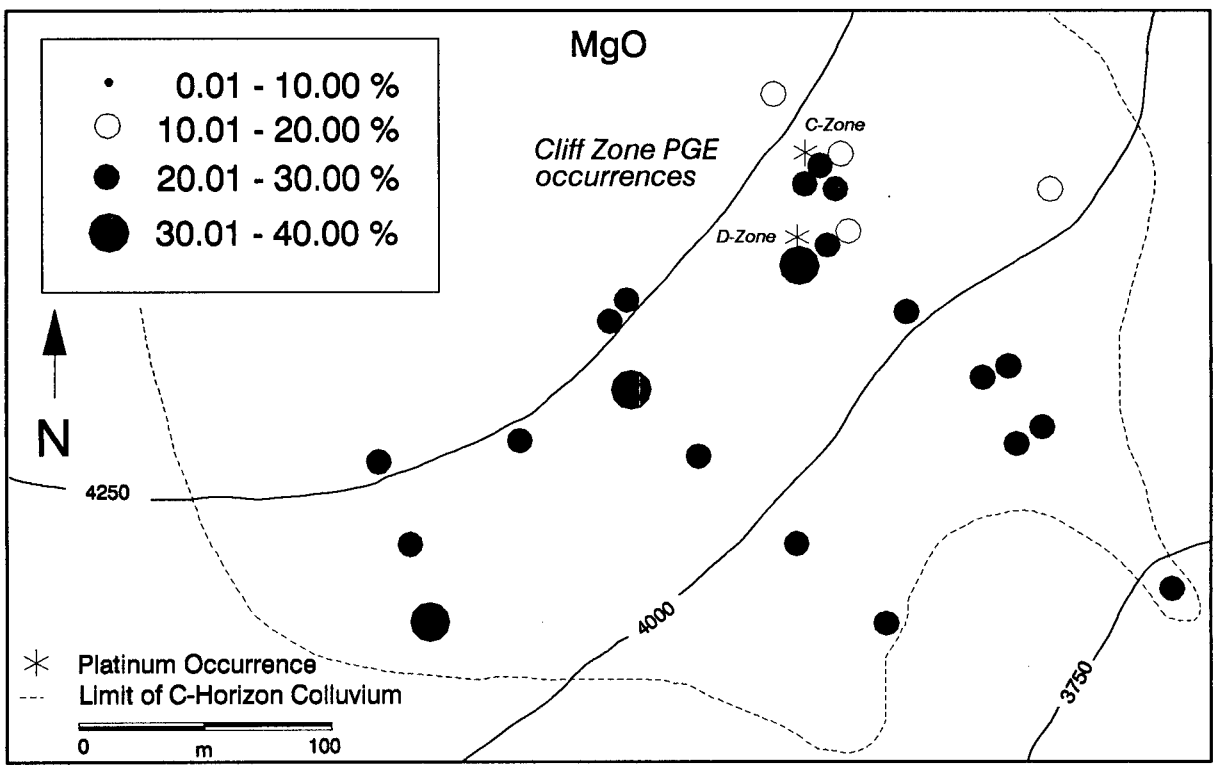

Figure 4-2. Distribution of MgO in C horizon colluvium, main study area (n=25), Grasshopper Mountain, B.C. (basemap adapted from Bohme, 1987).

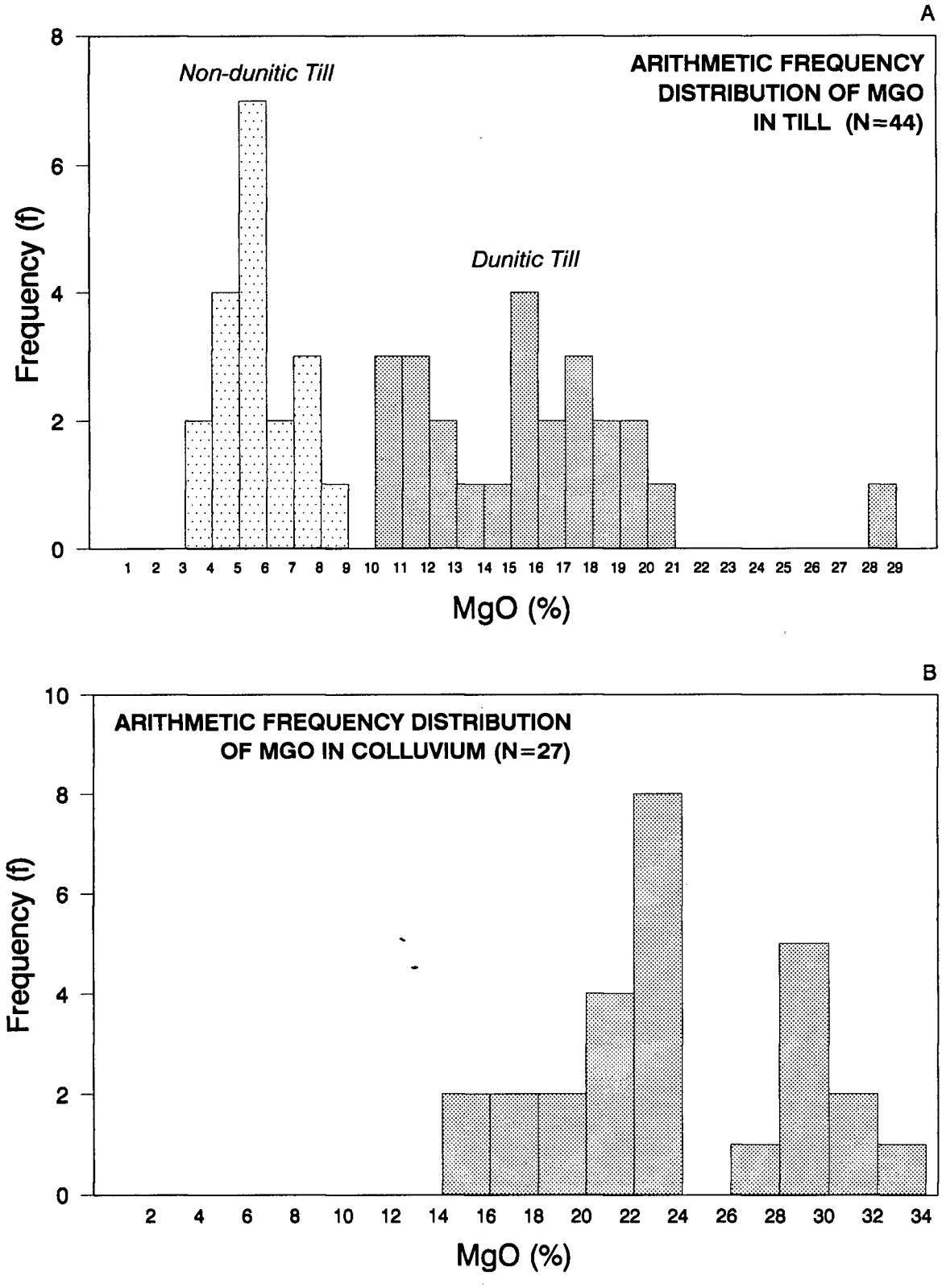

Figure 4-3. Arithmetic frequency distributions of MgO content (%) of overview C horizon soils in A. Till and B. Colluvium.

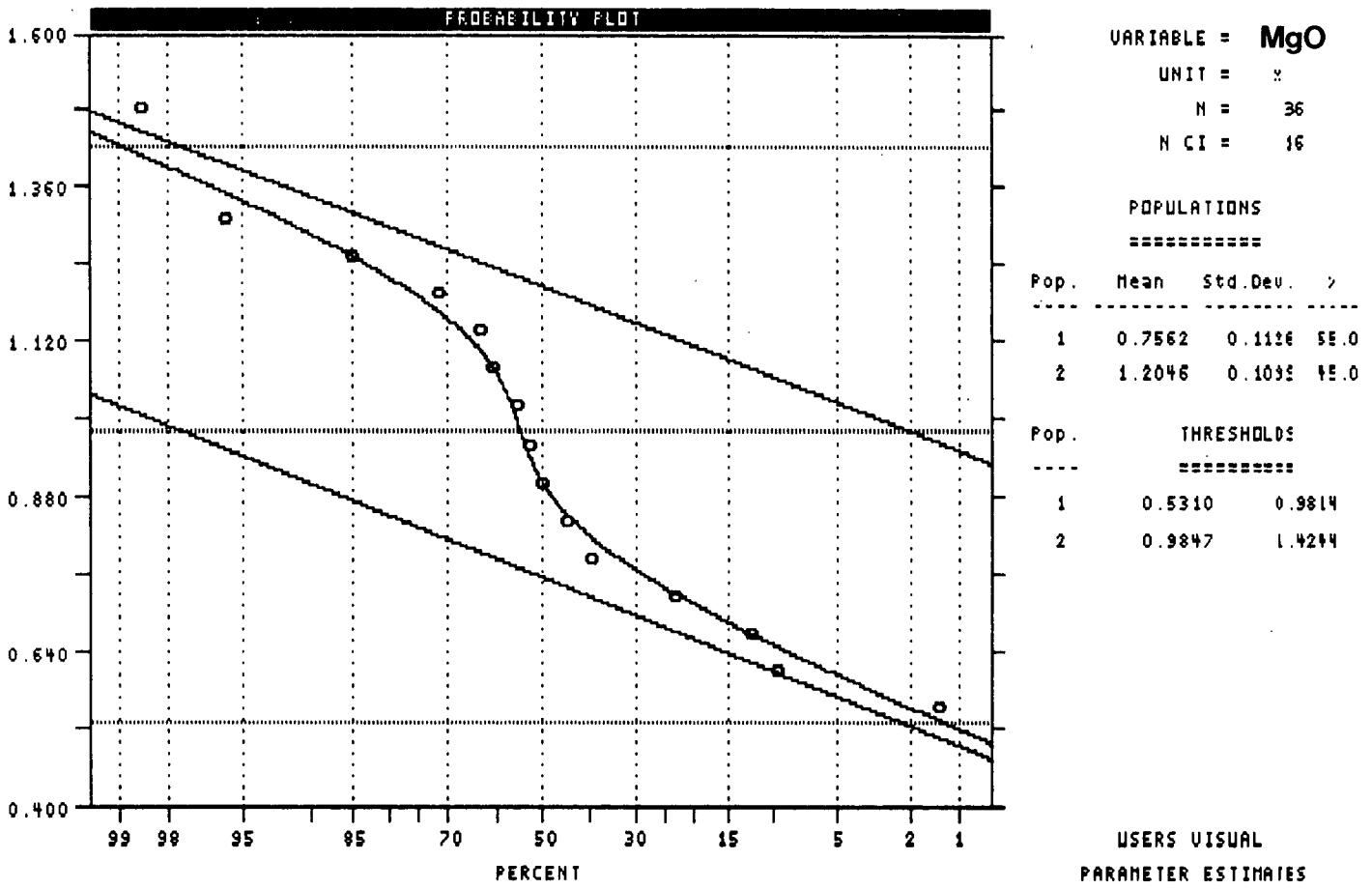

Figure 4-4. Log probability plot of MgO in till, main study area.

		MgO (%)	Cr2O3 (%)	Fe2O3 (%)	SiO2 (%)	Al2O3 (%)	CaO (%)	Na2O (%)	K2O (%)	TiO2 (%)	P2O5 (%)	MnO (%)	Ba (ppm)	LOI (%)
CLAY	x	5.01	0.04	9.50	53.14	16.00	4.02	2.54	1.39	1.00	0.20	0.19	587	6.9
Main Study Area	M	**5.01**	**0.04**	**9.50**	**53.14**	**16.00**	**4.02**	**2.54**	**1.39**	**1.00**	**0.20**	**0.19**	**587**	**6.9**
(n=2)	Min	4.22	0.04	9.11	51.87	15.41	3.75	2.52	1.33	0.98	0.16	0.12	555	6.5
	Max	5.80	0.04	9.89	54.41	16.58	4.29	2.56	1.45	1.02	0.24	0.26	619	7.3
NON-DUNITIC TILL	x	5.66	0.07	9.86	54.00	14.62	4.73	2.65	1.34	0.95	0.13	0.16	474	5.7
Main Study Area	M	**5.44**	**0.06**	**9.87**	**53.74**	**14.53**	**4.79**	**2.60**	**1.34**	**0.95**	**0.13**	**0.15**	**473**	**5.6**
(n=19)	Min	3.86	0.03	8.38	51.40	12.84	3.13	2.34	1.09	0.87	0.06	0.12	376	4.1
	Max	8.23	0.16	11.75	56.95	15.83	5.51	3.20	1.64	1.05	0.21	0.22	554	8.0
DUNITIC TILL	x	16.51	0.20	10.87	46.67	9.07	3.71	1.27	0.83	0.63	0.12	0.18	248	9.9
Main Study Area	M	**16.25**	**0.19**	**10.82**	**46.52**	**8.89**	**3.61**	**1.13**	**0.83**	**0.60**	**0.11**	**0.18**	**242**	**9.9**
(n=17)	Min	10.45	0.12	8.82	44.23	6.90	1.88	0.85	0.57	0.41	0.08	0.13	195	3.3
	Max	28.73	0.29	13.12	50.64	12.44	5.58	2.08	1.07	0.90	0.19	0.22	352	16.4
DUNITIC TILL	x	13.84	0.28	11.78	48.15	10.15	3.28	1.72	0.66	0.64	0.08	0.18	270	9.3
Secondary Study	M	**13.21**	**0.26**	**11.09**	**50.00**	**10.27**	**3.46**	**1.83**	**0.73**	**0.69**	**0.08**	**0.15**	**264.5**	**8.5**
Area (n=8)	Min	10.64	0.12	9.53	42.96	7.86	1.24	1.06	0.35	0.37	0.06	0.12	182	7.2
	Max	19.06	0.51	14.96	51.01	12.08	4.48	2.29	0.79	0.79	0.15	0.29	334	14.4
COLLUVIUM	x	24.16	0.33	11.89	40.67	5.51	1.73	0.83	0.30	0.35	0.12	0.27	125	13.8
Main Study Area	M	**23.29**	**0.32**	**12.10**	**40.65**	**5.57**	**1.90**	**0.85**	**0.22**	**0.37**	**0.11**	**0.25**	**112**	**12.7**
(n=25)	Min	14.29	0.20	9.37	34.60	1.21	0.35	0.08	0.05	0.08	0.07	0.15	38	9.4
	Max	32.78	0.50	13.72	46.38	9.73	3.29	1.44	0.82	0.62	0.22	0.57	226	22.8

x=mean
M=median
Min=minimum value
Max=maximum value

Table 4-3. Mean, median and range of major elements, subdivided by parent material grouping, in the -70 mesh fraction of C horizon soils.

and colluvium is shown in Figures 4-1 and 4-2, respectively. Frequency distributions (Figure 4-3) and a probability plot (Figure 4-4) show that two distinct non-overlapping lognormal MgO populations occur in till from the main study area. The S-SW trending boundary between the two is shown in Figure 4-1. The first population (range: 10.45-28.73% MgO) occurs in the western half of the area, has a mean MgO content of 16.51% (9.96% Mg) and is associated with generally higher values of Pt and Cr_2O_3. The second (range: 3.86-8.23% MgO) occurs in the eastern half of the area, has a mean MgO content of 5.66% (3.41% Mg) and is associated with lower Pt and Cr_2O_3 values. A t-test shows mean MgO contents of the two tills to be significantly different ($p = .05$). These are considered to be dunitic derived and nondunitic tills, respectively. Dunitic colluvium (range: 14.29-32.78% MgO) possesses an even greater mean MgO content of 24.16% (14.57% Mg). MgO content of main study area clay is very similar to that of non-dunitic till.

b) Overall Distribution of Platinum

Distribution of Pt in C horizon soils on Grasshopper Mountain is shown in Figure 4-5. Contour intervals for Pt were determined with log probability plots and histograms to separate individual Pt populations for soils developed on till (n=44). Lower and upper populations correspond in a general way to soils developed on non-dunitic and dunitic

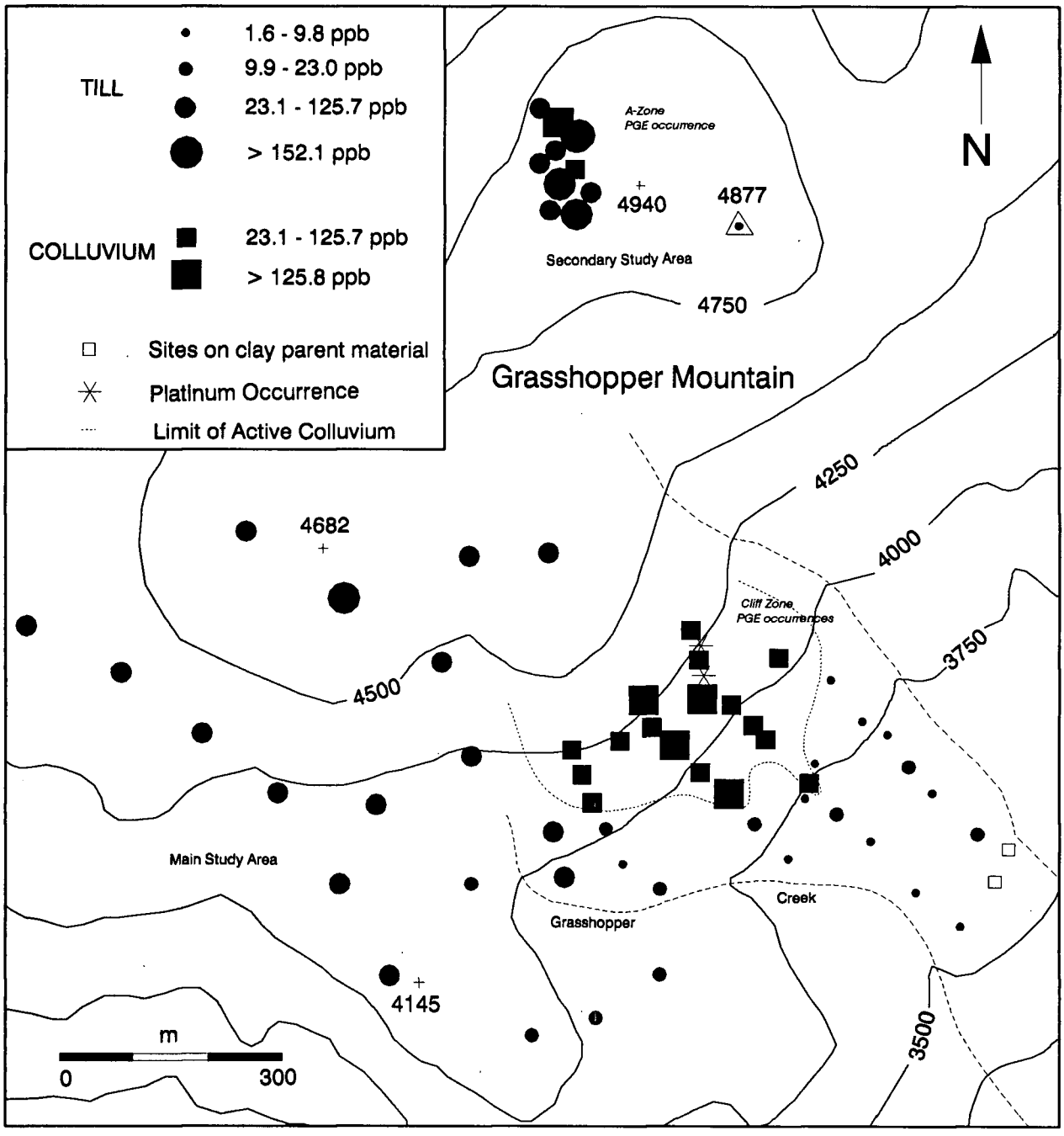

Figure 4-5. Pt content (ppb) of overiew -70 mesh C horizon soils in till (n=44) and colluvium (n=27) above the dunite core of the Tulameen ultramafic complex, Grasshopper Mountain, B.C. (basemap adapted from Bohme, 1987).

tills, reflected by the increase in soil Pt content from east to west across the main study area, and to a concentration of eight till/rubble (mean: 158.1 ppb Pt) and two colluvial Pt values clustered around known PGE mineralization at the secondary study area containing 0.024-0.039 oz/ton Pt (Bohme, 1988). Pt values in excess of 200 ppb occur in three till/rubble (maximum: 455 ppb Pt) and one stabilized colluvium site in this area (Figure 2-14B).

Pt content of colluvium (n=27) is approximately lognormally distributed, and contour interval values of Figure 4-5 were made to correspond to till intervals for ease of comparison. The greatest Pt concentration of all C horizon soils (855 ppb) occurred in active colluvium (soil site 16) beneath one of the Cliff Zone PGE occurrences.

c) Parent Material Groupings

i) Basic Statistics for Pt and Other Elements

Mean, median and range of concentrations for Pt and other selected elements in each categorical grouping are shown in Table 4-4. Original analytical data is in Appendix 5. Mean Pt content of overall colluvium (125.1 ppb) is considerably greater than that of overall till (53.3 ppb). However, further subdivision of till Pt data on the basis of

major element geochemistry provides a more meaningful grouping. When classified by MgO content and parent material, the mean Pt content of main study area colluvium (120 ppb) is more than double that of main study area dunitic till (52.8 ppb), while non-dunitic till exhibits the lowest mean Pt content (9.5 ppb) (Table 4-4). Median Pt values, unaffected by high outliers, give a better approximation of background Pt levels in surficial materials: 8 ppb in non-dunitic till, 36 ppb in dunitic till, and 88 ppb in colluvium.

Distribution of Cr_2O_3 is generally similar to that of Pt. Colluvium has the greatest mean Cr_2O_3 content (0.33%; 2257 ppm Cr), whereas soils on dunitic till and nondunitic till within the main study area have mean Cr_2O_3 contents of 0.20% (1368 ppm Cr) and 0.07% (479 ppm Cr), respectively. Locally-derived dunitic till in the secondary study area has a mean Cr_2O_3 content of 0.28% (1915 ppb Cr). The maximum Cr_2O_3 value of 0.51% (3,488 ppm Cr) occurred in this area.

The Pd content of the soils is very low in relation to Pt. Median values are 3 ppb in non-dunitic till, 6.5 ppb in dunitic till, and 2 ppb in dunitic colluvium.

The Au content of main study area colluvium (mean: 21.0 ppb) is 3-4x greater than in till. The secondary study area contains the least Au (5.1 ppb), while dunitic and non-

		Pt (ppb)	Pd (ppb)	Rh (ppb)	Au (ppb)	As (ppm)	Sb (ppm)
CLAY	x	5.5	2.5	2	5	11.9	0.9
Main Study Area	**M**	**5.5**	**2.5**	**2**	**5**	**11.9**	**0.9**
(n=2)	Min	4	2	2	5	9.4	0.5
	Max	7	3	2	5	14.3	1.2
NON-DUNITIC TILL	x	9.5	4.1	2	8.2	15.5	1.0
Main Study Area	**M**	**8**	**3**	**2**	**7**	**14.7**	**0.9**
(n=19)	Min	2	2	2	2	8.1	0.5
	Max	20	15	2	34	23.2	1.8
DUNITIC TILL	x	52.8	8.9	2.1	8.4	15.8	0.3
Main Study Area	**M**	**36**	**6.5**	**2**	**8**	**13.1**	**0.2**
(n=17)	Min	16	2	2	2	5.3	0.1
	Max	311	48	3	21	52.5	0.8
DUNITIC TILL	x	158.1	7.0	2.5	5.1	18.5	0.4
Secondary Study	**M**	**89**	**2.5**	**2**	**4**	**15.6**	**0.4**
Area (n=8)	Min	42	2	2	1	7.4	0.1
	Max	455	36	6	10	30.5	0.8
COLLUVIUM	x	120.0	2.6	2	21.0	21.3	0.6
Main Study Area	**M**	**88**	**2**	**2**	**18.5**	**15.8**	**0.5**
(n=25)	Min	24	2	2	2	7.5	0.2
	Max	885	5	3	56	56.3	1.2

x=mean
M=median
Min=minimum value
Max=maximum value

Table 4-4. Mean, median and range of PGE and other selected constituents of the -70 mesh fraction of C horizon soils in various parent materials, Grasshopper Mountain, B.C.

dunitic till have mean Au contents of 8.4 ppb and 8.2 ppb respectively. Rather high As values, ranging from 5.3 - 52.5 ppm in till and from 7.5 - 56.3 ppm in colluvium, occur throughout the study area, with 90% of the soils containing > 10 ppm As. Median As contents are relatively similar in all parent materials (Table 4-4).

ii) Correlation Analysis

Correlation matrices for the two genetic categorical groups, till and colluvium, are shown in Figure 4-6. The data were log-transformed prior to calculation because of the lognormal nature of the Pt distribution. Those linear correlation coefficients exceeding the critical value above which they are significantly different from zero at the 95% confidence level are listed, in order of decreasing strength, in Tables 4-5 and 4-6. Induced correlations between both major element oxides and Loss On Ignition (LOI) are omitted, as these sum to 100% and thus form proportions of a closed data set (Davis, 1986).

Forty-one significant correlations occur in the till group, whereas only sixteen occur in the colluvium group. The most important relation among the till correlations is the partioning of Pt with those elements forming mafic, as opposed to felsic, minerals. Pt exhibits positive

A. Till

	AU	PT	PD	RH	AS	SB	BI	SIO2	AL2O3	FE2O3	MGO	CAO	NA2O	K2O	TIO2	P2O5	MNO	CR2O3	BA	LOI
AU	1.00000																			
PT	-.06938	1.00000																		
PD	.41112	.26826	1.00000																	
RH	.18898	.24411	.05493	1.00000																
AS	.10194	-.00502	-.02390	.18252	1.00000															
SB	.11583	-.58420	-.28875	-.00023	.08572	1.00000														
BI	.01535	-.26191	-.15338	-.20680	-.03682	.11547	1.00000													
SIO2	-.00253	-.74773	-.32105	-.04905	-.04091	.53376	.23610	1.00000												
AL2O3	-.00202	-.70938	-.23219	-.14232	.06397	.56426	.10924	.87784	1.00000											
FE2O3	-.03699	.59846	.25734	.05461	.07701	-.37288	-.31865	-.48531	-.51479	1.00000										
MGO	-.02611	.74898	.27328	.15690	-.08263	-.61432	-.14578	-.91110	-.96240	.46643	1.00000									
CAO	.25976	-.55139	.11320	.00594	.07887	.32185	-.06302	.65088	.55428	-.11628	-.58810	1.00000								
NA2O	-.11116	-.66354	-.28799	-.06729	-.02445	.54661	.12254	.90776	.95621	-.44248	-.92687	.53253	1.00000							
K2O	.10718	-.81899	-.05814	-.19954	-.09326	.55980	.28820	.77222	.85055	-.64277	-.83336	.53402	.77496	1.00000						
TIO2	.11045	-.71046	-.07870	-.09530	.04130	.50482	.02652	.88419	.89298	-.28852	-.90714	.81354	.86501	.79571	1.00000					
P2O5	.29571	-.37210	.10843	-.20836	.06301	.27257	.13588	.03990	.21684	-.48978	-.21193	.03282	.06704	.42268	.11177	1.00000				
MNO	.08916	.40512	.36663	-.04449	.04032	-.11346	-.12327	-.59974	-.40684	.32653	.41174	-.38998	-.45226	-.30180	-.44217	.33110	1.00000			
CR2O3	-.23720	.83972	.13273	.10911	-.09824	-.57893	-.27839	-.79908	-.83457	.60605	.87566	-.56393	-.75432	-.85589	-.80603	-.44174	.28999	1.00000		
BA	-.02210	-.74263	-.29401	-.16941	-.05885	.62121	.17359	.87233	.96229	-.54219	-.94200	.45361	.93958	.86396	.83169	.22611	-.40354	-.81275	1.00000	
LOI	.06162	.62027	.30021	.01208	.27716	-.36613	-.23669	-.79260	-.55127	.20696	.61747	-.52275	-.66629	-.53361	-.64335	.08875	.44175	.55669	-.62690	1.00000

CRITICAL VALUE (1-TAIL, .05) = + Or - .25143
CRITICAL VALUE (2-tail, .05) = +/- .29694

N = 44

B. Colluvium

	AU	PT	PD	RH	AS	SB	BI	SIO2	AL2O3	FE2O3	MGO	CAO	NA2O	K2O	TIO2	P2O5	MNO	CR2O3	BA	LOI
AU	1.00000																			
PT	-.16428	1.00000																		
PD	-.12471	.02622	1.00000																	
RH	-.30014	.64792	-.15617	1.00000																
AS	.35451	.32746	-.19666	.30149	1.00000															
SB	.11945	.10484	.22438	-.02347	.47652	1.00000														
BI	.21649	.07873	.19984	.07935	.37718	.34467	1.00000													
SIO2	-.08093	-.29453	-.02671	-.16256	-.28751	-.03958	-.38109	1.00000												
AL2O3	-.21247	-.26623	.16495	-.10824	-.34747	-.02670	-.13881	.55803	1.00000											
FE2O3	-.21836	.34678	.01068	.10278	.16307	.18189	.16665	-.07994	.23019	1.00000										
MGO	.37223	.22693	-.25769	.18312	.24425	-.10592	-.00168	-.49770	-.86549	-.28977	1.00000									
CAO	-.10348	-.08915	.25483	-.11180	-.19792	-.00548	-.11108	.28444	.79665	.43016	-.67613	1.00000								
NA2O	-.24885	-.21632	.14998	-.06705	-.42616	-.08317	-.21618	.51458	.97723	.19238	-.79310	.79936	1.00000							
K2O	-.17707	-.28751	.21379	-.29113	-.09048	.05743	-.11477	.37640	.72809	.13173	-.74760	.58645	.71150	1.00000						
TIO2	-.17448	-.25160	.13552	-.11904	-.33725	-.02029	-.14008	.53302	.98580	.31302	-.85415	.84528	.96402	.70662	1.00000					
P2O5	.05633	.09879	.14094	.05984	.29180	.13281	.49063	-.62713	-.01064	.15393	-.11971	.15646	-.04477	.06880	.01880	1.00000				
MNO	.01449	.27552	-.06744	.09821	.50183	.17445	.45141	-.66624	-.16823	.41352	-.00210	-.01846	-.20963	.05042	-.14649	.79980	0000			
CR2O3	-.16175	.57683	.14640	.21907	-.10344	-.15229	-.10619	-.50541	-.52433	.05144	.52028	-.33853	-.42012	-.49493	-.52667	.06798	9950	1.00000		
BA	-.39982	-.21105	.23063	-.07831	-.19081	.08158	-.14141	.26706	.76249	.15397	-.82128	.60702	.74343	.83723	.74813	.16843	8978	-.45697	1.00000	
LOI	-.12015	.23464	.16486	.06062	.15721	-.02648	.35994	-.88532	-.35218	.01179	.16133	-.16945	-.32813	-.12040	-.35125	.75157	0040	.42814	.02022	1.00000

CRITICAL VALUE (1-TAIL, .05) = + Or - .32375
CRITICAL VALUE (2-tail, .05) = +/- .38009

N = 27

Figure 4-6. Log transformed correlation matrices for A. till and B. colluvium.

Pt	+	Cr_2O_3, MgO, LOI, Fe_2O_3, MnO
	-	K_2O, SiO_2, Ba, TiO_2, Al_2O_3, Na_2O, Sb, CaO, P_2O_5
Pd	+	Au, MnO, LOI
	-	SiO_2
Sb	+	Ba, Al_2O_3, K_2O, Na_2O, SiO_2, TiO_2, CaO
	-	MgO, Pt, Cr_2O_3, Fe_2O_3, LOI
Bi	-	Fe_2O_3
Ba	+	Al_2O_3, Na_2O, SiO_2, K_2O, TiO_2, Sb, CaO
	-	MgO, Cr_2O_3, Pt, LOI, Fe_2O_3, MnO
LOI	+	Pt, Pd
	-	Ba, Sb

Table 4-5. Significant correlations ($r > .29694$) in till (n=44). Listed from strongest to weakest.

Pt	+	Rh, Cr_2O_3
As	+	MnO, Sb
	-	Na_2O
Bi	+	P_2O_5, MnO
	-	SiO_2
Ba	+	K_2O, Al_2O_3, TiO_2, Na_2O, CaO
	-	MgO, Cr_2O_3, Au

Table 4-6. Significant correlations (r > .38009) in colluvium (n=27). Listed from strongest to weakest.

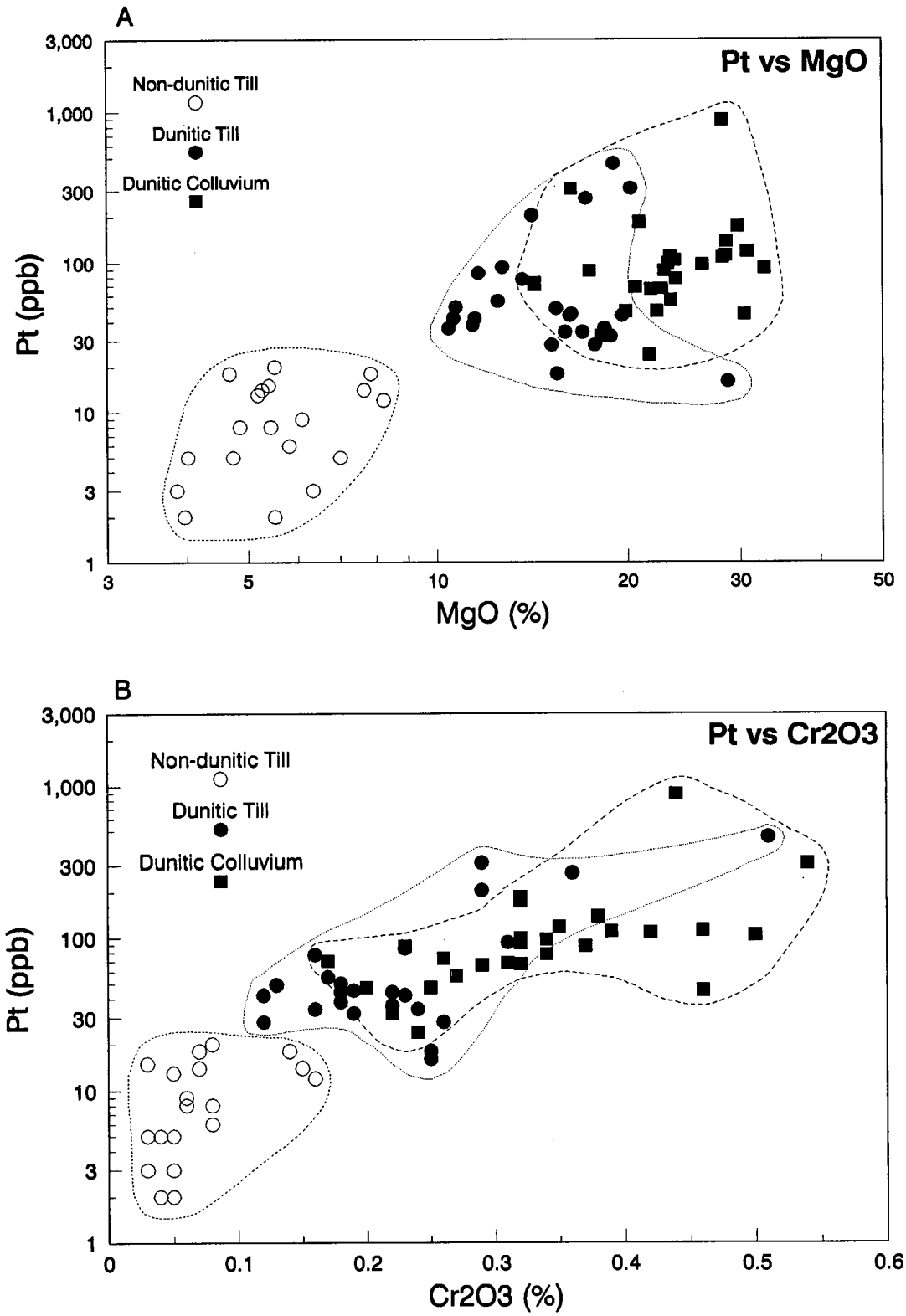

Figure 4-7. Scatterplots of -70 mesh overview Pt concentrations (ppb) with A. MgO and B. Cr2O3 from C horizon soils on various parent materials.

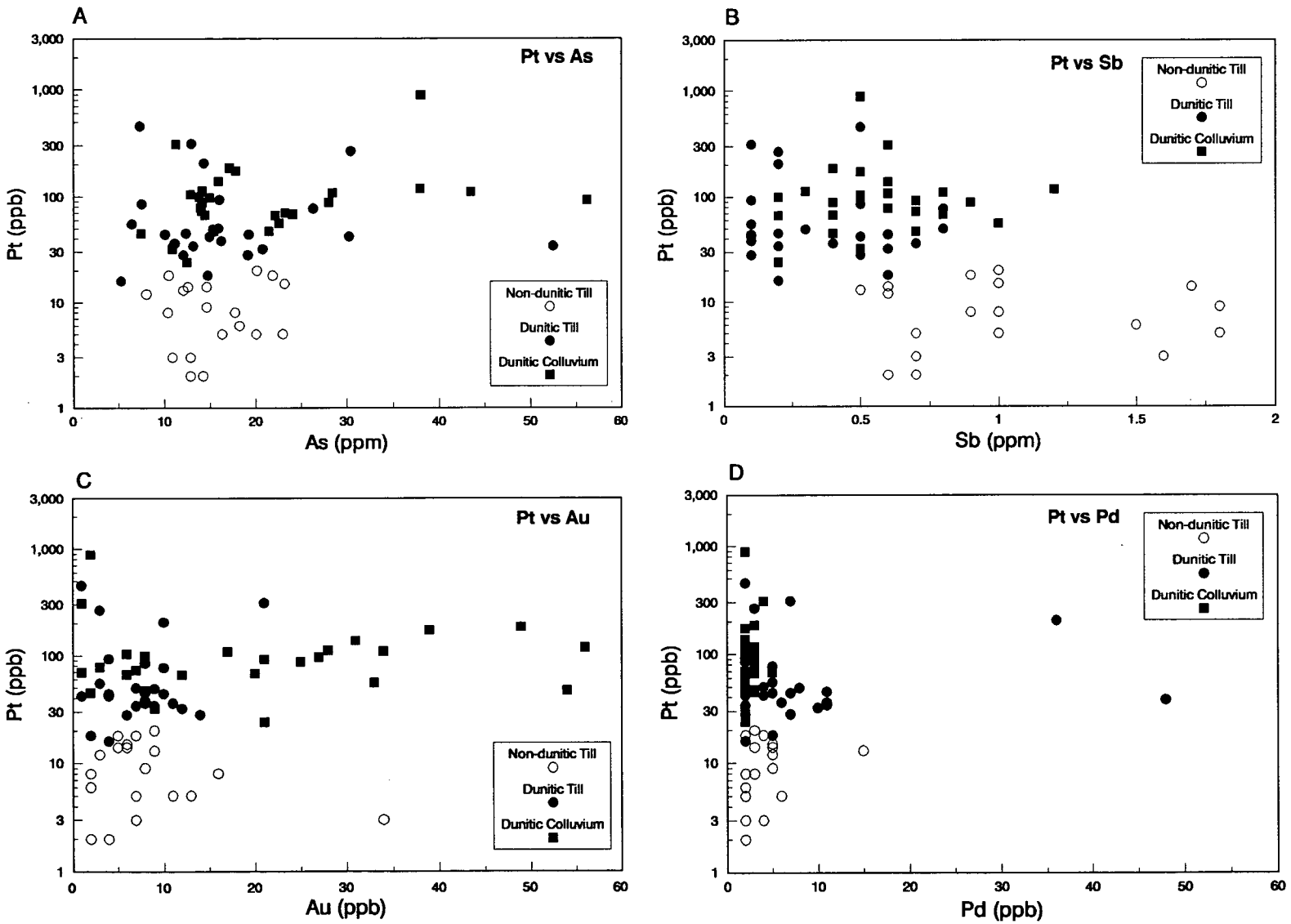

Figure 4-8. Scatterplots of -70 mesh overview soil Pt data (ppb) with selected elements: A. As; B. Sb; C. Au; and D. Pd.

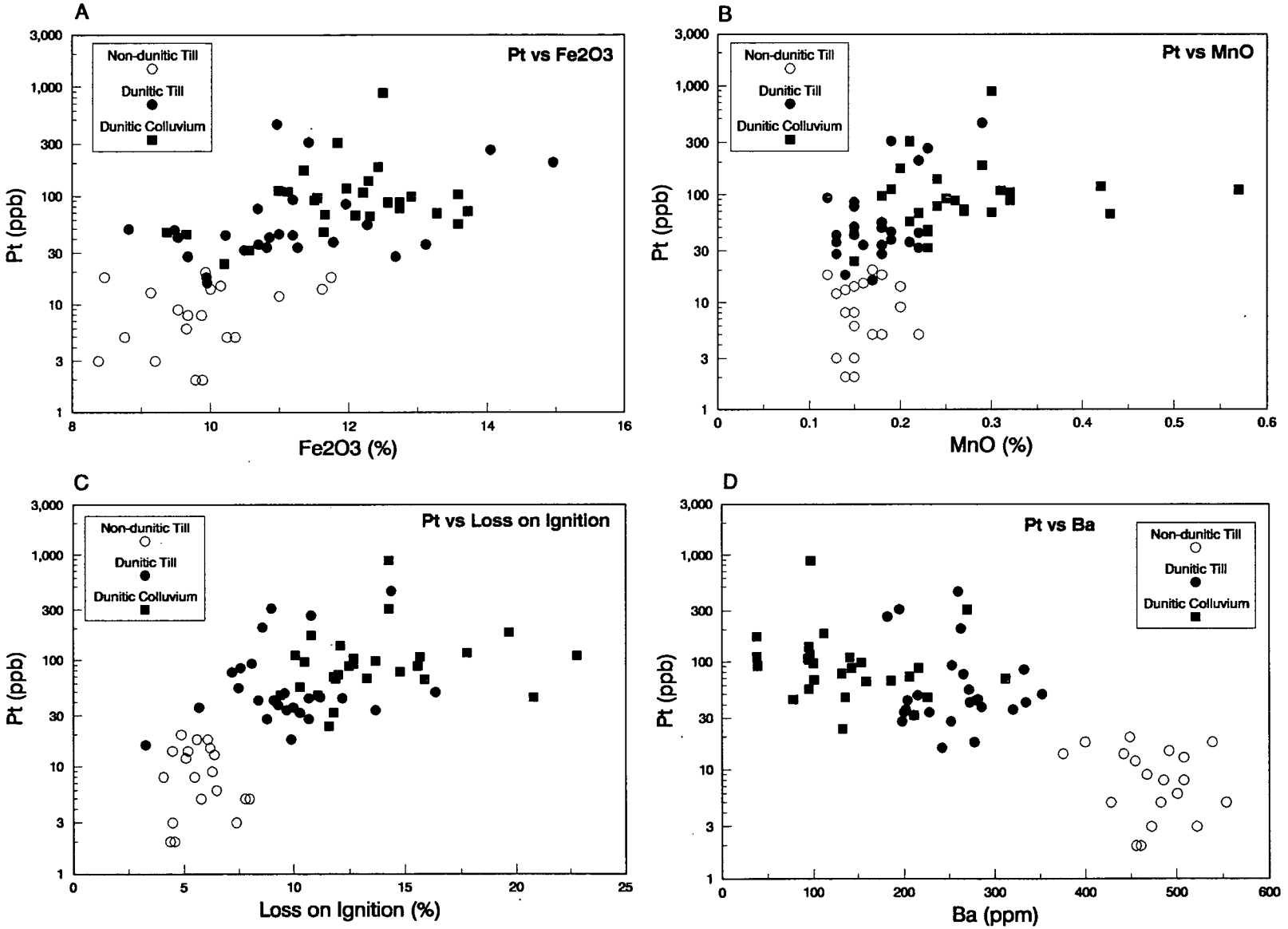

Figure 4-9. Scatterplots of -70 mesh overview soil Pt data (ppb) with selected elements/determinations: A. Fe2O3; B. MnO; C. LOI; D. Ba.

correlations with Cr_2O_3, MgO and, to a lesser extent, LOI, Fe_2O_3 and MnO. It exhibits negative correlations with K_2O, SiO_2, Ba, TiO_2, Al_2O_3 and others. In colluvium Pt correlates with Cr_2O_3, but not with MgO. Scatterplots of Pt with MgO and Cr_2O_3 are shown in Figure 4-7 and with other selected elements in Figures 4-8 and 4-9.

iii) Spatial Distribution of Pt and Other Selected Elements on Grasshopper Mountain

Partitioning of Pt, Cr_2O_3 and Pd data into separate populations within non-dunitic till, dunitic till and colluvium categorical groupings was performed with frequency distributions, ranked data, and probability plots. Arithmetic and log frequency distributions for till and colluvium are shown in Figure 4-10. Two separate lognormally-distributed Pt populations occur in non-dunitic till (Figure 4-11), but Pt distributions in both dunitic till and colluvium approximate single lognormal populations. Log frequency distributions of Cr_2O_3 and Pd in both till and colluvium are shown in Figure 4-12. Cr_2O_3, unlike MgO, shows a slight overlap between dunitic and non-dunitic till populations (Figure 4-7). Cr_2O_3 in dunitic till, like Pt, is lognormally distributed, while two separate Cr_2O_3 populations occur in non-dunitic till. Cr_2O_3 in colluvium

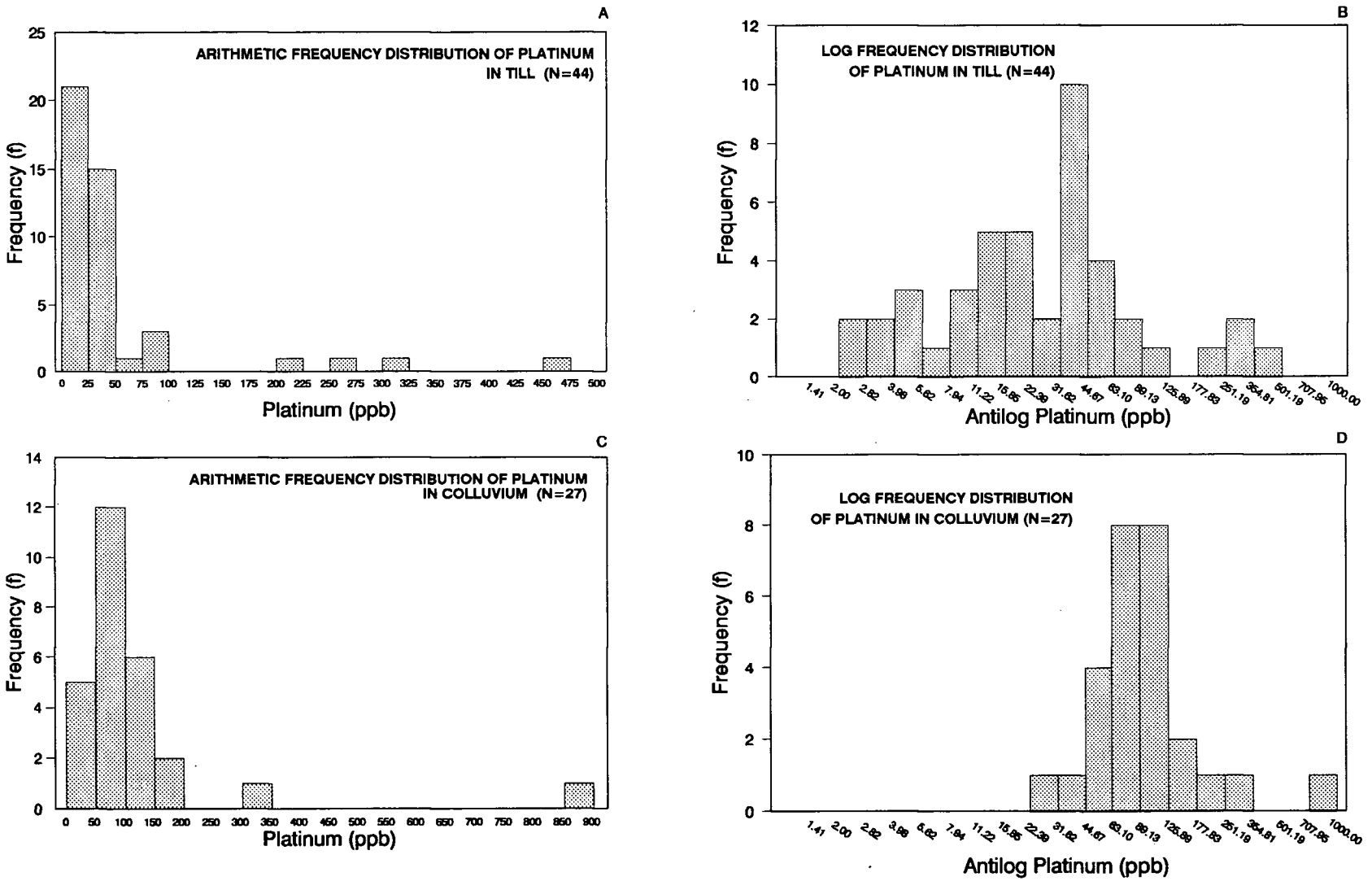

Figure 4-10. Arithmetic and log frequency distributions of Pt content (ppb) of overview C horizon soils in: A. and B. Till; and C. and D. Colluvium.

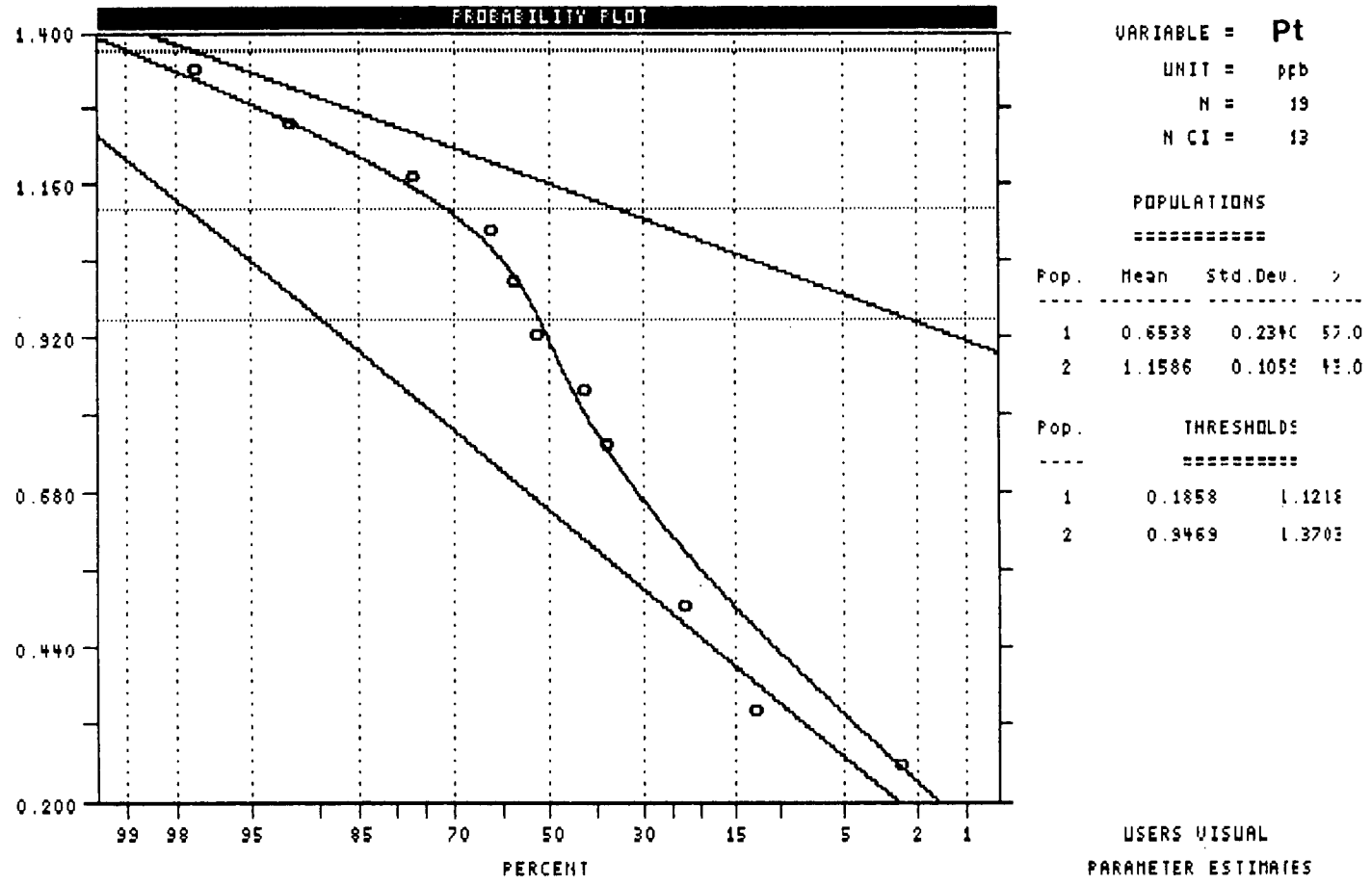

Figure 4-11. Log probability plot of Pt in non-dunitic till, main study area.

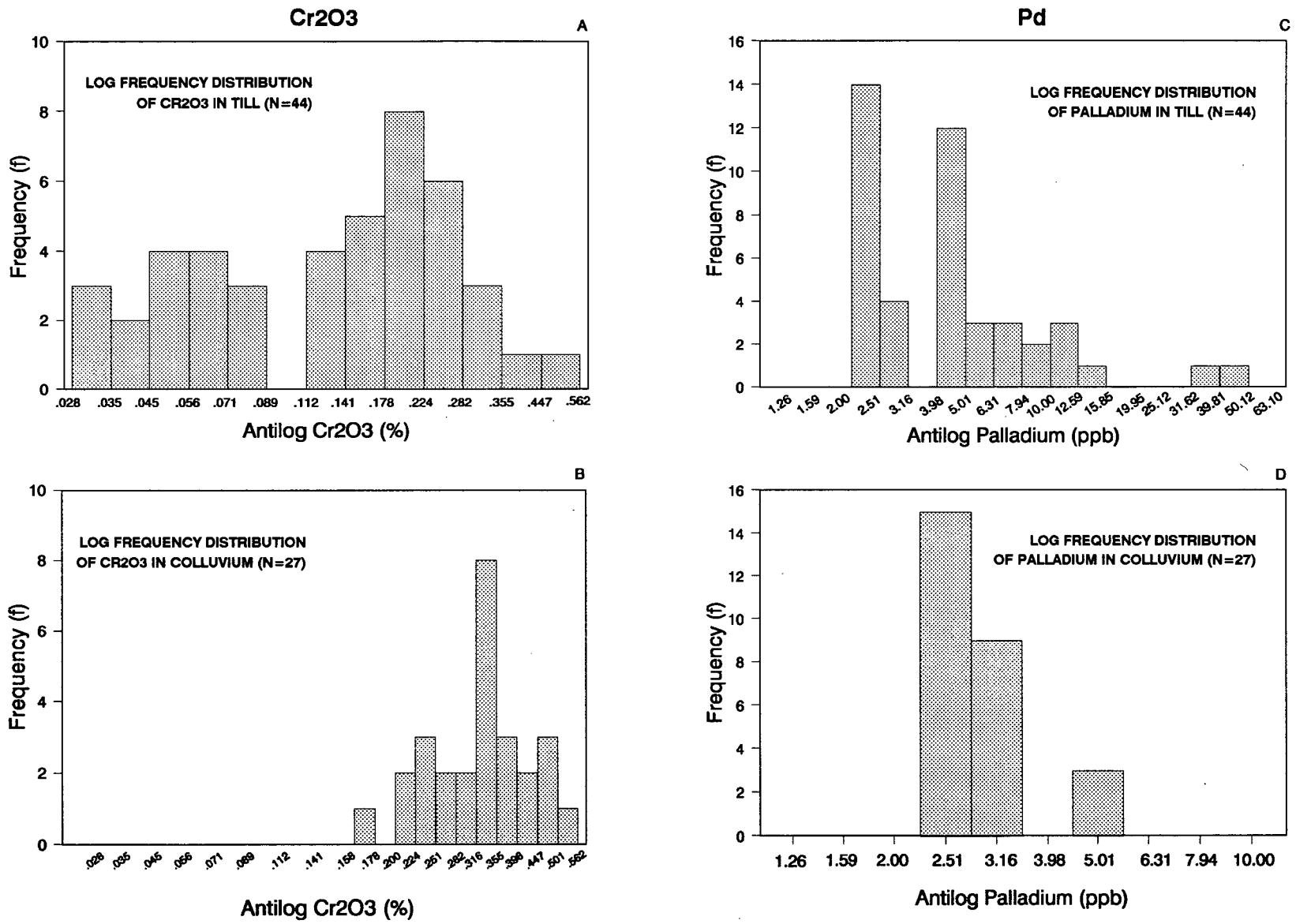

Figure 4-12. Antilog frequency distributions of: A. and B. Cr2O3 content (%) and C. and D. Pd content (ppb) of overview C horizon soils in till and colluvium

is also lognormally distributed (Figure 4-12B).

Only in the case of normal or lognormally distributed populations were upper populations partitioned on the basis of the top 2.5 percentiles (Sinclair, 1976; Rose et al, 1979); sometimes only a single very high value occurs in an otherwise lognormal population. The limited number of samples in the secondary study area (8 till, 2 colluvium), and its biased closely-spaced sampling in relation to the main study area, precluded the use of probability plots to define populations in this area. Threshold values in this area were therefore assigned on the basis of frequency distributions and ranked data, and were selected to facilitate comparisons with till data from the main study area.

Three upper-population Pt single values or zones occur in the main study area (Figures 4-13 and 4-16A), one within each grouping. Three Cr_2O_3 (Figures 4-14 and 4-16B) and Pd (Figures 4-15 ands 4-17) upper-population values or zones also occur in the main study area; the former are generally coincident with those defined for Pt, while the latter are not.

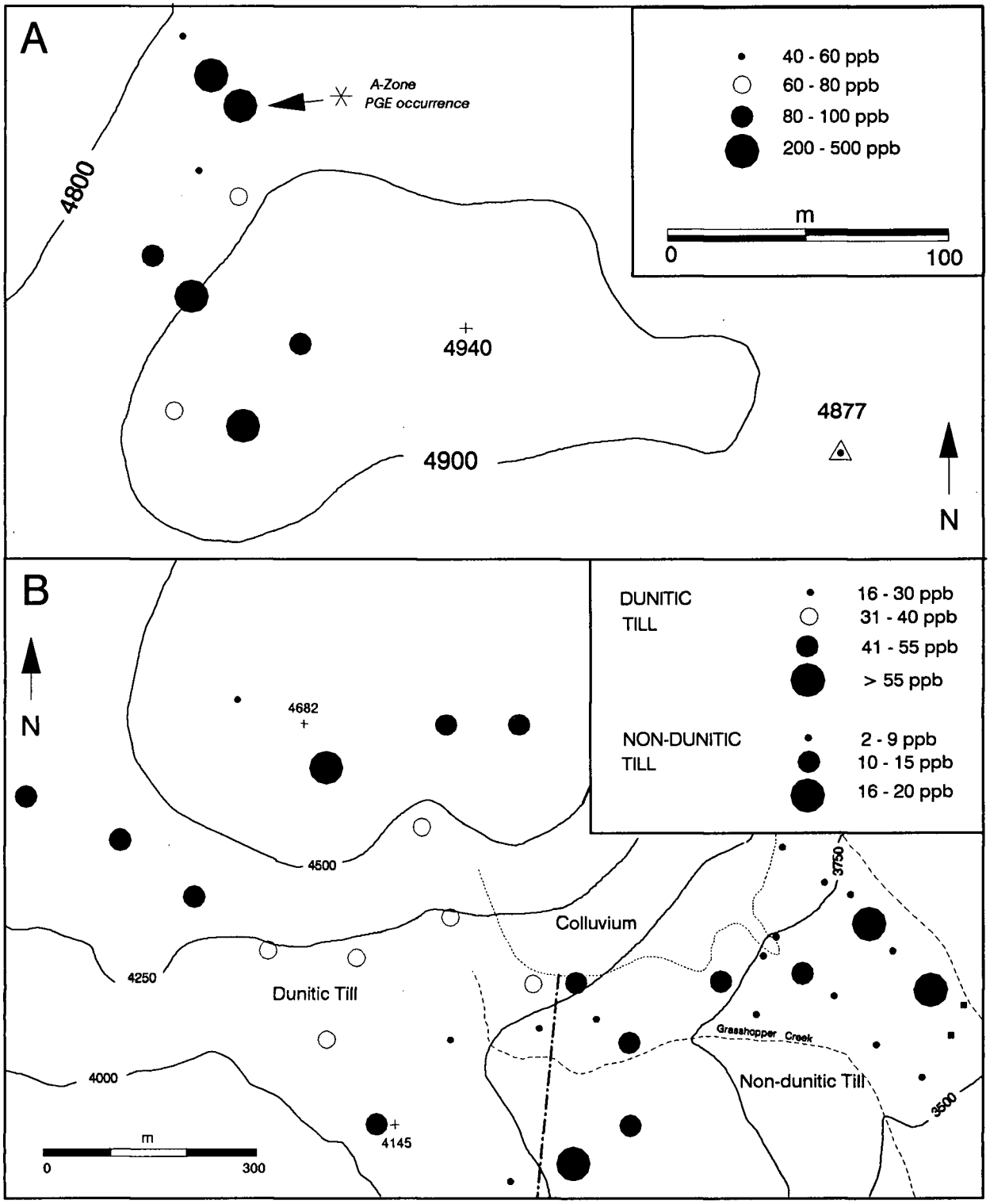

Figure 4-13. Pt content (ppb) of overview -70 mesh C horizon soils in A. dunitic till, rubble and colluvium adjacent to PGE mineralization in the secondary study area; and B. in dunitic and non-dunitic till in the main study area; Grasshopper Mountain, B.C. Dashed line at lower centre represents the boundary between dunitic and non-dunitic tills.

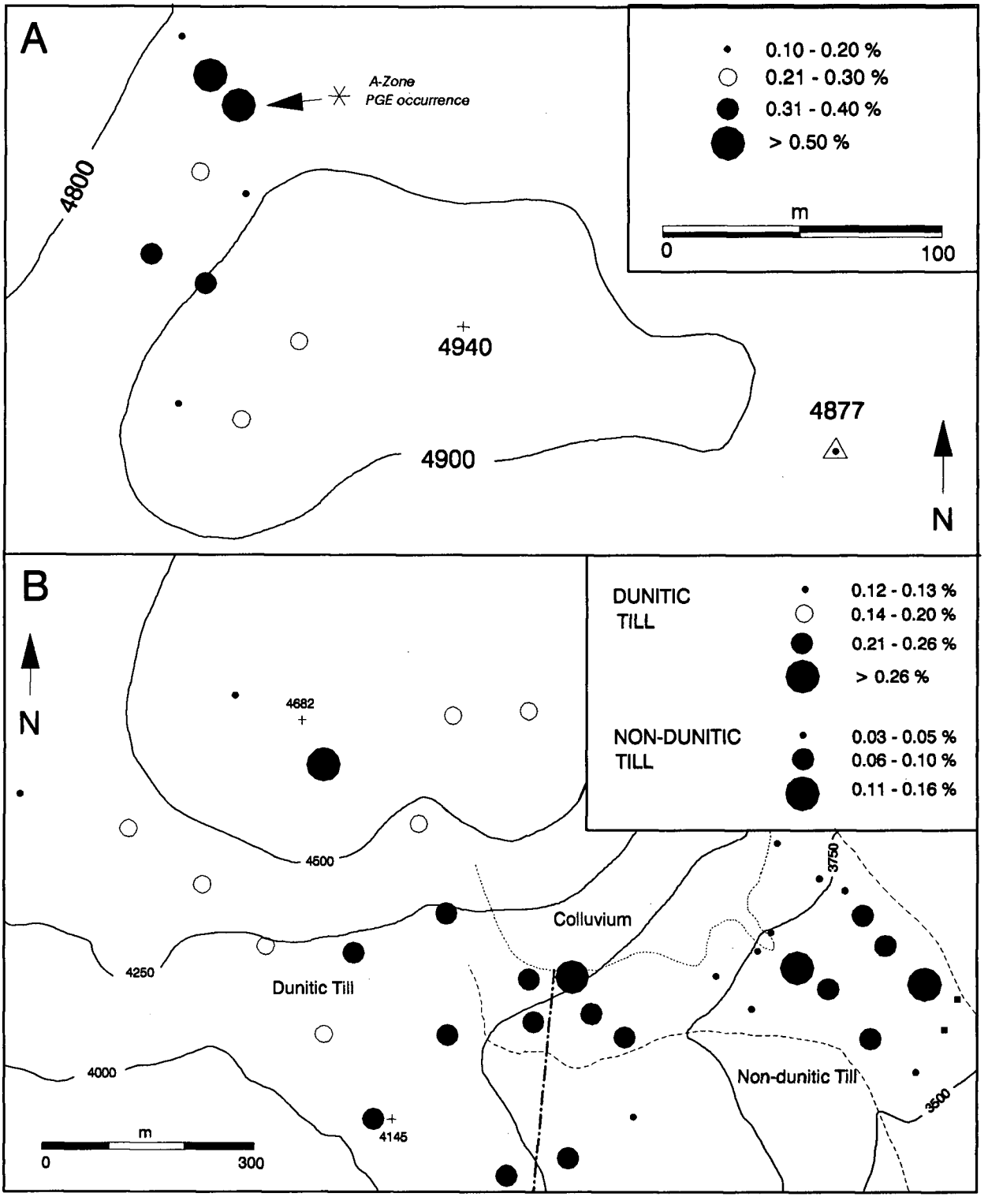

Figure 4-14. Cr2O3 content (%) of overview -70 mesh C horizon soils in: A. dunitic till, rubble and colluvium adjacent to PGE mineralization at the secondary study area; and B. in dunitic and non-dunitic till in the main study area, Grasshopper Mountain, B.C. Dashed line at lower centre represents the boundary between dunitic and non-dunitic tills.

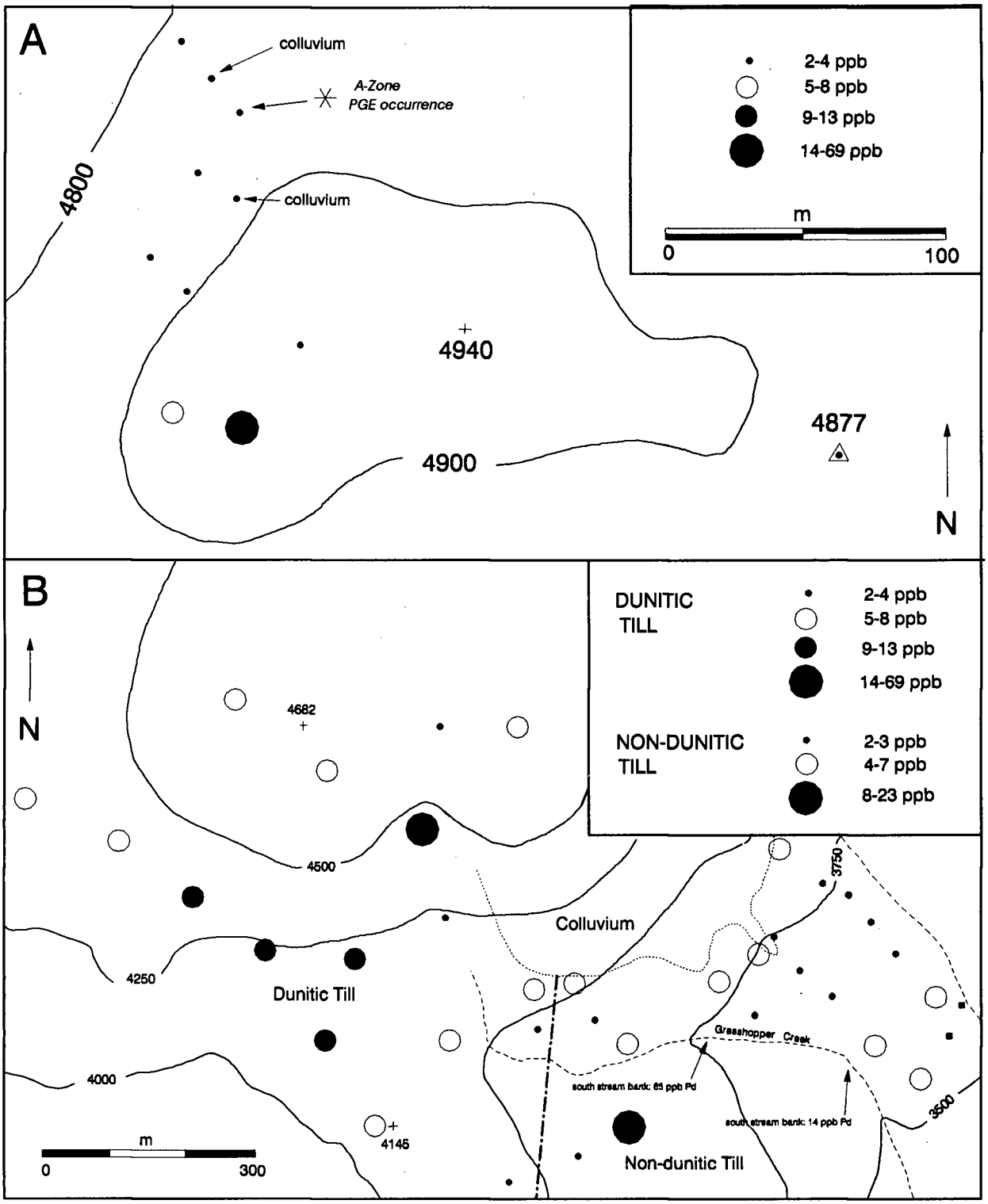

Figure 4-15. Pd content (ppb) of overview -70 mesh C horizon soils in A. dunitic till, rubble and colluvium adjacent to PGE mineralization in the secondary study area; and B. in dunitic and non-dunitic till in the main study area; Grasshopper Mountain, B.C. Dashed line at lower centre represents the boundary between dunitic and non-dunitic tills.

I. Dunitic till

The upper-population Pt site in dunitic till (311 ppb; Figure 4-13) occurs within a W-SW trend of enhanced background Pt values which is generally confined to the upper plateau area. This area has a thin till cover which, though more continuous than in the secondary study area, is thinner and closer to bedrock than that of many downslope sites with lower Pt concentrations. There are differences however, in the spatial distribution of Pt and Cr_2O_3 on a more detailed scale. A zone of higher Cr_2O_3 background values in dunitic till is not coincident with the zone of higher Pt values (Figure 4-14B), but is instead located farther downslope to the southeast. A zone of enhanced dunitic till Pd concentrations (Figure 4-15), comprising several closely-spaced sites containing 10-11 ppb Pd downice from the highest C-horizon Pd value (48 ppb), occurs approximately midway between the enhanced Pt and Cr_2O_3 zones. The upper-population Pd value in this area is one of the few sites where Pt is subordinate to Pd.

Upper-population Cr_2O_3 values in till at the secondary study area (Figure 4-14) seem to be much more locallized than upper-population Pt values (Figure 4-13). This may be related to the more disseminated nature of A-Zone chromite (Bohme, 1987, 1988) and to the occurrence of PGM in Mg-silicates as well as chromite. Upper-population Pd (Figure

4-15) is even more localized; a single value (36 ppb) occurs with a similar Pt value at the secondary study area, but is far removed from the A-Zone PGE occurrence. Three of the four highest till As values occur in the secondary study area.

II. Non-dunitic till

An upper-population Pt zone occurs in the east side of the non-dunitic till, and comprises subtle anomalies which would otherwise be swamped by higher background values farther to the west. Higher Pt values clustering along the till compositional boundary probably indicate gradational mixing with the dunitic till (Figure 4-13), and are not considered anomalous. The same mixing effect is also observed with Cr_2O_3; an upper-population Cr_2O_3 zone on the east side of the non-dunitic till is partially coincident with the corresponding Pt zone. With a mean Cr content of 479 ppm, the non-dunitic till apparently contains at least a minor dunite component.

The third-highest Pd value (15 ppb) occurs in non-dunitic till, just upslope from two stream bank sites containing 65 and 14 ppb Pd. Two bands, including one in the seepage zone area, of intermediate-level Pd concentrations (open circles on Figure 4-15) enclose an area of background-level Pd concentrations in this area. The

highest non-colluvial Au value (34 ppb) also occurs within a seepage zone gleysolic soil at one of these sites (soil site 6). Significantly, the seepage zone area also exhibits anomalous Sb values in the range 1.2 - 1.8 ppm, 3-6x higher than the mean Sb contents of other areas upslope (Table 4-4).

III. Colluvium

A single upper-population colluvial sample (885 ppb) pinpoints the Cliff Zone PGE occurrence (Figure 4-16A), although the remainder of the colluvial samples do not exceed 185 ppb Pt. It is coincident with an upper-population Cr_2O_3 value below the Cliff Zone (Figure 4-16B); other high-population Cr_2O_3 values in colluvium are not related to any known anomalous bedrock Pt values. The Cliff Zone Cr_2O_3 anomaly, however, extends considerably further downslope than does the more localized Pt anomaly.

The uppermost Pd population in colluvium is very subtle (4-5 ppb), and is located both above and below Cliff Zone PGE mineralization (Figure 4-17). High Au values of up to 54 ppb are found in serpentinized colluvium, although the highest (56 ppb) occurs beneath Cliff Zone Pt mineralization. Some of the highest As values also occur in colluvial soils immediately beneath the Cliff Zone Pt

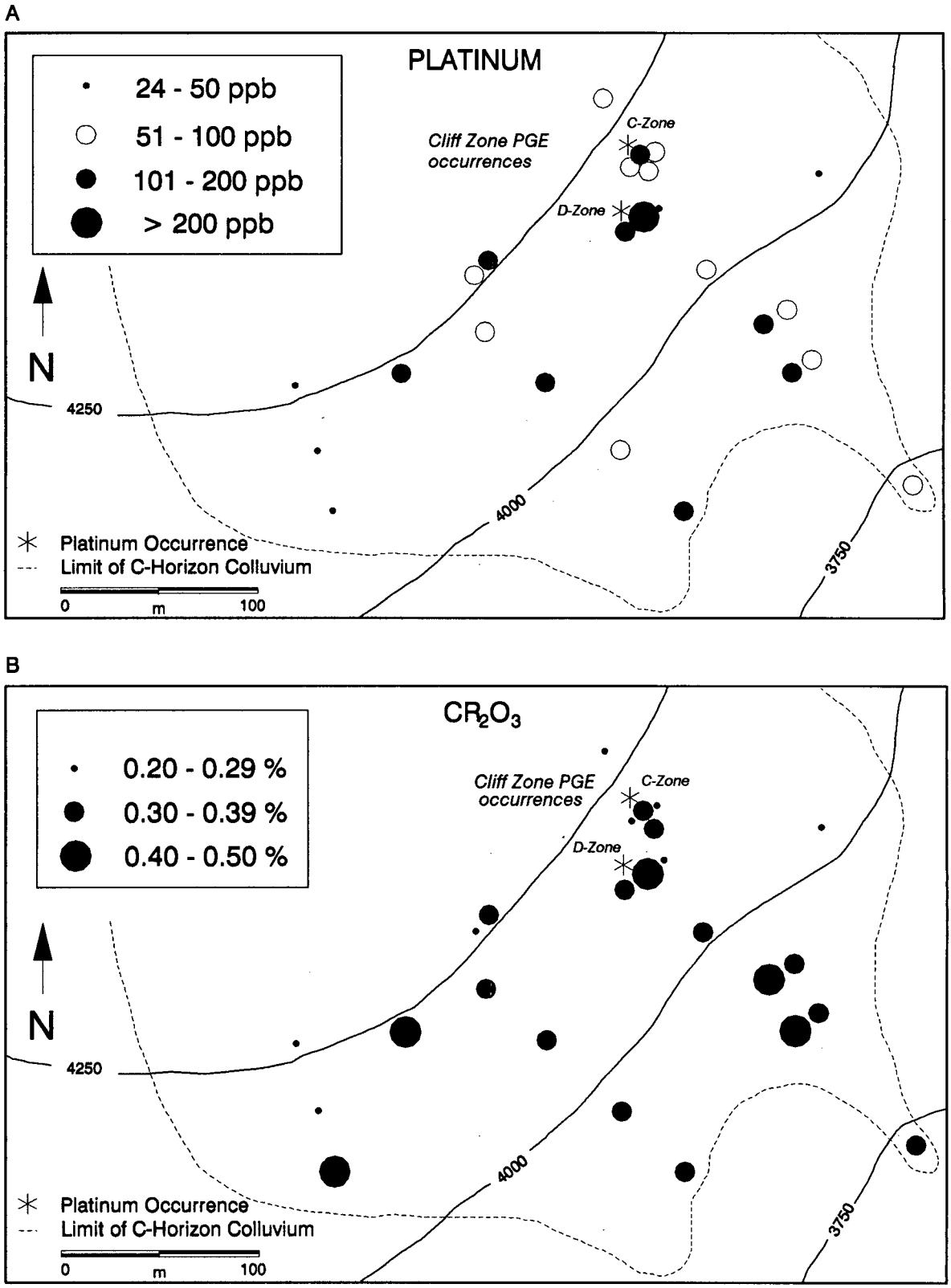

Figure 4-16. Distribution of A. Pt (ppb); and B. Cr2O3 (%) in C horizon colluvium, main study area (n=25), Grasshopper Mountain, B.C. (basemap adapted from Bohme, 1987).

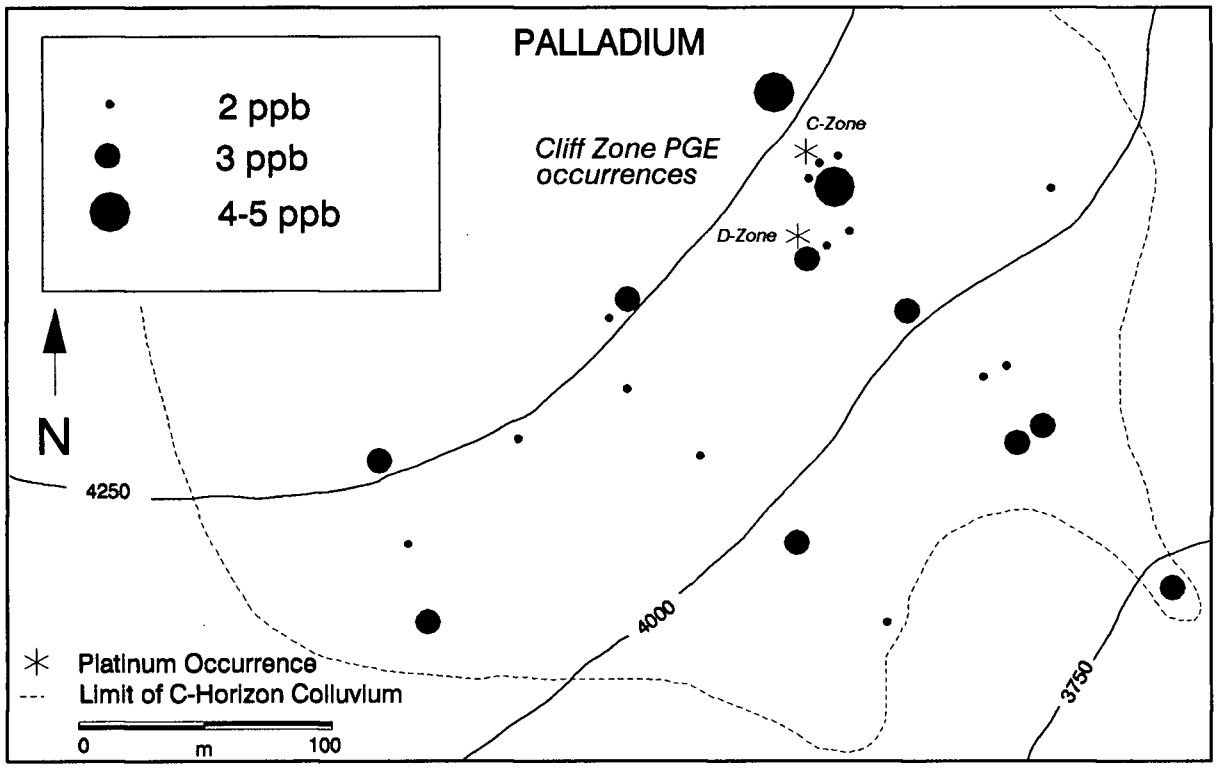

Figure 4-17. Distribution of Pd (ppb) in C horizon colluvium, main study area (n=25), Grasshopper Mountain, B.C. (basemap adapted from Bohme, 1987).

occurrences, while some of the lowest colluvial As values are associated with Pt-poor areas.

d) Regional Dispersion of Platinum

Background C horizon till samples were collected from 5 sites on the northern margin and to the west of the dunite core of the Tulameen complex to assess glacial transport and regional dispersion of Pt (section 3.2.2). Site locations on Grasshopper Mountain and Mount Britton are shown in Figure 4-18 along with Pt, Pd, MgO and Cr_2O_3 concentrations of C horizon soils.

Only one site, 402, is actually situated above the dunite core. Regarding the others, it is apparent that concentrations of these elements in C horizon soils at sites 403 and 404 are generally similar to those defined for non-dunitic till within the main study area. Relatively high MgO contents intermediate between those of the two till types (Table 4-3) suggest some degree of till mixing, however. Conversely, Pt, MgO and Cr_2O_3 concentrations at sites 405 and 406 are similar to those defined for main study area dunitic till. Pt concentrations are similar to those on the plateau of Grasshopper Mountain (Figure 4-13). Similarly, Cr_2O_3 concentrations equal or exceed those at most main study area sites on Grasshopper Mountain (Figure

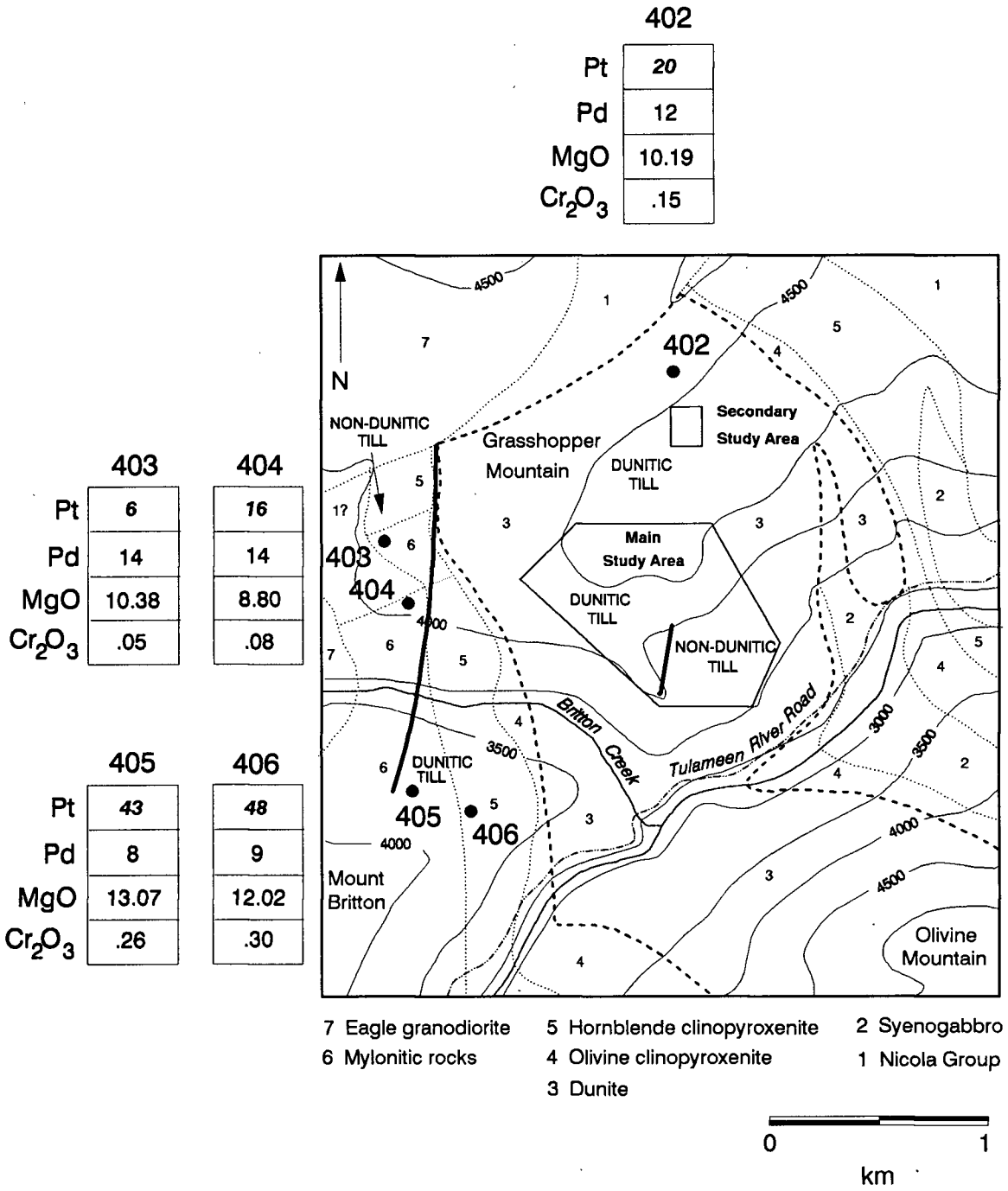

Figure 4-18. Concentrations of selected elements in background till samples on the northern margin and to the west of the dunite core of the Tulameen ultramafic complex. Solid lines indicate distribution of dunitic till. Pt and Pd concentrations in ppb; MgO and Cr2O3 concentrations in % (modified after Nixon and Rublee, 1988).

4-14). Based on these results and those of part a) of this section, solid dark lines in Figure 4-18 show the possible distribution limits of dunitic till in the Grasshopper Mountain-Mount Britton area. Later fluvioglacial outwash in the Britton Creek valley and post-glacial colluvium on Grasshopper Mountain are not shown.

4.2.1.3 X-Ray Diffraction Mineralogy Results

The mineralogy of 48 soil fractions, comprising both coarse -10+40 mesh (2mm-425um) and fine -270 mesh (<53um) fractions from 24 horizons in 11 profiles, was determined by X-ray diffraction (section 3.8). Results are summarized in Figure 4-19, and shown in Appendices 6.1 to 6.3 on the basis of soil parent material. Twenty-three minerals were identified, including two serpentine minerals, three chlorites, two micas, two clay minerals and three amphiboles.

a) Non-Dunitic Till

Horizons in both non-dunitic till profiles (Appendix 6.1) contain quartz, plagioclase, ferro hornblende and clinochlore. Serpentine group or other minerals indicative of an ultramafic origin are absent at site 20, although

chrysotile occurs at site 6. There are no major mineralogical variations with either particle size or horizon.

b) Dunitic Till

Serpentine-group minerals, particularly chrysotile, are ubiquituous in soil horizons of six dunitic till profiles (Appendices 6.1 and 6.2). Talc and vermiculite are locally important, but forsteritic olivine is relatively uncommon. Quartz and plagioclase occur at most sites.

Lizardite rather than chrysotile is the dominant serpentine mineral in the deepest sample directly above A-Zone Pt mineralization, although the two are difficult to distinguish. Talc and vermiculite are locally more dominant than crysotile in fine fractions, particularly at depth. Talc-bearing soils (sites 33, 73, 57) occur in both main and secondary study areas, but vermiculite-bearing soils are restricted to the plateau sites (69, 73). Chrysotile is a more common constituent of coarse fractions at these sites.

Mineralogy at site 43 (section 2.5.2) differs dramatically between the upper two (reworked till) and lower two (lodgement till) horizons. Near-surface horizons contain forsterite, chrysotile, quartz and plagioclase in all fractions. The two lower horizons, however, consist of

quartz with lesser plagioclase, saponite (Mg-smectite) and gonyerite (Mn-Mg chlorite). Detectable chromite occurs at sites 69, 56 and 57. Cooperite (PtS) was identified at site 73 in the coarse fraction of the Bm horizon. This, the only PGM detected by XRD, was confirmed in a second evaluation. The C horizon at this site contained 311 ppb Pt, one of the highest (Figure 4-13B) of the overview analyses.

c) Dunite Colluvium

Colluvial soil profiles beneath dunite cliffs are characterized by a limited mineralogy of serpentine group minerals and talc, and the absence of olivine, quartz, plagioclase and amphiboles (Appendix 6.3). There are important mineralogical differences between "dunitic colluvium" (site 16) and "serpentine colluvium" (sites 27 and 42), characterized by orange-coloured soil. Lizardite is the dominant mineral and sole serpentine group constituent of dunitic colluvium.

Lizardite is also the dominant mineral, particularly in coarse fractions, of the three samples from serpentine colluvium at site 27. Talc, however, is an important constituent of the fine fractions. Site 42 exhibits the most intense orange colouration of colluvium profiles. Crysotile and talc are the dominant minerals and lizardite

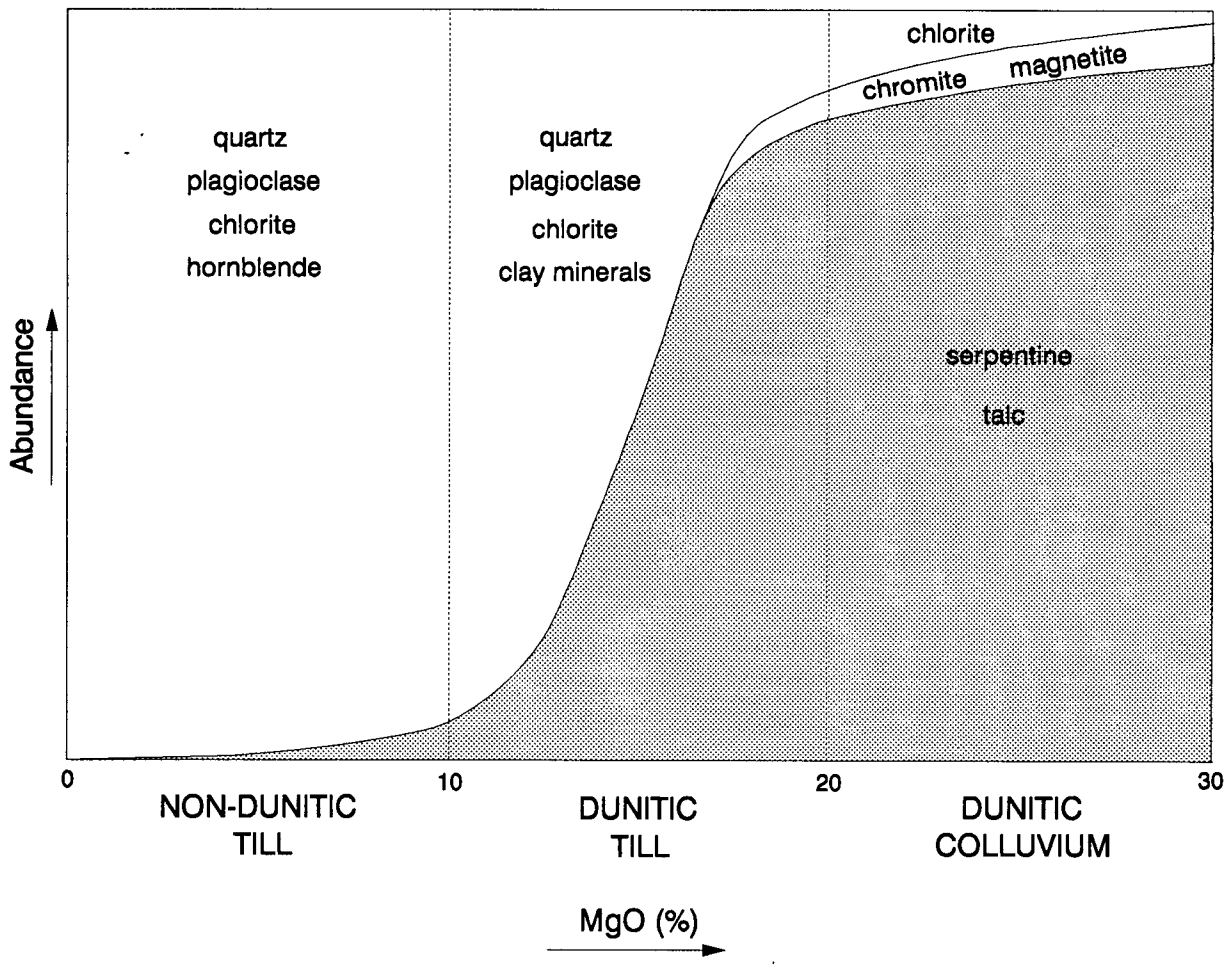

Figure 4-19. Schematic diagram illustrating the general relation of MgO content to soil mineralogy in surficial materials on Grasshopper Mountain (11 profiles).

is absent. Fine fractions of soils at both sites are dominated by talc.

4.2.2 LFH Horizons

LFH horizons were analyzed for Pt-Pd-Au-Rh by Pb fire assay with an ICP-AES finish, and subsequently for Fe by F-AAS (see section 3.4). Pt and Fe content of LFH horizons (Figure 4-20; Appendix 7) are summarized by parent material type in Table 4-7. Results are summarized as follows:

Weight % ash (remnant after ashing) content of almost all LFH samples lies in the range 5-24 %. It exhibits no obvious trends across the study areas (Figure 4-21). LFH horizons on active colluvium, however, have a considerably greater ash content (21.96%) than those on till.

Pt content generally increases gradually from southeast to northwest across the study area (Figure 4-22) in much the same manner as C-horizon soils. Concentrations are low and erratic however, and are generally less than 20 ppb on tills in the main study area. Median Pt concentrations over clay, non-dunitic till and dunitic till C-horizons in the main study area are 4 ppb, 7 ppb and 12.5 ppb, respectively. The greatest Pt values in LFH horizons on non-dunitic till occur in the southeast part of the study area near the base of the

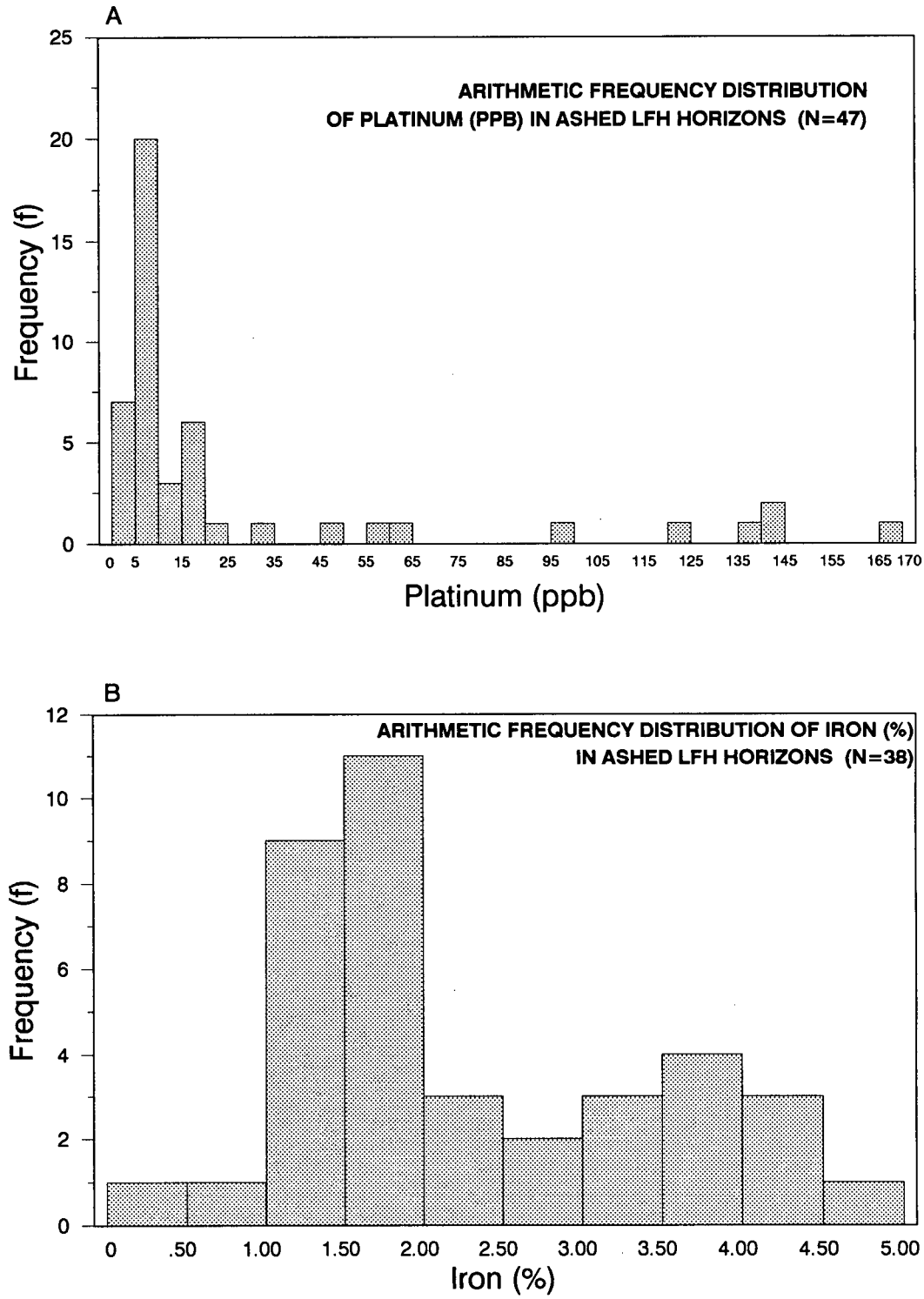

Figure 4-20. Arithmetic frequency distributions of A. Pt (ppb) and B. Fe (%) in LFH horizon ash.

Overburden	n	Pt (ppb)	Pd (ppb)	Au (ppb)	Weight Ash (%)	LFH/C Pt Ratio	Fe* (%)	Insoluble Residue* (%)
Clay	2	4.0	4.5	10	7.94	0.63	2.70	8.0
		4	**4.5**	**10**	**7.94**	**0.63**	**2.70**	**8.0**
		1	2	10	7.71	0.25	1.62	6.0
		7	7	10	8.16	1.00	3.78	10.00
Non-Dunitic Till	19	7.6	4.5	8.8	14.37	1.17	2.14	10.1
		7	**3**	**7**	**13.90**	**0.80**	**1.78**	**8.0**
		2	2	3	5.84	0.11	1.03	0.0
		18	19	46	37.67	3.50	3.67	32.0
Dunitic Till	16	14.0	2.0	3.1	13.54	0.37	1.52	4.7
		12.5	**2**	**2.5**	**11.45**	**0.36**	**1.46**	**4.0**
		6	2	1	7.07	0.06	0.38	0.0
		32	2	9	21.59	0.71	3.00	12.0
Dunitic Till/Rubble/ Colluvium (A-Zone)	7	104.7	2.7	6.1	12.33	1.14	3.64	15.8
		122	**2**	**6**	**11.34**	**1.36**	**3.62**	**14.0**
		9	2	3	5.54	0.12	2.83	7.0
		167	5	9	23.35	2.29	4.11	36.0
Dunite Colluvium	3	85.0	2.3	11.3	22.62	0.72	4.58	18.0
		65	**2**	**13**	**21.96**	**0.76**	**4.58**	**18.0**
		49	2	4	8.87	0.56	4.33	18.0
		141	3	17	37.03	0.83	4.83	18.0

Table 4-7. Mean, median, minimum value and maximum value of Pt, Pd, Au, weight percent ash, LFH/C horizon Pt ratio, Fe, and percent insoluble residue in LFH horizon samples. N=47 for all variables except those marked with an *, indicating sample sizes (n=38) of clay, n=2; non-dunitic till, n=14; dunitic till, n=15; A-Zone, n=5; dunite colluvium, n=2.

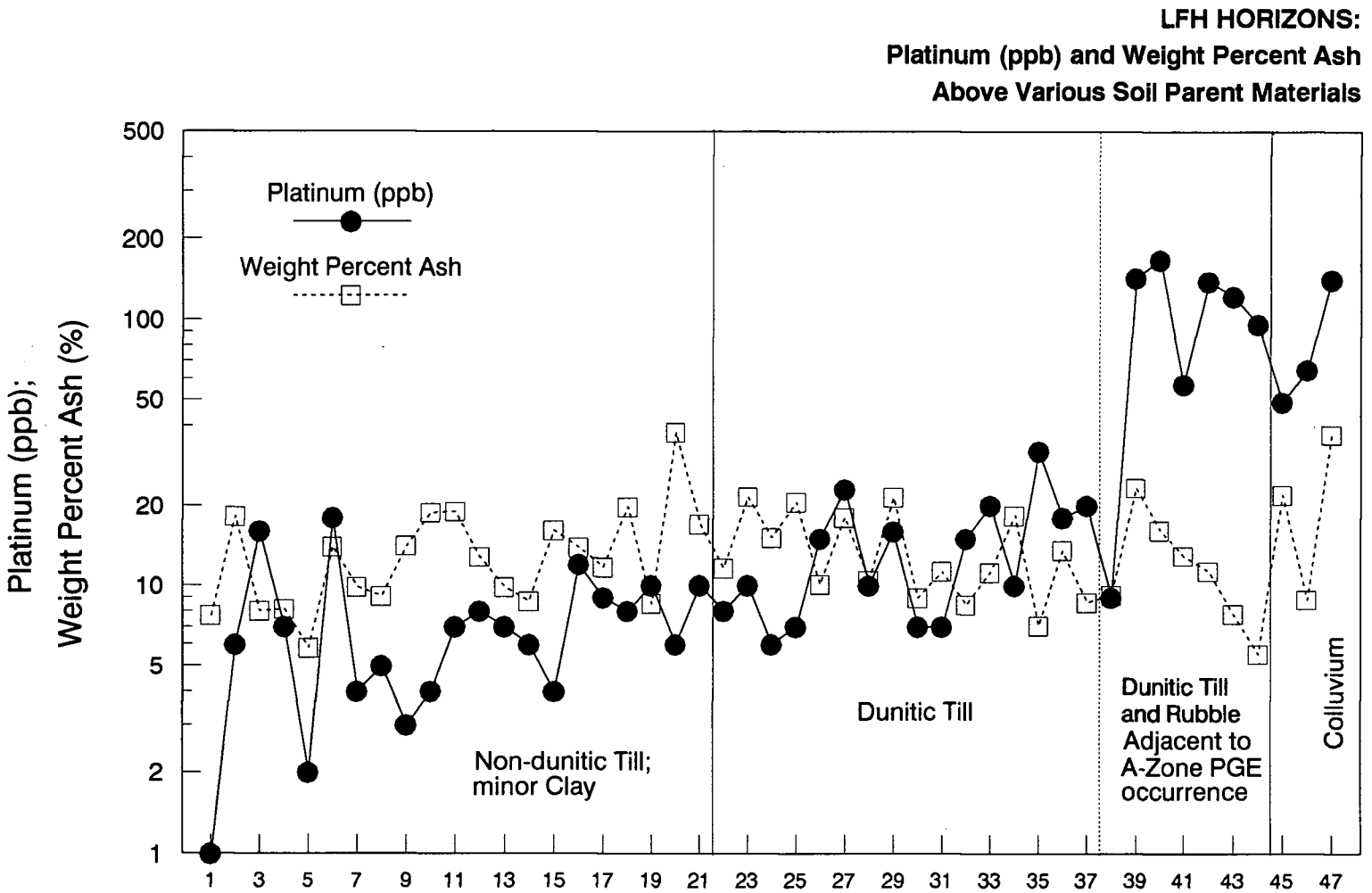

Figure 4-21. Relation of Pt (ppb) to weight percent ash in LFH horizons above various soil parent materials on Grasshopper Mountain.

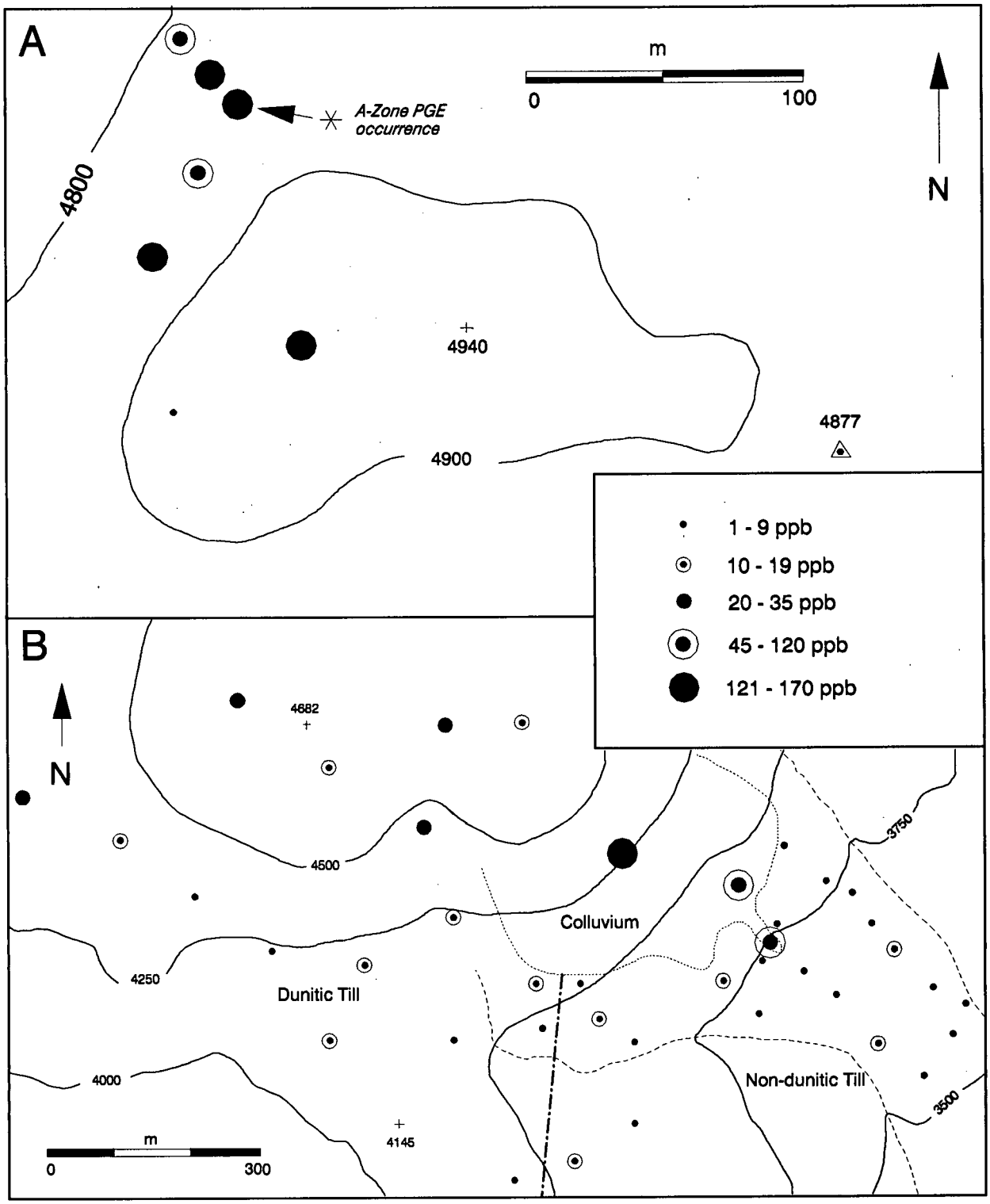

Figure 4-22. Pt distribution (ppb) in LFH horizons (n=47) of A. the secondary study area and B. the main study area on Grasshopper Mountain.

southern forested slope (Figure 4-22), whereas the greatest Pt values in LFH horizons on dunitic till occur on the plateau. Several LFH horizons in the dunitic till area are developed directly above stabilized dunite colluvium.

Pt content of LFH horizons increases dramatically above colluvium and in the secondary study area (Figure 4-22). LFH horizons on dunitic till, rubble and stabilized colluvium adjacent to the A-Zone occurrence in the secondary study area have a median Pt concentration of 122 ppb, almost 10x greater than those developed on dunitic till in the main study area. High Pt concentrations of up to 167 ppb appear to reflect underlying PGE mineralization, but are apparently very localized; a single site 125 m downice from the trenched A-Zone occurrence has an LFH Pt content of only 9 ppb (Figure 4-22).

Fe content of LFH horizon ash, determined to evaluate lithic contamination by underlying dunite or till, ranges from 0.38 to 4.83%. It is bimodally distributed into horizons containing < 2.4% Fe and those containing 3-5% Fe (Figure 4-20B). LFH horizons above dunite colluvium and adjacent to A-Zone Pt mineralization have much higher median Fe contents than do those on either dunitic or non-dunitic till (Table 4-7).

LFH correlation matrices (Figure 4-23) show that

significant correlations exist, among others, between Pt and Fe, between Pt content of the LFH horizon and that of the underlying C horizon soil, and between Pt and insoluble residue. Correlations between Pt and Fe are particularly evident in those LFH horizons developed on dunitic till, A-Zone till/rubble, and colluvium (Figure 4-24A). Significant correlations between Pd and Au, concentrations of both of which are subordinate to Pt in most LFH horizons (Table 4-7), are largely due to a few high-concentration samples. LFH Pt and Pd do not exhibit sympathetic relations above any type of underlying surficial material with the possible exception of non-dunitic till (Figure 4-24B).

The sympathetic increase in LFH Pt content with that of the underlying C horizon is shown in Figure 4-25. Pt content of the LFH horizon is generally less than that of the C horizon. Frequency distributions of the LFH/C Pt ratios are shown in Figure 4-26. Dunitic till ratios consistently plot below 1, indicative of low LFH Pt content relative to the C horizon. Erratic ratios both greater and less than 1 are present, however, at sites on non-dunitic till and on A-Zone till, rubble and colluvium.

The spatial distribution of LFH/C horizon Pt ratios on Grasshopper Mountain is shown in Figure 4-27. Sites with ratios > 1 are generally located on or near breaks in slope. Main study area high-ratio sites are clustered in the

	PT	PD	AU	PT-C	WT%ASH
PT	1.00000				
PD	-.07293	1.00000			
AU	.05653	.74807	1.00000		
PT-C	.63790	-.08709	-.05837	1.00000	
WT%ASH	.18827	-.07350	-.14235	.03555	1.00000

CRITICAL VALUE (1-TAIL, .05) = + Or - .24306
CRITICAL VALUE (2-tail, .05) = +/- .28723

N = 47

Figure 4-23A. LFH correlation matrix for Pt, Pd, Au, Pt (C horizon) and weight percent ash (n=47)

	PT	PD	AU	PT-C	WT%ASH	FE	%R
PT	1.00000						
PD	-.03794	1.00000					
AU	.06740	.77651	1.00000				
PT-C	.57714	-.05017	-.05155	1.00000			
WT%ASH	.24317	-.09865	-.11667	.09079	1.00000		
FE	.64126	.12714	.10741	.39766	.27199	1.00000	
%R	.44672	-.15002	-.10431	.11577	.32449	.63987	1.00000

CRITICAL VALUE (1-TAIL, .05) = + Or - .27114
CRITICAL VALUE (2-tail, .05) = +/- .31975

N = 38

Figure 4-23B. LFH correlation matrix for Pt, Pd, Au, Pt (C horizon), weight percent ash, Fe and percent insoluble residue (n=38).

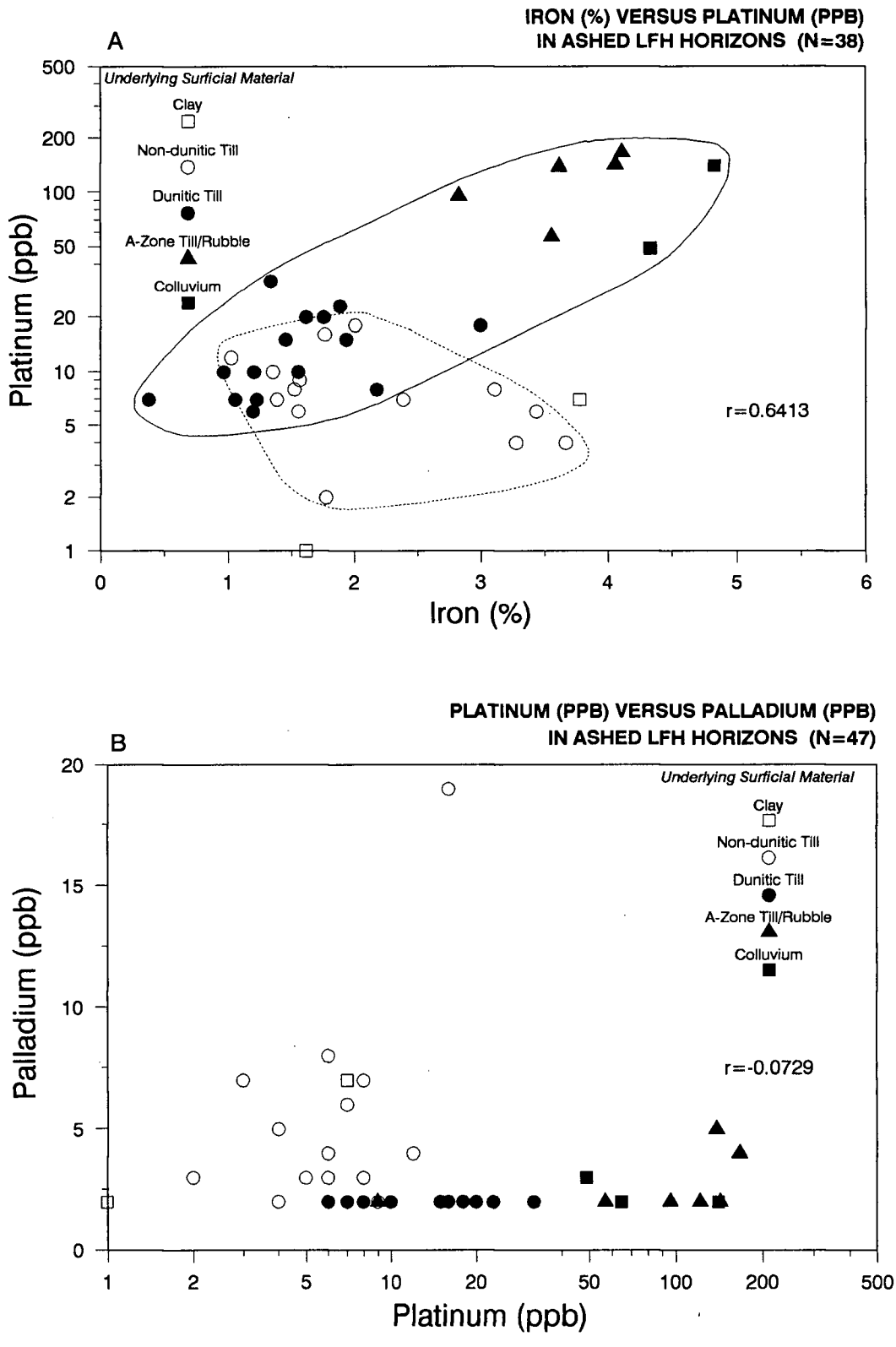

Figure 4-24. Scatterplots of Pt (ppb) versus A. Fe (%) and B. Pd (ppb) in ashed LFH horizons above various parent materials.

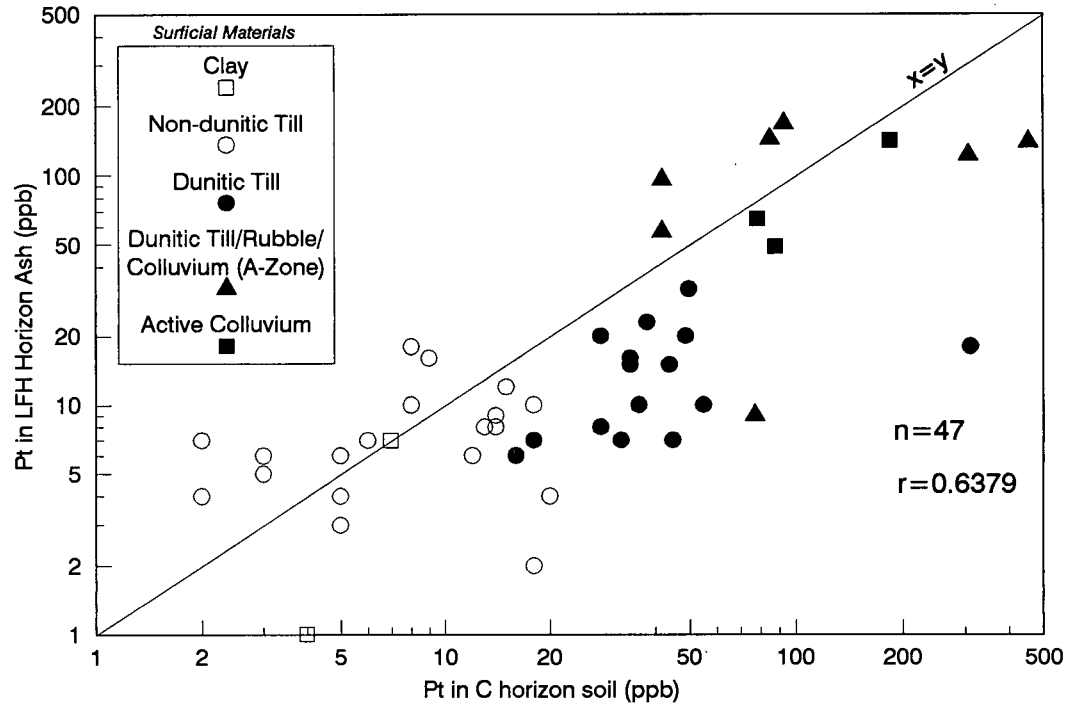

Figure 4-25. Scatterplot of Pt concentrations (ppb) of C horizon soils from various parent materials versus ash from corresponding LFH horizons. Points plotting above the unity line have LFH/C horizon Pt ratios of > 1.

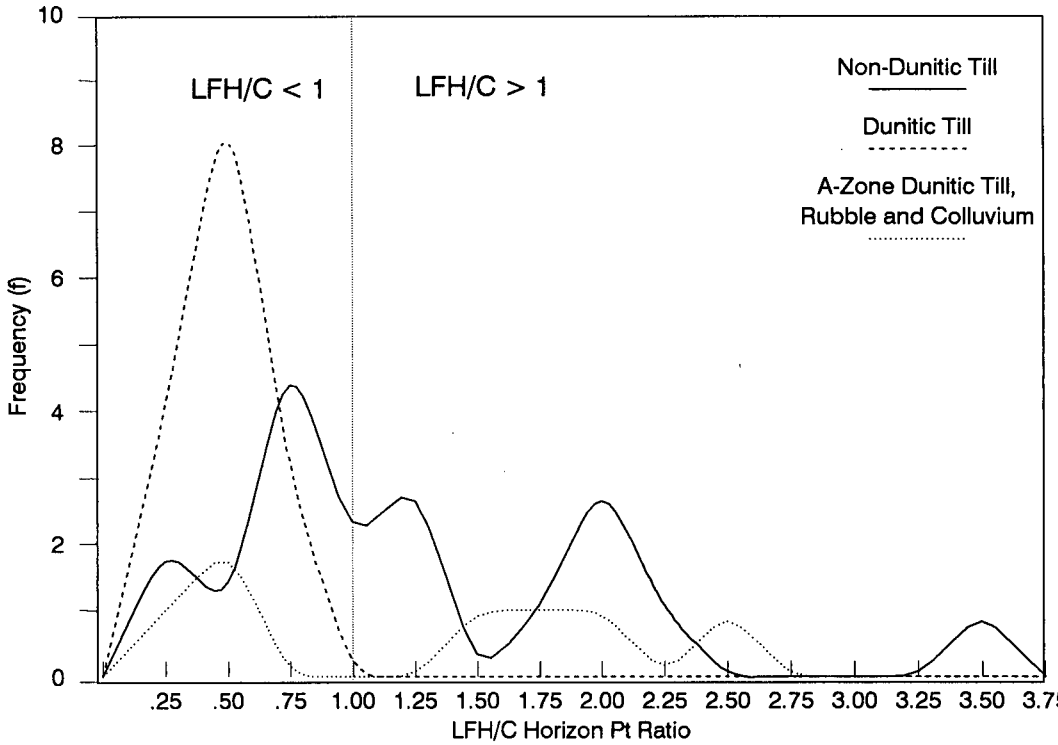

Figure 4-26. Frequency distributions of LFH/C horizon Pt ratios for non-dunitic till (n=19), dunitic till (n=16), and A-Zone dunitic till, rubble and colluvium (n=7).

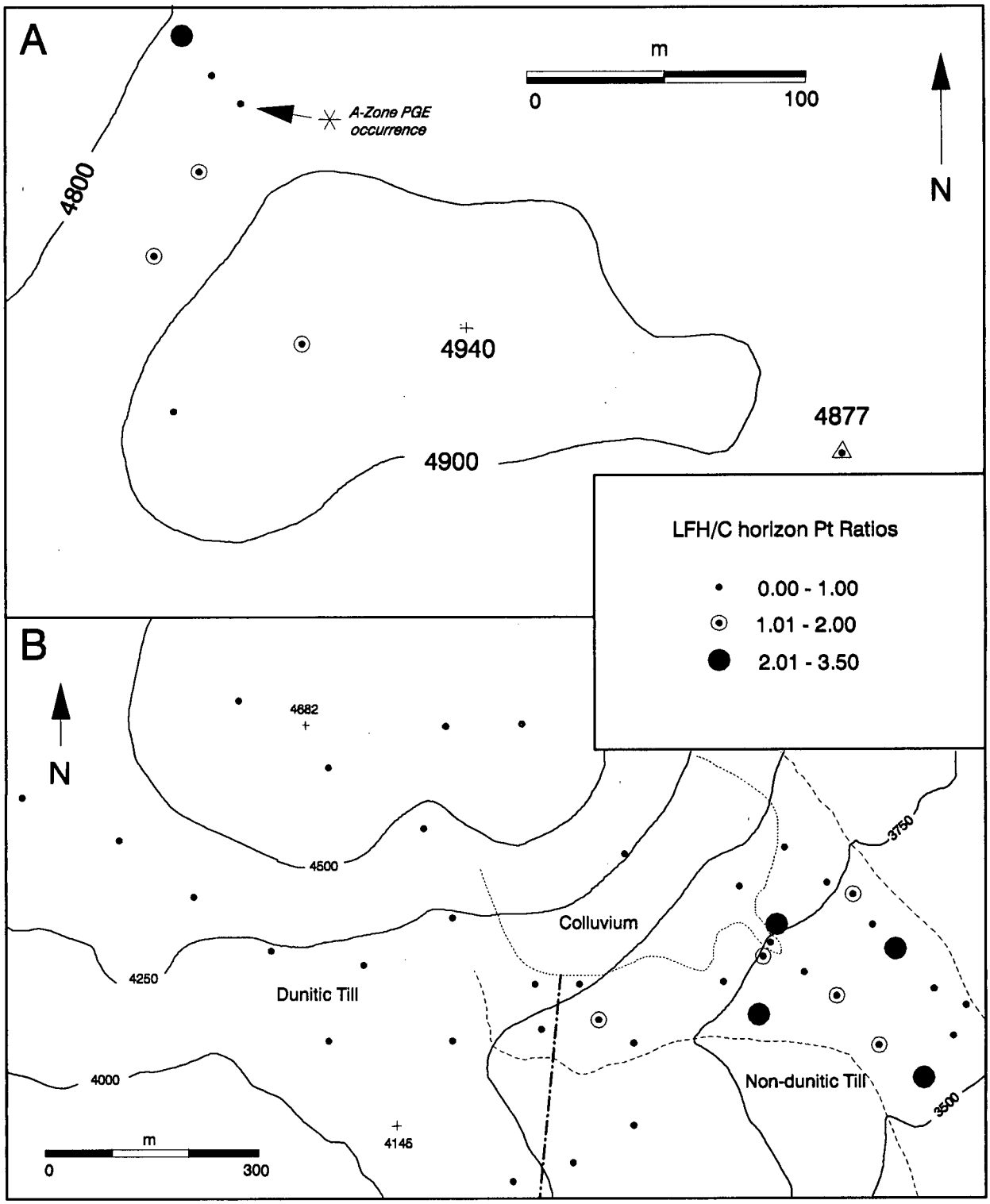

Figure 4-27. Distribution of LFH horizon/C horizon Pt ratios on Grasshopper Mountain. Solid dashed line at lower centre represents the boundary between dunitic and non-dunitic tills. The majority of the high-ratio soil sites are located in or near the seepage zone area in non-dunitic till.

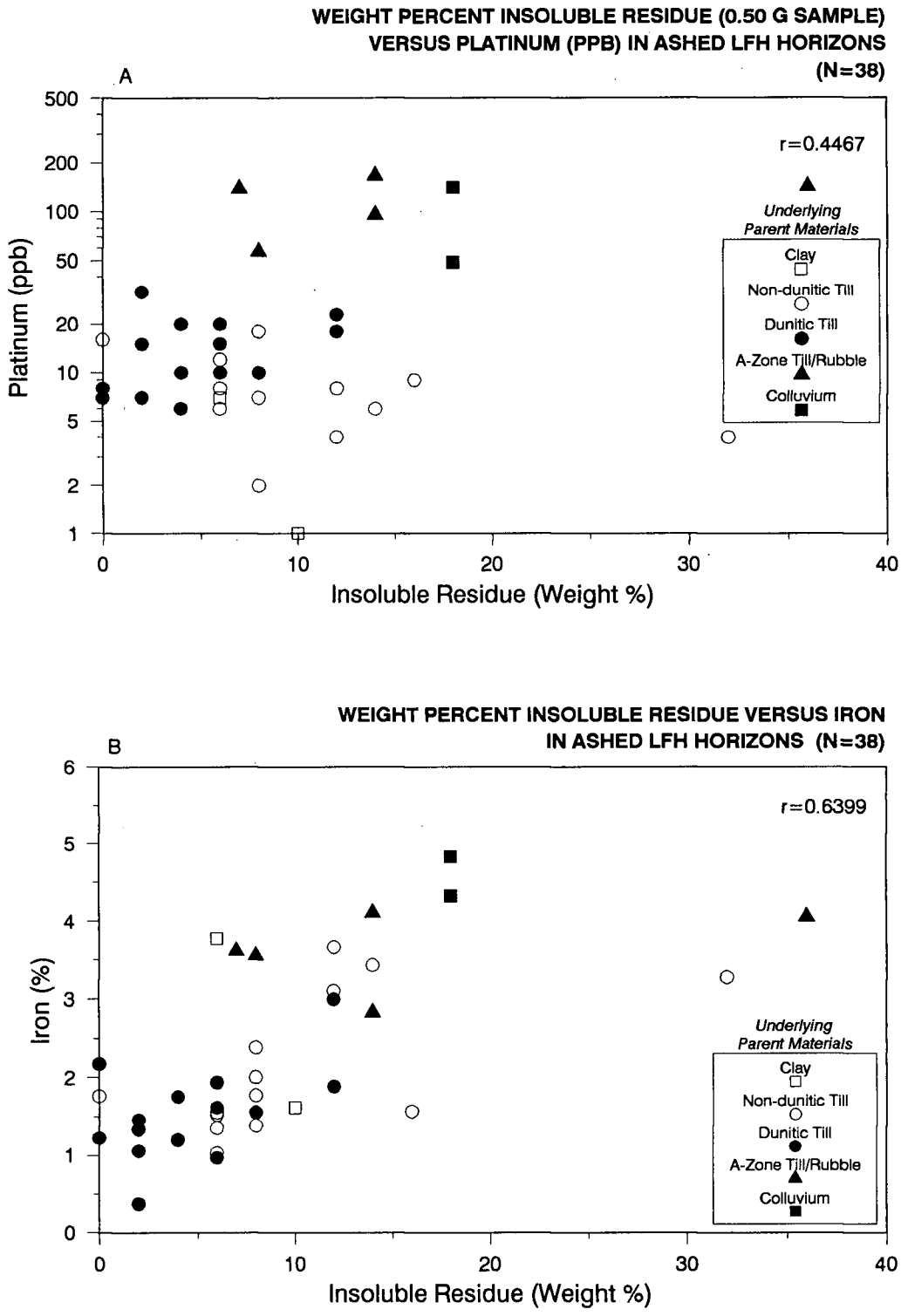

Figure 4-28. Scatterplots of weight percent insoluble residue versus A. Pt (ppb) and B. Fe (%); in ashed LFH horizons above various parent materials.

seepage zone/southern forested slope area above non-dunitic till, while the highest ratio in the secondary study area is immediately downslope of the A-Zone PGE occurrence.

Most LFH horizon ashes contain about 2-18% insoluble residue (Table 4-7; Appendix 7), comprising carbon or mineral matter, following acid digestion (see section 3.3.2). Median proportions of insoluble residue (Table 4-7) in LFH ash from active colluvium and the secondary study area are considerably higher than those from till sites in the main study area. Significant correlations exist between weight % insoluble residue and weight % ash, Pt content (Figure 4-28A), and Fe content (Figure 4-28B), indicating that the Pt content of the LFH is closely associated with particulate mineral matter.

4.2.3 Stream Sediments, Moss mats and Banks

Stream sediment, moss mat and bank samples were collected along Grasshopper Creek (section 3.2.3) and analyzed for the overview suite of elements. The distribution of Pt, Pd and Au in both stream sediments and moss mats (Appendix 8.1) is shown in Figure 4-29. Pt contents of different size/density/magnetic fractions (section 3.3.5) of sediment from site 2 are shown in Figure 4-30.

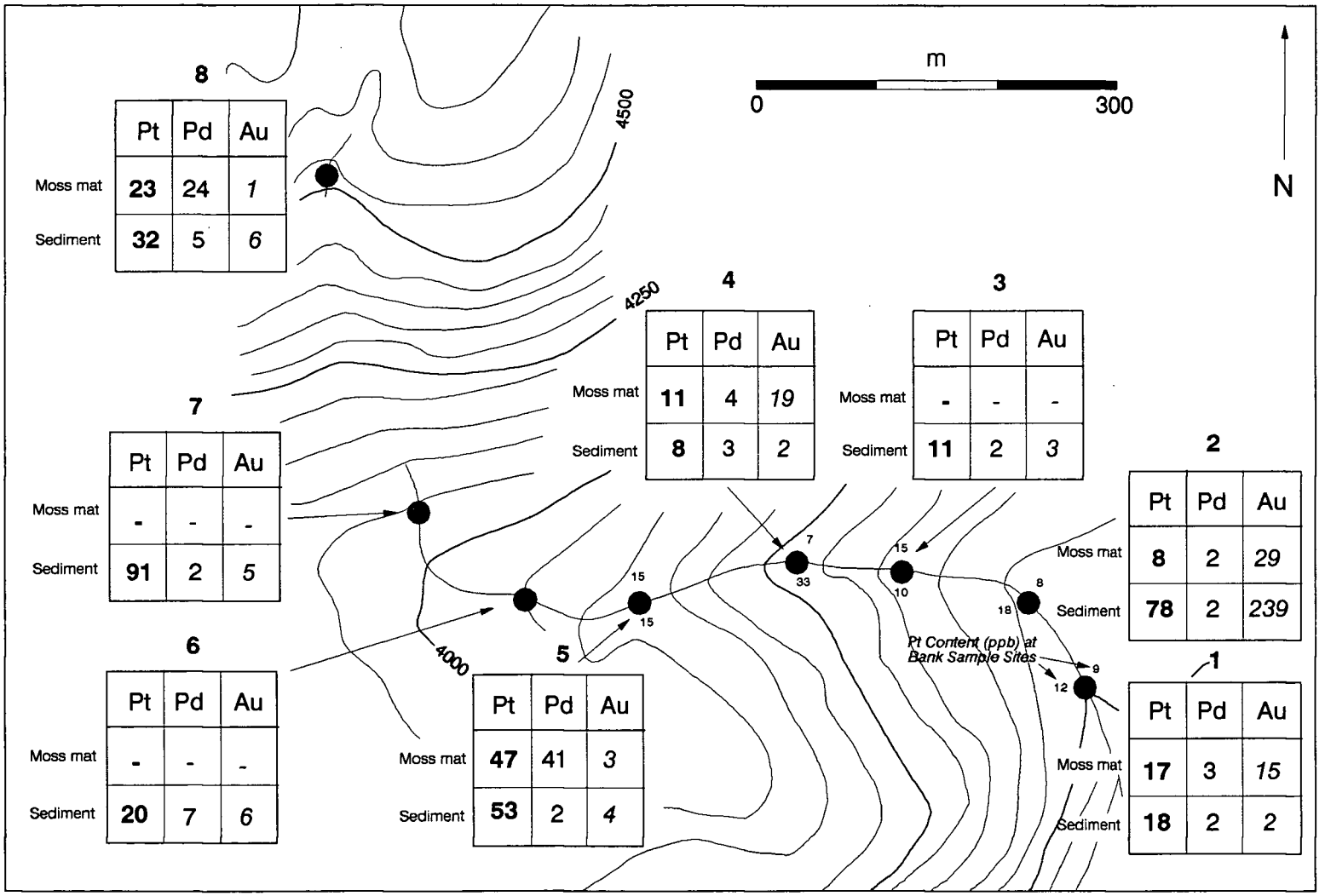

Figure 4-29. Pt, Pd, and Au contents (ppb) of stream sediments and moss mats at eight sampling sites along Grasshopper Creek on Grasshopper Mountain, B.C. Pt content (ppb) of bank samples at sites 1-4 are shown adjacent to the site marker. Stream sites are the same as those shown for water samples in Figure 4-33.

Grasshopper Creek is situated entirely on the dunite core of the Tulameen complex (Figure 2-1), but at lower elevations flows only through unconsolidated overburden, mostly till, of mixed dunitic and non-dunitic origin. Sample weight data for sediments and moss mats is shown in Appendix 8.2. The proportion of fine -70 mesh (<212 um) sediment, as weight % of the -10 mesh (<2mm) fraction, is consistently greater, by up to 4x at some sites, in moss mats (Table 4-8). The size fraction distribution of Pt at site 2 has Pt content increasing with decreasing particle size (Figure 4-30A).

Pt concentrations in sediments and moss mats are generally similar to, or slightly greater than, those in adjacent C horizon soils and appear to partly reflect local variations in stream gradient. Data is limited, but lower Pt concentrations occur where the gradient is gentle or steep, while higher concentrations occur at break of slope areas (Figure 4-31). Sediments generally have higher Pt contents (range: 8-91 ppb) than do moss mats (range: 8-47 ppb). The differences at most sites are usually small (Table 4-8), but Pt in sediment (78 ppb) is 4-10 x greater than in moss mats (8/17 ppb) at the most significant break of slope on the creek (site 2). Pt is most abundant in the -70+140 mesh heavy magnetic fraction (361 ppb), with the proportion of non-magnetic associated Pt increasing with decreasing grain size (Figure 4-30B).

Site	Pt in Sediment (ppb)	Pt in Moss-mat (ppb)	-70# Sediment (%)	-70# Moss-mat (%)	Stream Topography
1	18	17	10.7	40.7	L
2	78	8 (17)	9.5	36.3	B
3	11 (12)	-	25.2	-	M
4	8	11	20.2	25.5	M
5	53	47	18.1	41.8	G
6	20	-	26.7	-	G
7	91	-	33.6	-	B
8	32	23	51.6	75.6	B

L=Level to gentle
B=Break of slope
G=Gentle slope
M=Moderate slope

Site 8 is farthest upstream

-70#(mesh) as Wt.% of -10 mesh

Table 4-8. Weight percent -70 mesh fraction and Pt content of stream sediments and moss mats, Grasshopper Creek, Grasshopper Mountain, B.C.

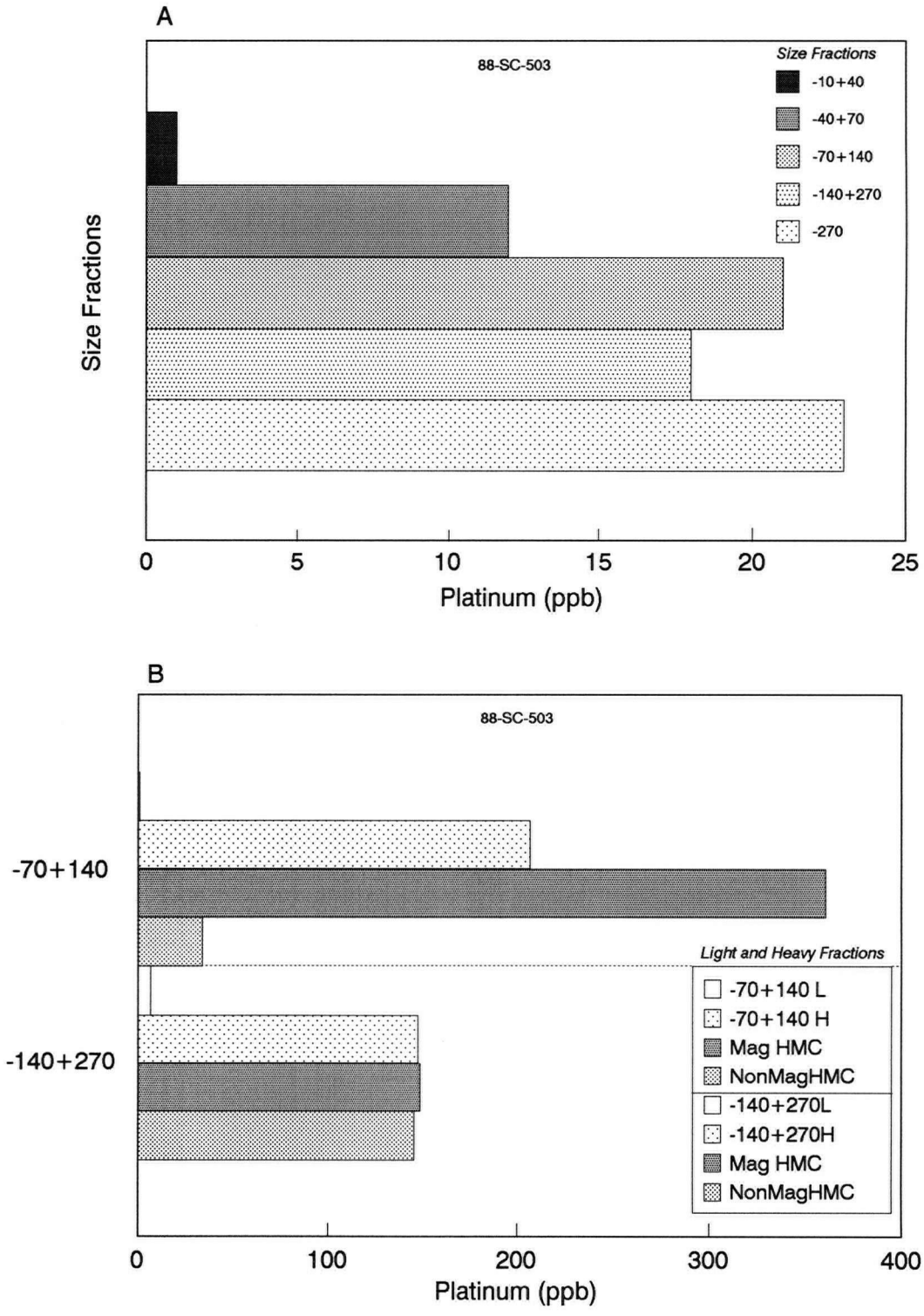

Figure 4-30. Pt distribution (ppb) in A. five size fractions and B. light, heavy, heavy magnetic and heavy non-magnetic mineral fractions of the -70+140 and -140+270 mesh size fractions, stream sediment site 2, Grasshopper Creek.

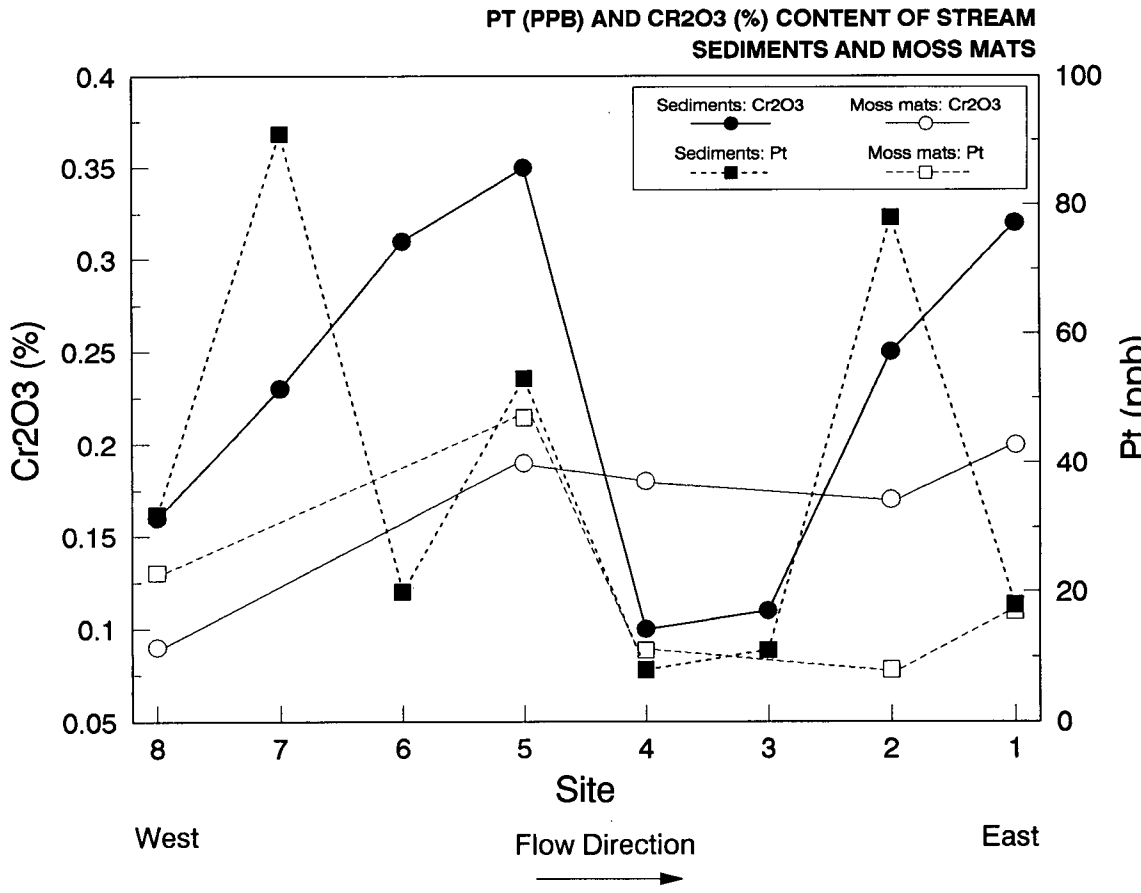

Figure 4-31. Pt (ppb) and Cr2O3 (%) content of sediments and moss mats at eight sites on Grasshopper Creek.

Cr_2O_3 content of sediments ranges from 0.10-0.35%; MgO content from 6.25-13.04%. MgO concentrations in both sediments and moss mats generally increase upstream into areas of dunitic till. Cr_2O_3 trends vary with the medium; concentrations in sediments increase downstream, while those in moss mats are relatively constant (Figure 4-31). Cr_2O_3 and MgO concentrations are greater in sediments than in moss mats at four out of five sites, with the differences being proportionally greatest for Cr_2O_3.

Pt content of bank samples at five sites (Figure 4-29; Appendix 8.3) varies from 7-33 ppb. All five sites are situated within non-dunitic till (Figures 4-1 and 4-13) and there is a general, if somewhat erratic, tendency for the Pt content to increase upstream toward the area of dunitic till. Low MgO and Cr_2O_3 contents of the banks are consistent with this interpretation.

Pd and Au contents of sediments and moss mats are low relative to Pt (Appendix 8.1) but vary considerably with the medium. Pd content of sediments (maximum: 7 ppb) is very low while that of moss mats (maximum: 41 ppb) at two sites in the upper dunitic till part of the creek are 5-20x greater than in corresponding sediments (Figure 4-29).

There are no obvious differences in the Au content of moss mats versus sediments on the upper half of the creek where water flow is the least. However, in the lower half of the creek Au is enriched 7-9x in moss mats relative to sediments at two sites on level/gentle and moderately steep slopes (Figure 4-29). Conversely, Au is 8x more abundant in sediments (239 ppb) than moss mats at the high-Pt base of slope site. Au, like Pt, content of this sediment increases with decreasing particle size, and very high Au concentrations (1659 ppb) occur in the -140+270 mesh heavy non-magnetic fraction.

4.2.4 Bogs

Separate splits of centre and margin organic sediments from three bogs (Figure 3-1) were either pulverized or ashed (section 3.3.4), prior to Pb-FA/ICP-AES analysis. Pt concentrations are shown in Figure 4-32; Pt, Pd, Rh and Au concentrations in Appendix 9.

Sample weight and ashing data (Appendix 9) show that the Loss On Ignition (LOI) content of unpulverized bog splits ashed at UBC are almost identical to those determined on pulverized bog splits at Acme Labs. However, perched bog 3 in the secondary study area has lower LOI values (65.9-67.4%) than the large seepage area bog 1 (84.1-93.1%).

Perched bog 3 also exhibits almost identical LOI values at bog centre and margin sites, whereas LOI values at seepage zone bog 1 decrease from the centre to the upslope margin where the proportion of mineral matter is greatest. Weight % ash content of organic bog soils are generally similar to those of LFH horizons (Table 4-7), particularly in the large seepage zone bog. The perched bog contains a somewhat greater proportion of post-ashing mineral matter, however, than do nearby LFH horizons.

High Pt concentrations in ashed samples (maximum: 67 ppb) are 2-17x greater than in corresponding pulverized samples (maximum: 21 ppb), reflecting the concentration of Pt during the ashing process. Reconstructed dry weight Pt concentrations for ashed samples, obtained by multiplying the Pt value by the weight % ash content, are invariably within 1-2.5 ppb of that of the pulverized split and indicate that Pt is not lost during ashing. Two bogs in the lower seepage-zone part of the main study area contain up to 9 ppb Pt in pulverized splits, concentrations similar to those on nearby soils on non-dunitic till. Perched bog 3 on dunite bedrock and thin discontinuous till in the secondary study area contains up to 21 ppb Pt in the pulverized split and 55 ppb in the ashed split.

An interesting relation is the association of higher Pt concentrations with samples from bog margins as opposed to

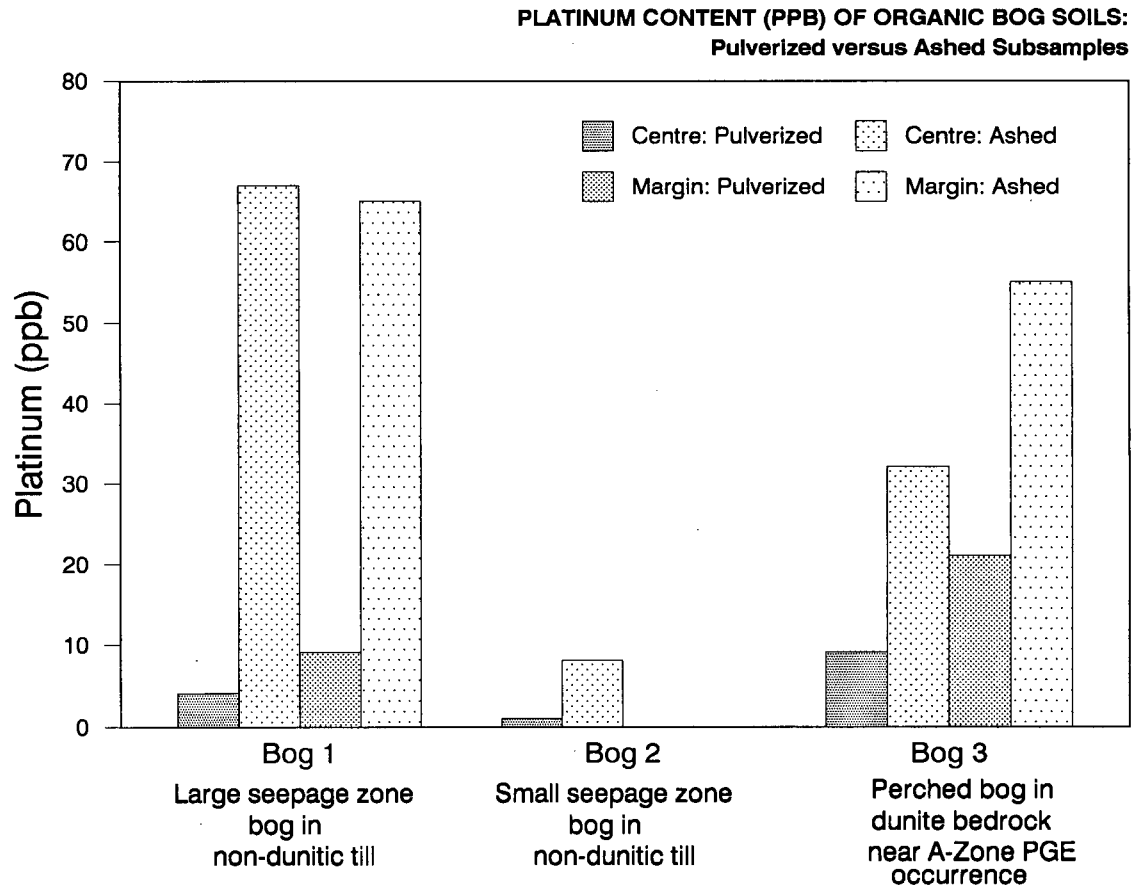

Figure 4-32. Pt contents (ppb) of pulverized and ashed organic bog soils in three Grasshopper Mountain bogs.

bog centres. This is particularly true for the pulverized splits from bog margins, which contain 2-3x as much Pt as do corresponding bog centres. The relation also holds for ashed splits of perched bog 3, but not for seepage zone bog 1, where Pt contents of margin and centre ashed samples are almost identical.

Pulverized bog samples also contain up to 4.1 ppm Sb (Appendix 9), with the highest values occcurring in seepage zone samples. These are more than 6x higher than the median Sb content of soils developed on till and colluvium, and are more than 2x greater than the highest Sb concentration in seepage zone soils.

4.2.5 Waters

The Pt content of Grasshopper Mountain water samples after field filtration to < 0.45 um is very low, but increases in the order (Table 4-9):

stream waters --> seepage zone waters --> plateau bog waters

Stream waters were collected from the same sites as the sediments (Figures 4-29 and 4-33). They almost always contain less than 1 ppt Pt (Appendix 10) with a mean Pt content of only 0.81 ppt (Table 4-9). Waters from seepage

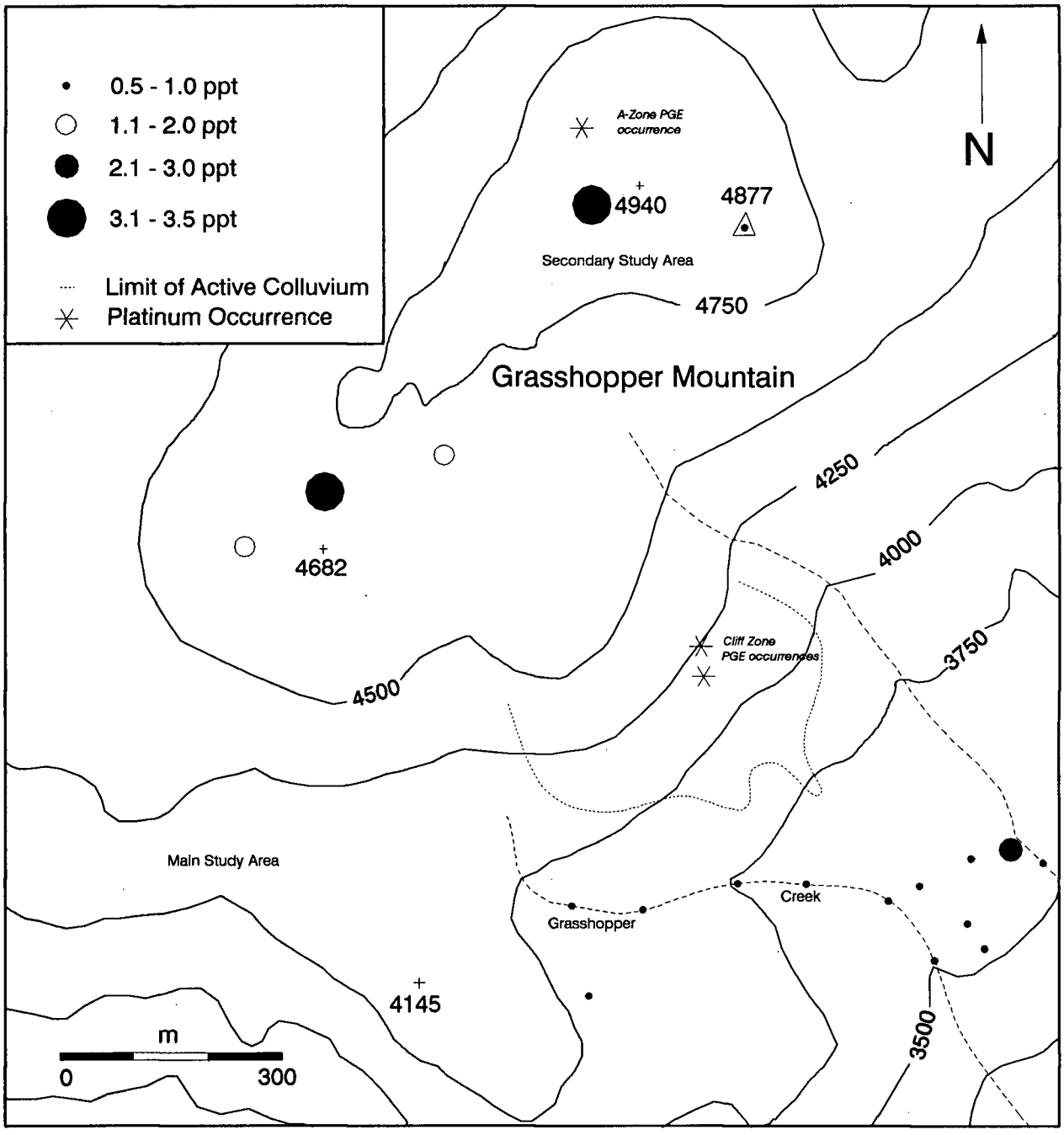

Figure 4-33. Pt content (parts per trillion) of filtered (<0.45 microns) stream, bog, and seepage waters (n=17), Grasshopper Mountain, B.C.

zones in bogs and soil pits in the lower part of the main study area average 1.05 ppt Pt. However, bog and pond waters from the plateau region of the mountain (Figure 4-33) contain 1.3 - 3.5 ppt Pt. Their mean Pt content (2.45 ppt) is 3x greater than that of stream waters. The trend to higher Pt values is associated with increasing intensity of water colour, from colourless to light brown or brown (Figure 4-34). Not all brown or light brown samples have high Pt contents, but all samples with high Pt contents have this colouration.

Water pH does not show any relation to Pt content (Figure 4-35) or categorical group (Table 4-9). Grasshopper Creek does, however, exhibit a general downstream increase in pH from 7.11 to 8.16 (Appendix 10). High-Pt plateau waters have a much narrower range of pH values (7.24-7.59) than stream and seepage zone waters (Figure 4-35).

A few other interesting relations occur in the water data. One is the relatively high (2.2/1.7 ppt) Pt content of water from the pit of soil site 46, which is situated on a clay parent material in an area of no currently-known Pt mineralization. Secondly, an unfiltered and unacidified duplicate of the 3.5 ppt sample contained only half as much Pt (1.8 ppt) as the original.

Sample Type	n	Pt (ppt)	pH
Stream waters	7	0.81 ± 0.15 (0.5 - 0.9)	7.79 ± 0.40 (7.11 - 8.16)
Seepage zone bogs and soil pits on non-dunitic till and clay	6	1.05 ± 0.58 (0.6 - 2.2)	7.04 ± 0.57 (6.30 - 7.99)
Plateau bogs and ponds on dunitic till	4	2.45 ± 1.07 (1.3 - 3.5)	7.38 ± 0.16 (7.24 - 7.59)

Table 4-9. Mean ± 1 s and range of Pt content (parts per trillion) and pH of various types of filtered (<0.45 microns) and acidified Grasshopper Mountain surface waters (n=17). Pt analyses courtesy of G.E.M. Hall, Geological Survey of Canada, Ottawa, Ontario

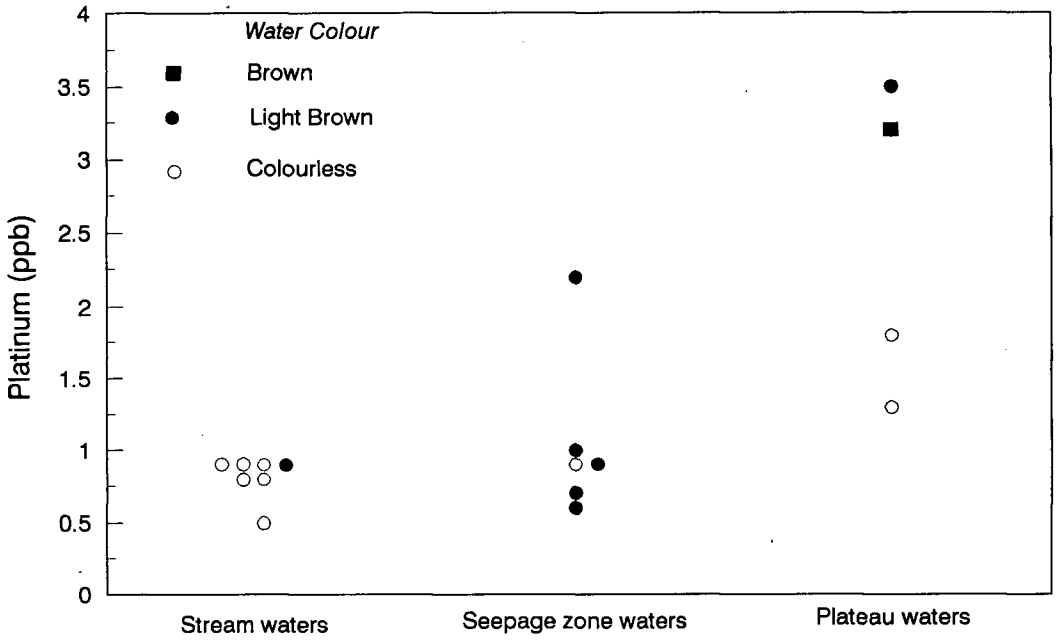

Figure 4-34. Relation between Pt content (ppt), sample type, and water colour for filtered Grasshopper Mountain surface waters.

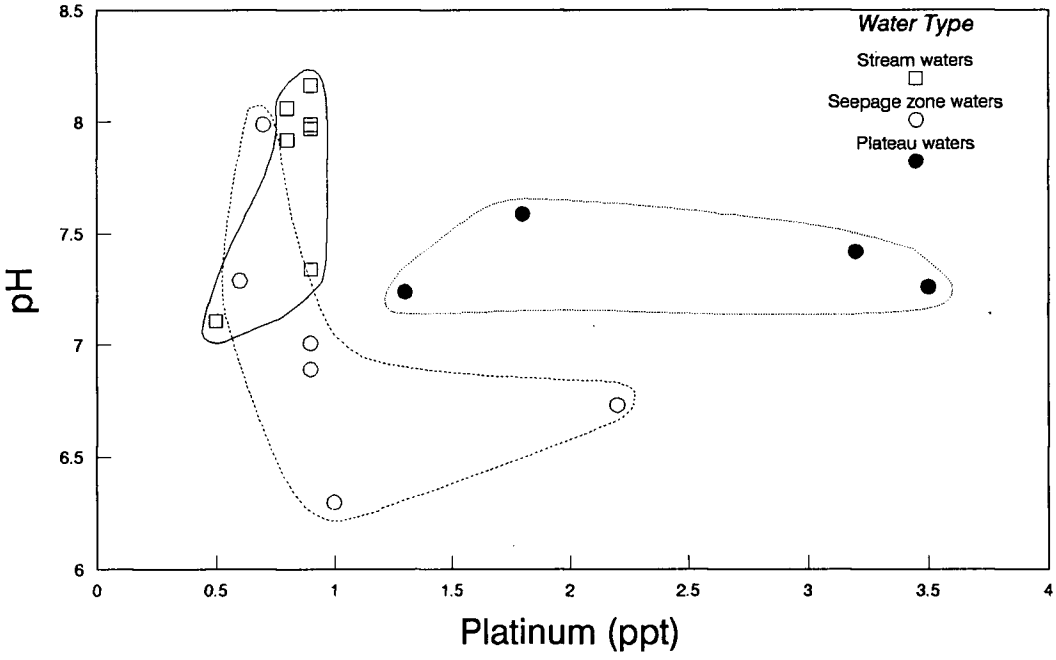

Figure 4-35. Scatterplot of Pt content (ppt) versus pH for filtered Grasshopper Mountain surface waters.

4.3 Part B - Detailed Soil Profile Results

4.3.1 Grain Size Distribution

4.3.1.1 Size Fractions

The grain size distribution among five size fractions of each horizon (Appendix 11.1), expressed as weight percent of the -10 mesh (< 2 mm) soil fraction, is shown in Appendix 11.2 and summarized by parent material type and horizon in Table 4-10.

All parent material and horizon types exhibit a bimodal grain size distribution (Table 4-10) with higher proportions in the coarse -10+40 mesh (2 mm - 425 um: coarse to very coarse sand) and fine -270 mesh (< 53 um: coarse silt to clay) fractions than in the three intermediate fractions. The highest proportion of sample in till parent materials occurs in the -270 mesh fraction; the lowest mean proportion of -270 mesh sample occurs in colluvium sites. The latter also contain the highest mean proportion of -10+40 mesh particles.

There are no strong trends in the vertical distribution of grain sizes (Appendix 11.2) within soil profiles. Colluvium exhibits relatively constant grain size distributions at all levels sampled. However, till C

Parent Material and/or Horizon	Size Fraction (ASTM)				
	-10+40 (%)	-40+70 (%)	-70+140 (%)	-140+270 (%)	-270 q(%)
NonDunitic Till: Near-Surface Horizons (3)	**22.57**[1]	**8.67**	**10.44**	**8.58**	**49.73**
	16.52[2]	8.57	9.08	8.41	46.35
	26.50[3]	8.86	12.29	8.72	53.60
NonDunitic Till: C Horizon (2)	**22.79**	**9.42**	**10.27**	**8.99**	**48.54**
	21.30	8.82	8.62	7.83	43.66
	24.27	10.01	11.91	10.15	53.42
Dunitic Till: Near-Surface Horizons (5)	**18.90**	**14.58**	**18.88**	**11.62**	**36.02**
	16.93	6.30	9.95	9.01	20.07
	22.82	23.02	26.85	13.13	56.23
Dunitic Till: C Horizon (6)	**29.10**	**13.07**	**12.12**	**8.34**	**37.38**
	22.69	9.96	9.04	7.28	19.21
	37.59	20.59	21.27	10.99	48.59
Dunitic Till (A-Zone): Near-Surface Horizons (5)	**24.35**	**6.74**	**11.74**	**9.96**	**47.21**
	21.17	4.88	9.15	8.44	45.74
	27.41	9.27	13.56	11.18	49.98
Dunitic Till (A-Zone): C Horizon (3)	**29.24**	**8.84**	**8.71**	**6.92**	**46.28**
	25.11	8.38	8.16	5.46	40.48
	37.35	9.59	9.51	8.18	50.91
Colluvium: (9)	**38.81**	**10.05**	**10.89**	**7.81**	**32.43**
	21.11	6.56	7.70	5.68	21.20
	51.03	11.68	14.95	10.19	47.19

Mean[1]
Minimum Value[2]
Maximum Value[3]

Table 4-10. Mean and range of grain size distribution of soils developed on different parent materials. All values in weight percent of the -10 mesh fraction. Numbers in parentheses ( ) at far left indicate the number of horizons in each grouping.

horizons usually contain a slightly greater proportion of -10+40 material than do near-surface horizons (Appendix 11.2). There is little change between near-surface and C horizons of the mean proportion of -270 mesh particles, although there are variations in individual profiles. For example, near-surface horizons of soil site 43 contain a disproportionally large amount of -40+70 and -70+140 mesh material and a small amount of -270 mesh material.

4.3.1.2 Density and Magnetic Fractions

Heavy mineral content (SG>3.3) content of the -70+140 and -140+270 mesh fractions (Appendices 11.3 and 11.4) ranges from 2.40-22.32 weight percent of the original fraction, with most samples in the range 5-15 weight percent (Figure 4-36). Pt content has no sympathetic relation with weight percent heavy minerals.

Relations exhibited by heavy mineral weight percent data are so varied as to render a categorical table similar to Table 4-10 meaningless, and data for each individual profile and horizon are instead shown in Table 4-11. The -70+140 mesh heavy concentrates comprise a slightly larger proportion of the original size fraction than do the -140+270 mesh concentrates (Figure 4-36 and Table 4-11), probably at least partly a function of the less efficient heavy liquid separation of the smaller particles. The lines

connecting same-profile horizons in Figure 4-36 indicate the downprofile trend of the heavy mineral content of each fraction.

Variations in the heavy mineral content with depth seem dependent on both parent material and pedogenic processes. Weight percent heavy mineral content in the -70+140 fraction decreases (or remains constant) with depth in non-dunitic till, but increases (or remains constant) with depth on dunitic till and rubble distal and proximal to A-Zone PGE mineralization. The proportion is relatively constant with depth in serpentine colluvium. Weight percent heavy minerals in the finer -140+270 fraction is generally similar to that of the coarser fraction (Table 4-11), but some profiles show very different trends with depth (Figure 4-36). Regarding pedogenic differences, the podzolic Bf horizon in soil site 20 is almost devoid of heavy minerals relative to Aej and C horizons (Table 4-11). Weight percent heavy minerals in stream sediment site 2 (88-SC-503) is similar to that in soils (Table 4-11).

Relative proportions of magnetic and non-magnetic heavy minerals in the heavy concentrates of each of the two fractions are shown in Table 4-11. Soils on non-dunitic till, and the stream sediment, have subequal proportions of magnetic and non-magnetic concentrates. The latter is usually predominant, although the podzolic Bf horizon of

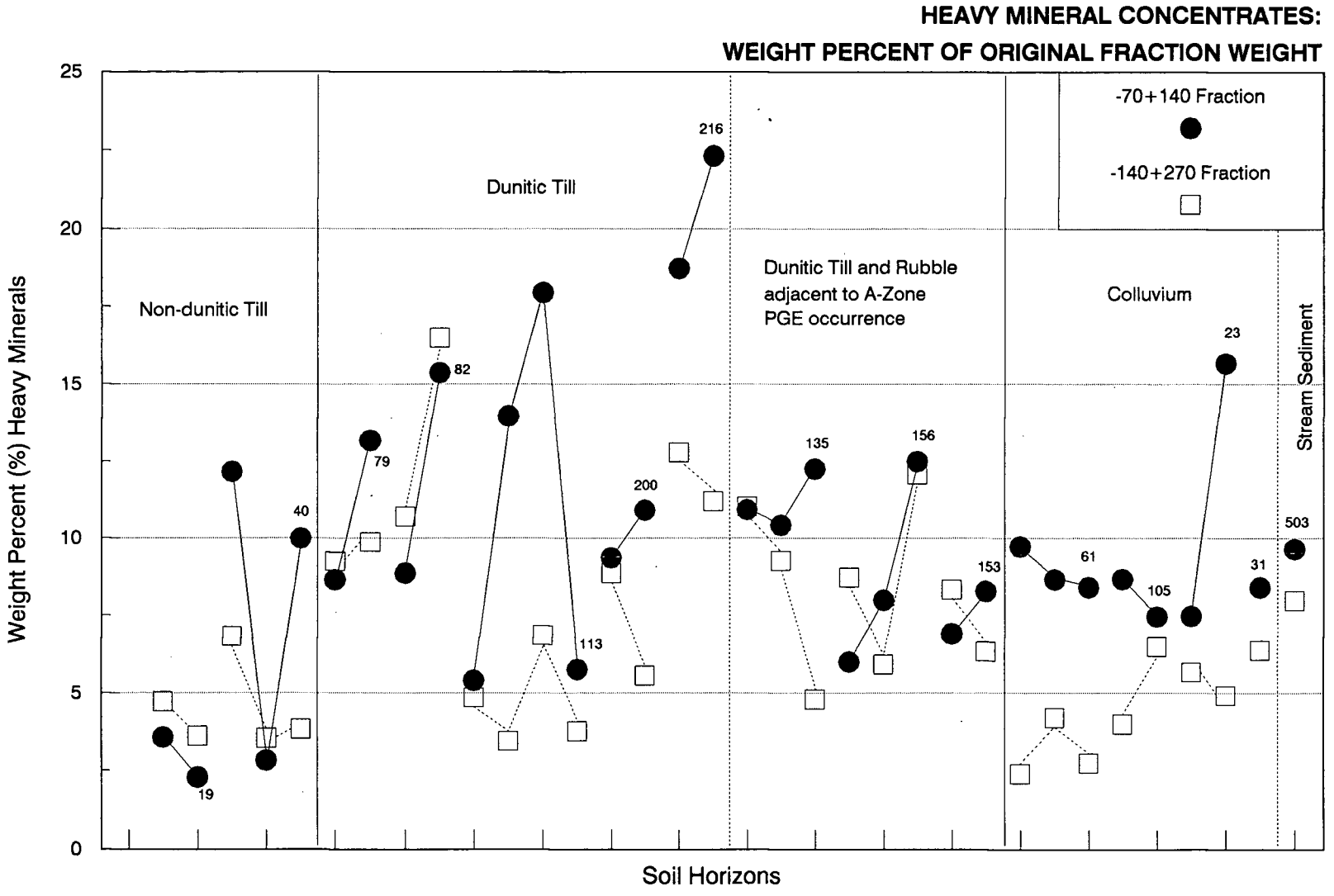

Figure 4-36. Weight percent heavy minerals (S.G.>3.3) in -70+140 and -140+270 mesh fractions of individual horizons from detailed soil profiles. Numbers are the C horizon sample numbers. Solid lines (-70+140 mesh fraction) and dashed lines (-140+270 mesh fraction) connect horizons of the same profile, and show changes in relative heavy mineral content with increasing depth in the profile.

	Soil Site	Sample Number	Horizon	Wt.% Heavy Minerals (-70+140)	Wt.% Heavy Minerals (-140+270)	Wt.% Mag Heavies (-70+140)	Wt.% Nonmag Heavies (-70+140)	Wt.% Mag Heavies (-140+270)	Wt.% Nonmag Heavies (-140+270)
Non-dunitic Till	6	18	Ah	3.57	4.72	58.90	41.10	64.23	35.77
	6	19	Cg	2.29	3.62	39.26	60.74	30.39	69.61
	20	38	Aej	12.16	6.83	15.88	84.12	31.62	68.38
	20	39	Bf	2.83	3.55	59.89	40.11	60.88	39.12
	20	40	C	10.00	3.84	23.95	76.05	44.43	55.57
Dunitic Till	33	78	Bm	8.65	9.25	70.61	29.39	64.43	35.56
	33	79	C	13.17	9.88	62.30	37.70	62.19	37.81
	34	81	IC	8.87	10.71	80.05	19.95	81.80	18.20
	34	82	IIC	15.37	16.50	58.65	41.35	53.89	46.11
	43	110	Bm	5.40	4.85	32.33	67.67	45.34	54.66
	43	111	Bm	13.97	3.45	11.56	88.44	47.40	52.60
	43	112	BC/C	17.95	6.86	9.59	90.41	28.59	71.41
	43	113	C	5.75	3.77	26.27	73.73	50.19	49.81
	69	199	Bm	9.37	8.87	63.60	36.40	66.11	33.88
	69	200	C	10.91	5.56	40.07	59.93	61.96	38.04
	73	215	Bm	18.73	12.79	19.51	80.49	31.79	68.20
	73	216	C	22.32	11.20	35.48	64.52	56.80	43.20
Dunitic Till/Rubble (A-Zone)	51	133	Bm	10.93	11.03	89.06	10.94	83.40	16.60
	51	134	BC	10.43	9.28	80.22	19.78	77.32	22.68
	51	135	C	12.25	4.79	72.51	27.49	67.42	32.58
	57	154	Bm/IC	6.00	8.73	90.15	9.85	71.20	28.80
	57	155	BC	7.99	5.92	79.44	20.55	69.65	30.34
	57	156	IIC	12.49	12.06	66.49	33.51	54.73	45.26
	56	152	C (upper)	6.91	8.34	87.01	12.99	77.29	22.71
	56	153	C (lower)	8.28	6.34	93.27	6.73	87.07	12.93
Colluvium	27	59	C (upper)	9.73	2.40	76.08	23.92	87.97	12.03
	27	60	C (middle)	8.66	4.20	83.11	16.89	87.36	12.64
	27	61	C (lower)	8.41	2.75	81.53	18.47	89.74	10.26
	42	104	C (upper)	8.67	3.99	83.72	16.28	76.65	23.35
	42	105	C (lower)	7.46	6.49	80.85	19.15	80.36	19.64
	9	24	C (upper)	7.48	5.67	82.53	17.46	82.65	17.35
	9	23	C (lower)	15.67	4.92	45.44	54.56	80.24	19.76
	16	31	C	8.41	6.37	83.67	16.33	83.22	16.77
	2	503	Sediment	9.65	7.98	53.05	46.95	52.82	47.18

Table 4-11. Weight percent heavy minerals (S.G.>3.3) in -70+140 and -140+270 mesh fractions of individual horizons of detailed soil profiles, and the proportions of magnetic and non-magnetic heavy minerals in each heavy fraction.

site 20 has a large proportion of magnetic minerals relative to other horizons in the profile. On dunitic till and colluvium, the magnetic component overwhelmingly dominates heavy concentrates of most soils. Thus, excepting soil site 43 which has a high proportion of non-magnetic heavy minerals, mean magnetic fraction weight percent of heavy concentrates from dunitic till and colluvium are 68.03% and 77.12% (-70+140 mesh), and 66.69% and 83.52% (-140+270 mesh), respectively.

Proportions of magnetic and non-magnetic concentrates vary erratically with depth in non-dunitic till but are relatively constant in serpentine colluvium. However, the proportion of magnetic concentrates generally decreases downprofile in dunitic till (Table 4-11). Dunitic rubble above the A-Zone occurrence presents one of the few exceptions to this relation.

4.3.2 Results: Platinum

A number of important trends are apparent. They relate to the general magnitude of soil Pt concentrations, its vertical distribution in soil profiles, and its residency in individual size/density/magnetic fractions. Pt distribution in size/density/magnetic fractions of all 14 detailed profiles are illustrated in Appendix 12.

4.3.2.1 Size Fractions

The Pt content of five size fractions from each horizon in 14 selected profiles was determined (Appendix 11.5). Median Pt contents of the various soil groupings are summarized in Table 4-12. Results for near-surface, intermediate and C horizons in each of the 5 size fractions are shown in Figures 4-37 to 4-39. The diagrams are arranged to show, from left to right, increasing proximity of till sites to known A-Zone PGE mineralization. Colluvium, including dunitic colluvium below the Cliff Zone PGE occurrences, is shown on the far right. Pt concentrations in each of the five fractions generally increase according to parent material, increasing in the order non-dunitic till --> dunitic till --> colluvium/A-Zone till and rubble (Table 4-12).

Pt concentrations among the five size fractions generally increase, or are constant, with depth (Figures 4-37 to 4-39). Specifically, Pt concentrations increase with depth in soils developed on non-dunitic till, usually increase or are relatively constant with depth in soils developed on dunitic till and rubble, and are usually constant with depth in unhorizonated colluvium. The highest single Pt concentration (722 ppb) occurred in the -10+40 (2mm-425 um) fraction of near-bedrock dunitic rubble above the A-Zone occurrence.

Parent material and/or horizon	Size Fraction (ASTM)				
	-10 +40	-40 +70	-70 +140	-140 +270	-270
A) Non-Dunitic Till: Near-Surface Horizons (n=3)	**7** (3-13)	**5** (3-11)	**4** (4-8)	**2** (2-9)	**7** (7-10)
Non-Dunitic Till: C Horizon (n=2)	**43** (9-77)	**15** (8-21)	**15** (6-23)	**14** (5-23)	**12** (9-14)
B) Dunitic Till: Near-Surface Horizons (n=5)	**49** (6-81)	**19** (1-113)	**20** (3-104)	**35** (6-172)	**36** (16-104)
Dunitic Till: C Horizon (n=6)	**34** (1-101)	**26** (1-76)	**24** (2-167)	**29** (7-50)	**23** (2-41)
C) Dunitic Till/Rubble (A-Zone): Near-Surface Horizons (n=5)	**92** (74-355)	**128** (103-402)	**83** (74-149)	**53** (38-90)	**76** (53-131)
Dunitic Till/Rubble (A-Zone): C Horizon (n=3)	**119** (96-722)	**588** (152-632)	**157** (155-278)	**164** (141-257)	**150** (89-260)
D) Colluvium: (n=9)	**106** (16-248)	**128** (53-388)	**74** (42-277)	**90** (41-167)	**89** (53-147)

Table 4-12. Median and range of platinum concentrations (ppb) among size fractions of soils developed on different parent materials.

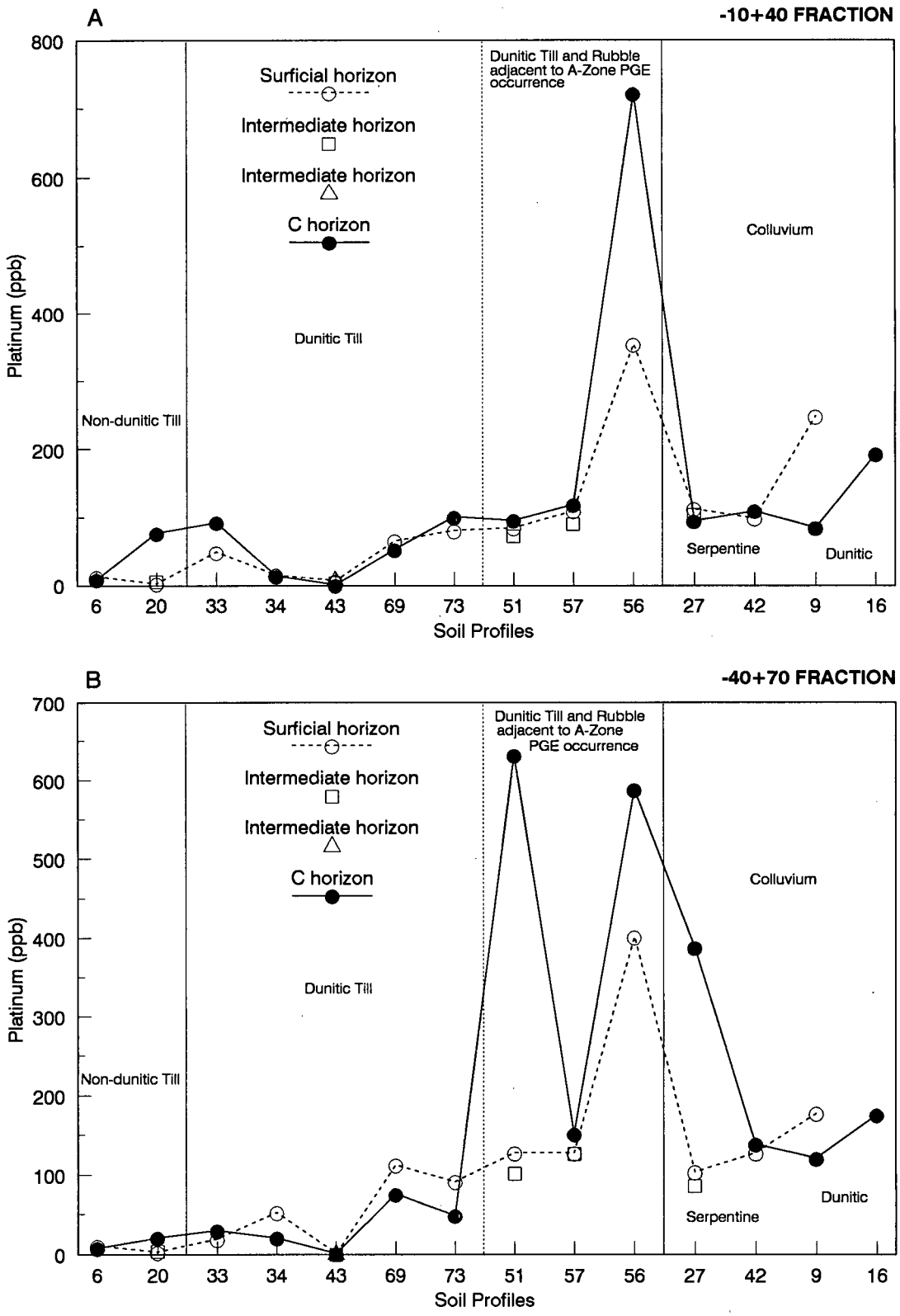

Figure 4-37. Pt content (ppb) of the A. -10+40 mesh fraction and the B. -40+70 mesh fraction of surficial, intermediate and C horizons in soils on various parent materials. Note that site 34 has a colluvium surficial horizon.

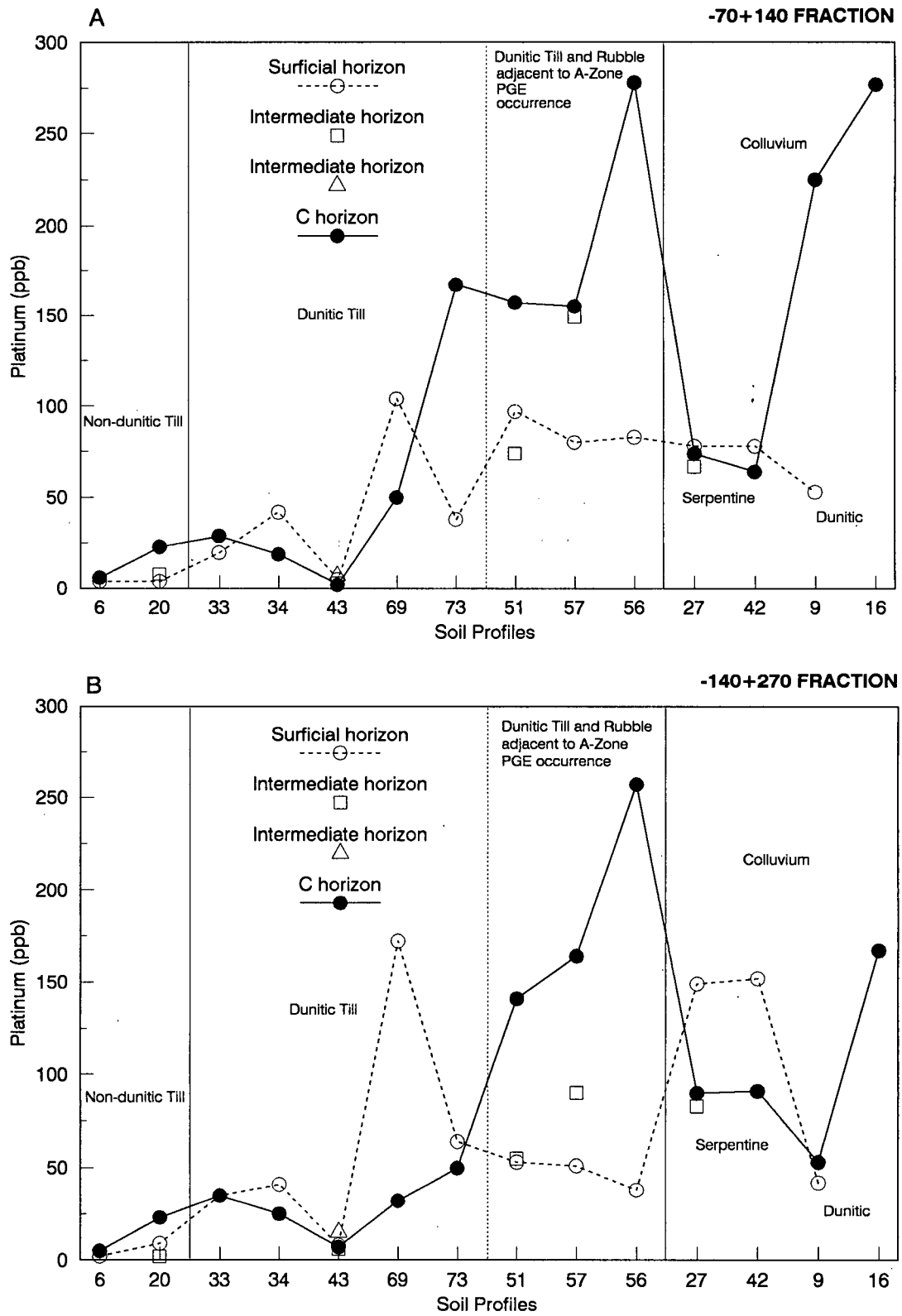

Figure 4-38. Pt content (ppb) of the A. -70+140 mesh fraction and the B. -140+270 mesh fraction of surficial, intermediate and C horizons in soils on various parent materials. Note that site 34 has a colluvium surficial horizon.

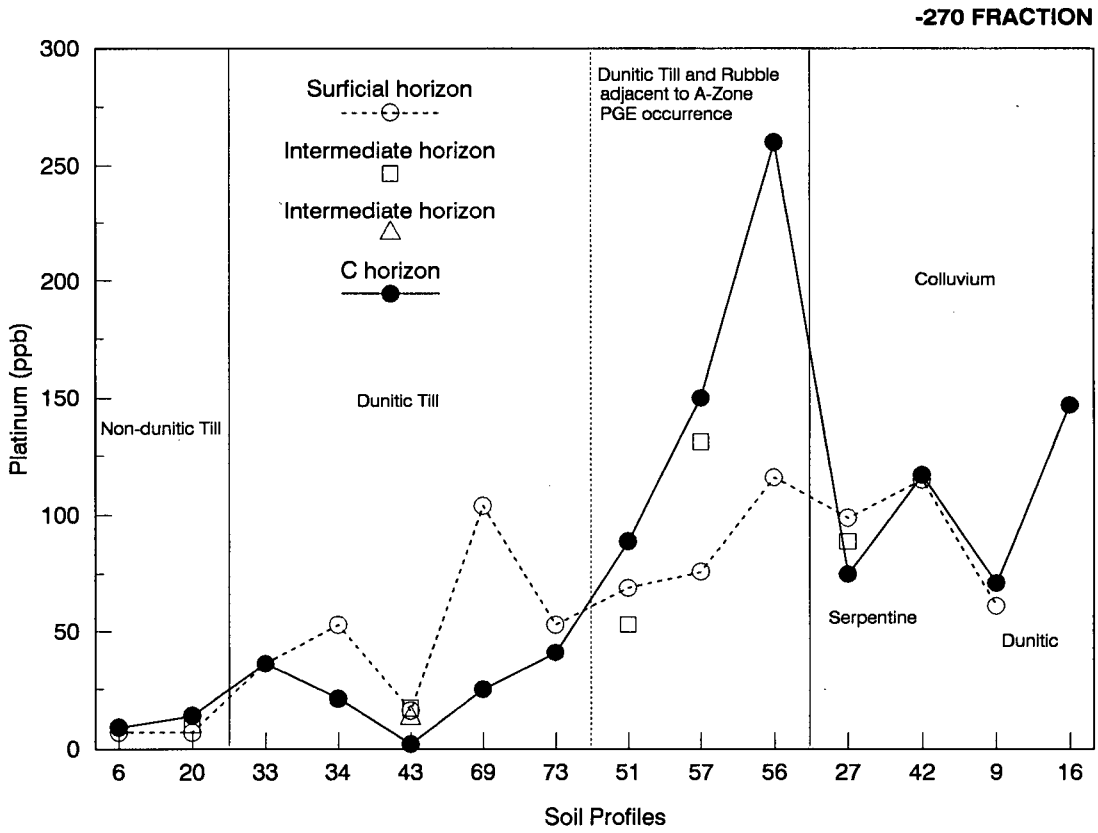

Figure 4-39. Pt content (ppb) of the -270 mesh fraction of surficial, intermediate and C horizons in soils on various parent materials. Note that site 34 has a colluvium surficial horizon.

Pt residence among the five size fractions varies slightly with parent material type (Figures 4-40 and 4-41). Low-level Pt concentrations in both surficial and C-horizons of non-dunitic till sites, although sometimes erratic, are relatively constant between size fractions. Most dunitic till horizons, including those immediately adjacent to the A-Zone occurrence, exhibit similarly-constant Pt concentrations among size fractions, although there are exceptions. For example, dunitic rubble at site 56, directly above the occurrence, contains higher Pt concentrations in the coarser size fractions. This is also observed in one colluvial site (site 9) beneath the Cliff Zone PGE occurrences, but not in the second (site 16), where Pt concentrations are remarkably constant between size fractions. Pt concentrations are also relatively constant between size fractions in serpentine colluvium (Figure 4-41).

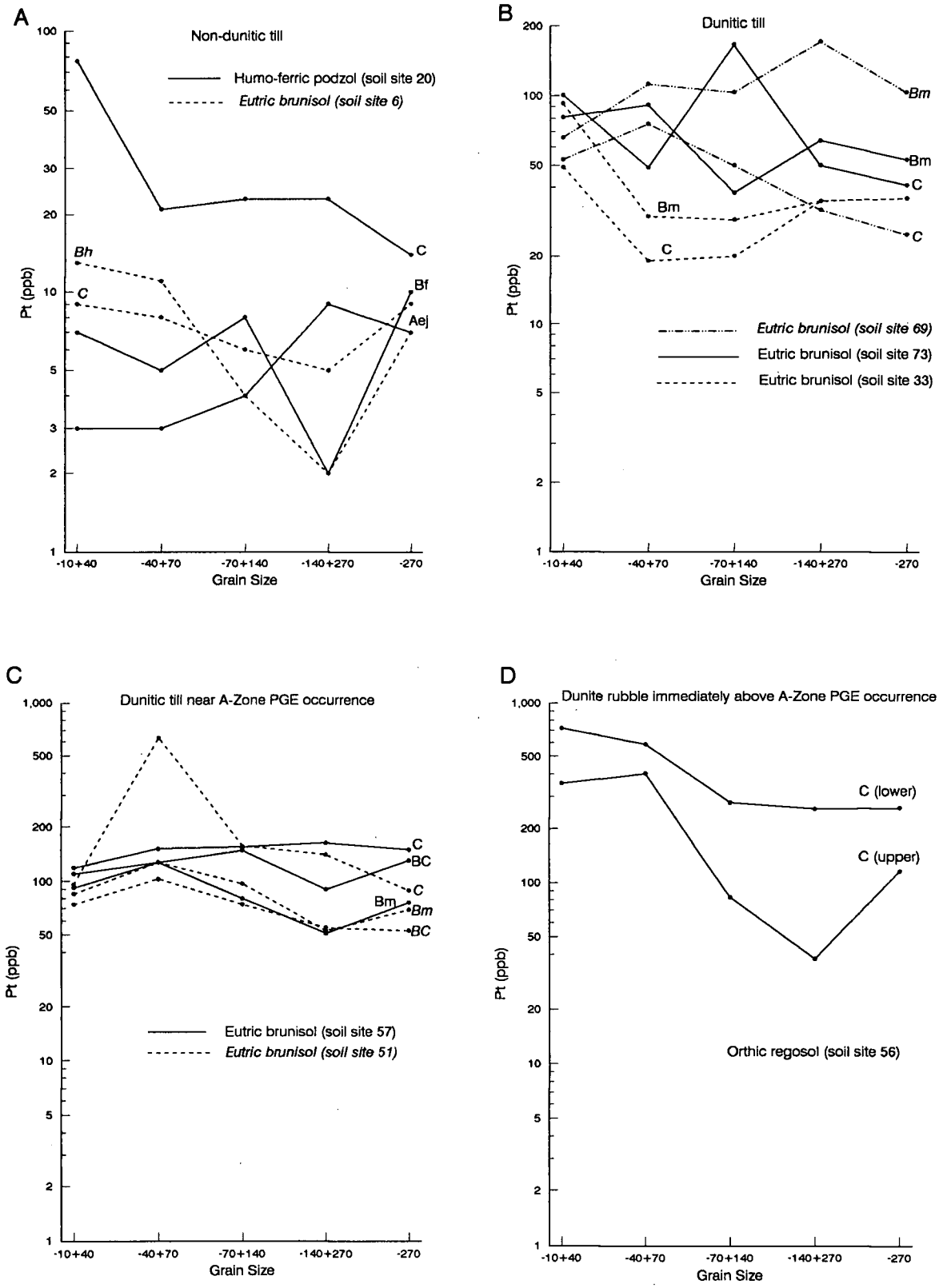

Figure 4-40. Pt distribution in size fractions of some Grasshopper Mountain soils from A. nondunitic till; B. dunitic till; C. dunitic till near the A-Zone PGE occurrence; and D. dunite rubble immediately above the A-Zone PGE occurrence

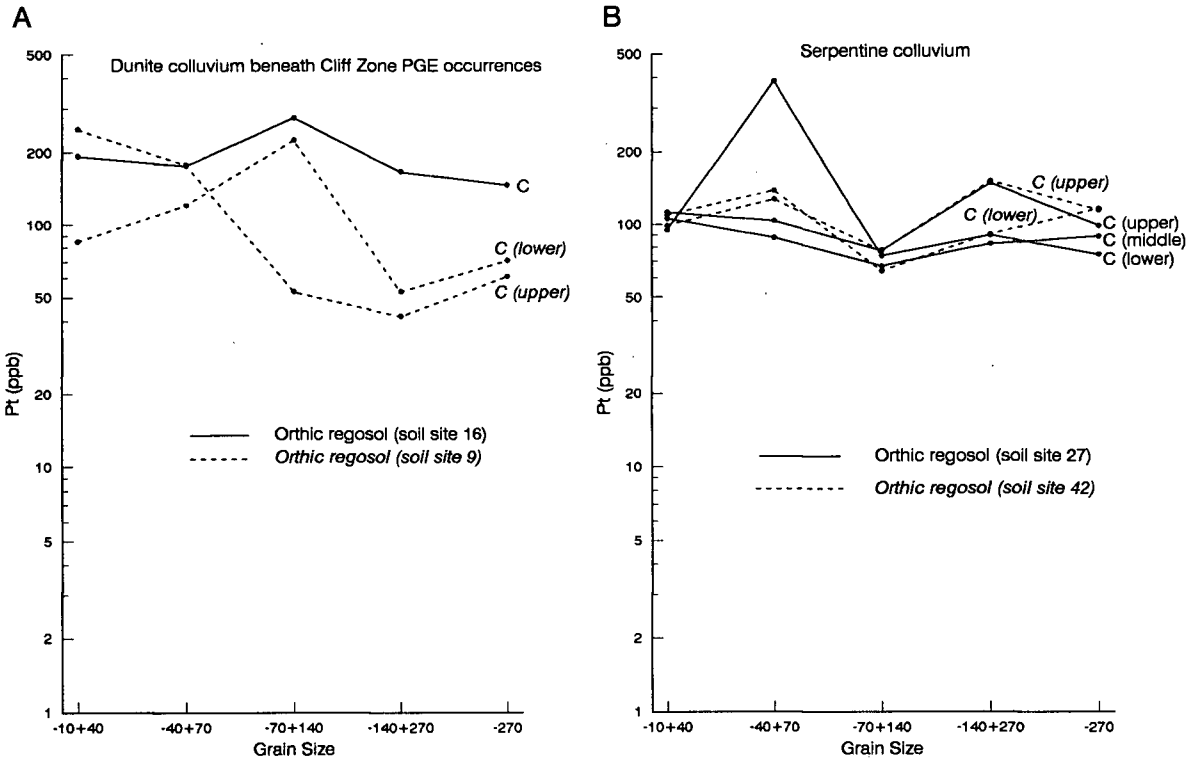

Figure 4-41. Pt distribution in size fractions of some colluvial Grasshopper Mountain soils: A. dunite colluvium beneath Cliff Zone PGE occurrences; B. serpentine colluvium.

4.3.2.2 Density and Magnetic Fractions (-70+140; -140+270)

a) Density Fractions

Pt concentrations in light and heavy mineral concentrates for the -70+140 and -140+270 mesh fractions from each horizon (Appendix 11.6) are summarized in Table 4-13 and Figure 4-42, where lines connect horizons of individual profiles.

Light Mineral Fractions

Pt concentrations in light mineral fractions (S.G. < 3.3) generally increase downprofile at till sites (Figure 4-42) and range from 1 ppb up to 160 ppb and 137 ppb in the -70+140 and -140+270 fractions, respectively. Trends in Pt concentrations follow, but are much lower than, those in the heavy mineral fractions. Maximum values are from a site directly over A-Zone PGE mineralization (Figures 4-42 and 4-48).

Heavy Mineral Fractions

Concentrations of Pt in the heavy mineral fraction (S.G. > 3.3) were obtained by calculation from analytical

results for the magnetic and non-magnetic heavy mineral concentrates. Pt concentrations in the heavy mineral fractions are typically 10 - 20x greater than in the corresponding light fraction (Appendix 11.6). They range from 11 ppb to 2538 ppb in the -70+140 size fraction, and from 22 ppb to 2027 ppb in the finer -140+270 size fraction. The highest value in the coarse fraction is from Cliff Zone colluvium, while the highest in the fine fraction is from rubble directly over A-Zone mineralization.

Pt content of the heavy mineral fraction increases (left to right in Figure 4-42) in the order nondunitic till -->dunitic till-->A-Zone dunitic till and rubble/colluvium. However, concentrations are highly variable. They increase downprofile in non-dunitic till, but decrease downprofile at some distal dunitic till sites. Concentrations increase or remain relatively constant with depth in dunitic till and rubble adjacent to mineralization, and are relatively constant with depth in colluvium.

Parent material and/or horizon	Size Fraction (ASTM)			
	Light		Heavy	
	-70 +140	-140 +270	-70 +140	-140 +270
A) Non-Dunitic Till: Near-Surface Horizons (n=3)	**3** (2-6)	**1** (1-6)	**22** (18-61)	**30** (22-46)
Non-Dunitic Till: C Horizon (n=2)	**8** (5-10)	**9** (3-14)	**105** (67-142)	**154** (66-242)
B) Dunitic Till: Near-Surface Horizons (n=5)	**9** (1-36)	**4** (3-50)	**142** (18-767)	**338** (78-1429)
Dunitic Till: C Horizon (n=6)	**13** (1-31)	**12** (1-20)	**90** (11-669)	**219** (98-329)
C) Dunitic Till/Rubble (A-Zone): Near-Surface Horizons (n=5)	**30** (21-50)	**24** (18-57)	**744** (526-1292)	**340** (193-607)
Dunitic Till/Rubble (A-Zone): C Horizon (n=3)	**70** (69-160)	**110** (74-137)	**787** (754-1590)	**817** (756-2027)
D) Colluvium: (n=9)	**40** (4-69)	**70** (2-128)	**388** (261-2538)	**503** (154-1000)

Table 4-13. Median and range of platinum concentrations (ppb) between light (S.G. < 3.3) and heavy (S.G. > 3.3) mineral fractions of soils on different parent materials.

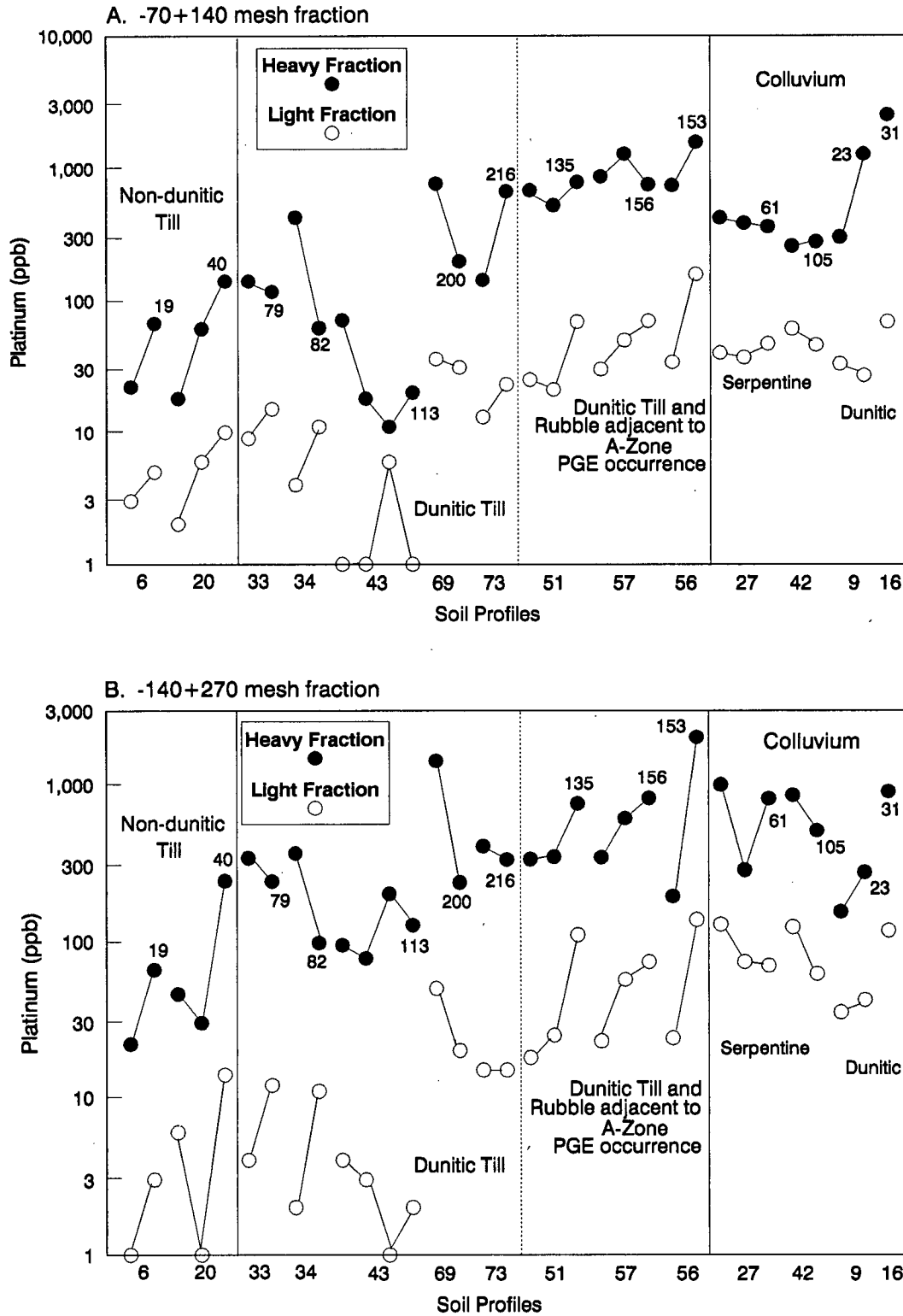

Figure 4-42. Pt distribution (ppb) in heavy and light mineral fractions of A. -70+140 mesh and B. -140+270 mesh size fractions from soil horizons in various parent materials. Solid lines connect individual horizons within soil profiles, and show changes in Pt concentration with increasing depth (left to right; numbers are C horizon sample numbers) in the profile.

b) Magnetic and Non-magnetic Fractions

Pt contents of -70+140 and -140+270 mesh magnetic and non-magnetic heavy fractions (Appendix 11.7) are summarized in Table 4-14. Maximum Pt concentrations are 4950 ppb in non-magnetic fractions and 2782 ppb in magnetic fractions. Bar graphs showing Pt contents of these and all other fractions of the 14 profiles are presented in Appendix 12.

Pt content of both magnetic and non-magnetic fractions increases in the general order non-dunitic till--> dunitic till --> A-Zone dunitic till and rubble/colluvium (Table 4-14; Figure 4-43). Pt is usually most abundant in the magnetic heavy mineral fraction in both non-dunitic till and dunitic till distal from known PGE mineralization. Concentrations are typically 10 - 20x times greater than in the corresponding non-magnetic fraction, with the difference being greatest in the -70+140 fraction. However, at dunitic till/rubble and colluvium sites immediately adjacent to both occurrences, Pt concentrations in non-magnetic fractions approach, equal or exceed those of the magnetic fractions. This also occurs in serpentine colluvium where it is most pronounced in the finer -140+270 fraction (Figure 4-43).

Pt concentrations in non-dunitic till generally increase downprofile (Figures 4-44 and 4-45; Appendices 12.1 and 12.2). For example, the magnetic-associated Pt content

Parent material and/or horizon	Magnetic		Non-magnetic	
	-70 +140	-140 +270	-70 +140	-140 +270
A) Non-Dunitic Till: Near-Surface Horizons (n=3)	**95** (34-96)	**47** (30-97)	**5** (4-8)	**9** (4-23)
Non-Dunitic Till: C Horizon (n=2)	**356** (148-563)	**330** (143-517)	**12** (9-15)	**28** (22-33)
B) Dunitic Till: Near-Surface Horizons (n=5)	**179** (51-1142)	**338** (95-1549)	**30** (10-112)	**95** (51-1195)
Dunitic Till: C Horizon (n=6)	**87** (58-1732)	**261** (59-525)	**10** (5-183)	**105** (5-539)
C) Dunitic Till (A-Zone): Near-Surface Horizons (n=5)	**759** (653-962)	**358** (185-413)	**57** (8-3225)	**261** (193-1053)
Dunitic Till (A-Zone): C Horizon (n=3)	**1075** (695-1671)	**987** (359-1857)	**466** (28-870)	**1371** (278-3172)
D) Dunite Colluvium: (n=4)	**1561** (331-2782)	**234** (168-855)	**361** (43-1601)	**673** (86-1128)
Serpentine Colluvium: (n=5)	**317** (253-393)	**284** (85-738)	**530** (257-587)	**2730** (1655-4950)

Table 4-14. Median and range of platinum concentrations (ppb) in magnetic and non-magnetic heavy mineral fractions in soils on different parent materials.

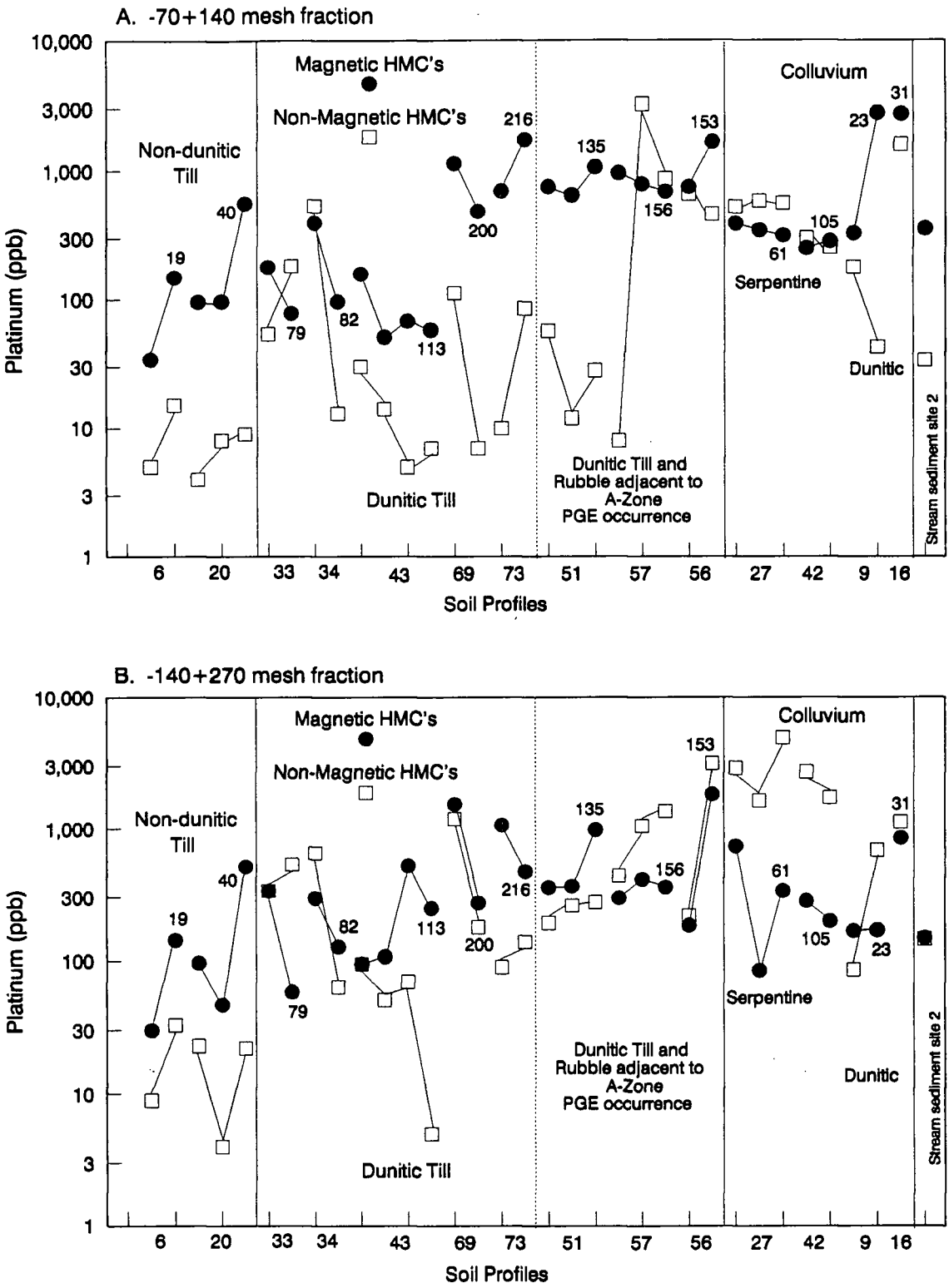

Figure 4-43. Pt distribution (ppb) in magnetic and non-magnetic heavy mineral fractions of A. -70+140 mesh and B. -140+270 mesh size fractions from soil horizons in various parent materials and a stream sediment. Solid lines connect individual horizons within soil profiles, and show changes in Pt concentration with increasing depth (left to right; numbers are C horizon sample numbers) in the profile.

of the C horizon in soil site 20 (Figure 4-46) is more than 5x greater than that of the surficial Aej horizon in both size fractions. The vertical Pt distribution is more complex in sites on dunitic till, which generally have much greater Pt concentrations than non-dunitic till sites (Figures 4-44 and 4-45; Appendices 12.3 to 12.10). Pt concentrations are quite variable with depth at sites distal to mineralization, but increase or remain constant with depth at sites adjacent to mineralization. The downprofile increase in Pt content with depth in dunitic till and rubble adjacent to and above the A-Zone PGE occurrence is illustrated in Figures 4-47 and 4-48, respectively.

The vertical distribution of magnetic and non-magnetic associated Pt in serpentine colluvium profiles is relatively constant with depth in the -70+140 fraction, but somewhat more erratic in the -140+270 fraction. Pt in dunite colluvium is erratically distributed at the single site where more than one sample was collected with depth (Figures 4-44 and 4-45; Appendices 12.11 to 12.14).

In a composite profile, where stabilized colluvium overlies dunitic till (Figure 4-49), the near-surface colluvial horizon contains 3-40x more Pt than corresponding fractions in the underlying till.

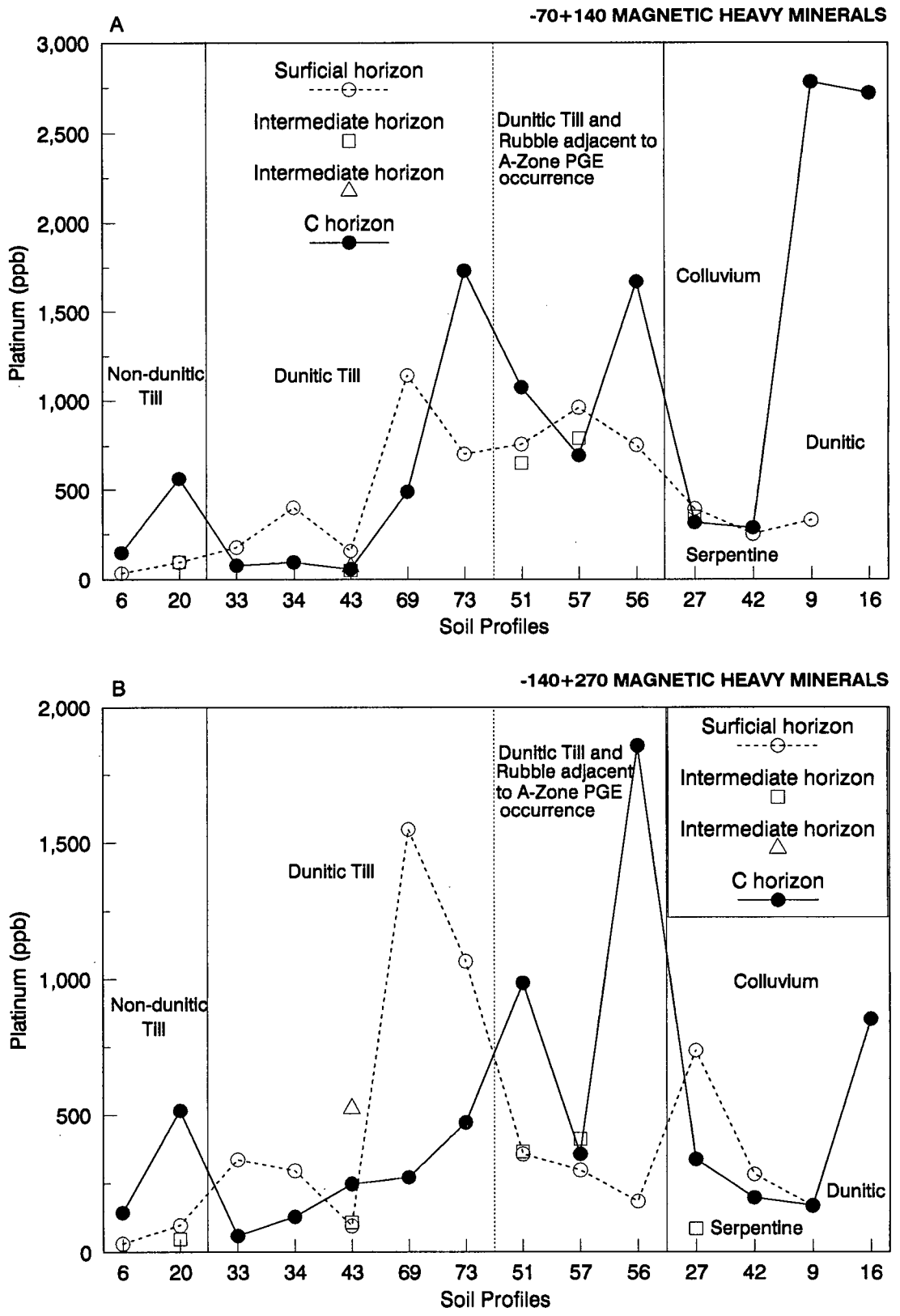

Figure 4-44. Pt content (ppb) of the A. -70+140 mesh and; B. -140+270 mesh magnetic heavy mineral fractions of surficial, intermediate and C horizons of soils on various parent materials. Note that site 34 has a colluvium surficial horizon.

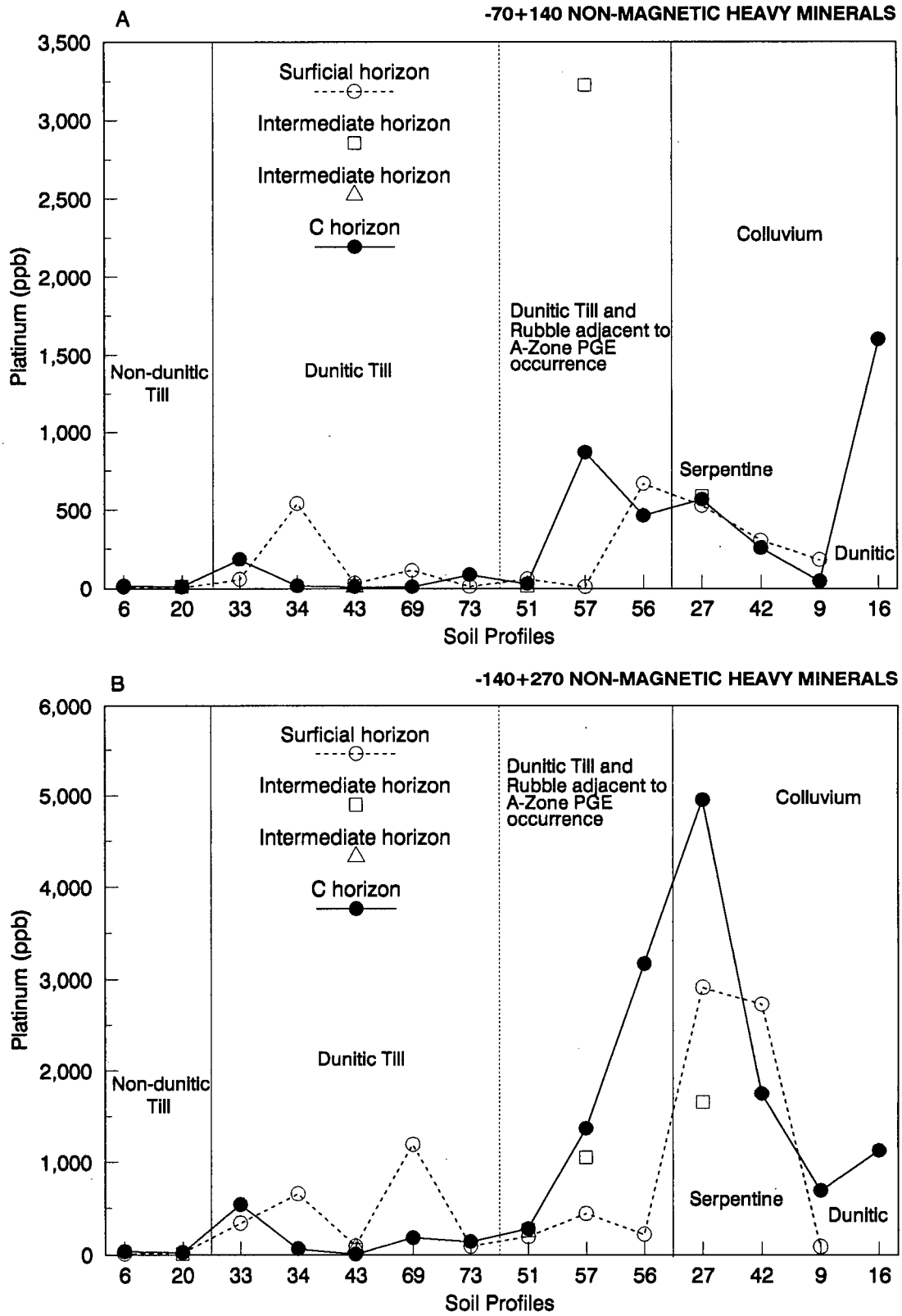

Figure 4-45. Pt content (ppb) of the A. -70+140 mesh and; B. -140+270 mesh non-magnetic heavy mineral fractions of surficial, intermediate and C horizons of soils on various parent materials. Note that site 34 has a colluvium surficial horizon.

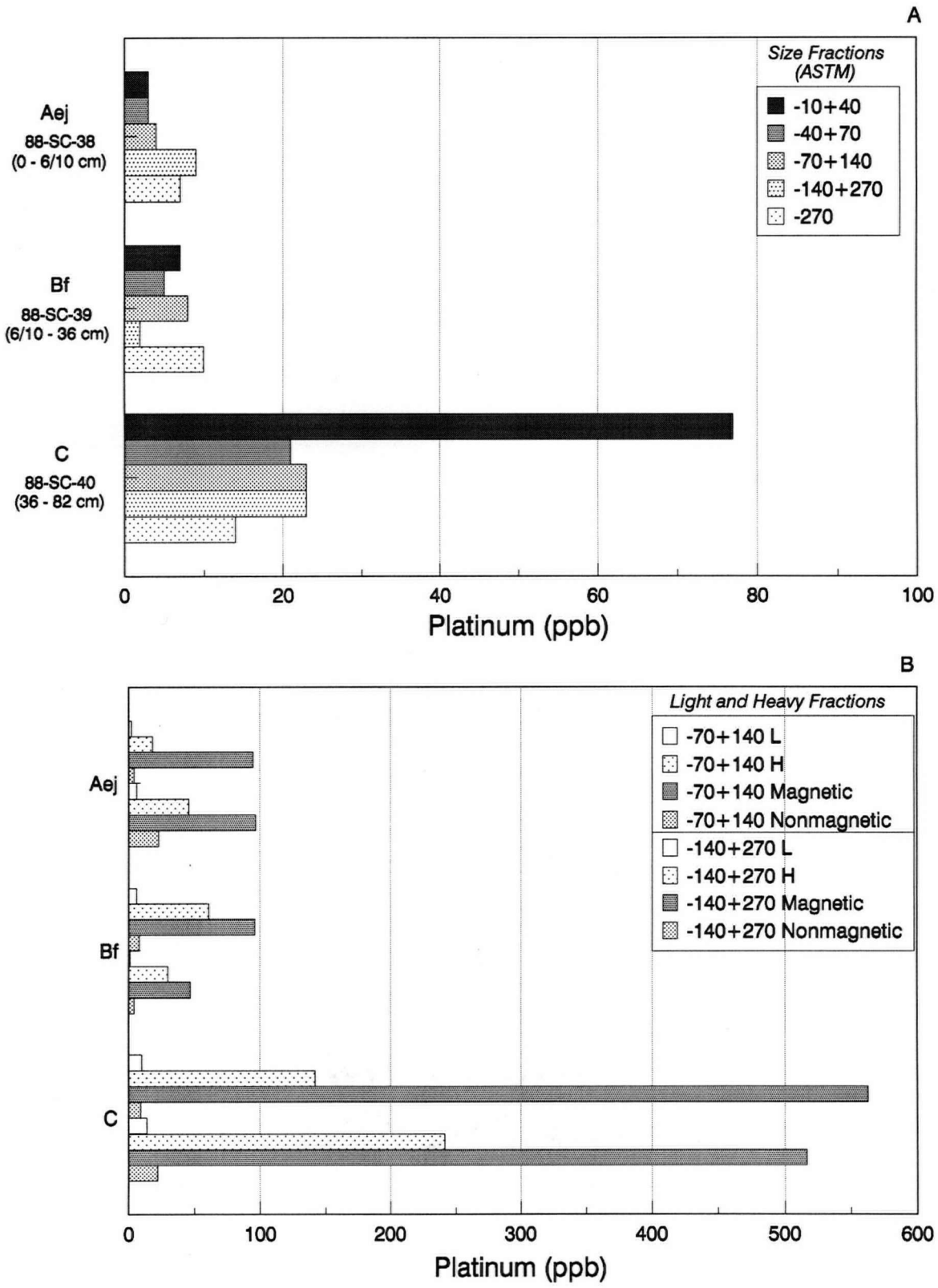

Figure 4-46. Pt distribution (ppb) in humo-ferric podzol (soil site 20) on non-dunitic till, showing A. Pt content of five size fractions and B. Pt content of light, heavy, heavy magnetic and heavy non-magnetic mineral fractions of the -70+140 (bars 1-4) and -140+270 (bars 5-8) mesh size fractions.

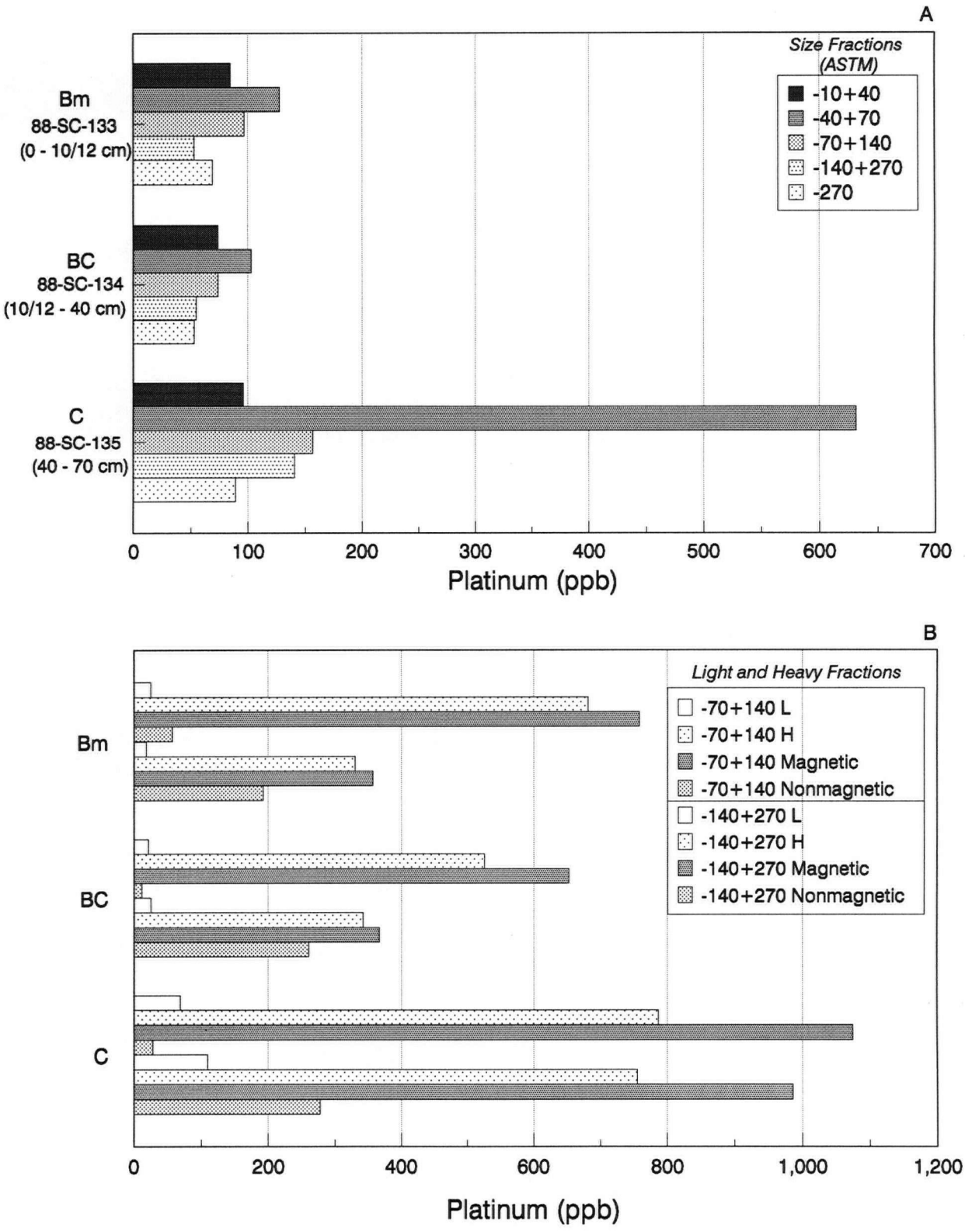

Figure 4-47. Pt distribution (ppb) in eutric brunisol (soil site 51) on dunitic till near A-Zone PGE occurrence, secondary study area, showing A. Pt content of five size fractions and B. Pt content of light, heavy, heavy magnetic and heavy non-magnetic mineral fractions of the -70+140 (bars 1-4) and -140+270 (bars 5-8) mesh size fractions.

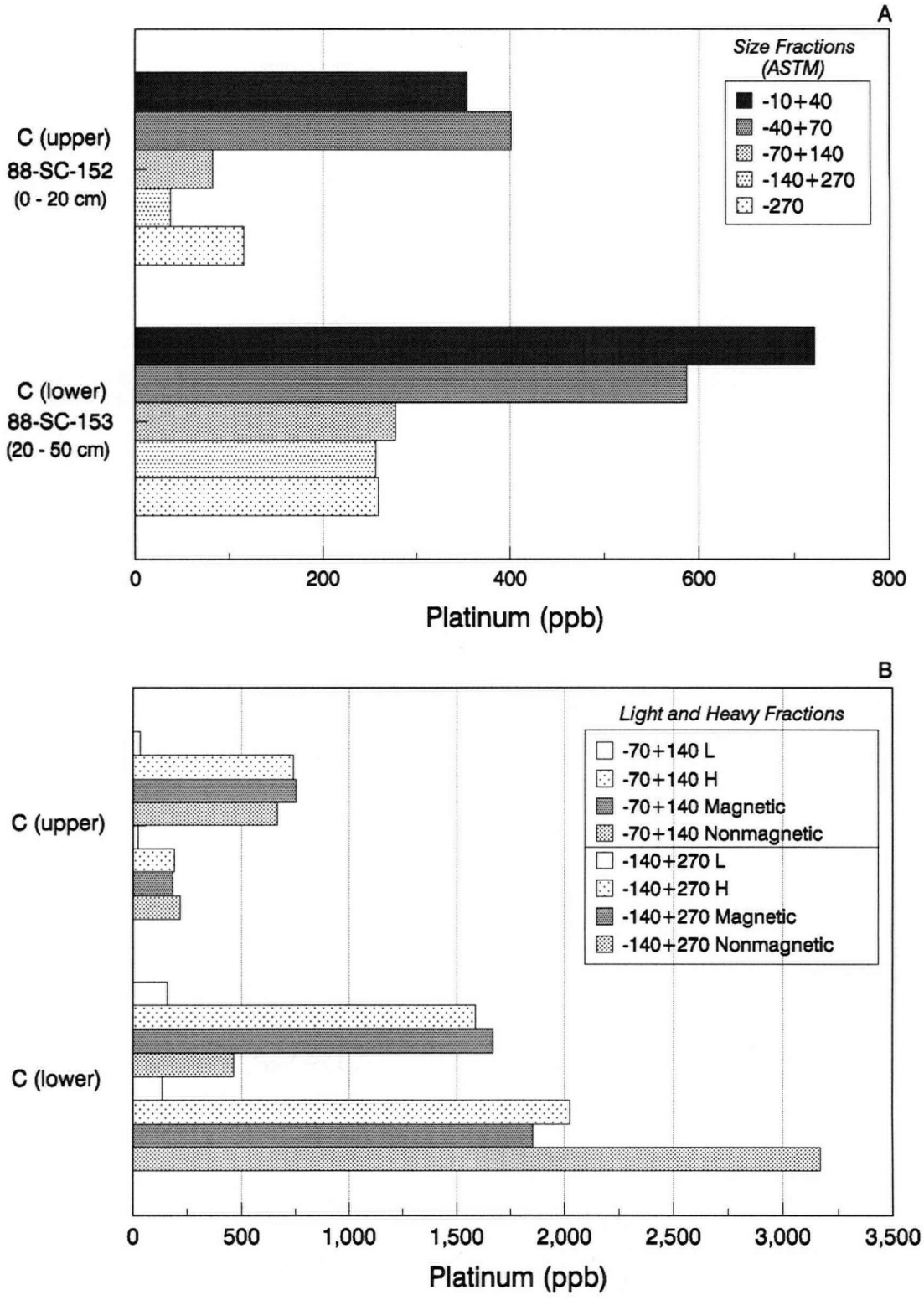

Figure 4-48. Pt distribution (ppb) in orthic regosol (soil site 56) on dunitic rubble immediately above A-Zone PGE occurrence, secondary study area, showing A. Pt content of five size fractions and B. Pt content of light, heavy, heavy magnetic and heavy non-magnetic mineral fractions of the -70+140 (bars 1-4) and -140+270 (bars 5-8) mesh size fractions.

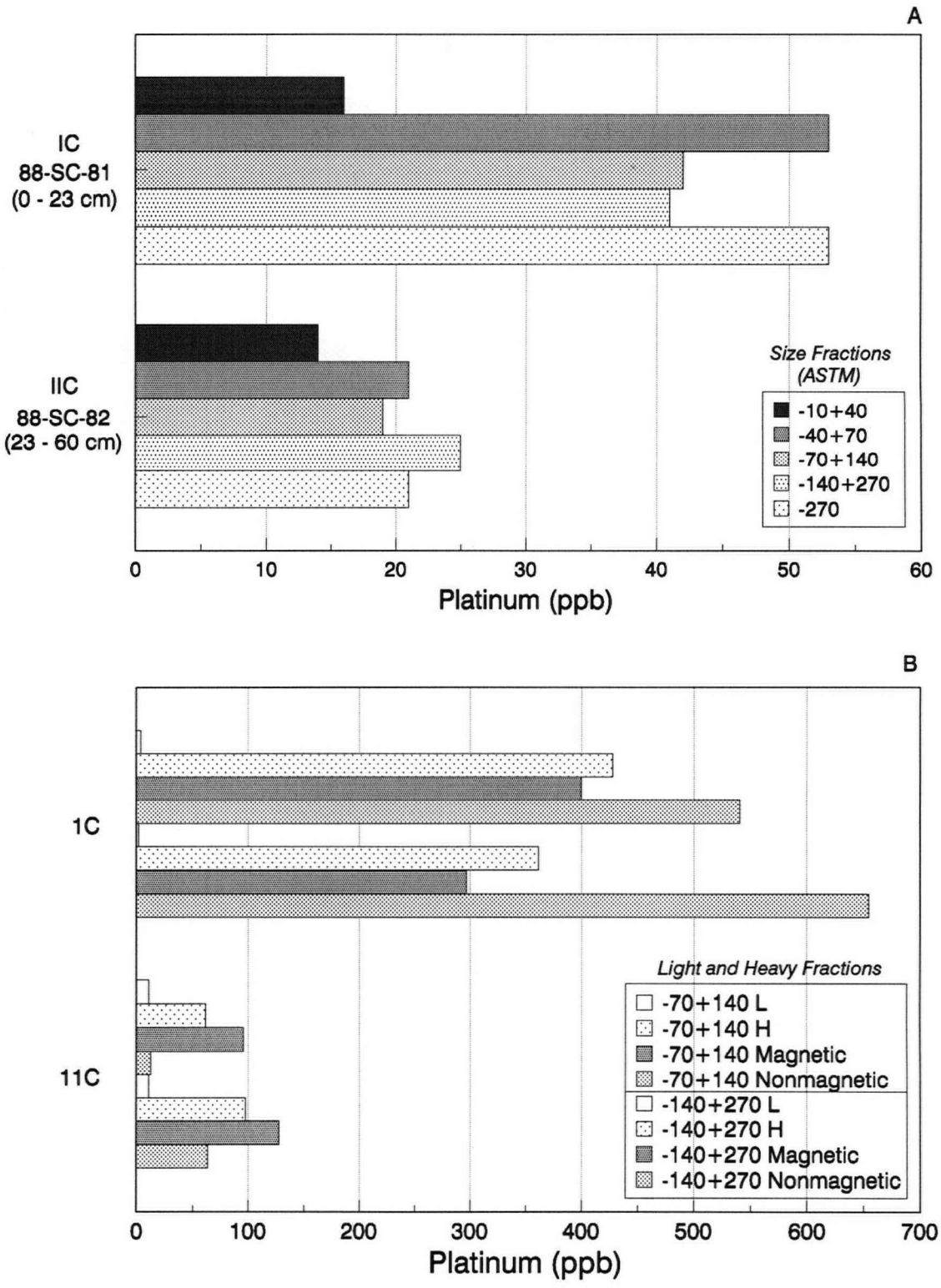

Figure 4-49. Pt distribution (ppb) in composite soil profile (soil site 34) of dunitic colluvium (IC) overlying dunitic till (IIC), showing A. Pt content of five size fractions and B. Pt content of light, heavy, heavy magnetic and heavy non-magnetic mineral fractions of the -70+140 (bars 1-4) and -140+270 (bars 5-8) mesh size fractions.

4.3.2.3 Total Pt Content of Selected Soils

Calculated total Pt contents of horizons from five selected profiles are given in Figures 4-50 and 4-51 along with stacked bar graphs showing the percent contribution of each of the five size fractions to the total Pt content of the <2mm soil. Downprofile increases in total Pt content (ppb) at 3 out of 4 till and rubble sites are consistent with previously-noted downprofile increases in Pt concentrations (section 4.3.2.1). However, one dunitic till profile (soil site 69; Figure 4-51A) exhibits a much higher Pt content in the Bm relative to the underlying C horizon.

The most striking relation in Figures 4-50 and 4-51 is that, in till, the -270 mesh fraction contains the greatest proportion of Pt and accounts for approximately one-half of total soil Pt content. In contrast, the -10+40 mesh fraction contains about one-half of the total Pt content of soils on colluvium and rubble parent materials.

There are also trends in the vertical distribution of Pt. The proportion of total Pt contained within finer-grained, particularly the -270 mesh, fractions increases toward the surface in three of the four till and rubble profiles (Figures 4-50 and 4-51). There is a coresponding decrease in the proportion of Pt in the coarser -10+40 mesh fraction of near-surface horizons. The only site (soil site

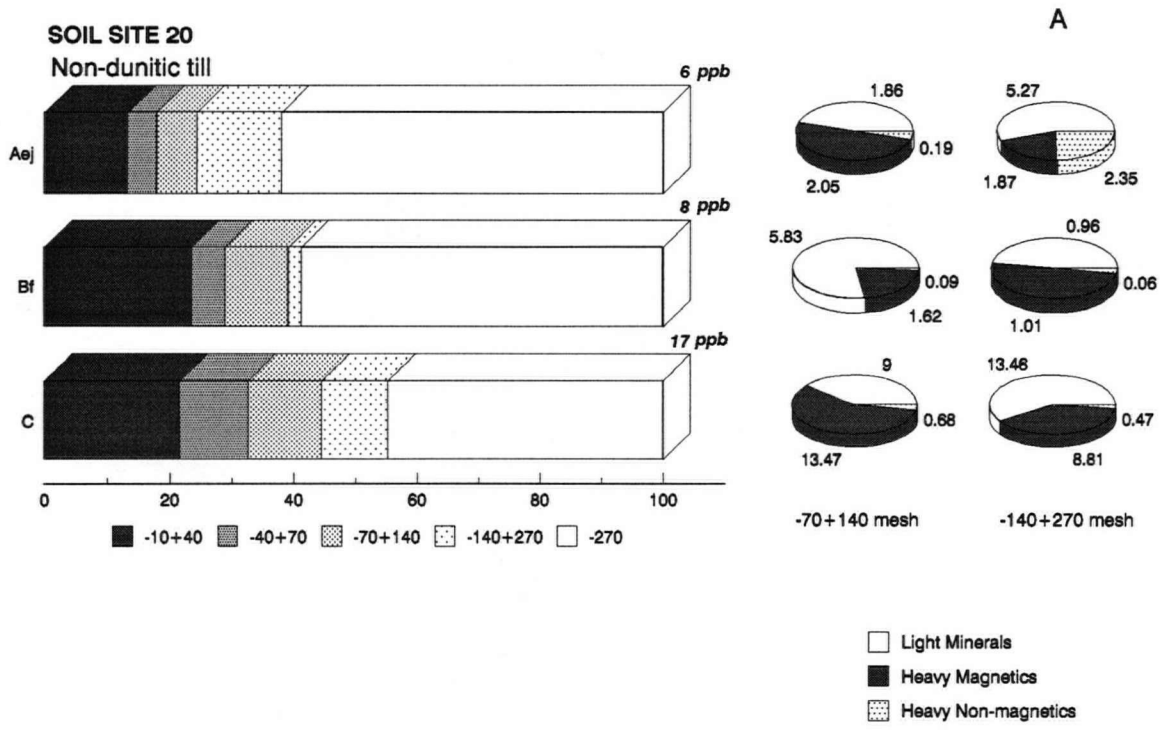

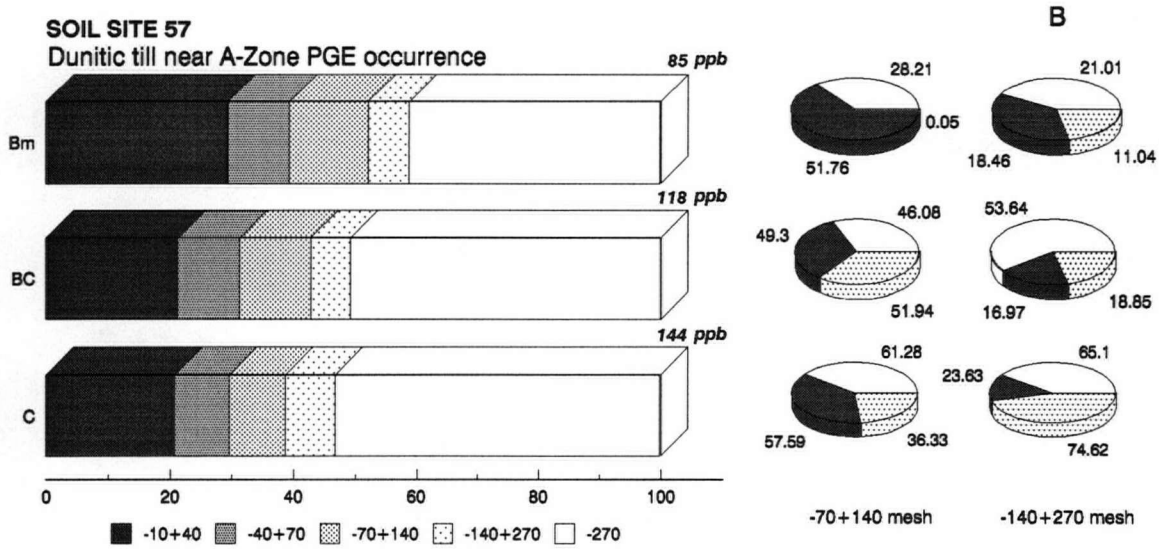

Figure 4-50. Percent contribution of individual size fractions to total Pt content (ppb; right side of each bar) of soil horizons developed in A. non-dunitic till and B. in dunitic till adjacent to the A-Zone PGE occurrence. Percent contributions of light, heavy magnetic and heavy non-magnetic mineral fractions to the -70+140 and -140+270 mesh fractions are shown in pie charts to the right of each horizon bar. Numbers indicate the Pt content (ppb) of each.

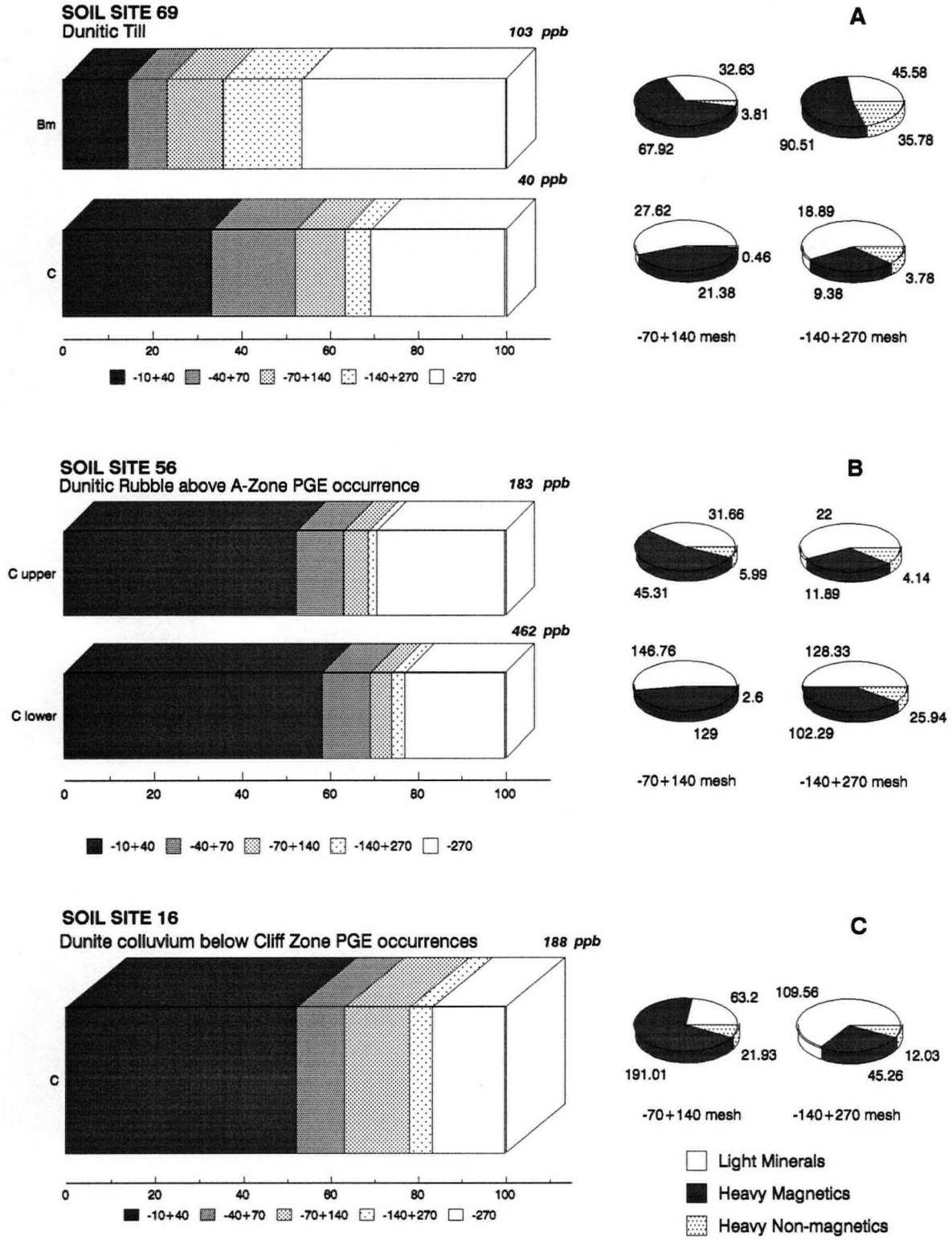

Figure 4-51. Percent contribution of individual size fractions to total Pt content (ppb; right side of each bar) of soil horizons developed in A. dunitic till; B. dunitic rubble above the A-Zone PGE occurrence; and C. dunite colluvium beneath the Cliff Zone PGE occurrences. Percent contributions of light, heavy magnetic, and heavy non-magnetic mineral fractions to the -70+140 and -140+270 mesh fractions are shown in pie charts to the right of each horizon bar. Numbers indicate the Pt content (ppb) of each.

57) at which the Pt content of the coarser fraction increases near the surface has colluvium, rather than a genetic Bm horizon, overlying till.

It is also apparent that a large proportion - about one-third to one-half - of the total Pt content of the -70+140 and -140+270 mesh size fractions is contained within the light mineral component, shown in pie graphs along with relative proportions of magnetic and non-magnetic heavy mineral fractions (Figures 4-50 and 4-51). This is despite the extremely high Pt concentrations in some heavy magnetic and non-magnetic concentrates (Table 4-14). Most Pt in the heavy mineral component occurs in the magnetic fraction, although the proportion of Pt in the non-magnetic fraction generally increases with decreasing grain size. Among the five profiles, large proportions of non-magnetic fraction Pt occur at only site 57 near the A-Zone PGE occurrence (Figure 4-50B).

4.4 Part C - Scanning Electron Microscopy and Microprobe Results

4.4.1 Introduction

Polished sections and grain mounts from eight soil sites were studied under the scanning electron microscope. Chromite grains from five magnetic fraction and five non- and paramagnetic fraction polished sections were subsequently analyzed with the electron microprobe (section 3.7). Mineralogical results for individual fractions of each of the eight soil heavy mineral concentrates are summarized in Tables 4-15 and 4-16.

4.4.2 Platinum-Group Minerals

Seven PGM grains were located in a search through 46 grain stub mounts and polished sections of magnetic, paramagnetic and nonmagnetic heavy mineral concentrates of -140+270 mesh soil fractions (see section 3.5). Five of the PGM were found in polished sections, and the other two in grain stub mounts. Tentative PGM identifications were made on the basis of EDS compositional signatures. Soil PGM occur as Pt-Fe-Ni-Cu alloys forming discrete free grains and inclusions within both chromite and Mg-silicates. They were identified only in the Cliff Zone and A-Zone areas in soil profiles proximal to known mineralization; none were found

Site	Sample	Wt.% of the Total HMC	Wt.% of the Total Size Fraction	Vol.% High Atomic No. Grains	Vol.% Low Atomic No. Grains	Magnetite: Total	Chromite: Total	Chromite: Irregular Crystals	Chromite: Fragments	Fe oxides/sulphides	Ilmenite	Zircon	Platinum-Group Minerals	Other	Pt content (ppb)	Chromite EDS Analysis Summary	Comments
	Proportion of High Atomic No. Grains: ● Dominant (>50%); ◉ Common (10-50%); • Subordinate (1-10%); X Trace (<1%)																
SITE 42	105 *Serpentine Colluvium*																
	MAGNETIC	68.64	5.28	95-100	0-5	●	•	●	◉	◉		X				199	Cr≥Fe	
	PARAMAGNETIC	12.03	0.93	85-90	10-15	X		X	●	●	•	◉		X		↓	Cr>Fe	
	NONMAGNETIC	19.33	1.49	30	70				●	●	◉	◉	•	•	X Fe-Ni sulphide	1749	Cr>Fe	chromite crystals more abundant than fragments
SITE 16	31 *Dunitic Colluvium*																
	MAGNETIC	66.67	1.71	95-100	0-5	●	X	●	◉	◉	X	X		X		855	Cr>Fe; Cr≥Fe	
	PARAMAGNETIC	13.84	0.35	50	50	•		•	●	◉	◉	◉		X	X 2 discrete Tulameenite grains	↓	Cr>Fe	chromite crystals more abundant than fragments
	NONMAGNETIC	19.49	0.50	15	85				●	X	●	◉	•	•	X Pt-Fe alloy in chromite fragment	1128	Cr>Fe	
SITE 56	153 *Dunitic Rubble (A-Zone)*																
	MAGNETIC	52.16	0.93	95-100	0-5	●	X	●	◉	◉		•			X Pt-Fe alloy in chromite crystal	1857	Fe=Cr	
	PARAMAGNETIC	10.49	0.19	90	10				●	◉	●	•	•			↓	Cr≥Fe (crystals) Cr>Fe (fragments)	primarily chromite
	NONMAGNETIC	37.35	0.67	5-10	90-95				●		●	X	•	X	X Pt-Fe alloy in chromite fragment	3172	Cr>Fe	
SITE 57	156 *Dunitic Till (A-Zone)*																
	MAGNETIC	67.15	5.59	95-100	0-5	●	•	●	◉	◉	•				X Pt-Fe alloy in Mg-silicate	359	Fe>Cr	
	PARAMAGNETIC	3.50	0.29	50	50	●		●	◉	•	◉	X				↓	Cr>Fe	
	NONMAGNETIC	29.35	2.44	10	90				•		•	X	●	•		1371	Cr>Fe	only 4 chromites

Table 4-15. Summary mineralogical results of SEM investigation of heavy mineral concentrates - Part A: colluvium and secondary study area dunitic till and rubble.

Site	Sample	Wt.% of the Total HMC	Wt.% of the Total Size Fraction	Vol.% High Atomic No. Grains	Vol.% Low Atomic No. Grains	Magnetite: Total	Magnetite: Crystals	Magnetite: Irregular	Chromite: Total	Chromite: Crystals	Chromite: Fragments	Fe oxides/sulphides	Ilmenite	Zircon	Platinum-Group Minerals	Other	Pt content (ppb)	Chromite EDS Analysis Summary	Comments
SITE 69	200 *Dunitic Till*																		
	MAGNETIC	58.87	3.25	95-100	0-5	●		●	•	•	•						273	Fe>Cr	chromites are primarily crystals
	PARAMAGNETIC	3.99	0.22	40	60	⊙	•	⊙	⊙	⊙	⊙	⊙	x				↓	Cr>Fe	chromite fragments more abundant than crystals
	NONMAGNETIC	37.14	2.05	10-15	85-90							x	●	x			179	No Chromite	
SITE 73	216 *Dunitic Till*																		
	MAGNETIC	56.80	6.35	80	20	●		●	⊙	⊙		x					474	Fe≥Cr	concentrates split from original; no duplicate
	NONMAGNETIC	43.20	4.83	0-5	95-100	⊙		⊙	•		•	x	⊙	x			139	Cr>Fe	concentrates split from original; no duplicate
SITE 20	40 *Non-dunitic Till*																		
	MAGNETIC	41.58	2.24	95-100	0-5	●	⊙	⊙	⊙	⊙	x	•					517	Fe=Cr	
	PARAMAGNETIC	2.39	0.13	50	50	⊙		⊙	•	•	•	•	⊙				↓	Cr>Fe	
	NONMAGNETIC	56.03	3.02	20	80				x	x		x	●	x		x REE mineral in apatite	22	Cr>Fe	1 chromite only
SITE 6	19 *Non-dunitic Till*																		
	MAGNETIC	21.03	0.88	95-100	0-5	●	⊙	⊙	•	•	x	x					143	Cr≥Fe	
	PARAMAGNETIC	4.81	0.20	60	40	⊙	x	⊙	⊙	⊙	⊙	⊙	⊙	x		x U-Nb-Y-K mineral in ilmenite	↓	Cr≥Fe; Cr>Fe	similar proportions of crystals and fragments
	NONMAGNETIC	74.17	3.10	10	90	•		•	•		•	•	●	⊙		x Discrete REE minerals	33	Cr>Fe	10 chromites only

Proportion of High Atomic No. Grains: ● Dominant (>50%); ⊙ Common (10-50%); • Subordinate (1-10%); x Trace (<1%)

Table 4-16. Summary mineralogical results of SEM investigation of heavy mineral concentrates - Part B: dunitic and non-dunitic tills.

in background-level dunitic or non-dunitic till profiles. No Pt-arsenides, antimonides or other non-Pt-Fe alloy PGM phases previously identified in Tulameen chromitites or placer nuggets (Aubut, 1978; St. Louis et al, 1986; Nixon et al, 1990) were found in the soils. With one exception, PGM were located exclusively in those heavy mineral fractions with a Pt concentration of at least 1000 ppb (1 ppm).

4.4.2.1 Discrete Free PGM

Two discrete free PGM grains were observed, both within the paramagnetic heavy fraction of C horizon colluvium (soil site 16; sample 88-SC-031) immediately beneath the Cliff Zone PGE occurrences. One grain (31PM-1) was observed in the grain stub mount, while the second (31PM-2) was observed in polished section (Figure 4-52). Both were by far the largest PGM grains encountered in the study. Grain 31PM-1 is about 115 um x 103 um, with an equant habit. Grain 31PM-2 is approximately 85 um x 53 um with an elongate prismatic shape and weakly crystalline outline in section.

Grain 31PM-1 was partially obscured by other grains in the stub mount. It is tentatively identified as *tulameenite* (Pt_2FeCu) on the basis of a Pt-Fe-Cu EDS analysis. The section of grain 31PM-2 is more informative. It also exhibits a Pt-Fe-Cu (tulameenite) surface/rim composition,

Figure 4-52

Discrete Free PGM

A. Backscatter SEM photomicrograph of free PGM grain (31PM-2) from paramagnetic heavy fraction of C horizon colluvium beneath Cliff Zone PGE occurrence.

B. Backscatter SEM photomicrograph showing close-up of 31PM-2. Pt-Fe-Cu alloy rim surrounds relict core of Pt-Fe alloy.

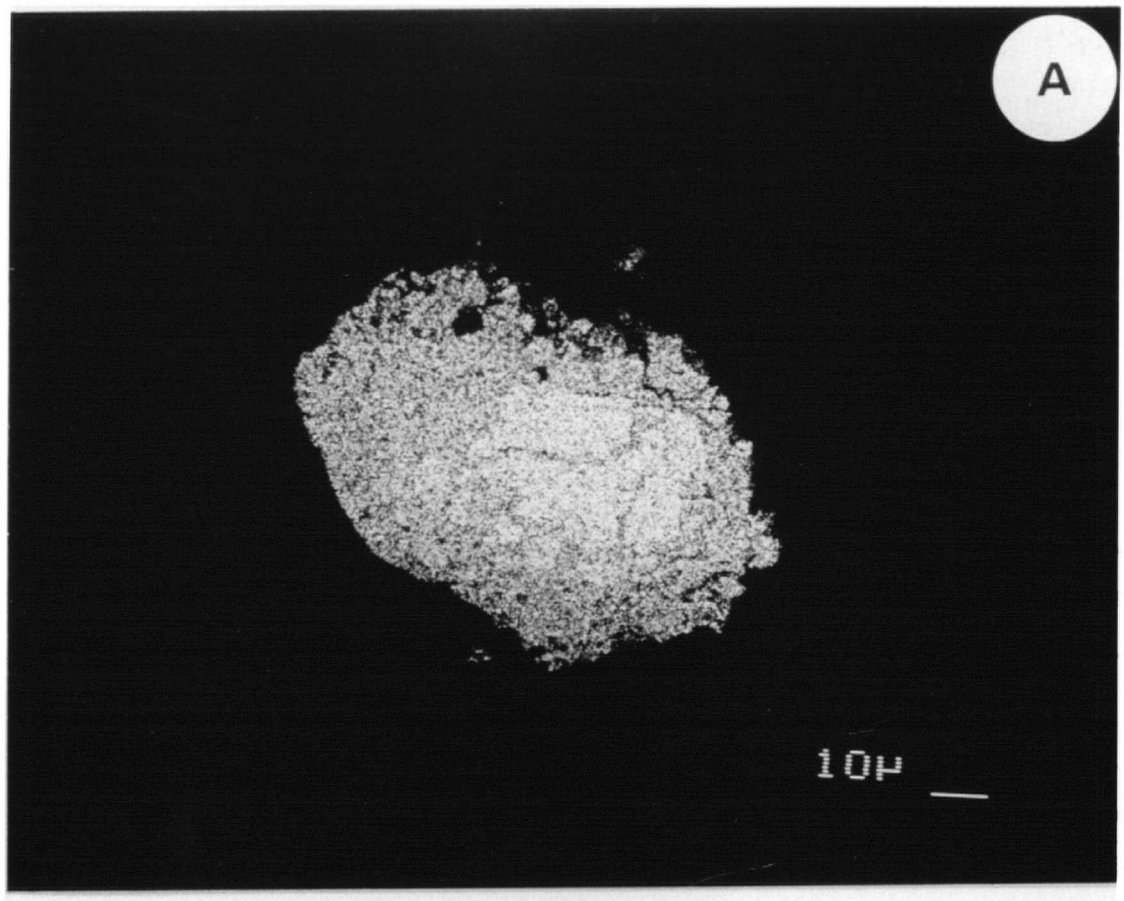
A
10μ

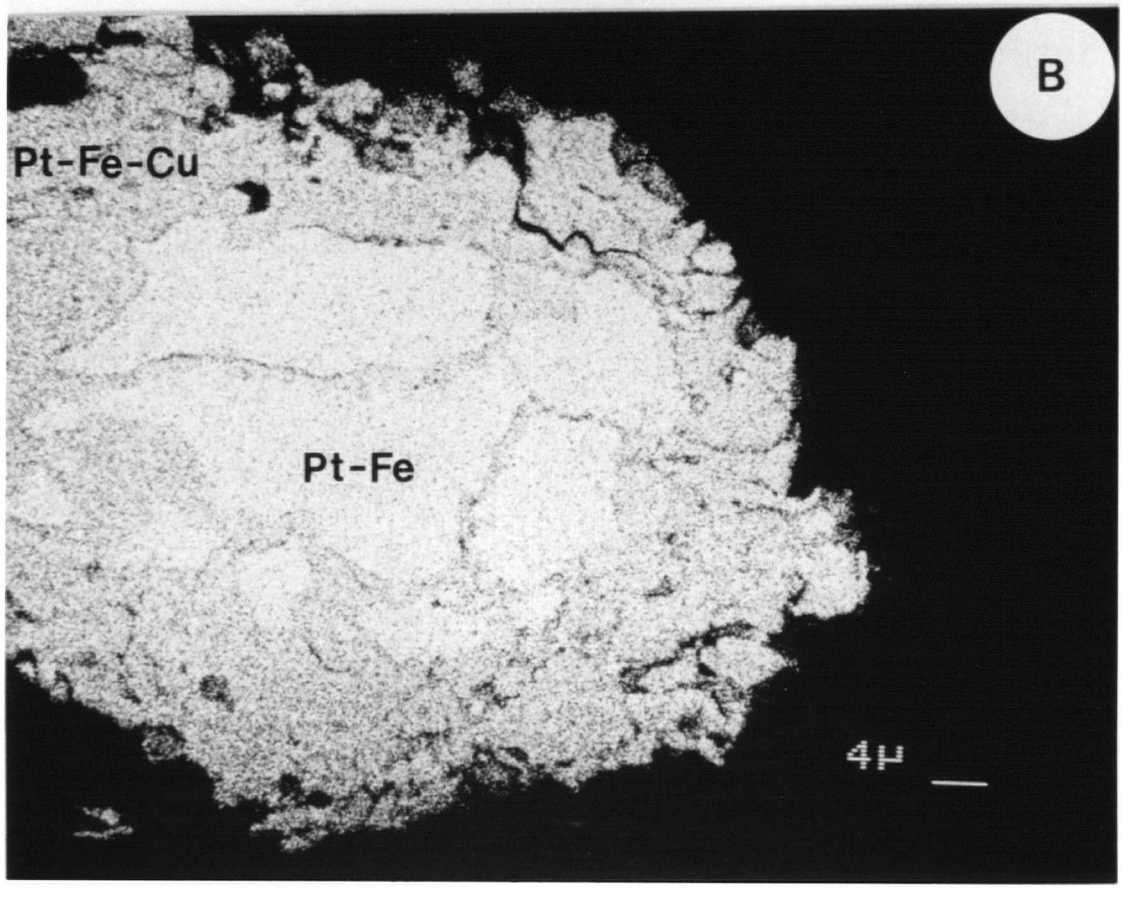
B
Pt-Fe-Cu
Pt-Fe
4μ

but contains a relict internal Pt-Fe alloy core tentatively identified as *isoferroplatinum* on the basis of relative peak heights. This, comprising about a third of the grain, is distinguished from the surrounding tulameenite in backscatter electron imaging (Figure 4-52) as a slightly brighter area indicative of a higher Pt content. Cu is virtually absent in the core compared to the surrounding tulameenite; the proportion of Fe, as estimated from peak heights, is approximately the same. The generally corroded appearance of the core and its transection by tulameenite suggests a replacement texture of Pt-Fe alloy by tulameenite. The corroded outer rim of the grain is suggestive of surface weathering.

4.4.2.2 PGM Inclusions in Mg-silicates

A single PGM inclusion (156M-1) was found in a Mg-silicate grain from the magnetic fraction of C horizon soil (sample 88-SC-156; soil site 57) in a dunitic till profile about 70 m SSW of known PGE mineralization at the A-Zone. The Mg-silicate grain is tentatively identified as talc ($Mg_3Si_4O_{10}[OH]_2$) on the basis of relative Mg and Si peak heights from EDS analyses, and from the x-ray diffraction determination of talc as the dominant Mg-silicate constituent of the -270 mesh fraction of this horizon (Appendix 6.2). The talc grain (Figures 4-53A and B) is

approximately 100 x 65 um and also contains disseminated magnetite and possibly chromite.

The PGM inclusion is triangular or heart-shaped, and is approximately 9 um x 9 um (Figure 4-53C). The lower third of the grain is partially obscured by covering talc; part of the upper two-thirds exhibits the remnant of a partially-shattered hexagonal crystal habit. Backscatter electron imaging (Figure 4-53D) and EDS analyses show it to be a Pt-Fe alloy with very little Cu or Ni, but considerable differences in the relative proportions of Pt and Fe as estimated by peak heights. Three darker areas exhibit a relatively high Fe composition relative to Pt, suggestive of a *tetraferroplatinum* (Pt_2Fe_2) composition. The proportion of Pt varies even within this grouping. The lower portion of the crystal exhibits a much darker backscatter image than the upper portion, and contains a much higher proportion of Fe to Pt. It may be a more Pt-poor variety of tetraferroplatinum. The top left corner of the PGM exhibits the reverse, a much higher proportion of Pt to Fe similar to that observed in free PGM grain 31PM-2. This portion of the PGM is tentatively identified as *isoferroplatinum* (Pt_3Fe).

Figure 4-53

PGM Inclusions in Mg-silicates

A. SEM photomicrograph of Pt-Fe alloy inclusion (156M-1) in Mg-silicate (talc?) grain with minor magnetite from magnetic heavy fraction of C horizon till (site 57) near the A-Zone PGE occurrence.

B. SEM photomicrograph showing close-up of Pt-Fe alloy inclusion 156M-1 in Mg-silicate (sil).

C. SEM photomicrograph of Pt-Fe alloy inclusion 156M-1.

D. Backscatter SEM photomicrograph of Pt-Fe alloy inclusion 156M-1. Brighter areas indicate locations of higher Pt content in the grain.

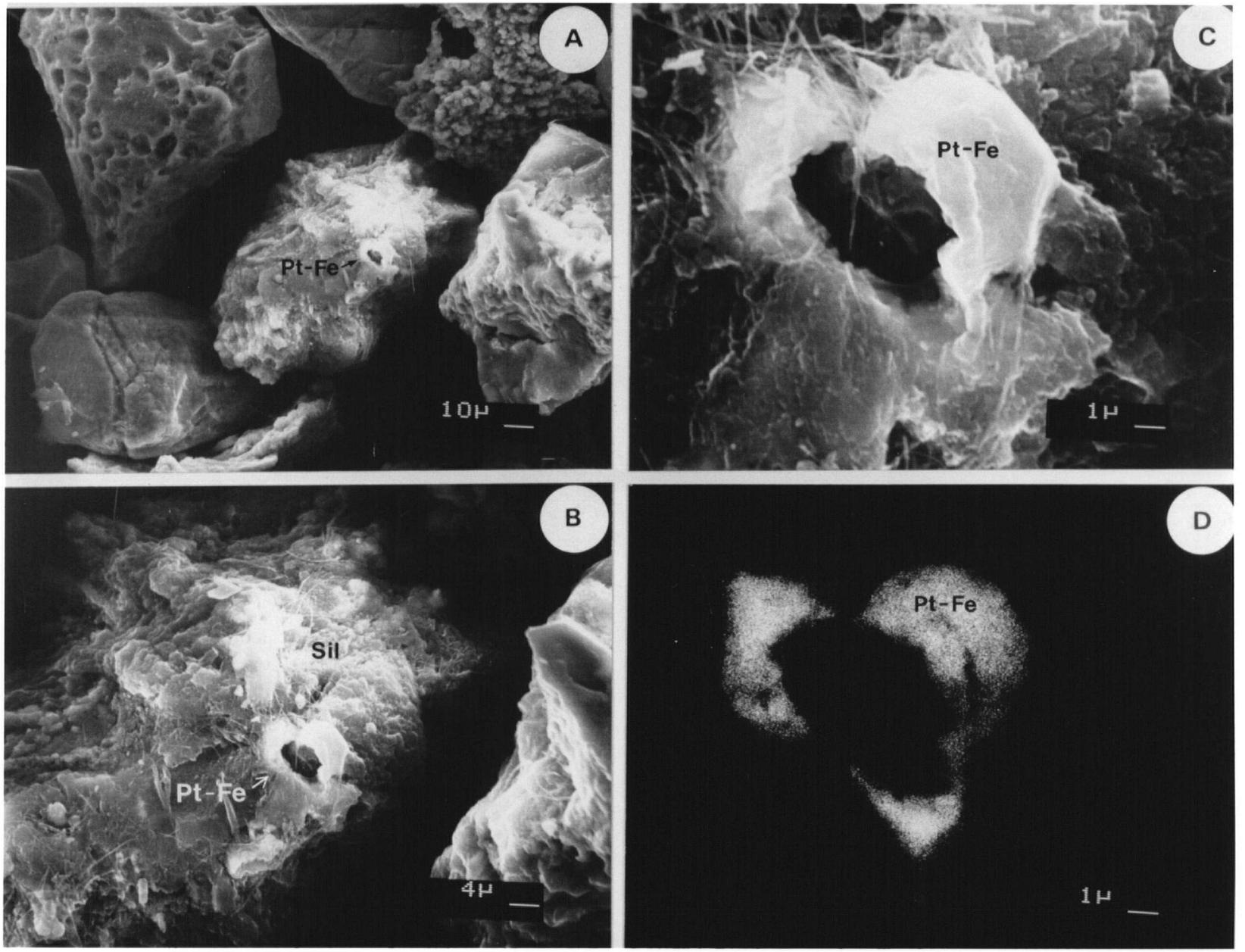
A
Pt-Fe
10μ
C
Pt-Fe
1μ
B
Sil
Pt-Fe
4μ
D
Pt-Fe
1μ

4.4.2.3 PGM Inclusions in Chromite

Four PGM inclusions (Figures 4-54 and 4-55) were found within three soil chromite grains, all from near known PGE mineralization. Three PGM, including two within the same host grain, were found within chromite from both the magnetic (153M-1, 153M-2) and non-magnetic (153NM-1) heavy fractions from C horizon dunitic rubble (soil site 56) directly above the A-Zone PGE occurrence. The fourth (31NM-1) was found in chromite of the non-magnetic heavy fraction from C horizon colluvium (soil site 16) beneath the Cliff Zone PGE occurrences.

The two PGM in the magnetic fraction occur within a single chromite crystal (Figure 4-54), while the two PGM in non-magnetic fractions occur as inclusions within chromite fragments (Figure 4-55). EDS analyses of the PGM-bearing fragments indicate a Cr>Fe composition similar to those of other fragments from these sites. EDS analysis of the PGM-bearing chromite crystal indicate a subequal Cr>Fe composition also similar to other crystals at that site (section 4.4.4). Characteristic of each of the PGM is their location near the edge of the host grains; none are found at the centre of a chromite.

The four PGM inclusions exhibit similar euhedral to subhedral habits. The largest PGM (153M-1) is prismatic and

Figure 4-54

PGM Inclusions in a Chromite Crystal

A. Backscatter SEM photomicrograph of PGM-hosting detrital chromite crystal (cmt) from magnetic heavy fraction of C horizon rubble (site 56) immediately above the A-Zone PGE occurrence.

B. Backscatter SEM photomicrograph showing location of two Pt-Fe alloy inclusions (153M-1, lower; and 153M-2, upper) in the same chromite crystal (cmt) as in A. above.

C. Backscatter SEM photomicrograph showing close-up of Pt-Fe alloy inclusion 153M-1 in detrital chromite crystal (cmt). Note absence of compositional zoning.

D. Backscatter SEM photomicrograph showing close-up of Pt-Fe alloy inclusion 153M-2 in detrital chromite crystal (cmt).

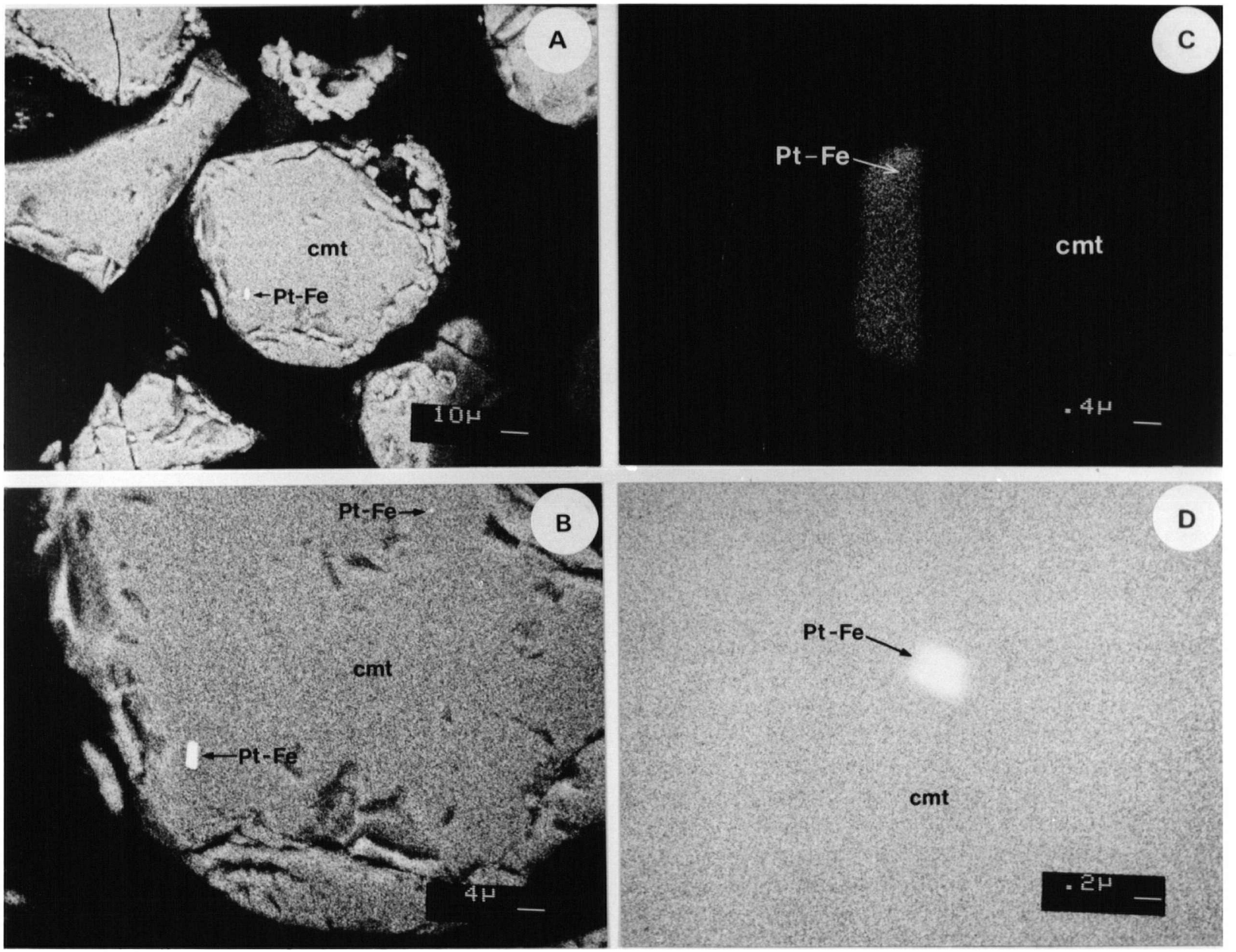
A
cmt
Pt-Fe
10μ
C
Pt-Fe
cmt
.4μ
B
Pt-Fe
cmt
Pt-Fe
4μ
D
Pt-Fe
cmt
.2μ

Figure 4-55

PGM Inclusions in Chromite Fragments

A. Backscatter SEM photomicrograph of PGM-hosting detrital chromite fragment (cmt) from non-magnetic heavy fraction of C horizon rubble (site 56) immediately above the A-Zone PGE occurrence.

B. Backscatter SEM photomicrograph showing close-up of Pt-Fe alloy inclusion from A. (153NM-1) in detrital chromite fragment (cmt).

C. Backscatter SEM photomicrograph of PGM-hosting detrital chromite fragment (cmt) from non-magnetic heavy fraction of C horizon colluvium (site 16) beneath Cliff Zone PGE occurrence.

D. Backscatter SEM photomicrograph showing close-up of Pt-Fe alloy inclusion from C. (31NM-1) in detrital chromite fragment (cmt).

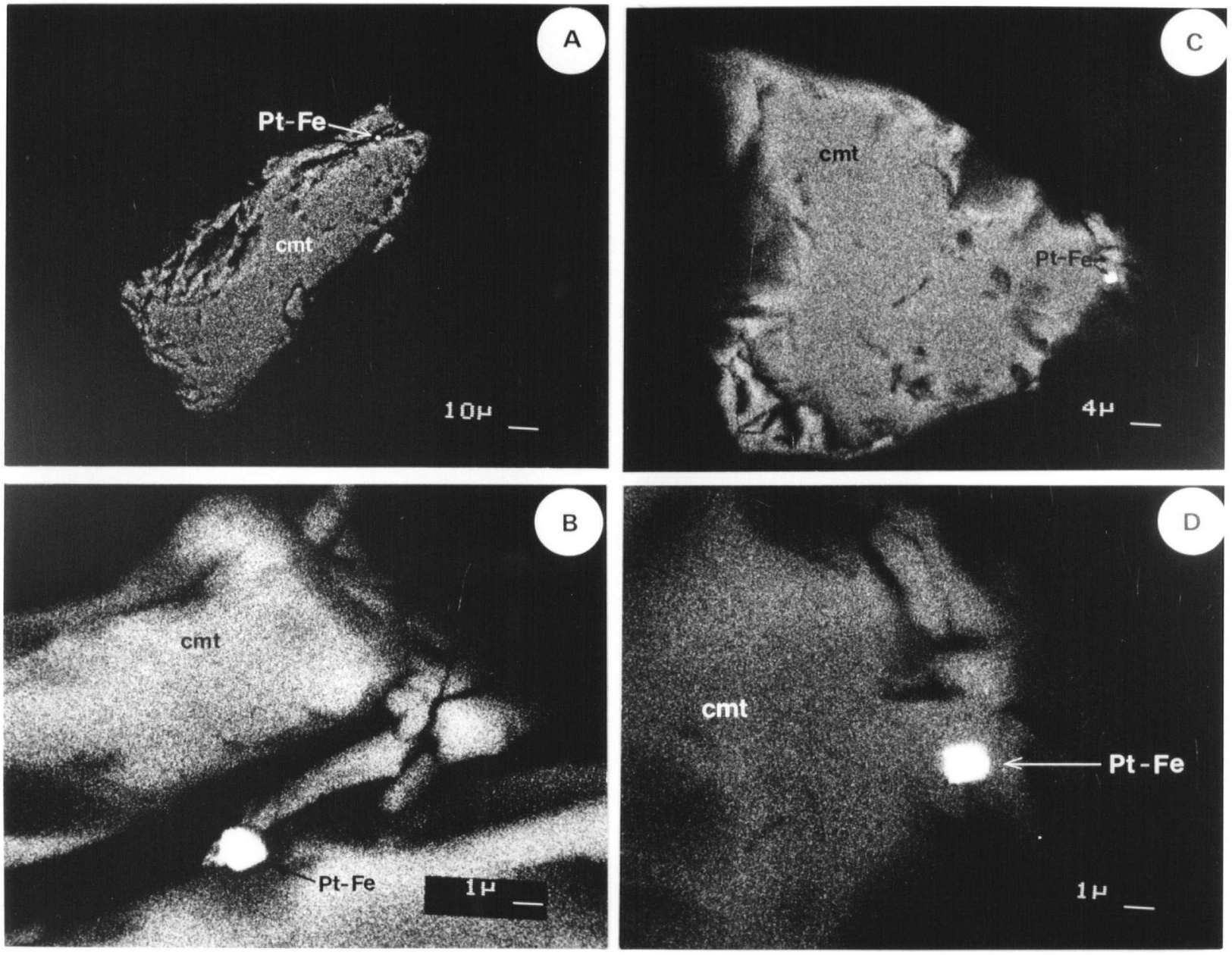
A
Pt-Fe
cmt
10μ
C
cmt
Pt-Fe
4μ
B
cmt
Pt-Fe
1μ
D
cmt
Pt-Fe
1μ

measures approximately 3 um x 1 um (Figure 4-54C). Its contact with chromite is planar on one side and slightly rounded on the other three, although the original grain orientation is unknown. The remaining three PGM are much smaller, less than 2 um in diameter, and are relatively equigranular. Their dimensions are approximately 0.4 um x 0.4 um (153M-2; Figure 4-54D); 1.4 um x 1.2 um (153NM-1; Figure 4-55B), 1.4 um x 1 um (31NM-1; Figure 4-55D).

The PGM inclusions are compositionally similar Pt-Fe-Ni-Cu alloys as determined from EDS analyses, tentatively identified as *isoferroplatinum* (Pt_3Fe). Ni is present in small amounts; it is a more important PGM constituent than Cu, and is particularly abundant in 31NM-1. Backscatter imaging of the largest PGM (153M-1; Figure 4-54C) shows it to be compositionally uniform and devoid of the zoning observed in free PGM grains and those in silicates.

4.4.3 Magnetite

Magnetite is the dominant mineral in magnetic heavy concentrates, usually comprising 70-90% of the metallic heavy grains (Tables 4-15 and 4-16). It most commonly occurs as irregular-shaped, rough-surfaced anhedral aggregate grains of magnetite and silicate, and as smoother, more angular fragments. Silicates in other heavy fractions

may contain a small proportion of magnetite inclusions. Crystals are a second, but less common, type of magnetite. They do not occur at all sites but are most abundant in magnetic concentrates from non-dunitic till (88-SC-19; -40), where they are a common constituent of the metallic grains. Crystals are generally octahedral but are rarely well-formed; those in non-dunitic till sites are generally subhedral-anhedral. Euhedral magnetite crystals are most common in serpentine colluvium (88-SC-105), where they exhibit prismatic cast marks more commonly observed on ilmenite grains.

The physical similarity of magnetite and chromite crystals in magnetic fractions neccessitated constant EDS analysis, from which magnetite was identified by the presence of characteristic Fe peaks. Magnetite was usually easily distinguishable from chromite in polished section by both its association with silicates and by the much more cracked and furrowed appearance of the surface. Fine magnetite, sometimes altered to hematite or limonite, frequently occurred together with Mg-silicate as a thin coating on chromite crystals (Figure 4-56). Magnetite crystals are sometimes titaniferous, but their compositions and distribution were not further investigated. No magnetite grains of any type were found directly associated with PGM grains.

4.4.4 Chromite

4.4.4.1 Scanning Electron Microscopy Results

Chromite is most abundant in the magnetic fraction, where it is a common to subordinate constituent (Tables 4-15 and 4-16). Magnetic fractions from sites adjacent to A-Zone PGE mineralization contain the greatest proportion of chromite (30-40%), while those from some background dunitic and non-dunitic till sites contain the least (5-10%). It is a relatively much more important constituent (up to 90%), however, of the heavy metallic component of many paramagnetic and non-magnetic fractions. Chromites, particularly fragments, are the only heavy metallic detrital grains found in direct association with PGM (section 4.4.2.3).

Chromite occurs as discrete grains comprising both euhedral-subhedral crystals and anhedral fragments. Crystals (Figure 4-56) are typically octahedral to subrounded, frequently have a partial coating of fine magnetite and Mg-silicate, and may exhibit minor weathering or erosional features such as scaling or pockmarked faces and chipped corners. Fragments (Figure 4-57) are elongate-to-blocky, often wedge or sliver-shaped, grains with sharp corners and an apparent conchoidal fracture. Chromite fragments usually have extremely smooth and unaltered

surfaces compared to those of crystals.

Chromites are grossly partitioned between heavy fractions on the basis of grain morphology (Tables 4-15 and 4-16). Crystals are common constituents of most magnetic fractions, consisting predominantly of magnetite, and are relatively more abundant than fragments which typically occur in only trace to subordinate amounts. Conversely, fragments are relatively more abundant than crystals in most (6 out of 8) non-magnetic fractions, which contain less chromite overall and consist predominantly of silicates. It should be stressed that while fragments are *relatively* more important than crystals in non-magnetic fractions, fragments are nevertheless more *numerically* abundant in the magnetic fractions than in the non-magnetic fractions.

The relative proportion of fragments in the non-magnetic fraction is highly variable. They are dominant constituents (65-90%) of the heavy metallic component at sites adjacent to both A-Zone and Cliff Zone PGE occurrences, but are common to trace constituents of most other non-magnetic fractions. However, chromite fragments were absent from non-magnetic fractions at two sites in non-dunitic till (88-SC-40) and background dunitic till (88-SC-200). The paramagnetic fraction, which contains both crystals and fragments, usually contains a relatively higher proportion of fragments than the non-magnetic fraction at

Figure 4-56

Morphology of Chromite Crystals

A. SEM photomicrograph of euhedral chromite crystal (cmt), with adhering Mg-silicate, beside an ilmenite (ilm) grain. Dunitic colluvium (site 16), 88-SC-31, paramagnetic fraction.

B. SEM photomicrograph of euhedral chromite crystal (cmt), with adhering magnetite-silicate, beside a magnetite-silicate (mag) aggregate grain. Non-dunitic till (site 20), 88-SC-40, paramagnetic fraction.

C. SEM photomicrograph of subhedral chromite crystal (cmt). Non-dunitic till (site 20), 88-SC-40, magnetic fraction.

D. SEM photomicrograph of subhedral chromite crystal (cmt) enveloped in Mg-silicate (sil). Non-dunitic till (site 6), 88-SC-19, paramagnetic fraction.

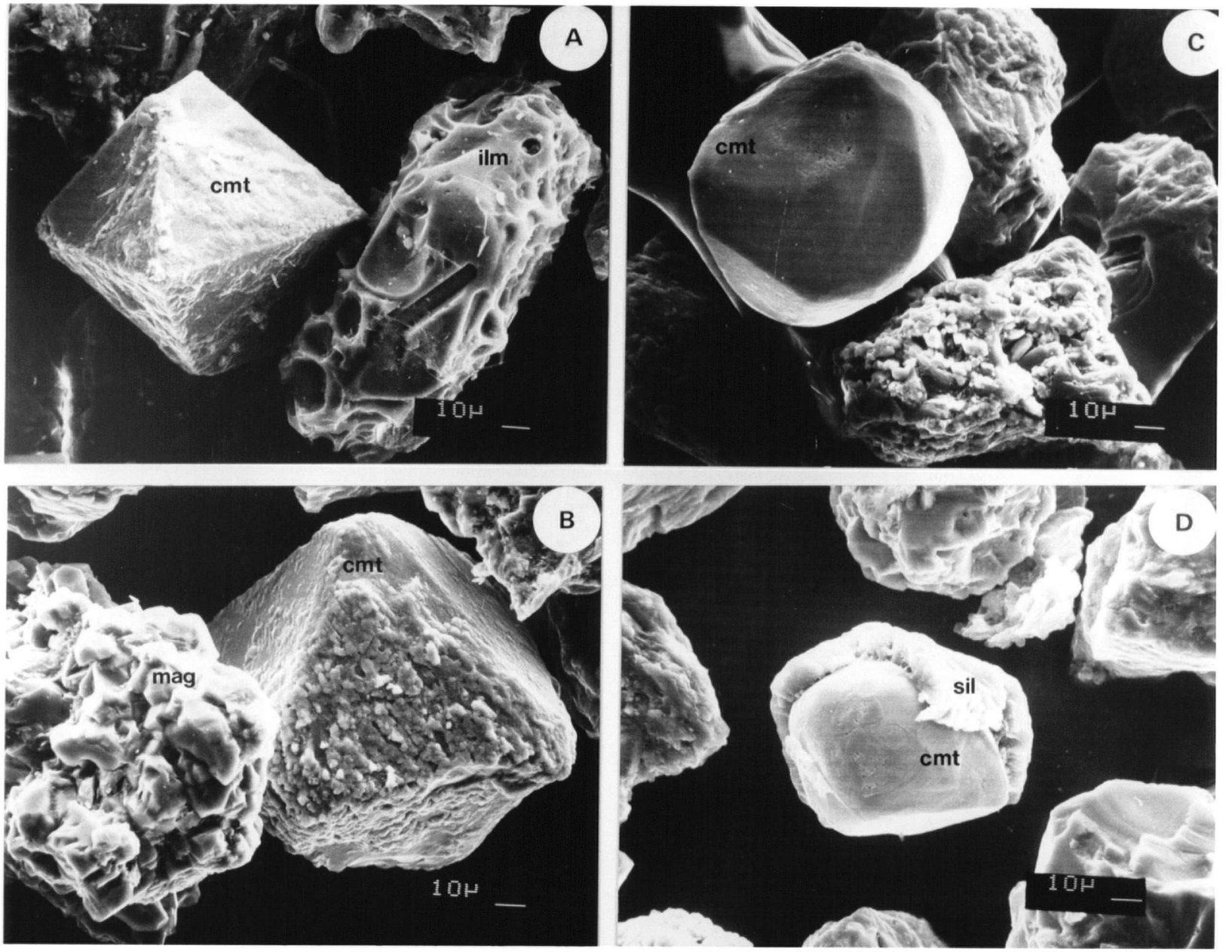
A
cmt
ilm
10μ
C
cmt
10μ
B
cmt
mag
10μ
D
sil
cmt
10μ

Figure 4-57

Morphology of Chromite Fragments

A. SEM photomicrograph of anhedral chromite fragment (cmt). Dunitic till (site 69), 89-SC-200, paramagnetic fraction.

B. SEM photomicrograph of anhedral chromite fragment (cmt). Non-dunitic till (site 6), 88-SC-19, paramagnetic fraction.

C. SEM photomicrograph of anhedral chromite fragment (cmt) from immediately above the A-Zone PGE occurrence. Dunitic rubble (site 56), 88-SC-153, non-magnetic fraction.

D. SEM photomicrograph of anhedral chromite fragment (cmt) from immediately above the A-Zone PGE occurrence. Dunitic rubble (site 56), 88-SC-153, paramagnetic fraction.

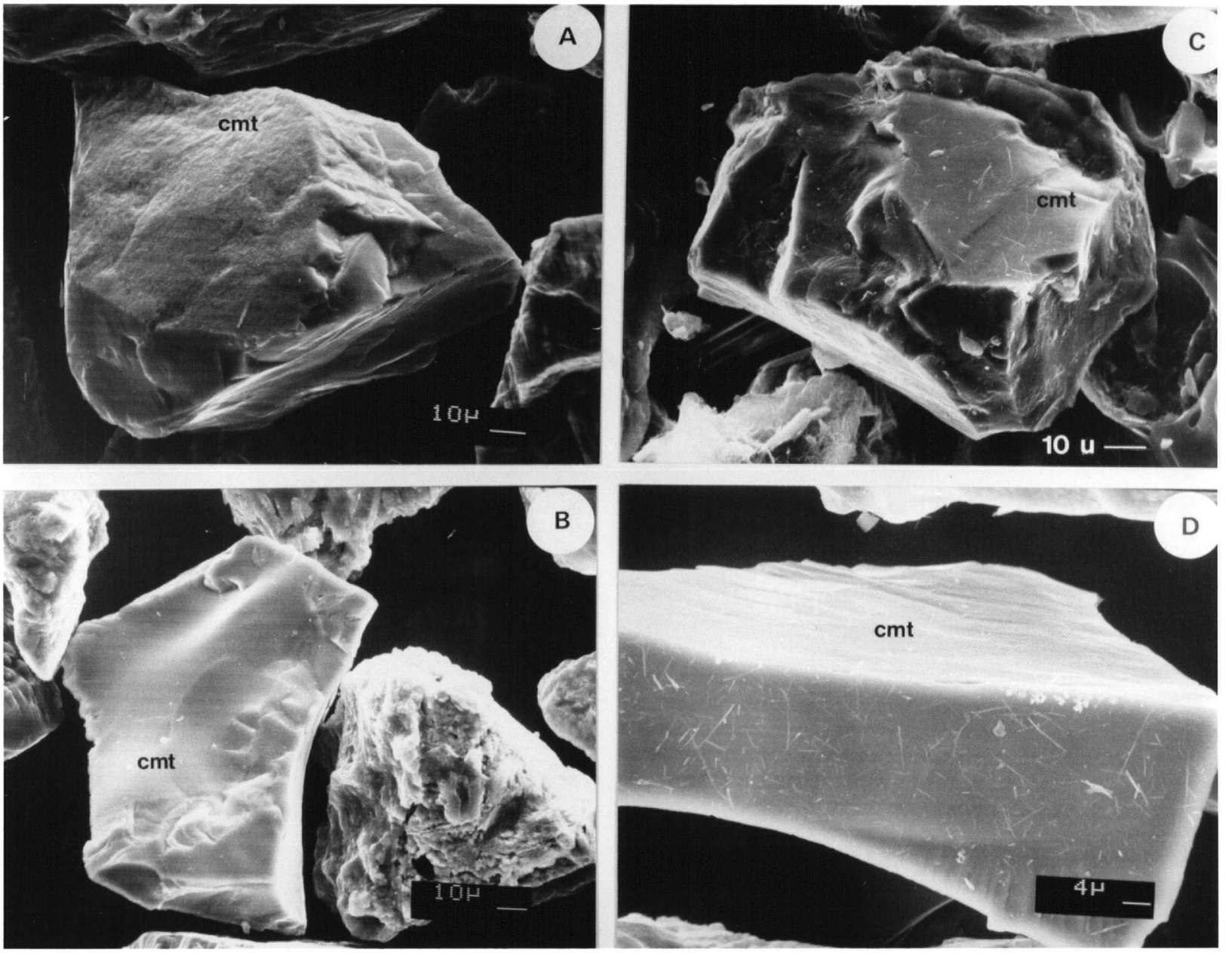
A
cmt
10μ
C
cmt
10 u
B
cmt
10μ
D
cmt
4μ

sites which are not immediately adjacent to known PGE mineralization.

The partitioning of chromite among heavy fractions is related to grain composition as well as morphology. Characteristic Cr and Fe peak heights observed during EDS analyses of chromites varied according to heavy fraction and grain morphology, indicating a systematic relation between the two. A summary of chromite EDS Cr:Fe signatures for each fraction of the eight samples is shown in Tables 4-15 and 4-16. Chromite crystals, relatively more abundant in the magnetic fraction, are generally more Fe-rich; chromite fragments, relatively more abundant in the non-magnetic fraction, are generally more Cr-rich. Fragments have greater proportions of Cr relative to Fe in all types of parent material at all sites, but crystal compositions are more variable. Crystals from serpentine colluvium, colluvium and till/rubble adjacent to known PGE mineralization, and non-dunitic till sites generally contain about subequal proportions of Cr and Fe in the order Cr=Fe or Cr>Fe. Those showing a Fe>Cr trend are only found at dunitic till sites (88-SC-156; -200; -216).

4.4.4.2 Electron Microprobe Results

Mean electron microprobe (EMP) compositions of chromite

crystals and fragments from each of five soil C horizons (section 3.7.3) are shown in Tables 4-17 and 4-18. Analysis of variance results for Cr_2O_3 and MgO concentrations of grain cores are given in Tables 4-19 and 4-20. Individual core analyses and mean values are plotted in Figures 4-58 and 4-59.

Nearly all chromites plot in the ferrian chromite field on the Fe^{3+}-Cr-Al ternary diagram (Figure 4-58) of the spinel prism (Stevens, 1944). The only exceptions are two fragments and five crystals which plot as aluminian chromite and chromian magnetite respectively. EMP results from grain cores (Table 4-17) indicate that considerable compositional differences may exist between crystals and fragments. In general, chromites have low Al (mean: 5.88-7.20 wt% Al_2O_3), minor Ti (mean: 0.57-1.02 wt% TiO_2) and minor Mn (mean: 0.23-0.71 wt% MnO) contents. Al and Ti are similar among both crystals and fragments. Cr, Fe,Mg and Mn contents, however, are variable and related to grain morphology and, to a lesser extent, proximity to known PGE mineralization. Chromite fragments have greater Cr, lesser Fe, and may have greater Mg and Mn contents than crystals from the same site. Cr/Total Fe ratios of cores (Table 4-17) range from 0.68-0.87 in Fe-rich crystals, but from 0.94-1.32 in Fe-poor fragments. Compositional differences between crystals and fragments are verified by a series of t-tests on selected elements at each of the five soil sites. Mean Cr_2O_3

A) CRYSTALS: CORES

	19 (n=9)	200 (n=9)	156 (n=15)	153 (n=15)	31 (n=15)
SiO_2	0.00	0.00	0.07	0.01	0.01
Al_2O_3	6.70	5.99	5.88	6.14	6.96
TiO_2	0.71	1.02	0.73	0.65	0.67
Cr_2O_3	36.60	35.23	36.17	36.59	39.54
Fe_2O_3	24.65	26.25	25.44	25.04	21.63
FeO	24.86	25.82	26.26	24.73	23.80
MnO	0.65	0.71	0.49	0.44	0.45
MgO	4.53	4.47	4.15	5.00	5.78
Total	98.70	99.49	99.19	98.60	98.84
Cr/Fe	0.74	0.68	0.70	0.74	0.87

B) FRAGMENTS: CORES

	19 (n=9)	200 (n=9)	156 (n=9)	153 (n=15)	31 (n=15)
SiO_2	0.00	0.00	0.01	0.01	0.01
Al_2O_3	7.10	7.20	5.98	6.57	6.93
TiO_2	0.66	0.57	0.60	0.64	0.61
Cr_2O_3	41.07	43.81	42.10	42.86	45.83
Fe_2O_3	19.92	17.92	20.48	20.20	17.54
FeO	23.49	21.65	24.11	18.75	17.17
MnO	0.52	0.51	0.36	0.24	0.23
MgO	5.92	7.12	5.59	9.07	10.19
Total	98.68	98.78	99.23	98.34	98.51
Cr/Fe	0.95	1.11	0.94	1.10	1.32

Table 4-17. Mean electron microprobe data (weight percent) for cores of detrital chromite crystals (magnetic heavy fraction) and fragments (partly magnetic and non-magnetic heavy fractions) from various C horizons: 19-non-dunitic till; 200-dunitic till; 156-dunitic till near A-Zone PGE mineralization; 153-dunitic till/rubble above A-Zone; 31-colluvium beneath Cliff Zone PGE mineralization.

A) CRYSTALS: EDGES

	19 (n=9)	200 (n=9)	156 (n=15)	153 (n=15)	31 (n=14)
SiO_2	0.00	0.00	0.07	0.00	0.01
Al_2O_3	6.49	5.77	5.83	6.02	6.72
TiO_2	0.70	0.92	0.70	0.67	0.67
Cr_2O_3	36.15	34.45	35.74	35.80	39.12
Fe_2O_3	24.29	27.19	25.74	25.63	22.18
FeO	25.55	25.54	26.86	25.05	24.00
MnO	0.83	0.77	0.59	0.60	0.57
MgO	4.18	4.44	3.67	4.63	5.54
Total	98.19	99.08	99.20	98.40	98.81
Cr/Fe	0.73	0.65	0.68	0.71	0.85

B) FRAGMENTS: EDGES

	19 (n=9)	200 (n=9)	156 (n=9)	153 (n=15)	31 (n=15)
SiO_2	0.00	0.00	0.01	0.01	0.00
Al_2O_3	6.94	7.25	5.97	6.63	6.93
TiO_2	0.71	0.58	0.60	0.61	0.61
Cr_2O_3	40.24	43.66	41.05	42.83	45.54
Fe_2O_3	20.35	18.16	20.72	19.87	17.51
FeO	23.78	21.57	25.81	18.64	17.21
MnO	0.58	0.51	0.36	0.26	0.23
MgO	5.59	7.22	4.42	9.02	10.07
Total	98.19	98.95	98.94	97.87	98.10
Cr/Fe	0.91	1.10	0.88	1.11	1.31

Table 4-18. Mean electron microprobe data (weight percent) for edges of detrital chromite crystals (magnetic heavy fraction) and fragments (partly magnetic and non-magnetic heavy fractions) from various C horizons: 19-non-dunitic till; 200-dunitic till; 156-dunitic till near A-Zone PGE mineralization; 153-dunitic till/rubble above A-Zone; 31-colluvium beneath Cliff Zone PGE mineralization.

concentrations of crystals and fragments are significantly different (p = .05) at all five sites. Furthermore, mean MgO concentrations of the two groups are significantly different (p = .05) at four of five sites; only in sample 19 from non-dunitic till are MgO contents of cystals and fragments similar.

Mean Cr content of crystals (range: 20.06-45.43 wt% Cr_2O_3) is remarkably similar (range of means: 35.23-39.54 wt% Cr_2O_3) at all five soil sites (Table 4-17) and is more uniform than suggested by EDS analyses. Mean Cr content of fragments (range: 37.66-50.25 wt% Cr_2O_3), although greater, is also similar between all soil sites (range of means: 41.07-45.83 wt% Cr_2O_3). Sample 31 (colluvium beneath Cliff Zone PGE occurrences) has the highest Cr_2O_3 content of both crystals and fragments.

Equivilency of mean core Cr_2O_3 concentrations was tested with one-way analysis of variance (p = .05) to determine if between-site variability is significantly greater than within-site variability. The null hypothesis (H_0) for each of crystals and fragments is:

$$u_1 = u_2 = u_3 = u_4 = u_5$$

Acceptance of H_0 indicates that the five population means are identical; rejection in favour of the alternate hypothesis (H_1) indicates that between-site variablity is so large that at least one population mean is significantly

different from the others. Results (Table 4-19) show that mean Cr_2O_3 concentrations are indeed homogenous in crystals at all five sites. However, this is not the case for at least one of the fragment means ($p = .05$); their Cr_2O_3 contents are significantly different between sites.

FeO and Fe_2O_3 contents are recalculated from total Fe_2O_3 on the basis of the spinel structural formula. Fe^{3+}, showing a trend generally opposite to that of Cr, ranges from 15.79-45.98 wt% Fe_2O_3 in crystals (range of means: 21.63-26.25 wt% Fe_2O_3) and from 12.89-23.18 wt% Fe_2O_3 in Fe-poor fragments (range of means: 17.54-20.48 wt% Fe_2O_3). Crystals in sample 200 (background dunitic till) have the highest mean Fe_2O_3 content.

Mean Fe^{2+} content, which is less variable than Fe^{3+}, ranges from 23.80-26.26 wt% FeO in crystals and from 21.65-24.11 wt% FeO in fragments at the three sites in which the paramagnetic fraction was used. However, FeO content of crystals at the two sites which non-magnetic fractions were used is considerably lower (range of means: 17.17-18.75 wt% FeO). Both sites (16 and 56) are adjacent to known PGE occurrences. This is paralled by a similar decrease in Mn, and corresponds to a Mg content (range of means: 9.07-10.19 wt% MgO) about 2x greater that of crystals (range of means: 4.15-5.78 wt% MgO) and fragments (range of means: 5.59-7.12 wt% MgO) from the other three sites. Equivilency of core

A. Cr_2O_3 (%) in chromite crystals (N=63)

	Sample	Mean ± 1s	n
1)	19	36.60 ± 3.41	9
2)	200	35.23 ± 8.83	9
3)	156	36.17 ± 3.37	15
4)	153	36.59 ± 2.30	15
5)	31	39.54 ± 3.45	15

Source of Variation	Sum of Squares	Degrees of Freedom	Mean Squares
Between groups	139.26	4	34.82
Within groups	1116.5	58	19.25
Total	1255.76	62	

$F = 1.81$; $F_{critical} = 2.53$ (0.05 significance level)

$F < F_{critical}$

Null hypothesis accepted; populations are not different

B. Cr_2O_3 (%) in chromite fragments (N=57)

	Sample	Mean ± 1s	n
1)	19	41.07 ± 1.54	9
2)	200	43.81 ± 3.81	9
3)	156	42.10 ± 1.82	9
4)	153	42.86 ± 1.12	15
5)	31	45.83 ± 2.07	15

Source of Variation	Sum of Squares	Degrees of Freedom	Mean Squares
Between groups	158.51	4	39.63
Within groups	239.02	52	4.60
Total	397.53	56	

$F = 8.62$; $F_{critical} = 2.53$ (0.05 significance level)

$F > F_{critical}$

Null hypothesis rejected; populations are different

Table 4-19. Anova tables showing one-way analysis of variance results for Cr_2O_3 analyses of five groups of A. chromite crystals and B. chromite fragments.

A. MgO (%) in chromite crystals (N=63)

	Sample	Mean ± 1s	n
1)	19	4.53 ± 1.55	9
2)	200	4.47 ± 1.74	9
3)	156	4.15 ± 1.07	15
4)	153	5.00 ± 0.90	15
5)	31	5.78 ± 1.00	15

Source of Variation	Sum of Squares	Degrees of Freedom	Mean Squares
Between groups	22.85	4	5.71
Within groups	84.74	58	1.46
Total	107.57	62	

$F = 3.91$; $F_{critical} = 2.53$ (0.05 significance level)
$F > F_{critical}$
Null hypothesis rejected; populations are different

B. MgO (%) in chromite fragments (N=57)

	Sample	Mean ± 1s	n
1)	19	5.92 ± 2.09	9
2)	200	7.12 ± 1.91	9
3)	156	5.59 ± 1.58	9
4)	153	9.07 ± 0.45	15
5)	31	10.19 ± 1.30	15

Source of Variation	Sum of Squares	Degrees of Freedom	Mean Squares
Between groups	187.28	4	46.82
Within groups	110.62	52	2.13
Total	297.90	56	

$F = 21.98$; $F_{critical} = 2.53$ (0.05 significance level)
$F > F_{critical}$
Null hypothesis rejected; populations are different

Table 4-20. Anova tables showing one-way analysis of variance results for MgO analyses (%) of five groups of A. chromite crystals and B. chromite fragments.

MgO concentrations in the five sites was also tested with one-way analysis of variance. Results (Table 4-20) indicate MgO inhomogeneity between sites for both crystals and fragments.

The compositional fields of some major rock types of Tulameen complex (Nixon et al, 1990) are shown on two faces of the spinel prism in relation to the compositions of individual detrital chromites (Figures 4-58 and 4-59). Crystals generally fall within the field of dunite and chromitiferous dunite and, to a lesser extent, olivine clinopyroxenite. Fragments almost always plot within the chromitite field. More significantly, fragments from rubble and colluvium (153 and 31) adjacent to known PGE occurrences plot within or near the magnesiochromite field (Figure 4-59). They also plot within the tightest compositional range, while those from dunitic till samples 200 and 156 plot within the widest. Dunitic till sample 200 also plots within the widest compositional range among crystals.

Mean analytical data of chromite cores and edges (Tables 4-17 and 4-18) indicate negligible compositional differences. It should be stressed that detrital grains were not acid purified or ultrasonically cleaned prior to mounting. Edge compositions may be affected by adhering minerals, although it is not readily apparent in the data. This would be expected to affect crystals more than

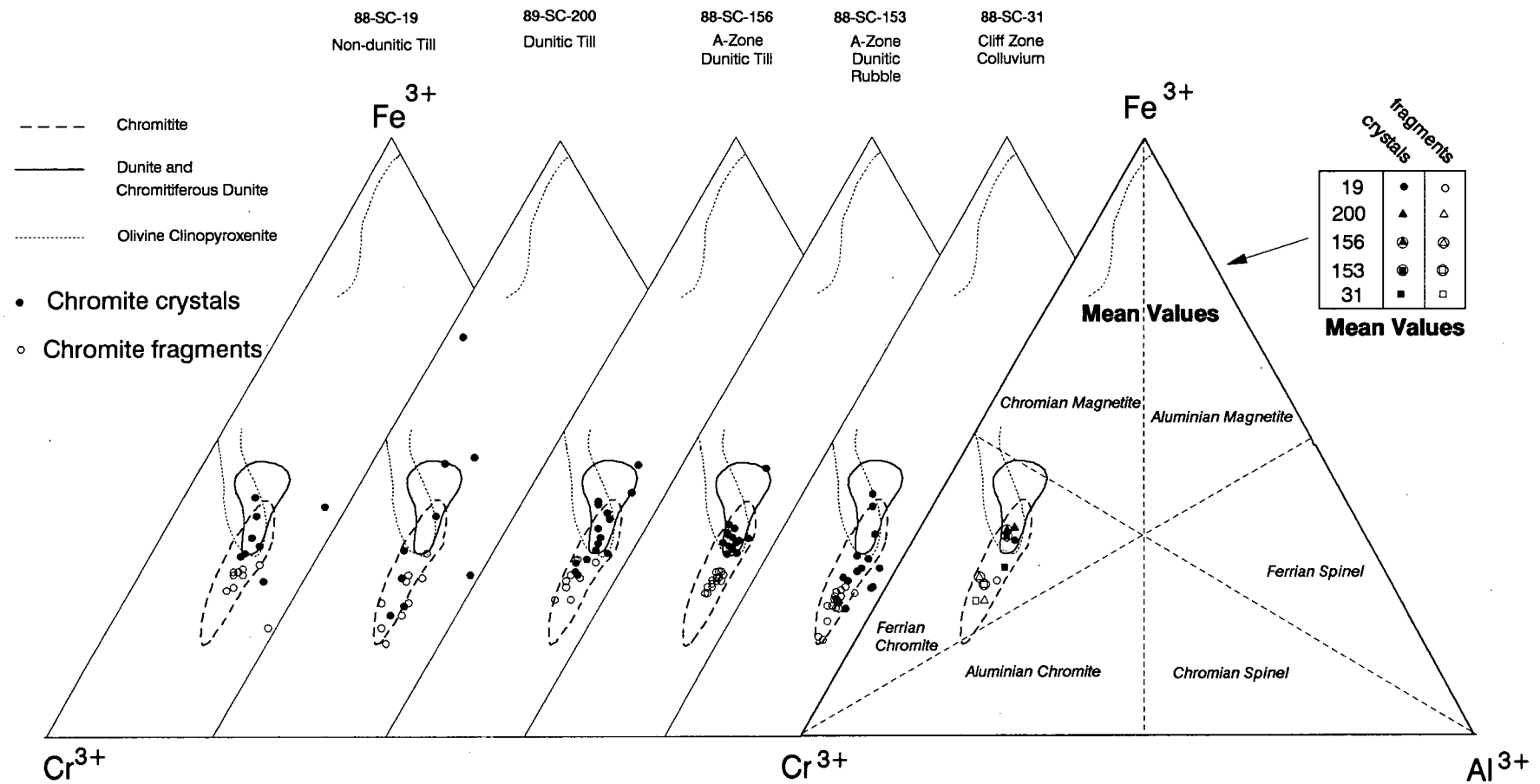

Figure 4-58. Fe-Cr-Al spinel composition plot of detrital chromite crystals (n=63) and fragments (n=57) from various C Horizon soils and from some major rock types of the Tulameen complex (adapted from Nixon et al, 1990; Stevens, 1944).

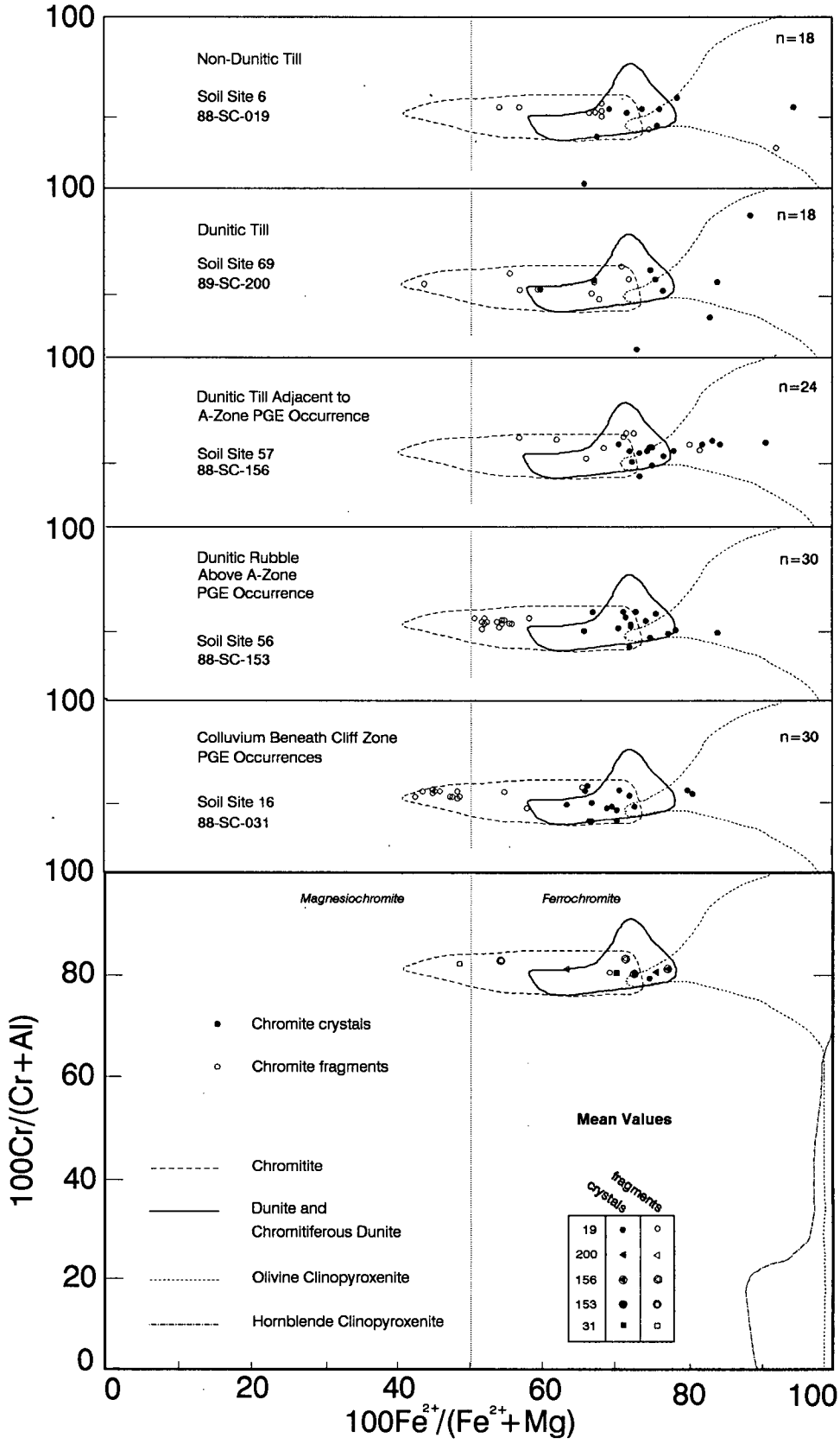

Figure 4-59. Plot of Fe2+/(Fe2+ + Mg2+) versus Cr/(Cr+Al) for detrital chromite crystals (n=63) and fragments (n=57) from various C horizon soils and major rock types of the Tulameen complex (adapted from Nixon et al, 1990).

fragments. Relative to cores, edges are slightly depleted in Cr_2O_3, usually slightly enriched in Fe_2O_3, and relatively constant in TiO_2 in both crystals and fragments. Behaviour of other elements differ between crystals and fragments. Crystal edges are slightly depleted in Al_2O_3 and MgO, and slightly enriched in FeO and MnO. Fragment edges, however, are constant in Al_2O_3, constant to slightly depleted in MgO, and relatively constant in FeO and MnO. Among conserved elements in fragments, those of sample 19 seem the least constant.

4.4.5 Ilmenite

Ilmenite was identified on the basis of characteristic Fe and Ti EDS peaks. It occurs as subhedral crystals exhibiting cast marks of attached prismatic silicates and as poorly-formed subhedral-anhedral grains with characteristic Ca-silicate inclusions or their casts.

Ilmenite is a common to subordinate constituent of paramagnetic and, in some cases, nonmagnetic heavy concentrates (Tables 4-15 and 4-16). It is most common in paramagnetic fractions from colluvium where it comprises 45% of the metallic grains in serpentine colluvium (88-SC-105), and 35% of that fraction in colluvium beneath Cliff Zone PGE occurrences (88-SC-31). Ilmenite is, however, relatively

uncommon adjacent to A-Zone PGE mineralization and has no apparent association with PGM grains.

4.4.6 Other Minerals

Other minerals, aside from common silicates, observed during SEM examination of heavy concentrates include Fe oxides and oxidized sulfides, zircon, rare earth element (REE) minerals and a U-Nb-Y-K mineral. A variety of metallic contaminants are also present.

Fe oxides and oxidized sulfides are most abundant in nonmagnetic concentrates. They are dominant constituents of this fraction at non-dunitic and some dunitic till sites, where they comprise nearly all of the heavy metallic grains (Tables 4-15 and 4-16), but are only a subordinate constituent of colluvium and dunitic till/rubble near known PGE mineralization. They occur as anhedral grains and masses of Fe oxide and as oxidized anhedral-euhedral pyrite pseudomorphs. These often contain irregular-shaped cores of relict pyrite, visible in polished section, and are particularly common at background dunitic till sites (88-SC-200;-216) and at a non-dunitic till site (88-SC-40). Pyrite pseudomorphs may show surface striiations or etch pits. A single irregular-shaped grain of Fe-Ni sulphide, possibly pentlandite, was observed in polished section of a

nonmagnetic concentrate from serpentine colluvium (88-SC-105). Subequal EDS peak heights decreased in the order: S > Fe > Ni.

Zircons occur as trace-to-subordinate constituents of non-magnetic concentrates of all types. They are most abundant in a non-dunitic till site (88-SC-19). Most are crystalline but a single well-rounded grain was observed in A-Zone dunitic till (88-SC-156) from the summit of Grasshopper Mountain.

A variety of rare minerals were found in polished sections of concentrates from non-dunitic till. An approximately 8 um x 4 um inclusion of an unidentified U-Nb-Y-K mineral was found in an ilmenite grain within a paramagnetic concentrate (88-SC-19). Two discrete Ce-bearing REE minerals were found within the nonmagnetic fraction of the same sample. One, measuring approximately 60 um x 35 um, was an unidentified Ce-Th-La-P mineral; the second, approximately 80 um x 25 um, was an unidentified Fe-Ca-Ce-La silicate. A third REE mineral was found in the nonmagnetic concentrate of the other non-dunitic till sample (88-SC-40). It occurred as several small inclusions, approximately 1-6 um in diameter, of an unidentified Ce-La mineral within an apatite (Ca-P) grain.

Chapter Five

DISCUSSION

CHAPTER FIVE: DISCUSSION

5.1 Introduction

Results of the distributions of Pt and other selected elements within various surficial materials on Grasshopper Mountain were presented in the previous chapter. In this chapter, they are used to present a model for mechanical and, to a lesser lesser degree, hydromorphic dispersion of Pt at this locality. Compositional variations of platinic chromite are shown to be theoretically predictable, and recommendations for geochemical exploration for chromitite-associated Pt deposits are outlined. It should be stressed that such recommendations are directly applicable only to similar deposits in temperate glaciated environments.

5.2 Detrital Chromites

5.2.1 Origin of Detrital Chromites

Chromite occurs in Tulameen dunite as both massive chromitite segregations and as accessory disseminated subhedral-euhedral crystals (Findlay, 1963; Nixon et al, 1990). Compositional and morphological evidence suggest that anhedral chromite fragments in soils represent the

fragmented remnants of chromitite segregations that may contain elevated Pt concentrations (St. Louis et al, 1986). Conversely, detrital chromite crystals represent relatively Pt-poor crystals liberated from dunite and, perhaps to a lesser extent, olivine clinopyroxenite (Figures 4-58 and 4-59).

5.2.1.1 Fragments

Compositional similarities of the detrital fragments to the composition of massive chromitite (Table 5-1) reported by Irvine (1967) and Nixon et al (1990), and compositional differences between these and detrital crystals, strongly suggest that detrital fragments derive from chromitite segregations. Higher Cr_2O_3, lesser Fe_2O_3 and FeO, and higher MgO contents (Tables 4-17 and 5-1, Figures 4-58 and 4-59) characterize both fragments and massive chromitites. A striking feature is the compositional uniformity of chromite fragments from soil sites spanning such a wide variety of parent material types and compositions (Table 4-17). Mean Cr_2O_3 and Fe_2O_3 contents are almost identical at all five sites, while only MgO and FeO contents vary significantly. The narrow range of fragment compositions from sites adjacent to PGE occurrences (Figures 4-58 and 4-59) illustrates the relatively restricted source areas of soils developed on

	Soil chromite fragments		Chromitite segregations				
	88-SC-153 (n=15)	88-SC-031 (n=15)	147[1] (n=16)	148[1] (n=12)	50[1] (n=8)	FJT60-55A[2]	FJT60-540[2]
SiO_2	0.01	0.01	0.27	0.19	0.19	0.61	0.02
Al_2O_3	6.57	6.93	6.31	7.28	7.45	6.90	8.10
TiO_2	0.64	0.61	0.78	0.42	0.51	0.58	0.86
Cr_2O_3	42.86	45.83	37.03	43.65	49.01	43.90	37.70
Fe_2O_3	20.20	17.54	26.70	20.88	15.36	20.80	25.10
FeO	18.75	17.17	20.71	18.40	17.20	18.50	19.50
MnO	0.24	0.23	0.47	0.45	0.35	0.40	0.39
MgO	9.07	10.19	7.96	9.57	10.49	8.80	8.50
CaO	-	-	-	-	-	<0.05	< 0.05
V_2O_3	-	-	-	-	-	0.06	0.12
NiO	-	-	-	-	-	0.06	0.08
Total	98.34	98.51	100.23	100.84	100.56	100.10	100.40

Table 5-1. Composition of detrital soil chromite fragments (non-magnetic fraction) from two sites adjacent to known PGE-chromite occurrences, with that of chromitite segregations. Tulameen chromitite data from 1: Nixon et al (1990) and 2: Irvine (1967).

dunitic colluvium and rubble, whereas the wider compositional variation in fragments from till sites is probably indicative of a larger source area. Similarly, the tight compositional grouping of chromite fragments in non-dunitic till (88-SC-19) probably indicates a relatively uniform source.

Morphologically, the absence of any recognizable crystal habit is the most obvious feature linking soil fragments to massive chromitite. Other features observed in detrital fragments, such as concentric lines and an apparent conchoidal fracturing on smooth surfaces, have been previously reported from layered chromite of ophiolitic podiform deposits (Leblanc, 1980). Smooth conchoidal surfaces represent the surfaces of three large-scale orthogonal cleavage planes along which the massive chromite splits, while the concentric lines were interpreted as groups of layers with concentric edges (Leblanc, 1980).

5.2.1.2 Crystals

Compositional similarity of detrital chromite crystals with those from dunite and possibly clinopyroxenite (Figures 4-58 and 4-59) suggest that they originated as disseminated grains in dunite. Data are lacking for a direct comparison of the compositions of disseminated chromite grains (Nixon

et al, 1990) with C horizon crystals, but compositions of chromite concentrates from dunite reported by Findlay (1963) are generally similar to those of this study. Findlay's (1963) magnetic concentrates have lower Cr_2O_3 and MgO contents, and higher Fe_2O_3 and FeO contents, than do corresponding non-magnetic concentrates. There is insufficient information about the morphological nature of Findlay's (1963) chromite to directly compare their compositions with those of the magnetic detrital crystals.

The strikingly similar mean compositions of magnetic-fraction chromite crystals in all five soils (Table 4-17) suggests a relatively homogenous crystal composition throughout the dunite core. Nevertheless, compositional ranges vary from site to site. The narrow compositional range of crystals from the two sites in dunitic rubble and colluvium adjacent to PGE occurrences (Figures 4-58 and 4-59) is indicative of the very limited provenance of these two soils. Conversely, crystals in dunitic and non-dunitic till sites exhibit much wider compositional ranges indicative of a larger source area.

The two morphological types of chromite crystals - euhedral and subhedral/anhderal (section 4.5.4) - may represent quite different cooling histories in spite of their relatively homogenous core compositions. Disseminated euhedral crystals represent the magmatic crystallization

habit of chromite, but subrounded multifaceted subhedral crystals within podiform chromite occurrences in ophiolites have been interpreted as a product of hydrothermal dissolution processes (Leblanc, 1980). Such crystals are most abundant on Grasshopper Mountain in colluvium (88-SC-105) derived from intensely serpentinized dunite. Although they superficially appear to have been rounded by abrasion, the presence of enveloping silicates around some subrounded chromites (Figure 4-56D) indicates that they were rounded, perhaps via dissolution by serpentinizing fluids, prior to being liberated from the rock. No microprobe analyses were performed on crystals from this site to determine the presence or absence of ferritchromite rims (Ramdohr, 1969; Kimball, 1990).

5.2.2 Chromite Chemistry: Relation Between Compositional Variations and Magnetic Properties

Chromite (AB_2O_4) is a member of the chromite series of the spinel group. The spinel unit cell contains 24 cations and has the general formula:

$$A_8^{2+}B_{16}^{3+}O_{32}$$

Spinel classification is dictated by the dominant B^{3+} and A^{2+} cations in solid solution (Deer et al, 1966; Stowe,

1987). Fe^{2+}, Mg^{2+} and trace Mn^{2+} occupy the tetrahedral coordination (A) sites, while variable proportions of Cr^{3+}, Fe^{3+}, Al^{3+} and lesser Ti^{4+} occupy octahedral coordination (B) sites. Considerable compositional variation occurs even within the same deposit (Hawkes, 1951; Peoples and Eaton, 1952).

Chromite is usually non-magnetic or weakly magnetic, and is rarely strongly magnetic. Its magnetic properties vary with variations in chemical composition due to ionic substitution (Stevens, 1944; Hawkes, 1951; Svoboda, 1987). Hawkes (1951), noting that one of three trivalent endmembers (Figure 4-58) of the spinel prism (magnetite) is magnetic whereas the other two (chromite and spinel) are not, suggested that increasing magnetic susceptibility of chromite is related to an increasing proportion of endmember magnetite ($FeO \cdot Fe_2O_3$). Increasing magnetic susceptibility with increasing iron content has been supported by studies from Indian occurrences (Rao, 1978; Radhakrishna Murthy and Gopalakrisha, 1982), the Stillwater Complex (Peoples and Eaton, 1952), and other localities (Stevens, 1944; Owada and Harada, 1985). It is unclear whether increased Fe^{2+} (Peoples and Eaton, 1952; Owada and Harada, 1985), Fe^{3+} (Rao, 1978), or both as $FeO \cdot Fe_2O_3$ is ultimately responsible for chromite magnetism. Peoples and Eaton (1952), for example, reported a linear relationship between magnetic susceptibility and the Fe/Fe+Mg (mol) ratio, but not with

weight percent total Fe.

Schwerer and Gundaker (1975) reported that greater magnetization of chromite was induced by mechanical crushing to finer particle sizes, a phenomenom attributed to defect structures on grain surfaces. This has intriguing implications for the magnetic behaviour of glacially-crushed chromite grains in till relative to those in rubble or colluvium. Chromite fragments are a relatively more important component of paramagnetic than non-magnetic fractions at all till sites, including one near A-Zone PGE mineralization (Tables 4-15 and 4-16), but there is insufficient evidence to suggest that crushing-induced magnetization significantly affects the primary magnetic properties of Tulameen chromitite.

Discussion of the magnetic properties of chromite assumes a homogenous grain composition. Occurrence of fracture-filling magnetite veinlets (Jenness, 1959), the formation of magnetite or ferritchromite rims by either hydrothermal alteration (Beeson and Jackson, 1969; Ramdohr, 1969; Kimball, 1990) or lateritic weathering (Michailidis, 1990), and the occurrence of fine coatings of magnetite or other iron oxides on detrital grains all serve to increase magnetic susceptibility. Chromites in the present study were not subject to any pretreatment to remove adhering particles, including magnetite, from grain edges prior to

microprobe analysis. However, grain cores are smooth and texturally homogenous; compositional similarity between edges and cores (Tables 4-17 and 4-18) suggests that contamination is not a major concern.

Tulameen chromite is generally magnetic and characterized by a high Fe^{3+} content (Findlay, 1963, 1969). This is typical of Alaskan-type ultramafic complexes (Irvine, 1967). Using mean compositions of colluvial chromite grains (88-SC-031) from beneath Cliff Zone PGE occurrences, the structural formula of chromite crystals (magnetic fraction) is:

$$(Fe^{2+}_{5.61}Mg_{2.43}Mn_{0.11})(Cr_{8.82}Fe^{3+}_{4.59}Al_{2.31}Ti_{0.14})O_{32.00}$$

and that of fragments (non-magnetic fraction) is:

$$(Mg_{4.15}Fe^{2+}_{3.93}Mn_{0.05})(Cr_{9.91}Fe^{3+}_{3.61}Al_{2.23}Ti_{0.13})O_{32.00}$$

It is apparent that detrital crystals are of chromite, or ferrochromite, ($FeCr_2O_4$) composition, while detrital fragments are not chromite but rather the Mg-rich chromite series end-member magnesiochromite ($MgCr_2O_4$), also known as picrochromite. This is best illustrated in Figure 4-59, where a $Fe^{2+}/(Fe^{2+} + Mg^{2+})$ cation ratio of 0.5 in the A site separates the two endmembers.

Chromite cation data shows that 12 out of 15 colluvial nonmagnetic chromite fragments from the Cliff Zone PGE occurrences (88-SC-031) are magnesiochromite, while none of the magnetic fraction chromite crystals are. Although several fragments are extremely close, neither the fragments nor crystals from dunitic rubble (88-SC-153) above the A-Zone PGE occurrence fall in the magnesiochromite field. This is not significant in itself, as the primary chromitite field (Nixon et al, 1990) spans both magnesiochromite and chromite compositions. Mean cation data of the same authors show one of three chromitites to be magnesiochromite, with a second quite close to the boundary. It may be significant that the MgO-rich Cliff Zone chromitite horizons contain massive to semi-massive segregations, whereas the A-Zone is the most widespread occurrence of wispy chromite lenses and coarsely disseminated grains (Bohme, 1987, 1988) which are slightly less magnesian. Detrital fragments from sites unrelated to known mineralization have similar Cr_2O_3 contents (Table 4-17) but are even less Mg-rich. There is only a single fragment in background non-dunitic till (88-SC-200) of magnesiochromite composition (Figure 4-59).

5.2.3 Origin of Compositional Variations in Detrital Chromite

Compositional and morphological evidence suggest a

correlation of nonmagnetic Cr-Mg-rich detrital fragments with massive chromitite, and of magnetic detrital crystals with disseminated grains. The origin of these observed variations among different lithologies is theoretically predictable, and is most adequately explained as systematic Mg/Mg+Fe and Cr/Fe variations due to magmatic differentiation trends. Chromite composition is indicative of chemical and thermal conditions of magma crystallization, and varies between deposit types (Irvine, 1965, 1967; Duke, 1983). Cr-rich chromite occurs in feldspar-free peridotites, Fe-rich chromite in pyroxene-rich stratiform complexes, and Al-rich chromites in alpine-type peridotites (Thayer, 1946; Irvine, 1967).

The preferential association of magnesian chromite with massive segregations relative to disseminated grains has been extensively documented. Nixon et al (1990) showed that Tulameen chromitites have a lower $Fe^{2+}/(Fe^{2+}+Mg^{2+})$ ratio (higher relative Mg^{2+}; Figure 4-59), as well as a lower $Fe^{3+}/(Fe^{3+}+Al+Cr)$ ratio (higher relative Cr^{3+}), than disseminated chromite within dunite. The latter ratio can also be interpreted as a higher Cr/Fe ratio in chromitite, as Al is relatively constant (Table 4-17; Figure 4-59). Similar Mg/Fe compositional variations have been reported from the Turnagain Alaskan-type complex in northwestern B.C. (Clark, 1978) and from stratiform complexes (Figure 5-1). For example, the cation fraction of Mg^{2+} relative to Fe^{2+}

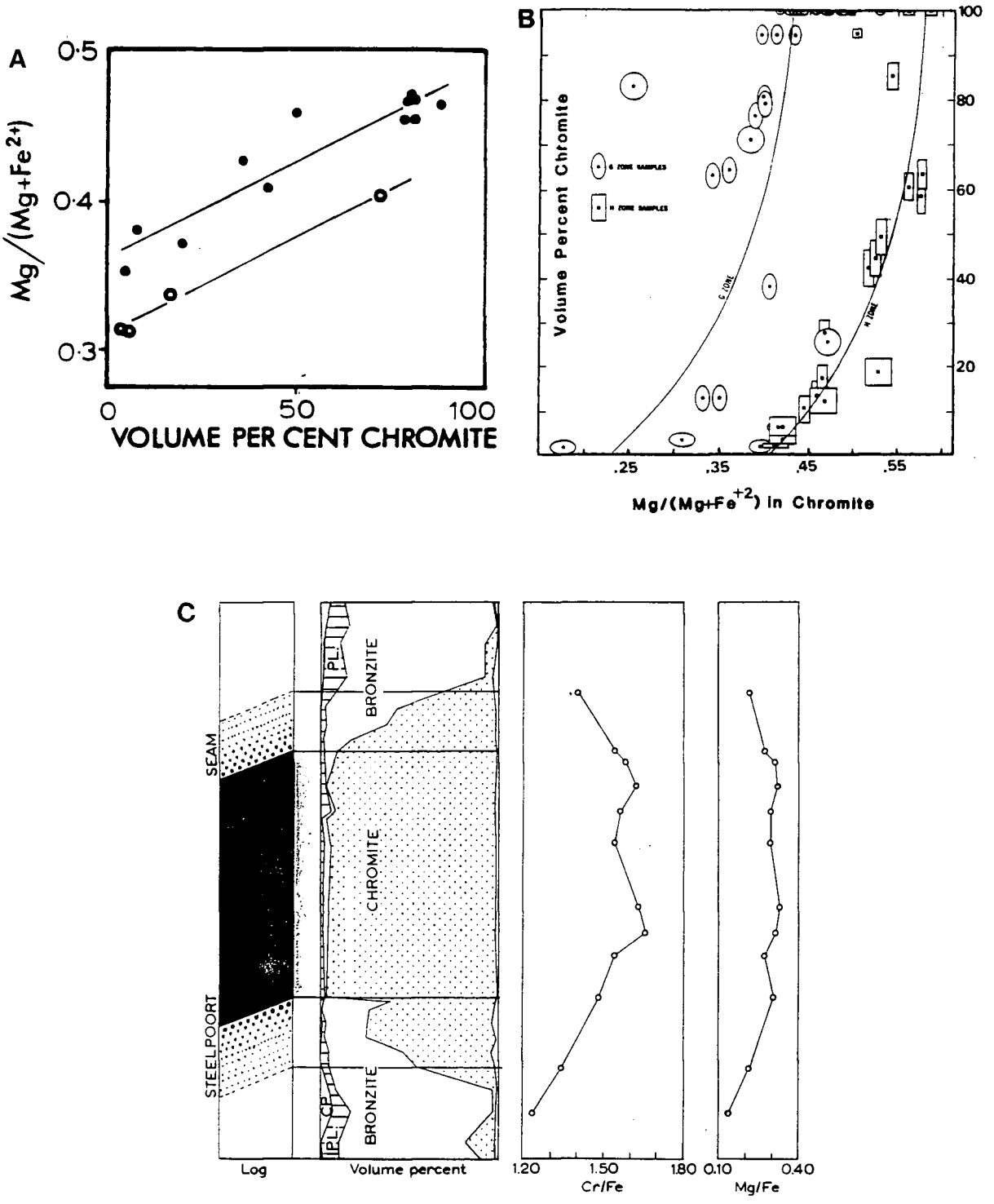

Figure 5-1. Relation between volume percent cumulus chromite and Mg/(Mg+Fe^{2+}) of the chromite, in A. UG2 seam sequences of the western Bushveld Complex (Eales, 1987); B. G and H chromitite zones of the Stillwater Complex (Jackson, 1969); and in C. relation between volume percent chromite and Cr/Fe and Mg/Fe ratios in the Steelpoort seam, eastern Bushveld Complex (Cameron and Desborough, 1969).

($Mg^{2+}/Mg^{2+}+Fe^{2+}$ ratio) increases with increasing modal chromite content in chromitite zones of both the Stillwater Complex (Jackson, 1969) and the Bushveld Complex (Van der Walt, 1941; Ulmer, 1969; Cameron and Desborough, 1969; Cameron, 1977; Eales, 1987). The maximum Mg^{2+} content occurs in massive chromitite containing no olivine (Jackson, 1987).

Compositional variations in stratiform complexes are not restricted to individual chromitite segregations, but occur systematically through the sequence (Duke, 1983). Cameron (1977) reported massive Bushveld Complex chromitite to have higher Mg/Mg+Fe and Cr/Fe ratios than disseminated (<5%) chromites in silicate-rich rocks. These ratios also decreased upward through the sequence of chromitite horizons. Similar upwardly-decreasing MgO and Cr_2O_3 contents of chromite horizons were also reported from the Great Dyke by Worst (1958), who observed coarse-grained chromite to be more Mg-rich than fine-grained chromite.

Variations of Mg/Mg+Fe and Cr/Fe ratios with increasing modal proportion of chromite have been attributed to fractional crystallization during magma cooling under equilibrium conditions (Cameron, 1975; Eales, 1987; Stowe, 1987). Cameron (1975) noted three main stages in chromite deposition in the eastern Bushveld Complex: a cumulus, or initial, stage of formation by settling crystals; a post-

cumulus stage of crystallization from intercumulus liquid; and a subsolidus stage involving reequilibration after the disappearance of the liquid phase.

Secondary subsolidus equilibration during slow cooling has been invoked as a mechanism for the increasing Mg^{2+} content of olivine and Fe^{2+} of chromite with increasing modal proportion of chromite (Irvine, 1967; Cameron, 1975; Clark, 1978; Nixon et al, 1989, 1990). However, fractional crystallization exerts the primary control on chromite compositional variations (Cameron, 1975, 1977; Clark, 1978). Cumulate chromites of stratiform complexes are early, locally-nucleating high-temperature precipitates initially enriched in Mg^{2+} when silicates are in low abundance. The Fe^{2+} content of the magma increases proportionally as large amounts of Mg^{2+} are preferentially partitioned into silicates. Later chromite differentiates become more Fe-rich as the Mg/Mg+Fe ratio decreases in oxides and increases in simultaneously-crystallizing ferromagnesian silicates (Van der Walt, 1941; Haggerty, 1976; Cameron, 1977). Clark (1978) stated that early Turnagain magmas were rich in Cr, and that the trend in spinel compositions was from chromite to magnetite, with slight rim enrichments of Fe^{2+} due to evolving magma composition. Postcumulus reactions may be important however, and have been invoked to account for the more heterogeneous compositions of accessory chromites of the Bushveld Complex relative to chromite-rich rocks

(Cameron, 1980). Interestingly, similar compositional relations occur between detrital chromite crystals and fragments in this study (Figure 4-59).

Tulameen cumulate chromite and associated PGM are products of early high-temperature coprecipitation from a primitive magma (Nixon et al, 1990). Early chromitite is therefore more Mg and Cr-rich than later disseminated chromites. Nixon et al (1990) have shown that chromite inclusions in some Tulameen placer PGM nuggets are among the most Mg and Cr-rich of all. Consequently, primary PGM can be expected to be preferentially associated with Mg and Cr-rich chromitite segregations, and PGE-hosting detrital chromite fragments in surficial materials are likely to be partitioned into the non-magnetic fraction of heavy mineral concentrates.

5.3 Soils

5.3.1 Introduction

Most studies of PGE geochemistry have focussed on their primary distribution and behaviour, and few data are available on their subsequent mobility in the surficial environment. This has been partly due to analytical limitations (Borthwick and Naldrett, 1984; Bloom, 1986)

which until recently hindered the availability of the ppb-level analyses necessary for systematic geochemical investigations of soils and other surficial media.

The most comprehensive study to date is that of Fuchs (1972) and Fuchs and Rose (1974), who studied distribution and behaviour of Pt and Pd in soils developed from mafic and ultramafic rocks of the Stillwater Complex, Montana. Pd was found to be relatively mobile in the weathering environment, having been depleted from surficial A horizons and concentrated in underlying B and C horizons in soils developed on both till and colluvium. Pt was found to be more uniformly distributed in the soil profile. The relative immobility of Pt was attributed to the occurrence of 70% of the element as either inclusions or in solid solution within chromite (Grimaldi and Schnepfe, 1969). Fuchs (1972) and Fuchs and Rose (1974) also studied the PGE speciation amongst the various soil components. Pd was most abundant within the magnetic, clay, and organic component fractions, whereas Pt was much more variable and occured primarily in the magnetic, silt, and Fe-oxide fractions.

Other studies of PGE in soils have centred on podiform chromite occurrences in the Unst ophiolite, Shetland Islands (Leake and Gunn, 1985; Gunn, 1989), the Howland Reef of the Stillwater Complex (Riese and Arp, 1986), Cu-Ni-PGE occurrences in Quebec (Wood and Vlassopoulos, 1990) and the

Northwest Territories (DiLabio, 1988; Coker et al, 1989), and a variety of chromite-PGE occurrences in southern British Columbia (Fletcher, 1989).

5.3.2 Overview Soils

The Pt content of -70 mesh Grasshopper Mountain soils is strongly dependent on the amount of contained dunite as estimated by MgO content. The mean MgO content of dunite colluvium (24.16%) is typically 2-4 times that of till, but less than than the mean MgO content of Grasshopper Mountain dunite (42.85%) from analyses of St. Louis et al (1986). Serpentine and talc are the principal soil minerals (Appendix 6.3). Grasshopper Mountain colluvium clearly represents a soil which is almost entirely derived from mechanical weathering and mass wasting of the dunite cliffs. Pedogenic modification is the probable cause of the differing MgO contents of C horizon colluvium and the dunite bedrock. Removal of Mg from surface horizons during weathering (Robinson et al, 1935; Walker, 1954; Rabenhorst et al, 1982) is much more likely to affect the MgO content of colluvial soils than those on till.

Cr_2O_3 has a very similar distribution to MgO because of the association of disseminated chromite and massive chromitite segregations with the dunite (Findlay, 1963; St.

Louis et al, 1986; Nixon et al, 1990). The mean Cr content of Grasshopper Mountain dunite and serpentinized dunite is 2902 ppm, based on analyses by St. Louis et al (1986). The mean Cr content of Grasshopper Mountain colluvium (2257 ppm) and dunitic till (1368 ppm) is within the range of 1000 - 5000 ppm Cr found in soils developed on ultramafic rocks (Kabata-Pendias and Pendias, 1984; Brooks, 1987).

The Pt content of active colluvium (88 ppb) more closely reflects the mean Pt content (48-180 ppb) of Tulameen dunite, serpentinite and serpentinized dunite (St. Louis et al, 1986) than does till, which has been subject to varying degrees of mixing and dilution. The relatively high MgO content of till from the western part of the main study area (16.51%) and from the secondary study area (13.84%) suggest that it is a relatively locally-derived dunitic till. Conversely, the much lower MgO content (5.66% MgO), its geographically-separate relation with dunitic till (Figures 4-1 and 4-3), and the south-southwesterly direction of glacial transport indicates a lesser dunite influence on till composition in the eastern part of the main study area. Non-dunitic till is probably derived largely from rock units north or northeast of the dunite core (Figure 2-1).

The lower background Pt contents of dunitic till (36 ppb) and non-dunitic till (8 ppb) relative to colluvium are a direct result of their lower content of dunite. However,

the terms "dunitic" and "non-dunitic" are not absolute and the range of major element composition suggests a degree of till mixing. Thus high CaO and Na_2O contents in dunitic till compared to those of colluvium suggest that dunitic till must contain some exotic component. Similarly, the mean Cr_2O_3 content of non-dunitic till (0.07%; 479 ppm Cr) indicates at least a minor dunite component as the Cr content of non-dunitic soils is usually less than 100 ppm (Brooks, 1987).

Major element analysis of the soil, particularly for MgO and Cr_2O_3, is a useful mapping tool to delineate the dispersion of dunitic till. XRD results (section 4.2.1.3) confirm genetic interpretations based on till geochemistry. Non-dunitic till has a mineralogy characterized by quartz, plagioclase, hornblende and chlorite, whereas dunitic till has a mineralogy characterized by ultramafic-related minerals such as serpentine, talc, vermiculite and chromite (Appendices 6.1 to 6.3). Locally-derived dunite colluvium might be expected to be effected by windlblown dilution, but XRD results (Appendix 6.3) show it to be devoid of detectable quantities of siliceous minerals such as quartz and plagioclase. These do, however, occur in dunitic till, indicating at least a minor component of till mixing.

Pt contents of soils on till and colluvium cannot, therefore, be directly compared. They must instead be

categorized on the basis of parent material and MgO content in order to delineate background and anomalous populations within each group. Anomalous C horizon soil Pt concentrations are derived from the dispersion of massive chromitite and chromitic dunite (>10% chromite) with mean Pt contents of 3410 ppb (St. Louis et al, 1986). Anomalous concentrations, as defined by probability plots and frequency distributions, are very subtle (>16 ppb) in areas of non-dunitic till. However, they are greater than 55 ppb in dunitic till and greater than 200 ppb in dunitic colluvium on Grasshopper Mountain.

Accurate recognition of parent material is also a prerequisite for tracing the mechanical dispersion of Pt. Till reflects upice sources whereas colluvium reflects upslope sources. The presence on Grasshopper Mountain of complex composite soil profiles where colluvium overlies till (Figure 4-49) suggests that routine near-surface sampling of the B horizon may lead to erroneous interpretations of both anomaly contrast and source unless the origin of the material is correctly identified.

The relation between Pt and other trace elements is variable. Relatively high Sb values in base of slope and bog samples may be related to hydromorphic dispersion of this element from the Pt antimonides St. Louis et al (1984) reported in chromitite. High As levels are more

problematic. Those in colluvium may be partly attributed to the local mechanical dispersion of sperrylite, but high As concentrations in soils occur with all parent materials. Nicola Group rocks generally contain less than 4 ppm As, but dunite and chromitite have very erratic As contents ranging from 1 - 26 ppm (G. Nixon, personal communication, 1989). The As content of standard PT-5 (Appendix 4.2), prepared from Grasshopper Mountain dunite, is also similar to soil As levels.

High Au concentrations probably originate from two sources. Relatively high Au concentrations in serpentine colluvium and beneath PGE-chromitite occurrences are consistent with, but greater than, lithogeochemical results (4.1 ppb and 8.2 ppb) for serpentinite and chromitite, respectively (St. Louis et al, 1986). High Au values in the -70 mesh fraction (34 ppb) and -70+140 mesh non-magnetic heavy fraction (718 ppb) from a nondunitic till site (soil site 6) may have been mechanically transported from Au occurrences in the Nicola Group (Rice, 1947) on northeastern Grasshopper Mountain.

In summary, soil Pt content is related to the dunite content of the parent material and is ultimately inherited from the primary dunite of the Tulameen complex. Pt content is greatest in dunite colluvium, but decreases in till with the dilution of locally-derived till by more exotic

material. Determination of MgO content is a useful method of estimating the degree of mixing and dilution and, by extension, the background Pt contents of tills in the vicinity of dunite bedrock.

5.3.3 Variations in Soil Pt Distribution With Depth

Several Pt concentration trends with depth occur on different surficial materials and landscapes of Grasshopper Mountain. Relatively constant, though locally erratic, Pt concentrations with increasing depth in active colluvium are consistent with the unhorizonated and constantly-evolving nature of the material. Pt concentrations in non-dunitic and distal dunitic tills increase with depth, whereas those of higher-concentration dunitic till/rubble adjacent to known mineralization either increase or remain constant with depth (section 4.3.2). Total Pt contents also increase downprofile at most sites (section 4.3.2.3). Relative increases in Pt concentrations in C horizons are generally more apparent in density/magnetitic fractions than in individual size fractions and are most pronounced in the non-dunitic till profiles. Vertical Pt variations within the soil profile may be a primary clastic dispersion feature within basal and/or ablation till, a result of more recent colluvial processes, or a product of secondary pedogenic processes. Clastic dispersion of basal till, however, is

probably the main control on Pt variations over most of the study area on Grasshopper Mountain.

5.3.3.1 Primary Clastic Dispersion

The vertical distribution of Pt in soils on tills on Grasshopper Mountain is most consistent with clastic dispersion plumes (Drake, 1983; Miller, 1984) of dunitic material. Mechanical dispersion fans in tills give negative exponential dilution of the element of interest downice from a mineral deposit (Shilts, 1976; Rose et al, 1979). Dispersion plumes, however, are three-dimensional features in which dunitic and/or chromititic material, entrained at the glacier base as lodgement till, would be mixed and diluted with exotic material as it gradually rises from the bedrock to the till surface (Drake, 1983).

Plumes may be diverted or displaced in alpine areas such as the Cordillera, however, where ridges and valleys obstruct and divert glacial flow directions (Shilts, 1976, 1982; Drake, 1983). Debris is transported for greater distances through valleys than across upland areas (Clark, 1987). Under such circumstances, glacial flow lines parallel the topography and debris rises from the glacier base in the lee of the obstruction (Boulton, 1978; Clark, 1987). The subparallel relation of the dunitic till/non-

dunitic till boundary with the topographic curvature of southeastern Grasshopper Mountain (Figures 4-1, 4-5 and 4-18) may be an example of this.

There is thus a gap between the subcrop of a geochemically distinct unit and the appearance of a related geochemical anomaly at the surface. In the present study, this is the distance between the margin of the dunite core and its geochemical appearance in near-surface till. The gap may be negligible, pinpointing the source in thin till as, for example, at the A-Zone, or it may increase with increasing till thickness (Drake, 1983).

There are two scales of Pt dispersion plumes on Grasshopper Mountain: a regional scale plume, similar to other large ultramafic dispersion fans (Shilts, 1976; Maurice, 1988) in which higher Pt values are related to high Pt content of contained dunite, and much smaller plumes containing considerably higher Pt concentrations derived from chromitite segregations within the dunite. These are shown in an idealized model of landscape elements and mechanical Pt dispersion in Figure 5-2.

On a regional scale, dunitic material is mixed with exotic material from outside the dunitic core. Serpentinized dunite, being a relatively soft rock, probably provided a relatively large amount of material to the

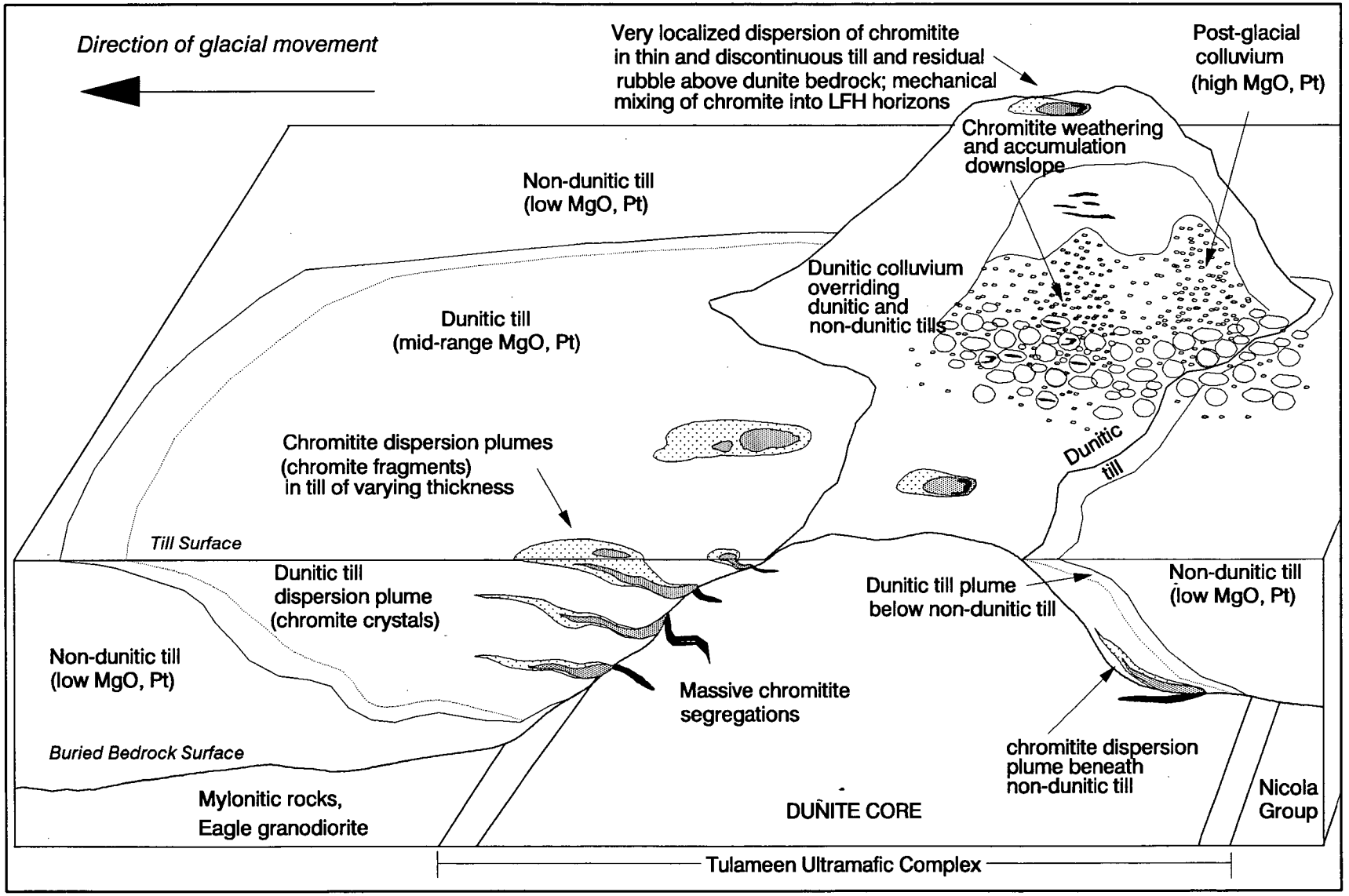

Figure 5-2. Idealized model for mechanical dispersion of Pt on Grasshopper Mountain.

dispersion plume (Shilts, 1982). The surface geochemical expression of the predominately dunitic till is not encountered until the dunitic/non-dunitic till boundary (Figure 4-13). Background sampling around the western edges of the dunite core (Figure 4-18) indicates, on the basis of MgO, Cr_2O_3 and Pt contents, that the regional dispersion plume persists downice beyond the western margin of the core. Evenson et al (1979) showed that glacial flow directions could be determined by analysis of heavy mineral suites. The glacial transport path in the Grasshopper Mountain area, and maximum extent of the regional plume southwest of the dunite core, could probably be outlined in a similar manner by tracking characteristic-composition chromite grains from heavy minerals in till. It should be noted that dispersion patterns of both dunitic and non-dunitic till may be obscured by their incorporation, at lower elevations, of pre-glacial colluvium lying in the path of the glacier. For example, Sibbick (1990) attributed the location of a gold dispersion train in southern B.C. to the incorporation of mineralized colluvium into till. There is no evidence of this on Grasshopper Mountain, but earthflows in south-central B.C. are nevertheless more common on serpentinized rocks than on unaltered dunite or peridotite, possibly because the platy habit of serpentine minerals act as earthflow boundary shear zones (Jones, 1988).

On a more detailed scale within the dunite plume, the

local occurrence of high Pt concentrations in till is dependent upon two factors: (i) source rock lithology; in particular, whether the till is derived from comminution of dunite containing only ubiquitous disseminated chromites, or contains an additional component from erosion of Pt-rich chromitites; and (ii) till thickness. Figures 4-50B and 4-51B show that total soil Pt contents are greatest just above bedrock, relative to higher parts of the profile, even in relatively thin till and residual rubble. Abrupt downprofile increases in Pt concentration at non-dunitic till sites probably indicate the subsurface top of the dispersion plume at those locations. This interpretation is supported, at soil site 20 (Figure 4-46), by near-identical low Pt concentrations in most Aej and Bf horizon magnetic concentrates and considerably greater Pt concentrations in the C horizon magnetic concentrates. Site 6 in non-dunitic till shows a similar relation. It is difficult to envision these differences arising from any type of post-glacial pedogenic processes.

Dispersion of relatively thin chromitite segregations within a softer dunite envelope is likely to be quite limited prior to dilution by barren dunite containing only background Pt concentrations. Consequently, displaced fragments of crushed PGE-rich segregations are unlikely to persist far from source, and high concentrations may only reach the till surface in areas of thin overburden (Figure

5-2). Even within individual profiles, weight percent distributions of non-magnetic relative to magnetic heavy minerals increase with depth at most dunitic till sites (Table 4-11). Thus, proximity to underlying bedrock exerts a major control on the vertical Pt distribution within the dunitic till-dominated part of the plume.

There are two alternative mechanisms for the vertical Pt distribution, but neither is as plausible as the dispersion plume model. The abrupt 5x enrichment of magnetic heavy mineral-associated Pt in C horizon soils at non-dunitic till sites (Figure 4-46) in relatively thick till suggests that PGM or PGE-hosting chromite grains may have been concentrated at depth by density segregation (Lakin et al, 1974). However, fragmentation and downward movement of heavy particles during soil creep cannot explain the subtle downprofile increase in the Pt content of the light mineral fraction. The upper horizons may alternately represent a poorly-compacted ablation till deposited above an earlier, more locally-derived, Pt-bearing lodgement till during glacial melt out (Flint, 1971). However, ablation tills typically have a lower fines content than lodgement tills (Flint, 1971). This is inconsistent with the grain size distribution of the -270 mesh fraction in individual profiles (Table 4-10, Appendix 11.2).

5.3.3.2 Post-glacial Processes

Post-glacial colluvial and pedogenic processes also influence the vertical distribution of Pt. Pt concentrations in active colluvium (Figure 5-2) are higher than in till, but variations with depth are minimal. The extent of Pt variations caused by thin colluvium overlying till are dependent on the relative magnitude of Pt concentrations in the two parent materials. For example, the covering of till by colluvium at soil site 34 (Figure 4-49) prior to vegetation of the area has resulted in near-surface Pt concentrations that are 2-6x that of the underlying till. The same relation is not, however, observed at A-Zone soil site 57 (Figure 2-14B; Appendix 12.9) because high Pt concentrations in the colluvial surface horizon are similar to those of the underlying till.

Secondary pedogenic processes may also modify the primary Pt distribution by redistributing it vertically in the profile during weathering. Here these processes appear minor compared to glacial dispersion and colluvial mass wasting. The more-widespread effect of weathering on Pt distributions within individual horizons will be discussed in a later section. However, prior development of composite profiles by colluvium (site 34), water reworking of till (site 43), or disruption by colluvial boulders (site 33) may have precluded pedogenic Pt enrichment or depletion at some

sites. Similarly, there are no apparent pedogenic modifications of Pt concentrations in active colluvium, as these horizons are juvenile and and constantly evolving.

One possible pedogenic modification of the soil Pt distribution occurs in the Bf horizon of a humo-ferric podzol (site 20) in non-dunitic till (Figure 4-46). Matelski and Turk (1947) reported that the greatest decomposition of both heavy opaque and ferromagnesian silicate minerals of some Michigan podzols occurred in the B horizon. They attributed this to the presence of organic coatings on mineral particles. Lower Pt concentrations in both -140+270 heavy fractions, lower weight percent heavy minerals and much greater proportions of magnetic heavy minerals relative to other horizons (Table 4-11) suggest a similar decomposition of non-magnetic PGE-bearing chromite or, more likely, silicates in this Bf horizon.

A second example of possible pedogenic redistribution of Pt involves its enrichment in the near-surface Bm horizon of a distal profile (site 69) on the plateau of Grasshopper Mountain. In a reversal of more common Pt concentration trends, Pt associated with the magnetic and non-magnetic heavy fractions are generally enriched 2-6x in the near-surface Bm horizon relative to the C horizon. Pt concentrations in the Bm horizon generally increase with decreasing grain size and the greatest difference between Pt

concentrations of the two horizons is in the finer size ranges (Figure 4-40B; Appendix 12.6). Total Pt content of the Bm horizon (103 ppb) is also much greater than the C horizon (40 ppb), as shown in Figure 4-51A.

XRD results of the -270 mesh fraction reveal interesting mineralogical differences between Bm and C horizons at this site (Appendix 6.2). Quartz and vermiculite are the most important minerals in the two respective horizons. The Bm horizon has more quartz and chromite, similar crysotile, and much less vermiculite than the underlying C horizon. The quartz may be indicative of windblown dilution of the Bm horizon by exotic material, while vermiculite is probably the result of pedogenesis in the C horizon (Rabenhorst et al, 1982). Chromitic dunite was also observed in Bm horizon fragments in the field, and the high Pt content of the Bm horizon relative to the C horizon is probably related to its higher chromite content. However, the origin of this is somewhat of an enigma. It seems unlikely that a later ablation till would contain more Pt than a locally-derived basal till, and eluvial concentration of chromites (Laznicka, 1985) is not a plausible explanation in this weathering environment.

In summary, vertical distribution of Pt in Grasshopper Mountain soils is primarily a clastic dispersion feature. In till, it occurs on both regional and local scales, and is

controlled by source rock lithology and proximity to bedrock. Downprofile variations are minimal in active colluvium, and relatively constant Pt concentrations are controlled by source lithology. Pedogenic modification of soil Pt distributions is relatively insignificant, and cannot be confidently invoked to explain features of more than a single profile.

5.3.4 Pt Residence Sites in Mineral Horizons

Pt residence sites among size, density and magnetic fractions of Grasshopper Mountain soils depend on overburden type, source mineralogy and proximity to bedrock.

5.3.4.1 Residence Sites

Similar Pt concentrations in all 5 size fractions (Figure 4-40) of horizons at non-dunitic till and many dunitic till sites indicate that Pt is not preferentially partitioned into any single size range of the -10 mesh (<2 mm) component. Non-dunitic till sites are all, however, located in relatively thick till compared to many dunitic till sites. Consequently, Pt distribution among size fractions in dunitic till, rubble and colluvium is much more influenced by proximity to bedrock. There is a tendency for

higher Pt concentrations to occur in the coarser size fractions of these materials (Figures 4-40 and 4-41), although this is not the case for every profile.

These results do not agree with previous work. DiLabio (1988) reported extremely erratic Pt concentrations in several size fractions of gossanous material from the Ferguson Lake Ni-Cu sulfide occurrence, N.W.T., with maximum concentrations generally occurring in the <63 um fraction. Variations from <10 ppb to 100-1000 ppb Pt in adjacent fractions were attributed to the presence of erratically-distributed micronuggets, but as no sample weight data was given, this cannot be evaluated.

Size fractionation of Pt in dunite colluvium beneath the Cliff Zone seems, on the basis of very limited evidence, to be partly dependent on slope morphology. Soil site 16 is situated within a uniform mass of colluvium (Figure 2-12) immediately beneath the D-Zone and exhibits remarkably uniform Pt concentrations among size fractions. Soil site 9, further downhill from the C-Zone, is located on the edge of a narrow gully which has been partially stabilized by vegetation (Figure 2-11A). It exhibits a much more erratic Pt distribution. At both sites the relatively coarse-grained -70+140 mesh fraction contains the highest Pt concentrations in 2 out of 3 samples.

Pt is preferentially partitioned into the heavy mineral fraction by a factor of 10-20x relative to the light mineral fraction. Nevertheless, one-third to one-half of the total Pt content of individual horizons is in the light mineral component (Figures 4-50 and 4-51). This, and the sympathetic increase in the Pt content of the light fractions with that of the heavy fractions, suggests that a considerable amount of soil PGM occur as either fine PGM grains or as inclusions within very fine chromite inclusions in larger olivine, serpentine and talc particles. PGM or oxides are evidently not abundant enough to cause the silicate grains to sink during heavy liquid separation.

There is abundant evidence to support this. PGM inclusions in Tulameen olivine have been reported by Bohme (1988) and occur in soil silicates (talc?) examined in this study. Silicate-associated PGE have been reported to constitute about a third of the total PGE in some Uralian dunites (Razin et al, 1965; Razin, 1971). Most occur in forsteritic olivine, with some adsorbed onto hydrous Fe-oxides associated with serpentine; this interpretation has, however, been questioned by Crocket (1974). Interstitial silicates containing discrete PGM have also been reported from Stillwater chromitites (Page and Jackson, 1967). Chromite is texture-independent in till dispersion fans from igneous sources (Shilts, 1973, 1976). Consequently, PGM inclusions such as those in chromites in the -140+270 mesh

fraction (Figures 4-54 and 4-55) would also be expected to occur in much smaller chromite grains within silicates.

Partitioning of Pt into magnetic and non-magnetic heavy mineral fractions appears to be related to distance from supposed source and, to a lesser extent, source rock mineralogy and grain size. The relation of the former to Pt-chromitite occurrences and landscape elements is depicted schematically in Figure 5-3 using data from several detailed profiles. Sites on both dunitic and non-dunitic till that are distal from known mineralization contain 10-20x more Pt in the magnetic than the non-magnetic heavy fraction. These results are consistent with those reported by Fletcher (1989) for Grasshopper Mountain soils. However, till, rubble and colluvium sites adjacent to known occurrences typically contain a much higher proportion of Pt in the non-magnetic fraction, in some cases exceeding that of the magnetic fractions. This relation has important implications for geochemical exploration for chromitite-associated PGM.

The highest proportions of Pt in the non-magnetic heavy fractions occur in serpentine colluvium. Although SEM examination of the -140+270 mesh heavy fractions of one sample (88-SC-105) revealed no discrete PGM, the very high Pt concentrations in the fine non-magnetic fraction (Appendix 11.7) probably reflect the original platinum-group

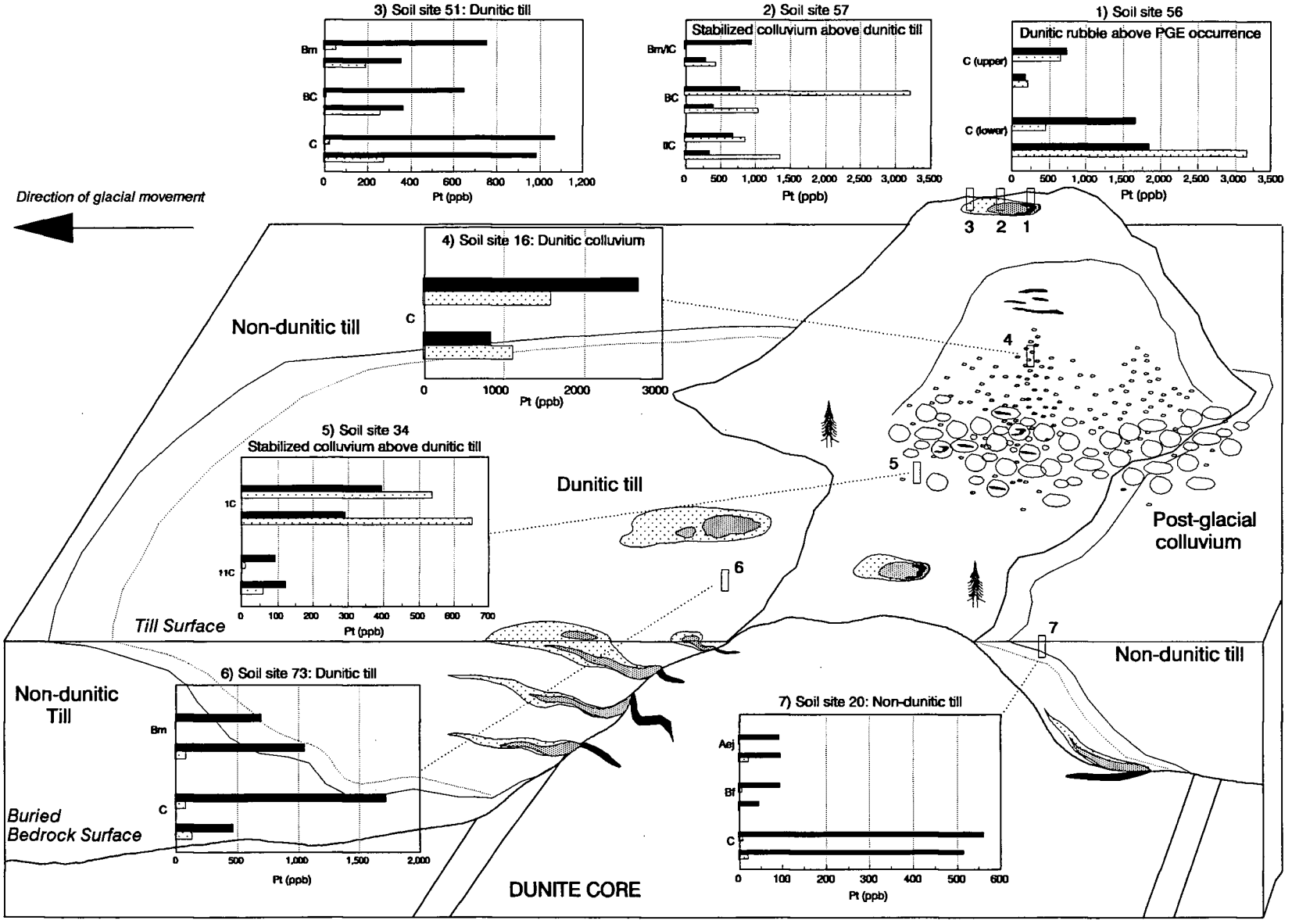

Figure 5-3. Pt distribution in magnetic (black bars) and non-magnetic (stippled bars) heavy fractions of selected soil profiles, and its relation to idealized Pt occurrences and landscape elements on Grasshopper Mountain. Symbols and surficial materials as in Figure 5-2. Pt distributions as in Appendix 12; for each horizon, upper two bars represent -70+140 mesh fraction and lower two bars represent -140+270 mesh fraction.

mineralogy of the serpentine source rocks. Whereas even the most minute PGM will partition into coarser fractions if encapsulated within a chromite host, those interstitial to chromite grains (St. Louis et al, 1986) would be liberated during erosion and fragmentation of the rock, and probably partition into the -270 mesh fraction. It was not, however, possible to make heavy mineral separations of the -270 mesh fraction to verify this. In contrast, partitioning of magnetic-fraction Pt from dunitic colluvium into the coarser -70+140 size range (Figure 5-3) probably reflects both platinum-group mineralogy and an initial state of dunite and chromite weathering. Large magnetic free PGM grains in dunitic colluvium beneath the Cliff Zone may exceed 100 um in diameter (section 4.4.2.1), and these sites have a much lower proportion of fine-grained fraction material than till (Table 4-10; Appendix 11.2).

Heavy non-magnetic soil fractions (-140+270 mesh) generally contain about 80-90% silicate minerals, primarily Mg-silicates, with the remainder comprising chromite, ilmenite, iron oxides, and oxidized sulfides (Tables 4-15 and 4-16). PGM were observed within chromite, but it is not possible to further speciate the Pt content of other metallic phases as no monomineralic separates were made or additional microprobe analyses performed.

In spite of the well-known sulfide-PGE association in

many deposits (Paktunc et al, 1990), there is no evidence that Pt is associated with Fe sulfides, oxidized sulfides or Fe-oxides in the non-magnetic heavy fraction of Grasshopper Mountain soils. No discrete PGM were observed in any oxidized sulfide grains. Sulfides are much less abundant than chromite in C horizons at 3 of the 4 highest-Pt sites, including those adjacent to known mineralization (Tables 4-15 and 4-16). Three additional till sites in which oxidized sulfides and iron oxides are a dominant constituent of the non-magnetic heavy fraction have very low Pt contents (22-179 ppb), although a fourth till contains 1371 ppb. Experimental evidence (Makovicky et al, 1986; Paktunc et al, 1990) indicates that pentlandite is the only sulfide in which some of the PGE can occur in solid solution, and that Pt is not among these.

In summary, morphological and analytical evidence show that higher Pt concentrations associated with non-magnetic heavy fractions of colluvium and dunitic till/rubble adjacent to known occurrences are related to the erosion and limited dispersion of nearby chromitite segregations (section 5.2). It would be simplistic to imply that all Pt is partitioned into non-magnetic fractions as that is obviously not the case at most sites. The occurrence of more Fe-rich chromite segregations, or near-segregation, Fe-rich, PGE-bearing chromite crystals which may be more broadly dispersed than the fragments themselves, are

possible explanations for the Pt content of the magnetic fractions. This is consistent with SEM observation of many magnetic and paramagnetic chromite fragments, the discovery of PGM inclusions within a magnetic fraction chromite crystal at the A-Zone occurrence, and the very high (563 ppb) Pt content of a magnetic fraction from non-dunitic till (site 20) containing no chromite fragments (Table 4-16).

5.3.4.2 Pedogenic Redistribution of Pt within Horizons

Contributions of different size fractions to the total Pt contents of individual horizons (Figures 4-50 and 4-51) provide evidence for the pedogenic redistribution of Pt during weathering. The total amount of Pt contained in individual fractions is primarily a function of parent material comminution. Approximately one-half the Pt within glacially-crushed till occurs in the -270 mesh fraction, whereas about one-half that in more juvenile colluvium and rubble occurs in the coarse -10+40 mesh fraction. Within these major bounds, however, there is considerable redistribution of the Pt within individual horizons.

Increases in the proportion of Pt in fine fractions towards the surface in most till and rubble profiles is clearly a result of grain size reduction during weathering. Although Bm horizon heavy concentrates were not observed

with the SEM, near-surface weathering and dissaggregation of silicate fragments would release both minute PGM and PGM-bearing silicate and chromite grains to finer size fractions.

5.3.5 Pt Residence Sites in LFH Horizons

Very little data is available on either the content or behaviour of PGE in LFH horizons. Humus or forest litter commonly contains a wide range of plant species and organs in various stages of decay (Dunn, 1986). Elemental partitioning between organs has been reported to be particularly well developed in conifers (Coker et al, 1989), and there are numerous reported North American examples of appreciable Pt in ashed organs of vascular plants. These include trees such as Black spruce (*Picea mariana*), Jack pine (*Pinus banksiana*) (Dunn, 1986; Dunn et al, 1989), Douglas fir (*Pseudotsuga menziesii*) (Riese and Arp, 1986) and Glandular birch (*Betula glandulosa*) (Coker et al, 1989), as well as understory shrubs such as Labrador tea (*Ledum groenlandicum*) (Dunn, 1986) and flowers such as *Eritrichium chamissonis* (Rudolf and Moore, 1972).

Pd (Coker et al, 1989) and Au (Curtin and King, 1983) are enriched in surficial humus by being mobilized in solution, taken up into vegetation through the root system,

concentrated in plant organs, and ultimately returned to the surface. Humus Pd concentrations of up to 340 ppb have been reported above Pd-Pt mineralization associated with Ni-Cu sulfides at Lac des Iles in northwestern Ontario (Fortesque et al, 1988). The dominance and sulfide association of more-hydromorphically mobile Pd at this locality is, however, probably of little relevance to chromite-associated, Pd-poor Pt deposits such as those of Grasshopper Mountain. It is unlikely that the Pt content of Grasshopper Mountain LFH horizons, which are 10x greater near known mineralization than in background areas (section 4.3.2.2), can be attributed to similar biogeochemical cycling. Biogeochemical methods have had only limited success on Grasshopper Mountain (Dunn, 1990). Ashed twigs and bark of Douglas fir, Lodgepole pine and Whitebark pine sampled directly above and adjacent to the A-Zone at the secondary study area have uniformly low Pt concentrations, rarely greater than 10 ppb (C. Dunn, personal communication, 1990) even at sites where LFH horizon ash contains 100-150 ppb Pt.

Chromium is most stable as Cr^{3+} in relatively inert and insoluble chromite and related spinel structures. Cr^{3+} is mobile only under acidic and highly oxidizing conditions (Bartlett and Kimble, 1976; Cary et al, 1977) unlikely to occur in Grasshopper Mountain soils. Plant roots are capable of dissolving and absorbing trace elements from the soil, but cannot reduce Cr^{3+} in soil chromite to soluble

Cr^{2+} (Kabata-Pendias and Pendias, 1984). Consequently, Cr is not readily available to plants (Gough et al, 1979; Kabata-Pendias and Pendias, 1984). Thus, the occurrence of Pt as inclusions encapsulated within resistant chromite (Figures 4-54 and 4-55) is the most probable cause of the poor biogeochemical response, inhibiting its mobilization in soil solutions and subsequent uptake into vegetation.

Several factors suggest that the Pt content of LFH horizons, particularly those near mineralization, is related to the presence of particulate dunite or chromite fragments within the LFH material. Foremost is the almost universal presence of a small proportion of insoluble residue of carbon and/or mineral particles, usually 2-18 weight percent remaining after acid digestion of the ash. Most silicate minerals, including olivine, talc, magnetite and hornblende (section 4.5), are decomposed in perchloric-hydrofluoric acid solutions (Langmyhr and Sveen, 1965). However, spinels and the sulfides pyrrhotite, pyrite and chalcopyrite are not readily decomposed by this acid mixture (Riley, 1958; Langmyhr and Sveen, 1965), and probably comprise the bulk of the residue. Higher proportions of insoluble residue are generally greater at, although not restricted to, the secondary study area and to colluvial sites where the LFH horizon is continually inundated with downslope-moving rock fragments (Table 4-7).

Mineral particles are a common constituent of LFH horizons (Dunn, 1986), particularly in the lowermost H horizon near the contact with mineral soil (Agriculture Canada Expert Committee on Soil Survey, 1987). Pt content of dunite and chromite particles in dunite-dominated areas appears to influence the Pt content of the LFH horizon in much the same manner that the proportion of dunite influences the background Pt content of mineral soils (section 5.2.2). Similarly, the presence of barren rather than Pt-bearing particles in non-dunitic soils would not contribute any Pt to the LFH horizon.

Lithic and mineral particles may be naturally incorporated into LFH horizons in several ways. Downslope movement of dunitic fragments is clearly the cause of high Pt concentrations in LFH horizons on active colluvium. The introduction of mineral particles into LFH horizons at forested till sites however, may be the result of wind action, bioturbation, tree uprooting or the incorporation of particle-laden forest litter into the humus. LFH Fe concentrations represent partial extractions exclusive of spinels or sulfides. Relatively high Fe contents of 3-5%, associated with both high LFH Pt contents at the A-Zone and on active colluvium, as well as with low LFH Pt contents at several non-dunitic till and clay sites, suggest that Fe-rich mineral grains are natural components of LFH horizons.

The positive correlation between LFH Pt and C horizon Pt (Figure 4-25) supports the mixing model of Pt introduction into the LFH horizon. The origin of high (>1) LFH/C horizon Pt ratios (Figure 4-26) is not always clear, however. High ratios in some A-Zone sites, although erratically distributed, are clearly the result of mixing of near-bedrock, high-Pt mineral soil into thin LFH horizons. The narrow normal distribution of low ratios at background-level dunitic till sites seems to be a distinctive feature of these tills. Furthermore, the five sites with the lowest ratios occur on relatively gentle topography where colluvial action and tree uprooting are uncommon. The origin of some higher ratios (>1) on non-dunitic till is more problematic. Some may be an artifact of reduced analytical precision at low C horizon Pt concentrations (Figure 3-8), but the clustering of high-ratio sites on the relatively thick non-dunitic till of the seepage zone and southern forested slope area suggests that biogenic accumulation of low-level Pt in LFH horizons may be comparatively more active in this area.

The secondary study area was the site of surface blasting and trenching during exploration of the A-Zone (Bohme, 1987, 1988). The possibility therefore exists that the high Pt concentrations in some LFH relative to C horizons (Figure 4-26) might reflect artificial contamination from airborne dunite fragments and dust rather than natural processes. Several factors however, suggest

this to be unlikely. Airborne contamination would probably result in these samples containing a higher proportion of lithic fragments than are found at other sites. However, there is no appreciable difference in the median weight percent ash (Table 4-9) of the A-Zone sites (11.34%) and that of sites on dunitic and non-dunitic till (11.45% and 13.90%, respectively), while that of inundated colluvium (21.96%) is much higher. Similarly, the proportion of insoluble residue at most A-Zone sites is not very different from that found elsewhere, and spatial distribution of insoluble residue values are not consistent with artificial contamination from blasting. Furthermore, the highest LFH Fe value above dunitic till (3.00%) coincides with the highest -70 mesh overview Pt value (311 ppb) in the main study area (site 73; Figure 2-8B). This site was not disturbed by exploration activity, indicating that higher LFH Fe values here and, by extension, at the A-Zone can result from naturally-occurring minerals in the underlying soil rather than from airborne dust.

5.4 Hydromorphic Transport of PGE: Evidence from Seepage Bogs and Waters

The PGE have historically been considered inert and insoluble, with a negligible aqueous geochemistry (Plimer and Williams, 1988). Renewed interest in hydrothermal Pt

deposits has raised questions concerning the role that chemical, or hydromorphic, transport mechanisms play in mobilizing PGE in the surficial environment. Several studies have provided evidence for hydromorphic redistribution of PGE in different weathering environments. These include soil profiles over the Stillwater Complex, Montana (Fuchs, 1972; Fuchs and Rose, 1974), nickel sulfide gossans in Western Australia (Travis et al, 1976; McGoldrick and Keays, 1981), oxide zones of the Bushveld Complex (Wagner and Reinecke, 1930; Cousins and Kinloch, 1976), lateritic weathering profiles in Brazil (Taufen and Marchetto, 1989), Ethiopia (Otteman and Augustithis, 1967) and Sierra Leone (Bowles, 1986, 1988), polluted sediments in Germany (Dissanayake et al, 1984), and alluvial PGM placers from a variety of localities (Cousins, 1973; Cousins and Kinloch, 1976; Stumpfl and Tarkian, 1976; Burgath, 1988).

Hydromorphic redistribution of PGE in the Canadian Cordillera is limited by the temperate climate, young age of the glacially-transported overburden, and immature soil development relative to that of tropical or older landscapes. With the exception of zoned Os-Ir placer PGM from Atlin and Discovery (Cousins and Kinloch, 1976), hydromorphic mobilization and/or secondary growth of surficial PGM in the Cordillera has not been proposed. Clastic glacial dispersion and post-glacial mass wasting have been shown as the dominant processes influencing Pt

distribution in Grasshopper Mountain soils. However, the distribution of PGE and other elements in seepage zone bogs and surface waters, together with the presence of soil PGM grains released from, or not encapsulated in, chromite (Figures 4-52 and 4-53) suggests the possibility of a minor hydromorphic modification of the clastic dispersion plume into a downslope area dominated by non-dunitic till. This section therefore examines the hydromorphic transport of Pt in groundwater, and its possible absorption onto organic matter in locally-reducing break of slope seepage zones and bogs. It is not the intention of the author to provide a quantitative estimation of PGE transport in surficial waters, but rather to review theoretical and field evidence for and against its occurrence on Grasshopper Mountain.

5.4.1 Constraints on PGE Mobility

Initial liberation of Pt from dunite and unconsolidated sediments prior to hydromorphic transport is largely dependent on particle size and host mineralogy. Weathering proceeds more rapidly in till than bedrock because of the greater abundance of fine-grained particles (FitzPatrick, 1980). Forsteritic olivine is a major constituent of serpentinized dunite although only a minor constituent of Grasshopper Mountain soils. It is the least resistant of the common silicates to surficial weathering (Goldich,

1938). Olivine dissolution occurs by hydrolysis; etch pits are formed along cleavage planes and lattice dislocations, surface area increases, and Mg^{2+} in the structure is replaced by H^{+} from the soil solution. Subsequent removal of Fe^{2+} completes the breakdown of the mineral surface (Grandstaff, 1978; FitzPatrick, 1980; Huang, 1989), causing more-resistant chromite and discrete PGM grains to be released to the weathering environment. Serpentine is similarly weathered to smectite (Rabenhorst et al, 1982). Although the weathering behaviour of fine magnetite (FitzPatrick, 1980) suggests that very fine-grained chromite may be somewhat more subceptible to decomposition than coarser grains, PGM encapsulated within resistant chromite generally remain isolated (Fuchs and Rose, 1974) from the weathering cycle. PGE occurring in solid solution, as free grains (Figure 4-52) or as inclusions in Mg-silicates (Figure 4-53) are, however, exposed and available to the weathering cycle.

Theoretical studies on the transport of Pt and Pd in aqueous solutions have been provided by Fuchs and Rose (1974), Mountain and Wood (1988a,b), Plimer and Williams (1988) and Wood et al (1989). Pt and Pd may occur as either 2+ or 4+ simple ions, particularly the former. Pd^{2+} is marginally more soluble than Pt^{2+} but both are immobile at $25^{o}C$ under all but the most acidic and oxidizing conditions. They have a preference for covalent bonding, however, and

form soluble stable inorganic complexes with chlorine (Cl^-), bromine (Br^-), iodine (I^-), cyanide (CN^-), thiocyanate (SCN^-), sulfite (SO_3^{-2}), thiosulfate ($S_2O_3^{-2}$), nitrite (NO_2^-), hydroxyl (OH^-), ammonia (NH_3) and bisulfide (HS^-). The relative scarcity of many of these ligands in surficial water, however, limits discussion of PGE transport to chloride, thiosulfate, and bisulfide complexes, and to poorly-understood organometallic complexes with soil organic matter such as humic or fulvic acids (Wood, 1990).

The relative importance of these complexing agents is partly dependent on their solubility under surficial conditions. An Eh-pH diagram of the system Pt-O-H-S at 25°C and 1 bar (Brookins, 1988) is shown in Figure 5-4, along with superimposed stability fields of some aqueous Pt-chloride and thiosulfate complexes and Eh-pH ranges of soils, peat bogs, shallow ground waters and British Columbia bog waters.

Native Pt is the dominant Pt species within the Eh-pH bounds of natural waters (Brookins, 1988; Figure 5-4). It is apparent, however, that aqueous chloride and thiosulfate complexes may be locally important. Pd depletion from surface horizons at the Stillwater Complex was attributed to chloride complexing (Fuchs and Rose, 1974). Chloride complexes, as $PtCl_4^{2-}$ are, however, capable of mobilizing Pt only in highly acidic and oxidizing environments (Mountain

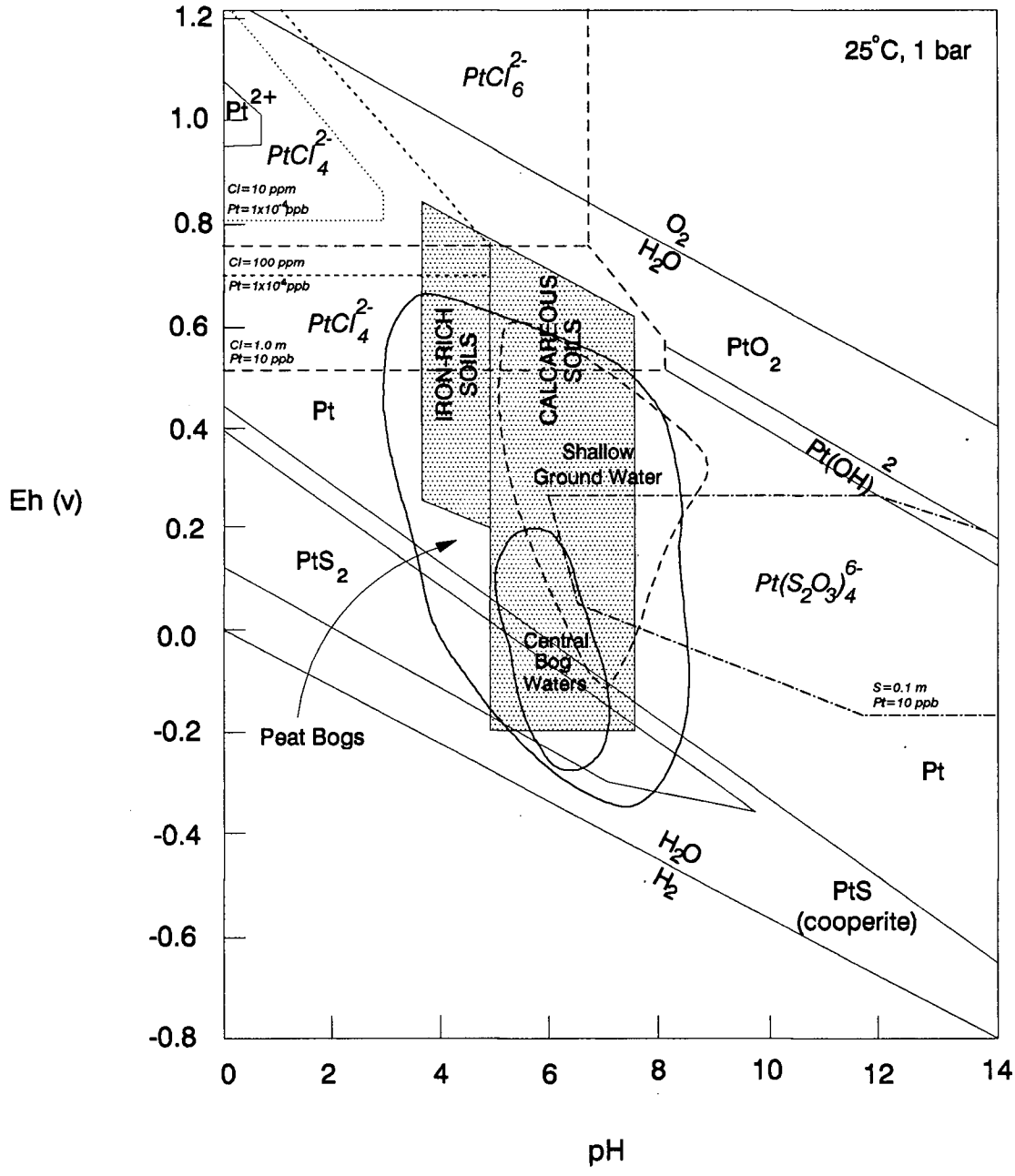

Figure 5-4. Eh-pH diagram for Pt at 25 °C and 1 bar, with superimposed stability fields of some chloride and thiosulfate complexes. Eh-pH ranges of iron-rich and calcareous soils, peat bogs, shallow ground water and British Columbia central bog waters are also shown. Eh-pH diagram after Brookins (1988). Chemical data after Fuchs and Rose (1974), Westland (1981), and Mountain and Wood (1988a). Environmental fields after Baas Becking et al (1960) and Lett (1978).

and Wood, 1988a,b; Wood and Mucci, 1988) such as those of lateritic soils (Bowles, 1986, 1988). Chloride concentration is a critical factor in determining PGE solution in soils (Bowles, 1986). Eh of $PtCl_4^{2-}$ formation is lower, hence surficial mobility greater, with increasing chloride concentration.

Cl^- concentrations in Grasshopper Mountain soils or groundwaters were not determined. However, a Cl^- value of 232 ppm has been reported for some Tulameen serpentinite (10-75% serpentine) by Stueber et al (1968). Other workers (Earley, 1958; Rucklidge, 1972) have also documented the very high Cl^- content of serpentinized dunites. The implications for hydromorphic PGE transport should not be overlooked. Cl^- occurs in solid solution within serpentine veinlets, where it may have been introduced during serpentinization, and attains maximum concentrations of 0.8% (Rucklidge, 1972). It is water-soluble (Stumpfl, 1974) and easily liberated during weathering (Goldschmidt, 1954). Although speculative, it would seem that the greater the Cl^- concentration of the dunitic soil solution, the more likely it might complex with available bedrock or soil PGM.

Among other inorganic ligands, thiosulfate complexes have been theorized to mobilize PGE over a near-neutral to slightly basic pH range of 5-9 during sulfide oxidation (Mountain and Wood, 1988a; Plimer and Williams, 1988). The

stability field of one thiosulfate complex, $Pt(S_2O_3)_4^{6-}$, overlaps the Eh-pH range of shallow groundwater (Figure 5-4) under more reasonable surficial conditions than those required for Pt chloride complexes to form. However, the importance of thiosulfate complexing may be minimal on Grasshopper Mountain because sulfides are not abundant (section 2.3). Low sulfide content may also limit Pt transport as bisulfide complexes. Solubility of these, although limited by the low activity of Pt^{2+} under reducing conditions where HS^- is dominant (Mountain and Wood, 1988), increases with increasing S content at basic pH (Wood and Mucci, 1988).

Fuchs and Rose (1974) stated that PGE mobility would be expanded by the existance of organic, as well as inorganic, complexes. Knowledge of the interaction of humic substances with the PGE is limited. Fulvic and synthetic phthalic acids are able to transport ppm-levels of Pt over a wide pH range, probably by stabilization of colloidal suspensions rather than by formation of soluble organometallic complexes (Wood, 1990). Dissanayake et al (1984) however, showed that Au, Pt and Pd are fixed as organometallic complexes in humic acid-rich organic sediments of the Rhine River. PGE were suggested to have been locally concentrated by being reduced through complexing with humic acids, in response to local changes in sediment redox conditions, and precipitated onto clay minerals in the sediment. Concentration of precious

metals, up to 1000 ppm Pd and 370 ppm Pt, near the base of the Kupferschiefer black shale in the Zechstein copper deposits of Poland have also been attributed to redox processes (Kucha, 1982).

5.4.2 Bogs

Numerous examples exist for the scavenging of Cu, among other metals, in Cordilleran bogs (Bradshaw, 1975; Lett and Fletcher, 1979). Bog interpretations are based on very limited data but suggest that low concentrations of hydromorphically mobile PGE may be similarly scavenged in a reducing environment. Evidence falls into two general areas: the relation of Pt concentrations in bog ash to those in the ash of adjacent LFH horizons, and the occurrence of higher Pt concentrations at bog margins relative to bog centres.

Ashed bog samples adjacent to Pt mineralization at the A-Zone (32-55 ppb) contain approximately the same, or lower, order of magnitude of Pt as nearby LFH horizons (Figures 4-21 and 4-32). Those from the larger of the seepage zone bogs (bog 2) in the main study area, however, contain the highest concentrations of Pt (65-67 ppb) and Pd (13-19 ppb) of any of the three bogs. Equally important, they also contain 3-30x the Pt concentrations and, with one exception,

2-4x the Pd concentrations of ash from adjacent LFH horizons. The lower Pd content is probably due to its lower abundance in the dunite core (St. Louis et al, 1986).

Pt enrichment in bog margins may be the result of different processes in different topographic settings. The 2-3x Pt enrichment at the margin relative to the centre of the perched A-Zone bog is probably related to mechanical runoff of clastic particles from adjacent dunite bedrock, an interpretation supported by a 3x enrichment of Cr_2O_3 (.02-.06%) in pulverized samples at the margin, and lower Loss on Ignition values (Appendix 9) than those found in the seepage zone bog. However, additional evidence supports a hydromorphic rather than mechanical origin for the 2x Pt enrichment at the margin relative to the centre of the seepage zone bog. Cr_2O_3 is almost absent (Appendix 9), and ashed splits from centre and margin locations have almost identical Pt contents.

Sb distributions are similar to those of Pt, and also support a hydromorphic origin for Pt in seepage zone bogs. Sb is a relatively mobile element in the surficial environment (Kabata-Pendias and Pendias, 1984; Rose et al, 1979), and may have been hydromorphically transported from upslope Pt-antimonide minerals on Grasshopper Mountain (St. Louis et al, 1986). No ash data is available, but Sb concentrations in pulverized organic material (3.9-4.1 ppm)

of the large seepage zone bog are more than 6x greater than the median Sb content of Grasshopper Mountain C horizon soils. Additionally, they are 2-4x greater than those of adjacent C horizons in the seepage zone area (Appendix 5.1). Sb content of the perched bog in the secondary study area (1.1 -1.5 ppm) is also higher than that of adjacent soils, but lower than that of the seepage zone bog. This may reflect the large upslope source area for the seepage zone bog relative to the A-Zone bog, which is located near the summit of Grasshopper Mountain with no source area other than adjacent dunite bedrock.

5.4.3 Waters

The limited data available on the PGE content of natural waters are from sulfide-associated rather than chromite-associated PGE occurrences, but support the transport of Pt in suspension and Pd in solution. Maximum Pt and Pd concentrations of 40 ppt (mean: 15 ppt) and 10 ppt (mean: 2.4 ppt) respectively were reported from stream waters draining a Cu-sulfide PGE occurrence in Transbaikal, USSR (Pogrebnyak et al, 1984). Pd occurred primarily (87.5%) in solution, with a minor component (12.5%) occurring in colloidal form (<0.3 microns) in high-concentration samples. Conversely, Pt was present entirely in suspension (0.3 - 10 microns) and interpreted as having

been adsorbed onto particulate Fe-hydroxides. Similar results were obtained in waters adjacent to Cu-Ni sulfide PGE showings in Quebec (Wood and Vlassopoulos, 1990). Pt (max: 0.5 ug/L) occurred in groundwater primarily as suspended and colloidal particles, while Pd (mean at two sites: 388 and 307 ng/L)) was found to be more soluble, occurring as both suspended particles and dissolved organic and hydroxide complexes. Pt and Pd contents of filtered and unfiltered groundwaters were considerably higher than those of lake waters, and increased closer to known showings.

The relatively low Pt content of Grasshopper Mountain stream waters (mean: 0.81 ppb) relative to plateau bog waters (mean: 2.45 ppt) is probably a function of dilution and the Pt content of the surrounding environment. Stream waters, probably composed largely of transient snowmelt, move through a mixed dunitic and non-dunitic till of relatively low Pt content with little interaction with the underlying dunite. Plateau bog waters, however, are subject to much lesser snowmelt dilution in a relatively high-Pt environment of dunite bedrock with a thin intermittent cover of locally derived till. One of the highest water Pt concentrations (3.2 ppt) occurs in a perched bog near the A-Zone PGE occurrence (section 4.2.5).

The sampled <0.45 um water fraction contains two principal components (Rose et al, 1979; Hem, 1985; Horowitz,

1985):

1) the dissolved load, consisting of simple and complex inorganic ions and organic complexes in solution.

2) inorganic and organic colloidal particles, transitional with dissolved particles, which may remain in suspension indefinitely.

It was not possible in this study to determine how Pt is speciated or transported in surface waters, as the > 0.45 um oversize fraction was not retained during the sampling procedure. Consequently, no information is available on the Pt content of the suspended particle fraction. A single Pt analysis of 340 ppb reported for an unfiltered but acidified water sample from an unspecified Tulameen area stream (Hall, 1988) suggests that Pt is far more abundant in the suspended fraction.

The colour of the filtered waters may provide a clue as to Pt speciation in the <0.45 um fraction, and ultimately to the mode of Pt transport. Waters with the highest Pt contents generally also have a brown or light brown colour (Figure 4-34; Appendix 10). This is caused by leaching of humic substances from decaying organic matter (Hem, 1985). Humic and fulvic acids have been shown to mobilize and transport Au under surficial conditions (Ong and Swanson, 1969; Baker, 1978; Coel, 1989), and are capable of reducing metal ions in natural waters (Skogerboe and Wilson, 1981).

In summary, increased Pt content of seepage zone bog soils, and association of higher Pt concentrations with darker water colour, provides evidence for both transport and scavenging of hydromorphic Pt on Grasshopper Mountain. Dunite-resident water containing appreciable organic acids may be more likely than clear stream water to transport Pt, perhaps as colloidal organic particles. There is therefore some evidence for hydromorphic mobility and accumulation of Pt under reducing conditions in seepage zone organic soils.

The lack of information on local groundwater flow limits further assessment of hydromorphic Pt transport. Few hydrologic studies have been made in mountainous terrain (Jamieson and Freeze, 1983). Seepage zones indicate the presence of a highly elevated water table (Jamieson and Freeze, 1983) on Grasshopper Mountain, and the presence of colluvium may cause complex groundwater flow patterns (Hodge, 1976), but a more thorough understanding of the groundwater regime is necessary to constrain both quantity and pathways of Pt transport.

5.5 Recommendations For Geochemical Exploration For Chromitite-Associated Platinum Deposits

The most notable application of geochemical exploration to Pt exploration was the role of soil and stream sediment

geochemistry in the initial discovery of mineralized zones of the Stillwater Complex (Conn, 1979; White, 1987). The use of exploration geochemistry in Pt exploration has also been discussed by Tintor (1986) and Buchanan (1988), and its importance will undoubtably increase with the greater need to probe beneath transported overburden. The application of geochemical methods to PGE exploration must, however, be based on an understanding of PGE mineralogy, residence, geochemical dispersion and landscape elements rather than on rigid adherence to inappropriate methods.

Anomalous Pt concentrations on Grasshopper Mountain occur in chromitite segregations, the remnants of which likely occur as short-ranged clastic dispersion plumes in till. Geochemical methods must take advantage of natural physical and chemical properties of the PGM and their host minerals in order to maximize contrast between anomalous and background Pt concentrations. Recommendations pertaining to sampling, preparation, and quality control techniques for soils and other media are given for regional, reconnaissance and detailed stages of Pt exploration (Table 5-2). For purpose of this section, the latter three terms are defined as follows. Regional geochemical exploration refers to the search for buried or unmapped ultramafic bodies, whereas reconnaissance exploration refers to property-scale exploration above a favourable geological target such as the dunite core of the Tulameen complex. Detailed exploration

refers to the follow-up of reconnaissance geochemical anomalies.

5.5.1 Sampling of Soils

Recommendations are given for the choice of soil horizon, size fraction and sampling density to be employed in Pt geochemical exploration. However, two other points are also critical for the correct interpretation of soil geochemical data. One is the correct field identification and careful sampling of the desired sample media, as stressed by Coker and DiLabio (1989). The second is the grouping of samples into similar categories (Sinclair, 1986), in this study according to parent material and MgO content, prior to the ranking of Pt concentrations within each group to identify background thresholds and anomalous concentrations within each. This is necessary to identify low-level anomalies which would otherwise be swamped by higher background Pt concentrations of samples in other groupings.

5.5.1.1 Choice of Soil Horizon

Near-surface B horizon soils are traditionally collected in geochemical exploration because they are

relatively inexpensive to collect and are enriched in soluble metals (Rose et al, 1979). However, soil development is juvenile in many parts of the Cordillera, and may vary considerably over short distances with variations in parent material, topography, drainage and biotic activity.

On Grasshopper Mountain, A and B horizons may bear little resemblance to those of nearby profiles whereas C horizons, representing oxidized till are relatively constant and unaffected by pedogenic or colluvial processes that may have disrupted the primary clastic PGM distribution in the upper horizons. Several additional factors suggest that the C horizon is the preferred sampling medium. These include the relation of major element geochemistry to Pt concentrations in till, the occurrence on slopes of mixed till-colluvium soil profiles, and the common occurrence of downward-increasing Pt distributions in soil profiles. Taking this further, till profiling or use of deep till samples from as close to bedrock as possible is recommended for detailed follow-up of reconnaissance Pt anomalies. Although more costly, this would have a greater chance of intercepting chromitite dispersion plumes rising from bedrock in thick till (Figure 5-2).

Geochemical sampling of colluvium requires a different approach. Colluvium has a relatively uniform Pt

distribution with depth, and strict sampling of a particular horizon is less important. The main consideration is probably to sample a section of the profile containing the greatest proportion of fine particles. In fact, field screening of coarse (>2 mm) gravel fragments, which constitute a large proportion of colluvial soils (section 4.2.1.2), is advisable in order to further increase the fines content of the field sample.

In a study of base of slope talus sampling as a complement to stream sediment geochemistry in the Cordillera, Hoffman (1977) stated that talus fines were derived from bedrock occurring 400 m to more than 1 km upslope. Cr is a useful pathfinder for Pt on Grasshopper Mountain, and the greater downhill extent of Cliff Zone Cr_2O_3 relative to Pt anomalies (Figure 4-16) illustrates the usefullness of base of slope colluvium sampling. However, the general trend of Cr_2O_3 to increase downslope along all lines on active colluvium on Grasshopper Mountain may hinder correct interpretation of anomalies.

Collection of LFH horizons is a relatively simple and inexpensive process, and 10x Pt enrichments in LFH horizons near A-Zone mineralization suggest that this medium might be an excellent prospecting tool. Unfortunately, the mechanical rather than hydromorphic or biogeochemical origin of LFH Pt anomalies on dunitic till suggests otherwise.

Thus, Pt content of LFH horizons is dependent on the Pt content of lithic and chromite particles of the immediately underlying overburden, and these are incorporated into the LFH only over colluvium, thin dunitic till or residual rubble. Consequently, effectiveness of LFH horizons as a sampling medium would likely decrease with increasing till thickness and distance from subsurface chromitite dispersion plumes, and they are best avoided completely over colluvium.

However, insofar as the biogeochemical behaviour of Pt remains poorly understood, the spatial distribution of LFH/C horizon Pt ratios (Figure 4-35) suggest some possibility of biogeochemical Pt enrichment of humus in soils on non-dunitic till.

5.5.1.2 Choice of Size Fraction

a) Effectiveness of -70 mesh Soils

Traditional -80 mesh soil sampling, particularly of the C horizon, would probably be successful in locating Pt anomalies in thin locally-derived dunitic till or rubble directly above bedrock during regional or reconnaissance scale exploration. Similar results could probably be achieved by surface prospecting, however, and a large proportion of the dunite core on Grasshopper Mountain is

covered by thicker and/or exotic till and clay on which traditional methods are largely ineffective. There are two reasons for this. First, sampling depths in thick till would probably be insufficient to intercept the most highly-concentrated portions of small chromitite dispersion plumes. Second, Pt concentrations are closely related to MgO and Cr_2O_3 contents indicative of source rock composition, and are reduced with dilution by barren material. It is essential to analyze for major elements, particularly MgO and Cr_2O_3, in order to assess the extent of till mixing and to set anomaly thresholds in a given area.

Thus, -70 or -80 mesh soil fractions may be used to delineate large dunitic dispersion plumes at the regional exploration level, but are unlikely to detect buried Pt mineralization beneath any but the thinnest of tills.

b) Preparation of Size Fractions versus Heavy Mineral Concentrates

The fourteen detailed soil profiles were chosen as representative of the range of profiles on Grasshopper Mountain, including those both adjacent to and distant from known Pt mineralization. The most useful soil fraction for geochemical exploration is the one which outlines and broadens the anomaly around the mineralized zone relative to distal sites. Both the -270 mesh fraction and the -140+270

mesh heavy concentrates fulfill these criteria on Grasshopper Mountain.

A-Zone Pt mineralization is detected in all five size fractions and all four heavy mineral fractions. While absolute concentrations are greatest in the two coarsest size fractions and in the two non-magnetic heavy mineral fractions, it is the two finest size fractions (-140+270, -270) which exhibit the broadest and most consistent till anomaly around all three A-Zone detailed sites (Figures 4-38 and 4-39). Results of heavy mineral concentrates are noisier, but broad C horizon till anomalies are exhibited by all four heavy fractions (Figures 4-44 and 4-45). In colluvium, relatively coarse -70+140 mesh size and magnetic heavy mineral fractions exhibit the greatest concentration difference between Cliff Zone and serpentine colluvium.

Magnetic rather than non-magnetic heavy mineral fractions are preferable for reconnaissance sampling. Pt is most abundant in magnetic fractions in non-dunitic till and in dunitic till distant from mineralization, and concentrations generally reach their maximum levels at sites adjacent to known mineralization (Figure 4-44). In comparison, high Pt concentrations in non-magnetic fractions have a very limited dispersion related to their origin in massive chromitite segregations, and are usually restricted to sites near known mineralization (Figures 4-43 and 4-45).

Consequently, non-magnetic heavy fractions are less suitable than magnetic heavy fractions for reconnaissance sampling, but are superior for detailed follow-up sampling because of their more limited dispersion and greater contrast.

Either of the two magnetic heavy mineral fractions, or the -270 mesh fraction, would probably provide the best chance of detecting anomalous Pt concentrations during reconnaissance geochemical sampling on Grasshopper Mountain. The occurrence of rare elements as very fine grains in soils and sediments is well-documented. For example, Sibbick (1990) showed that the -270 mesh fraction of Au in soils near a southern B.C. gold skarn provided a more reliable distinction between anomalous and background samples than heavy mineral concentrates. However, results of the current study suggest that use of the -270 mesh fraction would screen out any Pt occurring as inclusions in coarser chromite grains (Figures 4-54 and 4-55) in colluvium and, in some cases, in till. For example, high Pt concentrations in excess of 500 ppb occur in magnetic heavy fractions at site 20 in non-dunitic till (Figure 4-46). These Pt concentrations, higher than those of some nearby dunitic till sites, verify the overview designation of this site as "anomalous" (Figure 4-13) but are not found in the -270 mesh fraction.

In summary, use of the -270 mesh fraction is a suitable

and less-costly alternative to the preparation of magnetic heavy mineral concentrates for reconnaissance-scale Pt exploration in till. The possibility of coarse platinic chromite grains being sieved out of the fraction must be recognized, however, as a trade-off against the greater cost of the heavy concentrates. Use of the -70+140 mesh magnetic heavy mineral fraction is recommended for reconnaissance sampling of colluvium.

Detailed follow-up of Pt anomalies in both till and colluvium must be targeted toward identification of chromite fragments derived from chromitite-PGE horizons. Consequently, the more limited dispersion, greater contrast and chromite fragment association of Pt in the non-magnetic heavy mineral fraction, particularly that of the finer -140+270 mesh fraction, may be most useful in tracing anomalous Pt concentrations back to their bedrock source.

5.5.1.3 Sampling Density

No comparative evaluation of differing sample densities was attempted in the study. On the basis of MgO and Pt dispersion patterns, however, recommended soil or till sampling densities can be made for various stages of exploration. For a variety of reasons, relatively close sampling densities are recommended. At least 1 sample per

square kilometres is required for regional sampling, as a higher sample density may be insufficient to intercept a dunitic till dispersion plume (Figure 4-18) from a buried source.

A sampling density of at least 1 per 100 metres is suggested for reconnaissance-scale sampling because of the relatively small size of the PGE occurrences (Bohme, 1987, 1988) and narrow widths of individual chromitite segregations (Figures 2-4 and 2-7). Much smaller detailed sampling densities, in the order of one per tens of metres, are consequently required to trace reconnaissance soil anomalies back to their chromitite source. In contrast to till sampling, contour or base of slope-sampling of colluvium may require a much lower density during reconnaissance exploration because the direction of origin - uphill - is known.

5.5.2 Sampling of Other Media

5.5.2.1 Sediments

Gravel stream sediments yield less -70 mesh material than moss mats but their Pt content, on the basis of very limited data, offers better contrast than moss mats. Conversely, moss mats appear to concentrate Pd more

affectively than do stream sediments (Figure 4-29). Association of Pt with coarse sediments is undoubtably a function of the particulate nature of the PGM and, more importantly, their host chromites. Gravel et al (1990), on the basis of studies on southern Vancouver Island and the B.C. Lower Mainland, suggested that elements forming heavy detrital minerals such as Cr and Au are preferentially enriched in moss mats relative to sediments. Results from Grasshopper Creek do not support this, insofar as distribution of Cr_2O_3 and, to a lesser extent Pt and Au, appears to be related to differential accumulation of particulate grains under differing flow conditions (Fletcher, 1990).

Cr_2O_3 content of moss mats is relatively constant downstream, but the two increasing-downstream Cr_2O_3 cycles in gravel stream sediments (Figure 4-31) are similar to increasing-downstream concentrations of Au and magnetite described by Fletcher (1990). Stream sediment Cr_2O_3 content is greatest in areas of decreasing stream gradient and, like magnetite of Fletcher (1990), is probably derived from erosion of dunitic till banks in the upper reaches of the creek. The presence of two cycles rather than one may be just noise, or it may be related to the intermittent nature of stream flow in the upper half of the creek.

The collection of gravel stream sediments is

recommended, on the basis of very limited data, during regional and reconnaissance stages of Pt exploration. Among size fractions, the highest Pt content is found in the -270 mesh fraction, but differences in concentration between the three finest fractions are quite small (Figure 4-30). The highest Pt concentrations in Grasshopper Creek occur in the -70+140 magnetic heavy mineral fraction. This is in agreement with results of Fletcher (1989), who reported Pt in Olivine and Britton Creeks to be partitioned into the heavy mineral fraction. In summary, it appears that any fraction of gravel sediments finer than -70 mesh would be suitable for sampling of Grasshopper Creek, but that the best contrast would probably be obtained with magnetic heavy mineral concentrates. Fletcher (1990) stressed that very large samples be field-sieved to obtain a representative sample.

5.5.2.2 Waters and Bogs

The use of hydrogeochemistry in Pt exploration is limited by lack of data on speciation of Pt in natural waters, and the difficulty and unavailability of commercial analyses. However, slow-moving bog waters in dunite-dominated environments warrrant more study as a medium for detailed exploration. The effectiveness of sampling clear stream water for Pt seems to be much more limited. Organic

bog soils are abundant in the Cordillera, but data concerning the magnitude, nature, and origin of their Pt contents is presently far too limited to make meaningful recommendations for Pt exploration.

5.5.3 Sample Preparation Methodology

Sample preparation recommendations fall into two general groups: (i) the most effective methodology for concentrating PGM and PGM-bearing chromite in order to increase geochemical contrast, and (ii) the most effective pulverizing and subsampling methodologies, and analytical subsample size, to increase analytical precision and accuracy of the data.

5.5.3.1 Concentration Techniques

a) Recommended Methodology

Recommendations are given for *what* should be concentrated in order to increase geochemical contrast in Pt exploration, and *how* this is to be most satisfactorily accomplished. Results of the present study suggest that some PGM concentration techniques are inappropriate for geochemical exploration for chromite-PGE deposits. This can

be largely attributed to a failure to properly account for platinum-group mineralogy and mineralogical associations in the sampling design. For example, while magnetic separations are moderately more effective than gravity methods for concentrating PGM smaller than 200 mesh (Sabelin et al, 1986; Foley et al, 1987) and would probably be suitable for reconnaissance exploration, not all PGM are magnetic. More importantly, the absence of a corresponding non-magnetic heavy concentrate would hinder anomaly follow-up. Similarly, Pt exploration techniques utilizing conductive, magnetic, and high density properties of discrete PGM in order to concentrate them (Tintor, 1986) would seem ill-suited for detecting PGM encapsulated in chromite, which has quite variable magnetic properties (section 5.2.2).

Thus, the greater number of discrete PGM identified within this study as inclusions in chromite, relative to other forms (section 4.4.2), suggests that a technique targeted toward concentration of characteristic-composition host chromite rather than toward discrete PGM themselves would be a more logical approach to Pt geochemical exploration. PGM are associated with Mg-Cr-rich chromite which have been shown to be concentrated in the non-magnetic heavy mineral fractions.

Heavy concentrates are most easily prepared with

standard gravity methods such as panning, jigging, sluicing, superpanners, shaker tables, spiral concentrators and heavy liquids (Theobald, 1957; Muller, 1977; Wang and Poling, 1983; Stewart, 1986), but no single method is entirely satisfactory for concentrating the fine-grained chromite-associated PGM observed in Grasshopper Mountain soils. Thorough separations were obtained in this study with heavy liquids, but the method is slow, expensive and increasingly difficult for particle sizes finer than about 200 mesh. No comparative evaluations were made, but an at least partial alternative to heavy liquids is necessary to encourage a greater use of heavy mineral concentrates in geochemical exploration for Pt. Other methods are more useful for processing of large samples in the field, but unfortunately are also more subsceptible to the loss of fine PGM, chromite, Au and other heavy particles of <100 um in tailings water (Sobieraj and Laskowski, 1973; Wang and Poling, 1983; Giusti, 1986; Sabelin et al, 1986; Foley et al, 1987).

Thus, it is suggested that the most effective concentration methodology incorporate the speed and large sample capacity of field-based methods, the greater reproducibility of heavy liquids and the maximum retention of fine PGM. The recommended technique is an adaptation of those of Zhou and Zang (1975; as shown in Cabri and Laflamme, 1981), Ewing (1931) and Gunn (1989). Large till,

colluvium or sediment samples are dried, if necessary, and screened to -70 mesh. Partial concentrates, with a remaining silicate component, are prepared in a superpanner, shaking table or similar device. These are passed through magnetic and finally, heavy liquid separations using methylene iodide to obtain magnetic and non-magnetic heavy concentrates.

This approach offers several potential advantages. The nugget effect is minimized by using a large initial sample, and loss of fine heavy minerals minimized and reproducibility improved by using a heavy liquid finish. Regarding the magnetic separations, use of a Franz isomagnetic separator offers several advantages over a hand magnet. It produces more reproducible results (Mitchell, 1975) and permits a cleaner and more quantitative separation of non-magnetic PGM-bearing detrital chromite fragments from their magnetic counterparts. However, there is presently no data for the separation of different types of chromites at varying isomagnetic strengths. Consequently, repeated hand magnet separation of heavy concentrates into magnetic and non-magnetic fractions is probably sufficient for reconnaissance exploration.

b) Potential Improvements

The very fine grain size of most observed soil PGM suggests that heavy minerals of the -270 mesh fraction of till might provide the best geochemical contrast. Reliable gravity separations of such fine particles are difficult to perform (Day, 1988), but froth flotation techniques, generally confined to mineral processing and beneficiation, may have considerable potential for this purpose. A combination of gravity and flotation techniques has been suggested as the best method of concentrating very fine-grained chromite (Sagheer, 1966). Chromite flotation characteristics have been addressed by a number of workers (Sagheer, 1966; Sobieraj and Laskowski, 1973; Fuerstenau et al, 1986) but never utilized for Pt exploration, although similar flotation of <63 um gold particles has been proposed for stream sediment sampling (Giusti, 1986).

Selective flotation methods devised for one type of chromite are not directly applicable to another due to the wide compositional range of spinels (section 5.2). This is an advantage rather than an impediment to its use however, as it is selective flotation of only Mg-Cr-rich magnesiochromite, not all chromite, which is desired. Further research on the use of chromite flotation in Pt geochemical exploration is warranted.

5.5.3.2 Pulverizing and Subsampling Methodology

Recommendations to increase analytical precision and accuracy deal with the unique problems presented by chromitiferous concentrates. The entire heavy mineral concentrate should be crushed in its entirety to at least -270 mesh to minimize nugget effects, facilitate dissolution of chromite by the fire assay flux, and liberate as many PGM grains as possible from their refractory chromite host. Use of microsplitters as opposed to spatulas to obtain final subsamples is highly recommended to increase analytical reproducibility. Regarding the preparation of whole size fractions, use of a splitter at all stages to improve reducibility, and of a tungsten-carbide ring mill to prevent Cr contamination, is essential.

No specific field sample size recommendations are provided, but it should be stressed that dry sieving will produce a considerably smaller subsample of, for example, -270 mesh material than the wet sieving method employed in this study. Regarding the preparation of heavy mineral concentrates, subsamples large enough to yield at least 10 g of both magnetic and non-magnetic heavy minerals should be used in order to minimize nugget effects. These sizes differ for till and colluvium because of differing heavy mineral contents. For example, the -70+140 mesh fraction of C horizons from ten detailed till and rubble profiles (Table

4-11) have, on average, almost equal proportions of magnetic (5.92%) and non-magnetic (5.36%) heavy minerals. However, this fraction in the lowermost sample of four colluvium sites has, on average, 6.76% magnetic heavy minerals but only 3.23% non-magnetic heavy minerals. In fact, three out of the four colluvium sites contain, on average, only 1.45% non-magnetic heavy minerals in the -70+140 mesh fraction. Thus, in order to obtain at least 10 g of each of magnetic and non-magnetic heavy concentrates, it is recommended that -70+140 mesh fractions of at least 187 g till and 690 g colluvium be used.

In addition, the use of 30 g analytical subsamples should to be avoided in favour of 10 g subsamples when dealing with chromitiferous samples or concentrates unless the analytical laboratory has crucibles large enough to accomodate the extra flux and can demonstrate its ability to produce accurate results. Care must be taken to ensure that the laboratory does not further reduce the size of even 10 g subsamples prior to fire assay, but uses the entire amount.

5.5.4 Quality Control Monitoring

Systematic monitoring of data reliability is a necessity if geochemical data is expected to be a reliable indicator of either the presence or absence of Pt

mineralization. Major elements of quality control have been outlined by Fletcher (1981), and implementation of such a program begins in the field with the collection of large samples from, in the case of soils, C horizons. It should also include the regular collection of random field duplicates, the random insertion of preparation-stage duplicates, the insertion of reference standards of appropriate Pt concentrations and matrices to monitor accuracy, and the insertion of quartz blanks to monitor contamination. The routine re-analysis of all anomalous-population samples is recommended to verify their validity.

5.5.5 Application of Electron Microprobe Techniques to PGE Exploration

Nixon et al (1989) decried the limited use of the electron microprobe in exploration geochemistry. EMP analyses of detrital chromites in non-magnetic heavy mineral concentrates have the potential of becoming a very useful exploration tool by pinpointing the dispersed detrital remnants of Pt-hosting chromitite segregations. Although it would be impractical to probe a selection of grains from every sample, EMP results present a powerful method of prioritizing reconnaissance Pt anomalies outlined with magnetic heavy mineral concentrates. This would be accomplished by delineating areas containing detrital

chromite fragments having characteristic Mg and Cr-rich chromitite signatures.

5.5.6 Summary of Recommendations for Exploration for Chromitite-Associated Pt Deposits

A summary of recommended sample media and procedures for geochemical exploration for chromitite-associated Pt deposits is given in Table 5-2. The recommendations cover regional, reconnaissance, and detailed scales of exploration. It should be stressed that the data on which they are based is derived from an Alaskan-type ultramafic complex in a glaciated Cordilleran environment, and thus the recommendations are not universally applicable to all PGE deposits.

Level of Exploration	Preferred Soil Horizon	Preferred Size/density/magnetic Soil Fraction	Additional Elements	Sampling Density	Other Sample Media
REGIONAL	C	-70 mesh fraction for delineating distribution of dunitic till	Major Elements (MgO, Cr2O3)	1 km^2	1) gravel stream sediments
RECONNAISSANCE	C	TILL: -270 mesh fraction *or* -70+140/-140+270 mesh magnetic heavy mineral fractions COLLUVIUM: -70+140 mesh magnetic heavy mineral fraction	Major Elements (MgO, Cr2O3)	100 m	1) gravel stream sediments 2) bog waters
DETAILED	C or deep till; till profiling	Non-magnetic heavy mineral fractions: TILL: -140+270 mesh COLLUVIUM: -70+140 mesh	-	10's of m	electron microprobe analysis of chromite fragments

Table 5-2. Recommendations for geochemical exploration for chromitite-associated Pt deposits in Alaskan-type ultramafic complexes.

Chapter Six.

SUMMARY AND CONCLUSIONS

CHAPTER SIX. SUMMARY AND CONCLUSIONS.

A) Distribution and Behaviour of Pt

1) Glacial dispersion and mass wasting are the dominant processes influencing the surficial distribution of Pt on Grasshopper Mountain.

2) Pt content of the -212 um soil fraction ranges from 2-885 ppb and is dependent on the amount of contained dunite, as expressed by MgO content, in the parent material. Median Pt concentrations of dunite colluvium, dunitic till and non-dunitic till are 88 ppb, 36 ppb and 8 ppb, respectively.

3) Pt content generally increases or is relatively constant with depth in soils on till, and is constant with depth in soils on colluvium.

4) Pt is preferentially associated with heavy mineral fractions in soil. Partitioning of Pt between magnetic and non-magnetic heavy mineral fractions is dependent on both distance from supposed source and parent material mineralogy; sites adjacent to known occurrences contain a higher proportion of Pt in the non-magnetic fractions.

5) Detrital soil PGM, comprising Pt-Fe-Cu alloys, occur as free grains, as inclusions in Mg-silicates and, most

commonly, as inclusions within chromites.

6) Soil chromites occur as Fe-rich euhedral-subhedral crystals and as Cr-Mg-rich anhedral fragments. Crystals are relatively more abundant in magnetic heavy fractions and are interpreted to represent disseminated spinels in dunite. Fragments are relatively more abundant in non-magnetic heavy fractions and are interpreted to represent dispersed remnants of massive chromitite segregations. Their abundance in soils near known PGE occurrences accounts for the relatively high Pt content of corresponding non-magnetic heavy fractions.

7) Pt content of LFH horizons, which is up to 10x greater near known mineralization than elsewhere, is attributed to mixing of inorganic particles into the organic matrix. Pt content of Grasshopper Mountain bog water in a dunite-dominated environment is 3x that of streamwater flowing through dunitic and non-dunitic till. Enhanced Pt content of brown bog water and seepage zone bog ash suggests a minor hydromorphic modification of the clastic Pt dispersion.

B) Recommendations for Geochemical Exploration

8) C horizon soils are the preferred sampling medium.

9) Heavy mineral and -270 mesh fractions offer the greatest contrast for geochemical exploration, and their use provides the greatest likelihood of detecting hidden Pt mineralization beneath till. Magnetic heavy minerals would be most useful for detection of anomalous Pt concentrations during reconnaissance sampling, but the more limited dispersion, greater contrast and chromite fragment association of Pt in the -140+270 non-magnetic heavy fraction may be more useful for detailed follow-up surveys.

REFERENCES

REFERENCES

Agriculture Canada Expert Committee on Soil Survey. 1987. The Canadian System of Soil Classification, Second Edition. Agriculture Canada, Publication 1646, 164 pages.

Atmospheric Environment Service. 1974. Climate of British Columbia: Climatic Normals 1941 - 1970. British Columbia Department of Agriculture, Victoria, 90 pages.

Aubut, A.J. 1978. The Geology and Mineralogy of a Tertiary Buried Placer Deposit, Southern British Columbia. Unpublished M.Sc. Thesis, University of Alberta, 98 pages.

Baas Becking, L.G.M., Kaplan, I.R. and Moore, D. 1960. Limits of the Natural Environment in Terms of pH and Oxidation-Reduction Potentials. Journal of Geology, 68, pp. 243-284.

Baker, W.E. 1978. The Role of Humic Acid in the Transport of Gold. Geochimica et Cosmochimica Acta, 42, pp. 645-649.

Bartlett, R.J. and Kimble, J.M. 1976. Behavior of Chromium in Soils: I. Trivalent Forms. Journal of Environmental Quality, 5, pp. 379-382.

Beamish, F.E. and Van Loon, J.C. 1977. Analysis of Noble Metals: Overview and Selected Methods. Academic Press, New York, 327 pages.

Beeson, M.H. and Jackson, E.D. 1969. Chemical Composition of Altered Chromites from the Stillwater Complex, Montana. American Mineralogist, 54, pp. 1084-1100.

Blaise, B., Clague, J.J. and Mathewes, R.W. 1990. Time of Maximum Late Wisconsin Glaciation, West Coast of Canada. Quaternary Research, 34, pp. 282-295.

Bloom, L. 1986. Platinum Assays. The Northern Miner Magazine, 1, September issue, pp. 36-38.

Bohme, D.M. 1987. Geological, Geochemical and Geophysical Report on the Grasshopper Claims, Similkameen Mining Division, British Columbia (92 H/10W). Newmont Exploration of Canada Limited, 47 pages.

Bohme, D.M. 1988. Report on the 1987 Exploration Program: UM Project on the Grasshopper Claims, Similkameen Mining Division, British Columbia (92 H/10W). Newmont Exploration of Canada, 29 pages.

Borthwick, A.A. and Naldrett, A.J. 1984. Neutron Activation Analysis for Platinum Group Elements and Gold in Chromitites. Analytical Letters, 17 (A4), pp. 265-275.

Boulton, G.S. 1978. Boulder Shapes and Grain-Size Distributions of Debris as Indicators of Transport Paths Through a Glacier and Till Genesis. Sedimentology, 25, pp. 773-799.

Bowles, J.F.W. 1986. The Development of Platinum-Group Minerals in Laterites. Economic Geology, 81, pp. 1278-1285.

Bowles, J.F.W. 1988. Further Studies on the Development of Platinum-Group Minerals in the Laterites of the Freetown Layered Complex, Sierra Leone. *In* Geo-Platinum 87, H.M. Prichard, P.J. Potts, J.F.W. Bowles and S.J. Cribb, eds. Elsevier, pp. 273-280.

Boyle, R.W. 1979. The Geochemistry of Gold and its Deposits (Together with a Chapter on Geochemical Prospecting for the Element). Geological Survey of Canada, Bulletin 280, 584 pages.

Boyle, R.W. 1982. Gold, Silver, and Platinum Metal Deposits in the Canadian Cordillera - Their Geological and Geochemical Setting. *In* Precious Metals in the Northern Cordillera, A.A. Levinson, ed. Association of Exploration Geochemists, Special Volume 10, pp. 1-19.

Bradshaw, P.M.D. 1975. Conceptual Models in Exploration Geochemistry. Association of Exploration Geochemists, Special Publication 3. Elsevier, Amsterdam, 223 pages.

Brookins, D.G. 1988. Eh-pH Diagrams for Geochemistry. Springer-Verlag, New York, 176 pages.

Brooks, R.R. 1987. Serpentine and its Vegetation. Dioscorides Press, Portland, 454 pages.

Buchanan, D.L. 1988. Platinum-Group Element Exploration. Elsevier, 185 pages.

Bugbee, E.E. 1933. A Textbook of Fire Assaying. Second Edition. John Wiley and Sons, New York, 299 pages.

Burgath, K.P. 1988. Platinum-Group Minerals in Ophiolitic Chromitites and Alluvial Placer Deposits, Meratus-Bobaris Area, Southeast Kalimantan. *In* Geo-Platinum 87, H.M. Prichard, P.J. Potts, J.F.W. Bowles and S.J. Cribb, eds. Elsevier, pp. 383-403.

Cabri, L.J. 1981. The Platinum-Group Minerals. *In* Platinum-Group Elements: Mineralogy, Geology, Recovery, L.J. Cabri, ed. The Canadian Institute of Mining and Metallurgy, Special Volume 23, pp. 83-150.

Cabri, L.J. 1982. Classification of Platinum-Group Element Deposits with Reference to the Canadian Cordillera. *In* Precious Metals in the Northern Cordillera, A.A. Levinson, ed. Association of Exploration Geochemists, Special Volume 10, pp. 21-31.

Cabri, L.J. and Laflamme, J.H.G. 1981. Sample Preparation Techniques for Platinum-Group Element-Bearing Materials. *In* Platinum-Group Elements: Mineralogy, Geology, Recovery, L.J. Cabri, ed. The Canadian Institute of Mining and Metallurgy, Special Volume 23, pp. 65-70.

Cameron, E.N. 1975. Postcumulus and Subsolidus Equilibration of Chromite and Coexisting Silicates in the Eastern Bushveld Complex. Geochimica et Cosmochimica Acta, 39, pp. 1021-1033.

Cameron, E.N. 1977. Chromite in the Central Sector of the Eastern Bushveld Complex, South Africa. American Mineralogist, 62, pp. 1082-1096.

Cameron, E.N. 1980. Evolution of the Lower Critical Zone, Central Sector, Eastern Bushveld Complex, and Its Chromite Deposits. Economic Geology, 75, pp. 845-871.

Cameron, E.N. and Desborough, G.A. 1969. Occurrence and Characteristics of Chromite Deposits - Eastern Bushveld Complex. *In* Magmatic Ore Deposits: A Symposium, H.D.B. Wilson, ed. Economic Geology Monograph 4, pp. 23-40.

Camsell, C. 1913. Geology and Mineral Deposits of the Tulameen District, B.C. Geological Survey of Canada, Memoir 26, 188 pages.

Canmindex Files. 1986. Chromium - 92 H/10 - CR 1 - Grasshopper Mountain. Mineral Policy Sector, Department of Energy, Mines and Resources, 2 pages.

Cary, E.E., Allaway, W.H. and Olsen, O.E. 1977. Control of Chromium Concentrations in Food Plants. 2. Chemistry of Chromium in Soils and its Availability to Plants. Journal of Agricultural and Food Chemistry, 25, pp. 305-309.

Chao, T.T., Jenne, E.A. and Heppting, L.M. 1968. Prevention of Adsorption of Trace Amounts of Gold by Containers. U.S. Geological Survey, Professional Paper 600-D, pp. D16-D19.

Clark, P.U. 1987. Subglacial Sediment Dispersal and Till Composition. Journal of Geology, 95, pp. 527-541.

Clark, T. 1978. Oxidé Minerals in the Turnagain Ultramafic Complex, Northwestern British Columbia. Canadian Journal of Earth Sciences, 15, pp. 1893-1903.

Coel, R.J. 1989. Fulvic Acid as a Potential Agent of Gold Mobilization in the Surficial Environment. Geological Society of America, Cordilleran/Rocky Mountain Section Meeting, Program with Abstracts, 21, p. 67.

Coker, W.B. and DiLabio, R.N.W. 1989. Geochemical Exploration in Glaciated Terrain: Geochemical Responses. *In* Proceedings of Exploration '87: Third Decennial International Conference on Geophysical and Geochemical Exploration for Minerals and Groundwater, G.D. Garland, ed. Ontario Geological Survey, Special Volume 3, pp. 336-383.

Coker, W.B., Dunn, C.E., Hall, G.E.M., Rencz, A.N., DiLabio, R.N.W. and Campbell, J.E. 1989. The Behaviour of Platinum Group Elements in the Surficial Environment in Canada. *In* Rio 89 Abstracts, XIII International Geochemical Exploration Symposium - II Brazilian Geochemical Congress, pp. 25-26.

Conn, H.K. 1979. The Johns-Manville Platinum-Palladium Prospect, Stillwater Complex, Montana, U.S.A. Canadian Mineralogist, 17, pp. 463-468.

Cook, S.J. and Fletcher, W.K. 1990. Preliminary Report on the Distribution and Dispersion of Platinum in the Soils of the Tulameen Ultramafic Complex, Southern British Columbia (92 H/10). B.C. Ministry of Energy, Mines and Petroleum Resources, Geological Fieldwork 1989, Paper 1990-1, pp. 511-518.

Coombes, J.S. 1990. Platinum 1990. Johnson Matthey Public Limited Company, 64 pages.

Cousins, C.A. 1973. Platinoids in the Witwatersrand System. Journal of the South African Institute of Mining and Metallurgy, 73, pp. 184-199.

Cousins, C.A. and Kinloch, E.D. 1976. Some Observations on Textures and Inclusions in Alluvial Platinoids. Economic Geology, 71, pp. 1377-1398.

Crocket, J.H. 1974. Platinum Metals. *In* Handbook of Geochemistry, Volume II/4, K.H. Wedepohl, ed. Springer-Verlag, New York.

Curtin, G.C. and King, H.D. 1986. Utility of Mull in Geochemical Exploration. *In* Mineral Exploration: Biological Systems and Organic Matter, Rubey Volume V, D. Carlisle, W.L. Berry, I.R. Kaplan and J.R. Watterson, eds. Prentice-Hall, Englewood Cliffs, pp. 356-376.

Davis, J.C. 1986. Statistics and Data Analysis in Geology. Second Edition. John Wiley and Sons, New York, 646 pages.

Day, S.J. 1988. Sampling Stream Sediments for Gold in Mineral Exploration, Southern British Columbia. Unpublished M.Sc. Thesis, The University of British Columbia, 233 pages.

Deer, W.A., Howie, R.A. and Zussman, J. 1966. An Introduction to the Rock-Forming Minerals. Longman Group, London, 528 pages.

DiLabio, R.N.W. 1988. Residence Sites of Gold, PGE and Rare Lithophile Elements in Till. *In* Prospecting in Areas of Glaciated Terrain - 1988, D.R. MacDonald and K.A. Mills, eds. The Canadian Institute of Mining and Metallurgy, pp. 121-140.

Dissanayake, C.B., Kritsotakis, K. and Tobschall, H.J. 1984. The Abundance of Au, Pt, Pd, and the Mode of Heavy Metal Fixation in Highly Polluted Sediments from the Rhine River near Mainz, West Germany. International Journal of Environmental Studies, 22, pp. 109-119.

Douma, Y.L. and Knight, J.B. In Preparation. Mounting Samples in Methacrylate for SEM and EMP.

Drake, L.D. 1983. Ore Plumes in Till. Journal of Geology, 91, pp. 707-713.

Duke, J.M. 1983. Ore Deposits Models 7: Magmatic Segregation Deposits of Chromite. Geoscience Canada, 10, pp. 15-24.

Dunn, C. E. 1986. Biogeochemistry as an Aid to Exploration for Gold, Platinum and Palladium in the Northern Forests of Saskatchewan, Canada. Journal of Geochemical Exploration, 25, pp. 21-40.

Dunn, C.E. 1990. Biogeochemical Exploration for Noble Metals in Western Canada. *In* Methods of Geochemical Prospecting: Prague 1990, Extended Abstracts, J. Janatka, T. Hlavata, I. Barnet and E. Jelinek, eds. Geological Survey, Prague, page 245.

Dunn, C.E., Hall, G.E.M. and Hoffman, E. 1989. Platinum Group Metals in Common Plants of Northern Forests: Developments in Analytical Methods, and the Application of Biogeochemistry to Exploration Strategies. Journal of Geochemical Exploration, 32, pp. 211-222.

Eales, H.V. 1987. Upper Critical Zone Chromitite Layers at R.P.M. Union Section Mine, Western Bushveld Complex. *In* Evolution of Chromium Ore Fields, C.W. Stowe, ed. Van Nostrand Reinhold, New York, pp. 144-168.

Earley, J.W. 1958. On Chlorine in Serpentinized Dunite. American Mineralogist, 43, pp. 148-155.

Ercit, T.S. 1987. FORMULA: A General-Purpose Program for Formula Calculation.

Evenchick, C.A., Friday, S.J. and Monger, J.W.H. 1987. Potential Hosts to Platinum-Group Element Concentrations in the Canadian Cordillera. Geological Survey of Canada, Open File 1433.

Evenson, E.B., Pasquini, T.A., Stewart, R.A. and Stephens, G. 1979. Systematic Provenance Investigations in Areas of Alpine Glaciation: Applications to Glacial Geology and Mineral Exploration. *In* Moraines and Varves: Origin/Genesis/Classification, C. Schluchter, ed. A.A. Balkema, Rotterdam, pp. 25-42.

Ewing, C.J.C. 1931. A Comparison of the Methods of Heavy Mineral Separation. Geological Magazine, 68, pp. 136-140.

Findlay, D.C. 1963. Petrology of the Tulameen Ultramafic Complex, Yale District, British Columbia. Unpublished Ph.D. Thesis, Queen's University, 415 pages.

Findlay, D.C. 1965. Platinum in the Tulameen Ultramafic Complex, B.C. Geological Survey of Canada, Paper 65-2, page 40.

Findlay, D.C. 1969. Origin of the Tulameen Ultramafic-Gabbro Complex, Southern British Columbia. Canadian Journal of Earth Sciences, 6, pp. 399-425.

FitzPatrick, E.A. 1980. Soils: Their Formation, Classification, and Distribution. Longman Group Limited, London, 353 pages.

Fletcher, W.K. 1981. Analytical Methods in Geochemical Prospecting. Handbook of Exploration Geochemistry, Volume 1, G.V.S. Govett, ed. Elsevier, 255 pages.

Fletcher, W.K. 1989. Preliminary Investigation of Platinum Content of Soils and Sediments, Southern British Columbia (82 E/9, 92 H/7, 10, 92 I/14). B.C. Ministry of Energy, Mines and Petroleum Resources, Geological Fieldwork 1988, Paper 1989-1, pp. 607-610.

Fletcher, W.K. 1990. Dispersion and Behaviour of Gold in Stream Sediments. B.C Ministry of Energy, Mines and Petroleum Resources, Open File 1990-28, 28 pages.

Flint, R.F. 1971. Glacial and Quaternary Geology. John Wiley and Sons Inc., 892 pages.

Foley, J.Y., Mardock, C.L. and Dahlin, D.C. 1987. Platinum-Group Elements in the Tonsina Ultramafic Complex, Southern Alaska. Process Mineralogy VII, A.H. Vassiliou, D.M. Hausen and D.J.T. Carbon, eds. The Metallurgical Society, pp. 165-195.

Fortescue, J.A.C., Stahl, H. and Webb, J.R. 1988. Humus Geochemistry in the Lac des Iles Area, District of Thunder Bay. Ontario Geological Survey, Map 80 800, Geochemical Series.

Fuchs, W.A. 1972. Geochemical Behavior of Platinum, Palladium, and Associated Elements in the Weathering Cycle in the Stillwater Complex, Montana. Unpublished M.Sc. Thesis, Pennsylvania State University, 92 pages.

Fuchs, W.A. and Rose, A.W. 1974. The Geochemical Behavior of Platinum and Palladium in the Weathering Cycle in the Stillwater Complex, Montana. Economic Geology, 69, pp. 332-346.

Fuerstenau, M.C., Han, K.N. and Miller, J.D. 1986. Flotation Behavior of Chromium and Manganese Minerals. *In* Advances in Mineral Processing, P. Somasundaran, ed. Society of Mining Engineers, pp. 289-307.

Fulton, R.J. 1975. Quaternary Geology and Geomorphology, Nicola-Vernon Area, British Columbia. Geological Survey of Canada, Memoir 380, 50 pages.

Fulton, R.J. 1984. Quaternary Glaciation, Canadian Cordillera. *In* Quaternary Stratigraphy of Canada - A Canadian Contribution to IGCP Project 24, R.J. Fulton, ed. Geological Survey of Canada, Paper 84-10, pp. 39-47.

Fulton, R.J. and Smith, G.W. 1978. Late Pleistocene Stratigraphy of South-Central British Columbia. Canadian Journal of Earth Sciences, 15, pp. 971-980.

Giusti, L. 1986. The Morphology, Mineralogy, and Behaviour of "Fine-Grained" Gold from Placer Deposits of Alberta: Sampling and Implications for Mineral Exploration. Canadian Journal of Earth Sciences, 23, pp. 1662-1672.

Goldich, S.S. 1938. A Study in Rock Weathering. Journal of Geology, 46, pp. 17-58.

Goldschmidt, V.M. 1954. Geochemistry. Clarendon Press, Oxford, 730 pages.

Gough, L.P., Shacklette, H.T. and Case, A.A. 1979. Element Concentrations Toxic to Plants, Animals, and Man. U.S. Geological Survey, Bulletin 1466, 80 pages.

Grandstaff, D.E. 1978. Changes in Surface Area and Morphology and the Mechanism of Forsterite Dissolution. Geochimica et Cosmochimica Acta, 42, pp. 1899-1901.

Gravel, J.L and Matysek, P.F. 1989. 1988 Regional Geochemical Survey, Northern Vancouver Island and Adjacent Mainland (92E, 92K, 92L, 102I). B.C. Ministry of Energy, Mines and Petroleum Resources, Geological Fieldwork 1988, Paper 1989-1, pp. 585-591.

Gravel, J.L., Jackaman, W. and Matysek, P.F. 1990. 1989 Regional Geochemical Survey, Southern Vancouver Island and Lower Mainland (92B, 92C, 92F, 92 G). B.C. Ministry of Energy, Mines and Petroleum Resources, Geological Fieldwork 1989, Paper 1990-1, pp. 503-510.

Grimaldi, F.S. and Schnepfe, M.M. 1969. Mode of Occurrence of Platinum, Palladium, and Rhodium in Chromitite. U.S. Geological Survey, Professional Paper 650-C, pp. C149-C151.

Gunn, A.G. 1989. Drainage and Overburden Geochemistry in Exploration for Platinum-Group Element Mineralization in the Unst Ophiolite, Shetland, U.K. Journal of Geochemical Exploration, 31, pp. 209-236.

Haggerty, S.E. 1976. Opaque Mineral Oxides in Terrestrial Igneous Rocks. *In* Oxide Minerals, Reviews in Mineralogy, 3, D. Rumble III, ed. Mineralogical Society of America, pp. Hg101-Hg300.

Hall, G.E.M. 1988. The Determination of Pt and Pd in Waters. Explore, Number 64, pp. 12-13.

Hall, G.E.M. and Bonham-Carter, G.F. 1988. Review of Methods to Determine Gold, Platinum and Palladium in Production-Oriented Geochemical Laboratories, with Application of a Statistical Procedure to Test for Bias. Journal of Geochemical Exploration, 30, pp. 255-286.

Hall, G.E.M., Pelchat, J.-C. and Dunn, C.E. 1990. The Determination of Au, Pd and Pt in Ashed Vegetation by ICP-Mass Spectrometry and Graphite Furnace Atomic Absorption Spectrometry. Journal of Geochemical Exploration, 37, pp. 1-23.

Harris, J.F. 1982. Sampling and Analytical Requirements For Effective Use of Geochemistry in Exploration for Gold. *In* Precious Metals in the Northern Cordillera, A.A. Levinson, ed. Association of Exploration Geochemists, Special Volume 10, pp. 53-67.

Hawkes, H.E. 1951. Magnetic Exploration for Chromite. U.S. Geological Survey, Bulletin 973-A, 21 pages.

Hem, J.D. 1985. Study and Interpretation of the Chemical Characteristics of Natural Water. Third Edition. U.S. Geological Survey, Water-Supply Paper 2254, 264 pages.

Hickson, C.J. and Juras, S.J. 1986. Sample Contamination by Grinding. Canadian Mineralogist, 24, pp. 585-589.

Hills, L.V. 1962. Glaciation, Stratigraphy, Structure and Micropaleobotany of the Princeton Coalfield, British Columbia. Unpublished M.Sc. Thesis, The University of British Columbia, 141 pages.

Hodge, R.A.L. 1976. Regional Geology, Groundwater Flow Systems and Slope Stability. Unpublished M.A.Sc. Thesis, The University of British Columbia, 98 pages.

Hoffman, S.J. 1977. Talus Fine Sampling as a Regional Geochemical Exploration Technique in Mountainous Regions. Journal of Geochemical Exploration, 7, pp. 349-360.

Holland, S.S. 1976. Landforms of British Columbia: A Physiographic Outline. B.C. Department of Mines and Petroleum Resources, Bulletin 48, 138 pages.

Horowitz, A.J. 1985. A Primer on Trace Metal-Sediment Chemistry. U.S. Geological Survey, Water-Supply Paper 2277, 67 pages.

Huang, P.M. 1989. Feldspars, Olivines, Pyroxenes, and Amphiboles. *In* Minerals in Soil Environments. Second Edition. J.B. Dixon and S.B. Weed, eds. Soil Science Society of America, Madison, pp. 975-1050.

Hulbert, L.J., Duke, J.M., Eckstrand, O.R., Lydon, J.W., Scoates, R.F.J., Cabri, L.J. and Irvine, T.N. 1988. Geological Environments of the Platinum Group Elements. Geological Survey of Canada, Open File 1440, 148 pages.

Irvine, T.N. 1965. Chromian Spinel as a Petrogenetic Indicator: Part 1. Theory. Canadian Journal of Earth Sciences, 2, pp. 648-672.

Irvine, T.N. 1967. Chromian Spinel as a Petrogenetic Indicator: Part 2. Petrologic Applications. Canadian Journal of Earth Sciences, 4, pp. 71-103.

Jackson, E.D. 1969. Chemical Variation in Coexisting Chromite and Olivine in Chromitite Zones of the Stillwater Complex. *In* Magmatic Ore Deposits: A Symposium, H.D.B. Wilson, ed. Economic Geology Monograph 4, pp. 41-71.

Jackson, E.D. and Thayer, T.P. 1972. Some Criteria for Distinguishing Between Stratiform, Concentric, and Alpine Peridotite-Gabbro Complexes. Twenty-fourth International Geological Congress, Section 2: Petrology, pp. 289-296.

Jamieson, G.R. and Freeze, R.A. 1983. Determining Hydraulic Conductivity Distributions in a Mountainous Area Using Mathematical Modeling. Ground Water, 21, pp. 168-177.

Jenness, S.E. 1959. "Magnetic" Chromite from Shoal Pond, Northeastern Newfoundland. Economic Geology, 54, pp. 1298-1301.

Johnston, R.A.A. 1911. *In* Geological Survey of Canada, Summary Report: 1910, page 263.

Jones, P.S.A. 1988. Postglacial Chronology of Large Earthflows in South-Central British Columbia. Unpublished Ph.D. Thesis, The University of British Columbia, 446 pages.

Kabata-Pendias, A. and Pendias, H. 1984. Trace Elements in Soils and Plants. CRC Press, Boca Raton, 315 pages.

Kemp, J.F. 1902. Geological Relations and Distribution of Platinum and Associated Metals. U.S. Geological Survey, Bulletin 193, 95 pages.

Kimball, K.L. 1990. Effects of Hydrothermal Alteration on the Compositions of Chromian Spinels. Contributions to Mineralogy and Petrology, 105, pp. 337-346.

Kucha, H. 1982. Platinum-Group Metals in the Zechstein Copper Deposits, Poland. Economic Geology, 77, pp. 1578-1591.

Kurzl, H. 1988. Exploratory Data Analysis: Recent Advances for the Interpretation of Geochemical Data. Journal of Geochemical Exploration, 30, pp. 309-322.

Laflamme, J.H.G. 1990. The Preparation of Materials for Microscopic Study. *In* Advanced Microscopic Study of Ore Minerals, J.L. Jambor and D.J. Vaughan, eds. Mineralogical Association of Canada, Short Course Handbook 17, pp. 37-68.

Lakin, H.W., Curtin, G.C., Hubert, A.E., Shacklette, H.T. and Doxtader, K.G. 1974. Geochemistry of Gold in the Weathering Cycle. U.S. Geological Survey, Bulletin 1330, 80 pages.

Langmyhr, F.V. and Sveen, S. 1965. Decomposability in Hydrofluoric Acid of the Main and Some Minor and Trace Minerals of Silicate Rocks. Analytica Chimica Acta, 32, pp. 1-7.

Lavergne, P.J. 1988. Field and Laboratory Methods Used by the Geological Survey of Canada in Geochemical Surveys: Preparation of Geological Materials for Chemical and Spectrochemical Analysis; Separation and Concentration of Minerals; and a Guide to the Identification of Common Minerals. Geological Survey of Canada, Open File 1428, 57 pages.

Laznicka, P. 1985. Empirical Metallogeny-Depositional Environments, Lithological Associations and Metallic Ores: Volume 1. Elsevier, Amsterdam, 1002 pages.

Leake, R.C. and Gunn, A.G. 1985. Exploration for Platinum-Group Element Mineralization in the Unst Ophiolite, Shetland. *In* Geology in the Real World - The Kingsley Dunham Volume, Institute of Mining and Metallurgy, pp. 253-266.

Leblanc, M. 1980. Chromite Growth, Dissolution and Deformation from a Morphological View Point: SEM Investigations. Mineralium Deposita, 15, pp. 201-210

Lett, R.E.W. 1978. Secondary Dispersion of Transition Metals Through a Copper-Rich Bog in the Cascade Mountains, British Columbia. Unpublished Ph.D Thesis, The University of British Columbia, 244 pages.

Lett, R.E.W. and Fletcher, W.K. 1979. The Secondary Dispersion of Transition Metals Through a Copper-rich Hillslope Bog in the Cascade Mountains, British Columbia. *In* Geochemical Exploration 1978, J.R. Watterson and P.K. Theobald, eds. Association of Exploration Geochemists, pp. 103-115.

Lord, T.M. and Green, A.J. 1974. Soils of the Tulameen Area of British Columbia. Agriculture Canada, British Columbia Soil Survey Report No. 13, 163 pages.

MacAulay, R.M. 1919. The Source of Placer Platinum in the Tulameen District of British Columbia. Engineering and Mining Journal, 107, pp. 303-306.

Macdonald, A.J. 1987. Ore Deposits Models 12. The Platinum Group Elements Deposits: Classification and Genesis. Geoscience Canada, 14, pp. 155-166.

Makovicky, M., Makovicky, E. and Rose-Hansen, J. 1986. Experimental Studies on the Solubility and Distribution of Platinum Group Elements in Base-Metal Sulphides in Platinum Deposits. *In* Metallogeny of Basic and Ultrabasic Rocks, M.J. Gallagher, R.A. Ixer, C.R. Neary and H.M. Prichard, eds. Institution of Mining and Metallurgy, pp. 415-425.

Matelski, R.P. and Turk, L.M. 1947. Heavy Minerals in Some Podzol Soil Profiles in Michigan. Soil Science, 64, pp. 469-487.

Mathews, W.H. 1944. Glacial Lakes and Ice Retreat in South-Central British Columbia. Royal Society of Canada, Proceedings and Transactions, 38, Section 4, pp. 39-57.

Maurice, Y.T. 1988. Repartition du Cr, Pt, Pd, et Ir dans les depots de surface de l'Estrie-Beauce, Quebec. *In* Current Research, Part B, Geological Survey of Canada, Paper 88-1B, pp. 1-8.

McGoldrick, P.J. and Keays, R.R. 1981. Precious and Volatile Metals in the Perseverence Nickel Deposit Gossan: Implications for Exploration in Weathered Terrains. Economic Geology, 76, pp. 1752-1763.

Mertie, J.B., Jr. 1969. Economic Geology of the Platinum Metals. U.S. Geological Survey, Professional Paper 630, 120 pages.

Michailidis, K.M. 1990. Zoned Chromites with High Mn-Contents in the Fe-Ni-Cr-Laterite Ore Deposits from the Edessa Area in Northern Greece. Mineralium Deposita, 25, pp. 190-197.

Mihalik, P., Jacobsen, J.B.E. and Hiemstra, S.A. 1974. Platinum-Group Minerals from a Hydrothermal Environment. Economic Geology, 69, pp. 257-262.

Miller, J.K. 1984. Model for Clastic Indicator Trains in Till. *In* Prospecting in Areas of Glaciated Terrain 1984. Institution of Mining and Metallurgy, pp. 69-77.

Mitchell, W.A. 1975. Heavy Minerals. *In* Soil Components: Volume 2 - Inorganic Components. Springer-Verlag, Berlin, pp. 449-480.

Moloughney, P.E. 1986. Assay Methods Used in Canmet for the Determination of Precious Metals. Canada Centre for Mineral and Energy Technology, SP86-1E, 33 pages.

Mortimer, N. 1987. The Nicola Group: Late Triassic and Early Jurassic Subduction-Related Volcanism in British Columbia. Canadian Journal of Earth Sciences, 24, pp. 2521-2536.

Mountain, B.W. and Wood, S.A. 1988a. Solubility and Transport of Platinum-Group Elements in Hydrothermal Solutions: Thermodynamic and Physical Chemical Constraints. *In* Geo-Platinum 87, H.M. Prichard, P.J. Potts, J.F.W. Bowles and S.J. Cribb, eds. Elsevier, pp. 57-82.

Mountain, B.W. and Wood, S.A. 1988b. Chemical Controls on the Solubility, Transport, and Deposition of Platinum and Palladium in Hydrothermal Solutions: A Hydrothermal Approach. Economic Geology, 83, pp. 492-510.

Muller, L.D. 1977. Laboratory Methods of Mineral Separation. *In* Physical Methods in Determinative Mineralogy, Second Edition, J. Zussman, ed. Academic Press, London, 720 pages.

Naldrett, A.J. and Cabri, L.J. 1976. Ultramafic and Related Mafic Rocks: Their Classification and Genesis with Special Reference to the Concentration of Nickel Sulfides and Platinum-Group Elements. Economic Geology, 71, pp. 1131-1158.

Nasmith, H., Mathews, W.H. and Rouse, G.E. 1967. Bridge River Ash and Some Other Recent Ash Beds in British Columbia. Canadian Journal of Earth Sciences, 4, pp. 163-170.

Nixon, G.T. 1990. Geology and Precious Metal Potential of Mafic-Ultramafic Rocks in British Columbia: Current Progress. B.C. Ministry of Energy, Mines and Petroleum Resources, Geological Fieldwork 1989, Paper 1990-1, pp. 353-358.

Nixon, G.T., Cabri, L.J. and Laflamme, J.H.G. 1989. Origin of Platinum Nuggets in Tulameen Placers: A Mineral Chemistry Approach with Potential for Exploration. B.C. Ministry of Energy, Mines and Petroleum Resources, Exploration in British Columbia - 1988, pp. B83-B89.

Nixon, G.T., Cabri, L.J. and Laflamme, J.H.G. 1990. Platinum-Group Element Mineralization in Lode and Placer Deposits Associated with the Tulameen Alaskan-Type Complex, British Columbia. Canadian Mineralogist, 28, pp. 503-535.

Nixon, G.T. and Rublee, V.J. 1988. Alaskan-type Ultramafic Rocks in British Columbia: New Concepts of the Structure of the Tulameen Complex. B.C. Ministry of Energy, Mines and Petroleum Resources, Geological Fieldwork 1987, Paper 1988-1, pp. 281-294.

O'Neill, J.J. and Gunning, H.C. 1934. Platinum and Allied Metal Deposits of Canada. Geological Survey of Canada, Economic Geology Series No. 13, 165 pages.

Ong, H.L. and Swanson, V.E. 1969. Natural Organic Acids in the Transportation, Deposition, and Concentration of Gold. Quarterly of the Colorado School of Mines, 64, pp. 395-425.

Ottemann, J. and Augustithis, S.S. 1967. Geochemistry and Origin of "Platinum-Nuggets" in Lateritic Covers from Ultrabasic Rocks and Birbirites of W. Ethiopia. Mineralium Deposita, 1, pp. 269-277.

Otto, G.H. 1933. Comparative Tests of Several Methods of Sampling Heavy Mineral Concentrates. Journal of Sedimentary Petrology, 3, pp. 30-39.

Owada, S. and Harada, T. 1985. Grindability and Magnetic Properties of Chromites from Various Localities in Relation to their Mineralogical Properties. Journal of the Mineralogical and Metallurgical Institute of Japan, 101, page 781.

Owen, R.M. 1978. Geochemistry of Platinum-Enriched Sediments of the Coastal Bering Sea. *In* Geochemical Exploration 1978. Association of Exploration Geochemists, pp. 145-152.

Page, N.J. and Jackson, E.D. 1967. Preliminary Report on Sulfide and Platinum-Group Minerals in the Chromitites of the Stillwater Complex, Montana. U.S. Geological Survey, Professional Paper 575-D, pp. D123-D126.

Paktunc, A.D., Hulbert, L.J. and Harris, D.C. 1990. Partitioning of the Platinum-Group and Other Trace Elements in Sulfides from the Bushveld Complex and Canadian Occurrences of Nickel-Copper Sulfides. Canadian Mineralogist, 28, pp. 475-488.

Peoples, J.W. and Eaton, G.P. 1952. Magnetic Susceptibility of Chromite from Montana and its Relation to Other Physical and Chemical Properties. American Mineralogist, 37, page 298.

Plimer, I.R. and Williams, P.A. 1988. New Mechanisms for the Mobilization of the Platinum-Group Elements in the Supergene Zone. *In* Geo-Platinum 87, H.M. Prichard, P.J. Potts, J.F.W. Bowles and S.J. Cribb, eds. Elsevier, pp. 83-92.

Pogrebnyak, Yu.F., Kondratenko, L.A. and Tat'yankina, E.M. 1984. Forms of Platinum and Palladium Migration in Water of Dispersion Trains. Doklady Academy Nauk SSSR, 279, pp. 460-462.

Poitevin, E. 1924. Platiniferous Rocks from Tulameen Map-Area, Yale District, British Columbia, and Ural Mountains, Russia. Geological Survey of Canada, Summary Report 1923, Part A, pp. 84A-110A.

Rabenhorst, M.C., Foss, J.E. and Fanning, D.S. 1982. Genesis of Maryland Soils Formed from Serpentinite. Soil Science Society of America Journal, 46, pp. 607-616.

Radhakrishna Murthy, I. V. and Gopalakrishna, G. 1982. Remanence Hysteresis Properties of Chromites. Indian Academy of Sciences, Proceedings, Earth and Planetary Sciences, 91, pp. 159-166.

Rao, A.T. 1978. Magnetic Chromites from Kondapalli, Andhra Pradesh, India. Mineralogical Magazine, 42, page 406.

Razin, L.V. 1971. Problem of the Origin of Platinum Metallization of Forsterite Dunites. International Geology Review, 13, pp. 776-788.

Razin, L.V., Khvostov, V.P. and Novikov, V.A. 1965. Platinum Metals in the Essential and Accessory Minerals of Ultramafic Rocks. Geochemistry International, 2, pp. 118-131.

Rice, H.M.A. 1947. Geology and Mineral Deposits of the Princeton Map-Area, British Columbia. Geological Survey of Canada, Memoir 243, 136 pages.

Riese, W.C. and Arp, G.K. 1986. Biogeochemical Exploration for Platinum Deposits in the Stillwater Complex, Montana. *In* Mineral Exploration: Biological Systems and Organic Matter, Rubey Volume V, D. Carlisle, W.L. Berry, I.R. Kaplan and J.R. Watterson, eds. Prentice-Hall, Englewood Cliffs, pages 170-182.

Riley, J.P. 1958. The Rapid Analysis of Silicate Rocks and Minerals. Analytica Chimica Acta, 19, pp. 413-428.

Robinson, W.O., Edgington, G. and Byers, H.G. 1935. Chemical Studies of Infertile Soils Derived from Rocks High in Magnesium and Generally High in Chromium and Nickel. U.S. Department of Agriculture, Technical Bulletin 471, pp. 1-28.

Rose, A.W., Hawkes, H.E. and Webb, J.S. 1979. Geochemistry in Mineral Exploration. Second Edition. Academic Press, London, 657 pages.

Rublee, V.J. and Parrish, R.R. 1990. Chemistry, Chronology and Tectonic Significance of the Tulameen Complex, Southwestern British Columbia. Geological Association of Canada - Mineralogical Association of Canada, Annual Meeting, Program with Abstracts, 15, page A114.

Rublee, V.J. 1986. Occurrence and Distribution of Platinum-Group Elements in British Columbia. B.C. Ministry of Energy, Mines and Petroleum Resources, Open File 1986-7, pp. 6-12.

Rucklidge, J. 1972. Chlorine in Partially Serpentinized Dunite. Economic Geology, 67, pp. 38-40.

Rudolph, W.W. and Moore, J.R. 1972. A New and Strange Prospecting Guide. Alaska Construction and Oil Report, February: pp. 40-42.

Sabelin, T., Iwasaki, I. and Reid, K.J. 1986. Platinum-Iron Alloys in the Duluth Gabbro Complex: Mineralogy and Beneficiation. *In* Process Mineralogy VI, R.D. Hagni, ed. The Metallurgical Society, pp. 431-440.

Sagheer, M. 1966. Flotation Characteristics of Chromite and Serpentine. American Institute of Mining, Metallurgical and Petroleum Engineers, Transactions, 235, pp. 60-67.

Schwerer, F.C. and Gundaker, W. 1975. Magnetic Properties of Natural Chromites: Mechanical and Thermal Effects. American Institute of Mining, Metallurgical and Petroleum Engineers, Transactions, 258, pp. 88-95.

Shilts, W.W. 1973. Glacial Dispersion of Rocks, Minerals, and Trace Elements in Wisconsinan Till, Southeastern Quebec, Canada. Geological Society of America, Memoir 136, pp. 189-219.

Shilts, W.W. 1976. Glacial Till and Mineral Exploration. *In* Glacial Till: An Interdisciplinary Study, R.F. Legget, ed. Royal Society of Canada, Special Publication 12, pp. 205-224.

Shilts, W.W. 1982. Glacial Dispersal - Principles and Practical Applications. Geoscience Canada, 9, pp. 42-47.

Sibbick, S.J.N. 1990. The Distribution and Behaviour of Gold in Soils in the Vicinity of Gold Mineralization, Nickel Plate Mine, Hedley, Southern British Columbia. Unpublished M.Sc. Thesis, The University of British Columbia, 205 pages.

Sinclair, A.J. 1976. Applications of Probability Graphs in Mineral Exploration. The Association of Exploration Geochemists, Special Volume 4, 95 pages.

Sinclair, A.J. 1986. Statistical Interpretation of Soil Geochemical Data. *In* Exploration Geochemistry: Design and Interpretation of Soil Surveys, James M. Robertson, ed. Society of Economic Geologists, Reviews in Economic Geology, Volume 3, pp. 97-115.

Skogerboe, R.K. and Wilson, S.A. 1981. Reduction of Ionic Species by Fulvic Acid. Analytical Chemistry, 53, pp. 228-232.

Sobieraj, S. and Laskowski, J. 1973. Flotation of Chromite: 1-Early Research and Recent Trends; 2-Flotation of Chromite and Surface Properties of Spinel Minerals. Institution of Mining and Metallurgy, Transactions, pp. C207-C213.

Stanley, C.R. 1987. Probplot: An Interactive Computer Program to Fit Mixtures of Normal (or Log-Normal) Distributions with Maximum Likelihood Optimization Procedures. The Association of Exploration Geochemists, Special Volume 14.

Steger, H.F. 1986. Certified Reference Materials. Canada Centre for Mineral and Energy Technology, CM84-14E, Revised Edition, 42 pages.

Stevens, R.E. 1944. Composition of Some Chromites of the Western Hemisphere. American Mineralogist, 29, pp. 1-34.

Stewart, R.A. 1986. Routine Heavy Mineral Analysis Using a Concentrating Table. Journal of Sedimentary Petrology, 56, pp. 555-556.

St. Louis, R.M. 1984. Geochemistry of the Platinum-Group Elements in the Tulameen Ultramafic Complex, British Columbia. Unpublished M.Sc. Thesis, University of Alberta, 127 pages.

St. Louis, R.M., Nesbitt, B.E. and Morton, R.D. 1986. Geochemistry of Platinum-Group Elements in the Tulameen Ultramafic Complex, Southern British Columbia. Economic Geology, 81, pp. 961-973.

Stowe, C.W. 1987. The Mineral Chromite. *In* Evolution of Chromium Ore Fields, C.W. Stowe, ed. Van Nostrand Reinhold, New York, pp. 1-22.

Stueber, A.M., Huang, W.H. and Johns, W.D. 1968. Chlorine and Fluorine Abundances in Ultramafic Rocks. Geochimica et Cosmochimica Acta, 32, pp. 353-358.

Stumpfl, E.F. 1974. The Genesis of Platinum Deposits: Further Thoughts. Minerals Science Engineering, 6, pp. 120-141.

Stumpfl, E.F. 1986. Distribution, Transport and Concentration of Platinum Group Elements. *In* Metallogeny of Basic and Ultrabasic Rocks, M.J. Gallagher, R.A. Ixer, C.R. Neary and H.M. Prichard, eds. Institution of Mining and Metallurgy, pp. 379-394.

Stumpfl, E.F. and Tarkian, M. 1976. Platinum Genesis: New Mineralogical Evidence. Economic Geology, 71, pp. 1451-1460.

Svoboda, J. 1987. Magnetic Methods for the Treatment of Minerals. Developments in Mineral Processing, 8. Elsevier, Amsterdam, 692 pages.

Taufen, P.M. and Marchetto, C.M.L. 1989. Tropical Weathering Control of Ni, Cu, Co and Platinum Group Element Distributions at the O'Toole Ni-Cu Sulphide Deposit, Minas Gerais, Brazil. Journal of Geochemical Exploration, 32, pp. 185-197.

Thayer, T.P. 1946. Preliminary Chemical Correlation of Chromite with the Containing Rocks. Economic Geology, 41, pp. 202-217.

Theobald, P.K. 1957. The Gold Pan as a Quantitative Geologic Tool. U.S. Geological Survey, Bulletin 1071-A, 54 pages.

Thompson, M. and Howarth, R.J. 1978. A New Approach to the Estimation of Analytical Precision. Journal of Geochemical Exploration, 9, pp. 23-30.

Tintor, N. 1986. The Platinum Group. The Northern Miner Magazine, 1, May Issue, pp. 55-57.

Travis, G.A., Keays, R.R. and Davison, R.M. 1976. Palladium and Iridium in the Evaluation of Nickel Gossans in Western Australia. Economic Geology, 71, pp. 1229-1243.

Ulmer, G.C. 1969. Experimental Investigations of Chromite Spinels. *In* Magmatic Ore Deposits: A Symposium, H.D.B. Wilson, ed. Economic Geology Monograph 4, pp. 114-131.

Van der Walt, C.F.J. 1941. Chrome Ores of the Western Bushveld Complex. Geological Society of South Africa, Transactions, 44, pp. 79-112.

Wagner, P.A. 1929. The Platinum Deposits and Mines of South Africa. 1973 Reprint. Struik, Capetown, 338 pages.

Wagner, P.A. and Reinecke, L. 1930. Mineral Deposits of the Union of South Africa. Third (Triennial) Empire Mining and Metallurgical Congress, Johannesburg, 310 pages.

Walker, R.B. 1954. The Ecology of Serpentine Soils: II. Factors Affecting Plant Growth on Serpentine Soils. Ecology, 35, pp. 259-266.

Wang W. and Poling, G.W. 1983. Methods for Recovering Fine Placer Gold. Canadian Institute of Mining and Metallurgy, Bulletin, 76 (860), pp. 47-56.

Weberling, R.P. and Cosgrove, J.F. 1965. Flame Emission and Absorption Methods. *In* Trace Analysis: Physical Methods, G.H. Morrison, ed. John Wiley and Sons, New York, pp. 245-269.

Westland, A.D. 1981. Inorganic Chemistry of the Platinum-Group Elements. *In* Platinum-Group Elements: Mineralogy, Geology, Recovery, L.J. Cabri, ed. Canadian Institute of Mining and Metallurgy, Special Volume 23, pp. 5-18.

White, G.V. 1987. Olivine Potential in the Tulameen Ultramafic Complex: Preliminary Report. B.C. Ministry of Energy, Mines and Petroleum Resources, Geological Fieldwork 1986, Paper 1987-1, pp. 303-307.

White, L. 1987. Stillwater Adds a New Source to World Platinum Supplies. Engineering and Mining Journal, 188, October Issue, pp. 38-43.

Whittaker, P.J. and Watkinson, D.H. 1985. Platinum-Group Minerals from Chromitite in Alpine-Type Peridotite of the Cache Creek Group, British Columbia. Canadian Mineralogist, 23, page 320.

Wood, S.A. 1990. The Interaction of Dissolved Platinum with Fulvic Acid and Simple Organic Acid Analogues in Aqueous Solutions. Canadian Mineralogist, 28, pp. 665-673.

Wood, S.A., Mountain, B.W. and Fenlon, B.J. 1989. Thermodynamic Constraints on the Solubility of Platinum and Palladium in Hydrothermal Solutions: Reassessment of Hydroxide, Bisulfide, and Ammonia Complexing. Economic Geology, 84, pp. 2020-2028.

Wood, S.A. and Mucci, A. 1988. The Solubility of Platinum as Bisulfide and Hydroxide Complexes at 25°C. V.M. Goldschmidt Symposium, Program with Abstracts, p. 83.

Wood, S.A. and Vlassopoulos, D. 1990. The Dispersion of Pt, Pd and Au in Surficial Media About Two PGE-Cu-Ni Prospects in Quebec. Canadian Mineralogist, 28, pp. 649-663.

Worst, B.G. 1958. The Differentiation and Structure of the Great Dyke of Southern Rhodesia. Geological Society of South Africa, Transactions, 61, pp. 283-354.

Wright, T.L. and Fleischer, M. 1965. Geochemistry of the Platinum Metals. U.S. Geological Survey, Bulletin 1214-A, 24 pages.

Zhou, Z., and Zhang, D. 1975. Heavy Mineral Separation for Platinum-Group Minerals in Platinum-Bearing Chromite Deposits. Acta Geologica Sinica, 2, pp. 187-193 (Chinese with English abstract).

APPENDICES

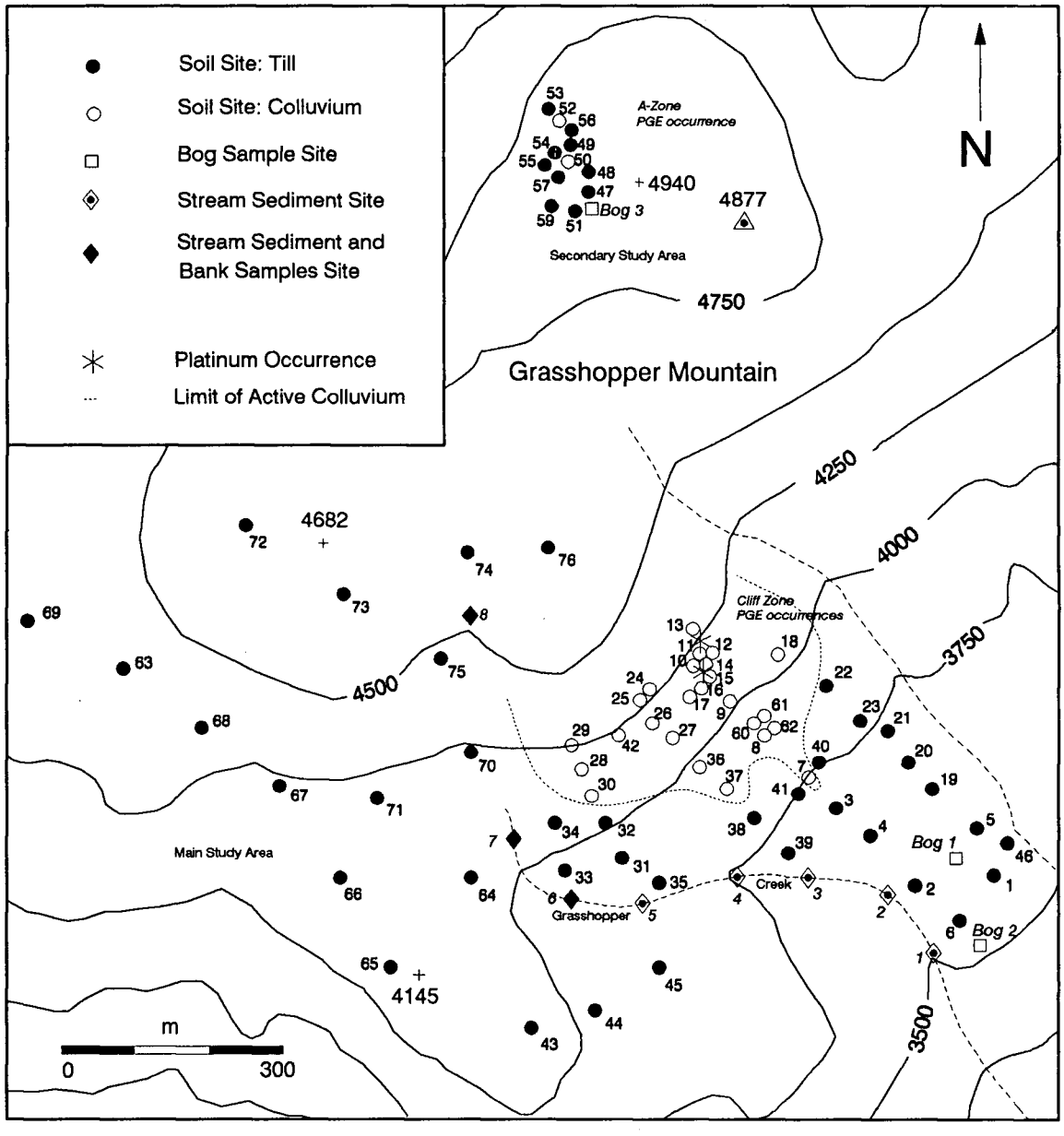

Appendix 1. Sample location map of soil, sediment and bog sites within the dunite core of the Tulameen complex (basemap adapted from Bohme, 1987).

Appendix 2.1
Subsample Size Experiment:
Analytical Results for 10 g versus 30 g Subsamples
of Drift Monitors RK-05 and PT-5

Batch	Lab	Sample	Standard	Weight (g)	Pt (ppb)	Pd (ppb)	Rh (ppb)	Au (ppb)
1	A	TU-4-01	RK-05	10	34	5	3	4
1	A	TU-4-04	RK-05	10	31	11	5	3
1	A	TU-4-05	RK-05	10	33	2	8	3
1	A	TU-4-07	RK-05	10	31	2	5	3
1	A	TU-4-09	RK-05	10	31	3	6	3
1	A	TU-4-12	RK-05	10	34	7	4	4
1	A	TU-4-14	RK-05	10	35	3	6	6
1	A	TU-4-02	PT-5	10	439	10	6	1
1	A	TU-4-03	PT-5	10	434	9	6	1
1	A	TU-4-06	PT-5	10	464	9	12	11
1	A	TU-4-08	PT-5	10	449	6	13	3
1	A	TU-4-10	PT-5	10	396	2	6	2
1	A	TU-4-11	PT-5	10	465	8	10	5
1	A	TU-4-13	PT-5	10	448	6	7	2
1	A	TU-4-16	RK-05	30	32	3	9	2
1	A	TU-4-18	RK-05	30	32	2	7	3
1	A	TU-4-19	RK-05	30	32	2	10	2
1	A	TU-4-21	RK-05	30	32	2	8	3
1	A	TU-4-23	RK-05	30	32	2	7	3
1	A	TU-4-26	RK-05	30	31	2	8	1
1	A	TU-4-27	RK-05	30	31	2	8	2
1	A	TU-4-15	PT-5	30	438	3	6	3
1	A	TU-4-17	PT-5	30	319	3	4	2
1	A	TU-4-20	PT-5	30	274	3	3	3
1	A	TI-4-22	PT-5	30	408	2	6	3
1	A	TU-4-24	PT-5	30	381	5	10	3
1	A	TU-4-25	PT-5	30	321	3	6	4
1	A	TU-4-28	PT-5	30	325	3	5	1
2	A	TU-5-01	PT-5	10	522	7	20	12
2	A	TU-5-02	PT-5	10	501	10	17	6
2	A	TU-5-03	PT-5	10	567	7	9	7
2	A	TU-5-04	PT-5	10	488	4	13	6
2	A	TU-5-05	PT-5	10	489	10	7	5
2	A	TU-5-06	PT-5	10	488	2	8	1
2	A	TU-5-07	PT-5	10	528	2	7	399
2	A	TU-5-08	PT-5	30	522	4	10	2
2	A	TU-5-09	PT-5	30	434	4	7	1
2	A	TU-5-10	PT-5	30	481	4	6	1
2	A	TU-5-11	PT-5	30	447	6	5	2
2	A	TU-5-12	PT-5	30	385	6	8	1
2	A	TU-5-13	PT-5	30	453	4	5	2
2	A	TU-5-14	PT-5	30	432	2	5	5
3	B	TU-8-01	PT-5	10	650	< 10	-	20
3	B	TU-8-02	PT-5	10	650	< 10	-	10
3	B	TU-8-03	PT-5	10	600	< 10	-	< 10
3	B	TU-8-04	PT-5	10	650	< 10	-	< 10
3	B	TU-8-05	PT-5	10	600	< 10	-	50
3	B	TU-8-06	PT-5	10	650	< 10	-	20
3	B	TU-8-07	PT-5	10	650	< 10	-	< 10

Appendix 2.2
Certified Reference Standard PTA-1:
Analytical Results from Two Commercial Laboratories
(A = Acme Labs, B = Chemex Labs)

Batch	Lab	Sample	Standard	Weight (g)	Pt (ppb)	Pd (ppb)	Rh (ppb)	Au (ppb)
2	A	TU-5-51	PTA-1	10	7078	64	35	536
2	A	TU-5-52	PTA-1	10	5729	32	32	26
2	A	TU-5-53	PTA-1	10	2618	40	24	534
2	A	TU-5-54	PTA-1	10	3375	33	23	68
2	A	TU-5-55	PTA-1	10	5082	48	35	107
2	A	TU-5-56	PTA-1	10	3032	24	25	57
2	A	TU-5-57	PTA-1	10	3657	28	49	41
3	B	TU-8-08	PTA-1	10	4700	40	-	900
3	B	TU-8-09	PTA-1	10	3300	30	-	100
3	B	TU-8-10	PTA-1	10	3000	30	-	40
3	B	TU-8-11	PTA-1	10	4200	30	-	70
3	B	TU-8-12	PTA-1	10	3700	30	-	490
3	B	TU-8-13	PTA-1	10	3400	30	-	330
3	B	TU-8-14	PTA-1	10	2100	20	-	300

Appendix 3.1
Duplicate Pt, Pd and Au Analyses:
Overview (-70 mesh) Sample Suite
(n = 12)

Batch	Soil Site	Sample	Pt-1 (ppb)	Pt-2 (ppb)	Pd-1 (ppb)	Pd-2 (ppb)	Au-1 (ppb)	Au-2 (ppb)
1	21	88-SC-44	3	6	2	3	7	9
1	31	88-SC-72	8	3	2	2	2	16
1	6	88-SC-19	3	9	4	4	34	21
1	43	88-SC-112	16	16	2	2	4	1
2	72	89-SC-213	28	32	7	11	14	8
2	67	89-SC-193	32	41	10	14	12	15
1	56	88-SC-153	455	363	2	2	1	1
1	29	88-SC-66	47	46	3	2	54	55
1	15	88-SC-30	47	47	2	4	8	11
2	BS03	88-SC-708	21	19	7	5	3	3
1	SS03	88-SC-505	11	12	2	5	3	4
2	MS02	88-SC-504	8	17	2	4	29	76

Appendix 3.2
Duplicate Arsenic Analyses of Selected C Horizon Soils
and Standards - As-1: Acme Labs,
As-2: B.C. Geological Survey

Number	Lab Label	As-1 (ppm)	As-2 (ppm)	Comments
1	TU-1-02	14.7	18.0	
2	TU-1-04	0.1	1.2	Standard RK-05
3	TU-1-13	10.4	16.0	
4	TU-1-34	43.5	42.0	
5	TU-1-44	14.5	19.0	Standard PT-5
6	TU-1-45	56.3	73.0	
7	TU-1-68	16.1	22.0	
8	TU-1-95	7.5	10.0	

Appendix 3.3
Duplicate Pt, Pd and Au Analyses:
Ashed LFH Horizons and Organic Bog Soils
(n = 10)

Soil Site	Sample	Media	Underlying Material	Pt-1 (ppb)	Pt-2 (ppb)	Pt-3 (ppb)	Pd-1 (ppb)	Pd-2 (ppb)	Pd-3 (ppb)	Au-1 (ppb)	Au-2 (ppb)	Au-3 (ppb)
6	88-SC-017	LFH	Nondunitic Till	6	5	-	8	8	-	5	7	-
7	88-SC-020	LFH	Dunite Colluvium	49	116	-	3	3	-	4	4	-
22	88-SC-045	LFH	Nondunitic Till	4	2	-	2	3	-	6	1	-
24	88-SC-053	LFH	Dunite Colluvium	141	114	-	2	3	-	17	29	-
32	88-SC-074	LFH	Nondunitic Till	6	11	9	4	2	2	4	5	2
34	88-SC-080	LFH	Dunitic Till	10	7	-	2	2	-	4	6	-
-	88-SC-099	LFH	Nondunitic Till	11	7	-	2	3	-	6	3	-
47	88-SC-125	LFH	Dunitic Till (A)	143	112	104	2	2	2	3	10	1
75	89-SC-220	LFH	Dunitic Till	23	13	-	2	2	-	1	1	-
-	88-SC-708	Bog	Organic	55	52	-	3	5	-	4	5	-

Appendix 3.4
Duplicate Sample (Post-grinding) Analytical Data
(n = 47)

Site	Sample	Batch	Size Fraction	Pt-1 (ppb)	Pt-2 (ppb)	Pd-1 (ppb)	Pd-2 (ppb)	Au-1 (ppb)	Au-2 (ppb)
34	88-SC-082	3	-10+40	14	21	6	10	1	4
57	88-SC-155	3	-10+40	92	96	6	4	4	4
51	88-SC-133	3	-40+70	128	131	8	7	1	2
27	88-SC-061	3	-40+70	388	269	2	5	17	18
6	88-SC-018	3	-70+140L	3	1	3	4	16	8
57	88-SC-155	3	-70+140L	50	47	10	8	6	6
42	88-SC-105	3	-140+270L	62	70	4	2	19	16
56	88-SC-152	3	-140+270L	24	29	3	2	3	1
6	88-SC-019	3	-270	9	10	11	4	4	7
34	88-SC-082	3	-270	21	24	8	7	15	8
20	88-SC-040	3	-70+140H NON	9	12	7	10	13	6
34	88-SC-082	3	-70+140H NON	13	16	10	11	16	15
51	88-SC-135	3	-70+140H NON	28	34	28	23	69	58
34	88-SC-082	3	-140+270H NON	64	43	17	12	328	81
57	88-SC-156	3	-140+270H NON	1371	1265	13	12	509	26
33	88-SC-079	3	-70+140H MAG	78	100	6	9	5	2
51	88-SC-135	3	-70+140H MAG	1075	972	9	9	182	17
56	88-SC-152	3	-70+140H MAG	755	1123	6	8	1	1
27	88-SC-060	3	-70+140H MAG	348	556	6	7	6	9
34	88-SC-082	3	-140+270H MAG	128	128	14	10	5	5
51	88-SC-133	3	-140+270H MAG	358	252	5	2	1	2
57	88-SC-156	3	-140+270H MAG	359	794	2	11	1	2
20	88-SC-040	3	-40+70	21	19	10	3	5	3
33	88-SC-078	3	-40+70	19	19	4	9	3	1
57	88-SC-156	3	-270	150	132	10	5	8	13
42	88-SC-105	3	-270	117	126	2	2	39	36
56	88-SC-153	3	-270	260	219	4	4	4	1
73	89-SC-216	4	-10+40	101	123	6	7	7	7
43	88-SC-112	4	-40+70	1	5	5	2	11	2
43	88-SC-113	4	-70+140L	1	2	6	4	4	2
16	88-SC-031	4	-140+270L	117	90	2	5	8	4
73	89-SC-216	4	-270	41	43	2	5	7	7
56	88-SC-153	4	-10+40	1584	1003	7	7	7	5
69	89-SC-200	4	-40+70	54	68	4	8	2	5
43	88-SC-112	4	-70+140H NON	5	8	4	5	1	2
69	89-SC-200	4	-70+140H NON	7	8	7	3	18	16
73	89-SC-216	4	-70+140H NON	85	76	6	4	2	8
43	88-SC-112	4	-140+270H NON	70	66	6	11	3	3
73	89-SC-215	4	-140+270H NON	90	406	6	5	100	343
73	89-SC-216	4	-140+270H NON	139	129	9	7	115	98
69	89-SC-199	4	-70+140H MAG	1142	1088	8	7	21	20
73	89-SC-216	4	-70+140H MAG	1732	1696	3	10	72	22
16	88-SC-031	4	-70+140H MAG	2721	4740	12	13	73	69
69	89-SC-199	4	-140+270H MAG	1549	1577	3	3	10	25
73	89-SC-216	4	-140+270H MAG	474	406	7	8	15	17
43	88-SC-110	4	-270	16	10	7	8	2	1
69	89-SC-200	4	-270	25	4	6	6	12	25

SPLITTER DUPLICATE SAMPLE DATA: -10+40 FRACTION

SAMPLE	STATUS	Pt (ppb)	Pd (ppb)	Au (ppb)
88-SC-019	Original	9	6	1
	Duplicate	9	3	5
88-SC-040	Original	77	7	3
	Duplicate	17	7	12
88-SC-079	Original	93	6	1
	Duplicate	38	5	4
88-SC-135	Original	96	4	1
	Duplicate	89	7	4
88-SC-153	Original	722	7	1
	Duplicate1	1584 (1003)	7 (7)	7 (5)
	Duplicate2	1473	7	9
88-SC-156	Original	119	7	1
	Duplicate	121	2	6
88-SC-031*	Original	193	4	7
	Duplicate	199	5	6
89-SC-216*	Original	101 (123)	6 (7)	7 (7)
	Duplicate	60	3	5
88-SC-503*	Original	1	7	3
	Duplicate	1	7	20

Appendix 3.5. Analytical data for splitter-stage duplicate samples: -10+40 fraction. Asterix (*) indicates that originals and duplicates were analyzed in the same batch; all duplicates were analyzed in batch 4. The third value inside parentheses ( ) denotes concentration of a conventional post-grinding duplicate from that sample.

SPLITTER DUPLICATE SAMPLE DATA: -40+70 FRACTION

SAMPLE	STATUS	Pt (ppb)	Pd (ppb)	Au (ppb)
88-SC-061	Original	388 (269)	2 (5)	17(18)
	Duplicate	148	4	19
88-SC-112	Original	1 (5)	5 (2)	11 (2)
	Duplicate*	10	2	1
88-SC-135	Original	632	5	9
	Duplicate	121	7	5
88-SC-155	Original	128	2	1
	Duplicate	113	8	2
89-SC-200*	Original	76	5	9
	Duplicate	54 (68)	4 (8)	2 (5)
89-SC-215*	Original	92	3	28
	Duplicate	18	4	9

Appendix 3.6. Analytical data for splitter-stage duplicate samples: -40+70 fraction. Asterix (*) indicates that originals and duplicates were analyzed in the same batch; all duplicates were analyzed in batch 4. The third value inside parentheses ( ) denotes concentration of a conventional post-grinding duplicate from that sample.

Appendix 4.1
Drift Monitor RK-05
Analytical Results
(n = 20)

Analytical Batch	Lab Label	Pt (ppb)	Pd (ppb)	Au (ppb)
1	TU-1-04	29	2	2
1	TU-1-23	33	2	1
1	TU-1-58	37	2	2
1	TU-1-77	32	3	1
2	TU-3-120	33	9	3
2	TU-3-130	37	6	1
3	TU-6-05	33	5	1
3	TU-6-31	30	4	4
3	TU-6-58	30	5	1
3	TU-6-94	33	2	1
3	TU-6-108	29	2	1
3	TU-6-124	30	5	1
3	TU-6-147	30	2	2
3	TU-6-175	26	3	1
3	TU-6-208	29	3	3
4	TU-9-05	34	2	2
4	TU-9-39	26	2	1
4	TU-9-60	25	2	2
4	TU-9-92	28	2	1
4	TU-9-119	32	5	1

Appendix 4.2
Drift Monitor PT-5
Analytical Results
(n = 21)

Analytical Batch	Lab Label	Pt (ppb)	Pd (ppb)	Au (ppb)
1	TU-1-38	623	2	7
1	TU-1-44	637	2	1
1	TU-1-71	746	2	1
1	TU-1-89	621	4	3
2	TU-3-106	463	5	1
2	TU-3-136	546	3	3
3	TU-6-28	488	4	1
3	TU-6-45	494	7	1
3	TU-6-50	495	3	3
3	TU-6-64	513	8	1
3	TU-6-89	447	6	5
3	TU-6-132	503	7	1
3	TU-6-153	499	2	1
3	TU-6-193	435	3	4
3	TU-6-246	505	5	4
4	TU-9-15	534	5	4
4	TU-9-33	511	3	1
4	TU-9-64	566	3	2
4	TU-9-82	509	5	4
4	TU-9-102	478	2	5
4	TU-9-133	496	2	1

Appendix 4.3
Certified Reference Standard PTA-1
Analytical Results
(n = 7)

Analytical Batch	Lab Label	Pt (ppb)	Pd (ppb)	Au (ppb)
3	TU-6-217	1626	21	57
3	TU-6-225	4941	35	38
3	TU-6-252	3269	29	40
3	TU-6-264	3551	33	59
4	TU-9-124	2959	37	65
4	TU-9-142	2685	24	84
4	TU-9-147	1836	29	89

Appendix 4.4
Composite Ash Vegetation Standard V-3
Analytical Results
(n = 3)

Analytical Batch (LFH)	Lab Label	Subsample Weight (g)	Pt (ppb)	Pd (ppb)	Au (ppb)	Rh (ppb)
1	88-SC-064	10.00	72	223	55	7
1	88-SC-182	10.00	75	215	31	4
2	89-SC-187	2.86	74	180	28	14

Blank	Batch	Sample	Pt (ppb)	Pd (ppb)	Au (ppb)
1	1	TU-1-98	1	2	1
2	1	TU-1-99	1	2	1
3	2	TU-3-143	3	2	1
4*	3	TU-6-218	2	2	3
5*	3	TU-6-226	3	2	1
6*	3	TU-6-265	4	2	4
7*	4	TU-9-125	19	2	18
8*	4	TU-9-143	23	7	18
9*	4	TU-9-148	24	2	1

Appendix 4.5. Pt, Pd, and Au contents of silica blanks. All values in ppb. Samples marked with an asterix (*) indicate that the blank was inserted immediately after Certified Reference Standard PTA-1 in the sequence.

Appendix 5.1
Overview Analytical Results: Till
Non-dunitic Till and Clay (Page 1)

	Site	Sample	Parent Material	Pt (ppb)	Pd (ppb)	Rh (ppb)	Au (ppb)	As (ppm)	Sb (ppm)	Bi (ppm)	Ge (ppm)	Se (ppm)	Te (ppm)
1	Soil Site 2	88-SC-006	Nondunitic Till	9	5	2	8	14.7	1.8	0.4	0.2	0.2	0.3
2	Soil Site 3	88-SC-009	Nondunitic Till	14	3	2	6	12.6	1.7	0.1	0.2	0.2	0.3
3	Soil Site 4	88-SC-012	Nondunitic Till	6	2	2	2	18.3	1.5	0.2	0.2	0.2	0.3
4	Soil Site 5	88-SC-016	Nondunitic Till	18	4	2	5	21.9	0.9	0.6	0.2	0.3	0.3
5	Soil Site 6	88-SC-019	Nondunitic Till	3	4	2	34	10.9	1.6	0.2	0.3	0.2	0.3
6	Soil Site 19	88-SC-036	Nondunitic Till	8	3	2	16	17.8	0.9	0.3	0.2	0.2	0.3
7	Soil Site 20	88-SC-040	Nondunitic Till	20	3	2	9	20.2	1.0	0.2	0.2	0.2	0.3
8	Soil Site 21	88-SC-044	Nondunitic Till	3	2	2	7	12.9	0.7	0.2	0.2	0.2	0.3
9	Soil Site 22	89-SC-048	Nondunitic Till	5	6	2	7	16.4	1.0	0.2	0.4	0.4	0.5
10	Soil Site 23	88-SC-051	Nondunitic Till	5	2	2	13	20.1	1.8	0.3	0.2	0.4	0.3
11	Soil Site 31	88-SC-072	Nondunitic Till	8	2	2	2	10.4	1.0	0.2	0.2	0.2	0.3
12	Soil Site 32	88-SC-076	Nondunitic Till	12	5	2	3	8.1	0.6	0.2	0.2	0.2	0.3
13	Soil Site 35	88-SC-088	Nondunitic Till	14	5	2	5	14.7	0.6	0.3	0.3	0.2	0.3
14	Soil Site 38	88-SC-163	Nondunitic Till	15	5	2	6	23.2	1.0	0.3	0.2	0.2	0.3
15	Soil Site 39	88-SC-098	Nondunitic Till	2	2	2	4	14.3	0.6	0.2	0.2	0.2	0.3
16	Soil Site 40	88-SC-102	Nondunitic Till	2	2	2	2	12.9	0.7	0.4	0.2	0.2	0.3
17	Soil Site 41	88-SC-108	Nondunitic Till	5	6	2	11	23.0	0.7	0.4	0.2	0.3	0.3
18	Soil Site 44	88-SC-117	Nondunitic Till	18	2	2	7	10.5	0.6	0.3	0.2	0.2	0.3
19	Soil Site 45	88-SC-120	Nondunitic Till	13	15	2	9	12.1	0.5	0.3	0.2	0.2	0.3
20	Soil Site 1	88-SC-003	Clay	4	2	2	5	9.4	0.5	0.5	0.2	0.2	0.3
21	Soil Site 46	88-SC-124	Clay	7	3	2	5	14.3	1.2	0.3	0.2	0.2	0.3

Appendix 5.1
Overview Analytical Results: Till
Non-dunitic Till and Clay (Page 2)

	Site	Sample	Parent Material	SiO2 (%)	Al2O3 (%)	Fe2O3 (%)	MgO (%)	CaO (%)	Na2O (%)	K2O (%)	TiO2 (%)	P2O5 (%)	MnO (%)	Cr2O3 (%)	Ba (ppm)	LOI (%)	Total (%)
1	Soil Site 2	88-SC-006	Nondunitic Till	53.70	14.27	9.53	6.10	4.87	2.44	1.32	0.96	0.10	0.20	0.06	468	6.3	99.93
2	Soil Site 3	88-SC-009	Nondunitic Till	52.12	13.04	11.62	7.66	5.51	2.34	1.09	0.90	0.10	0.20	0.15	376	5.2	99.99
3	Soil Site 4	88-SC-012	Nondunitic Till	52.95	14.86	9.65	5.82	4.74	2.60	1.37	0.91	0.11	0.15	0.08	501	6.5	99.83
4	Soil Site 5	88-SC-016	Nondunitic Till	51.40	13.20	11.75	7.85	4.74	2.36	1.23	0.88	0.13	0.18	0.14	400	6.1	100.03
5	Soil Site 6	88-SC-019	Nondunitic Till	53.74	14.39	8.38	6.35	4.81	2.52	1.15	0.87	0.15	0.15	0.05	473	7.4	100.04
6	Soil Site 19	88-SC-036	Nondunitic Till	54.19	14.79	9.87	5.44	4.92	2.46	1.32	0.93	0.13	0.15	0.06	508	5.5	99.85
7	Soil Site 20	88-SC-040	Nondunitic Till	54.87	14.46	9.93	5.52	4.79	2.58	1.24	0.97	0.14	0.17	0.08	449	4.9	99.73
8	Soil Site 21	88-SC-044	Nondunitic Till	56.54	15.64	9.20	3.86	4.68	2.87	1.29	1.05	0.12	0.13	0.03	522	4.5	100.00
9	Soil Site 22	89-SC-048	Nondunitic Till	52.31	13.97	8.76	7.02	4.53	2.57	1.50	0.89	0.21	0.18	0.05	428	8.0	100.08
10	Soil Site 23	88-SC-051	Nondunitic Till	52.76	15.53	10.36	4.02	4.21	2.60	1.37	0.92	0.13	0.17	0.04	554	7.8	100.00
11	Soil Site 31	88-SC-072	Nondunitic Till	56.36	14.24	9.67	4.86	4.96	3.06	1.38	0.96	0.07	0.14	0.08	486	4.1	99.96
12	Soil Site 32	88-SC-076	Nondunitic Till	52.90	12.84	11.00	8.23	4.87	2.50	1.13	0.94	0.06	0.13	0.16	455	5.1	99.94
13	Soil Site 35	88-SC-088	Nondunitic Till	55.18	14.34	10.00	5.27	5.26	2.76	1.23	0.95	0.13	0.15	0.07	442	4.5	99.92
14	Soil Site 38	88-SC-163	Nondunitic Till	52.76	15.50	10.15	5.40	4.60	2.65	1.40	1.04	0.15	0.16	0.03	492	6.2	100.12
15	Soil Site 39	88-SC-098	Nondunitic Till	55.12	14.53	9.88	5.52	5.28	2.51	1.34	0.98	0.16	0.15	0.05	456	4.4	100.00
16	Soil Site 40	88-SC-102	Nondunitic Till	55.03	15.28	9.78	3.97	5.01	3.20	1.64	1.04	0.11	0.14	0.04	461	4.6	99.92
17	Soil Site 41	88-SC-108	Nondunitic Till	52.89	15.83	10.24	4.74	4.76	2.75	1.44	1.04	0.21	0.22	0.03	483	5.8	100.03
18	Soil Site 44	88-SC-117	Nondunitic Till	56.95	15.65	8.47	4.68	3.13	2.66	1.58	0.91	0.11	0.12	0.07	539	5.6	100.02
19	Soil Site 45	88-SC-120	Nondunitic Till	54.29	15.22	9.14	5.19	4.15	2.84	1.43	0.95	0.13	0.14	0.05	508	6.4	100.02
20	Soil Site 1	88-SC-003	Clay	54.41	16.58	9.11	4.22	3.75	2.52	1.33	1.02	0.16	0.12	0.04	619	6.5	99.87
21	Soil Site 46	88-SC-124	Clay	51.87	15.41	9.89	5.80	4.29	2.56	1.45	0.98	0.24	0.26	0.04	555	7.3	100.18

Appendix 5.1
Overview Analytical Results: Till
Dunitic Till (Page 1)

	Site	Sample	Parent Material	Pt (ppb)	Pd (ppb)	Rh (ppb)	Au (ppb)	As (ppm)	Sb (ppm)	Bi (ppm)	Ge (ppm)	Se (ppm)	Te (ppm)
22	Soil Site 33	88-SC-079	Dunitic Till	28	2	2	6	19.2	0.5	0.3	0.2	0.2	0.5
23	Soil Site 34	88-SC-082	Dunitic Till	36	6	2	11	11.2	0.4	0.2	0.2	0.2	0.3
24	Soil Site 43	88-SC-112	Dunitic Till	16	2	2	4	5.3	0.2	0.4	0.2	0.2	0.3
25	Soil Site 63	89-SC-178	Dunitic Till	44	7	2	10	19.3	0.6	0.5	0.1	0.1	0.1
26	Soil Site 64	89-SC-182	Dunitic Till	18	5	2	2	14.8	0.6	0.2	0.3	0.1	0.4
27	Soil Site 65	89-SC-184	Dunitic Till	44	5	2	4	10.1	0.1	0.2	0.1	0.1	0.1
28	Soil Site 66	89-SC-189	Dunitic Till	34	11	2	9	13.2	0.2	0.2	0.1	0.1	0.1
29	Soil Site 67	89-SC-193	Dunitic Till	32	10	2	12	20.8	0.6	0.2	0.3	0.4	0.5
30	Soil Site 68	89-SC-197	Dunitic Till	45	11	2	8	12.4	0.2	0.4	0.2	0.1	0.4
31	Soil Site 69	89-SC-200	Dunitic Till	49	8	2	9	15.4	0.3	0.6	0.1	0.1	0.2
32	Soil Site 70	89-SC-203	Dunitic Till	34	2	2	7	52.5	0.2	0.1	0.1	0.2	0.4
33	Soil Site 71	89-SC-209	Dunitic Till	36	11	2	8	11.1	0.7	0.2	0.2	0.2	0.4
34	Soil Site 72	89-SC-213	Dunitic Till	28	7	2	14	12.1	0.1	0.2	0.1	0.1	0.1
35	Soil Site 73	89-SC-216	Dunitic Till	311	7	3	21	13.0	0.1	0.3	0.1	0.1	0.2
36	Soil Site 74	89-SC-219	Dunitic Till	50	4	2	7	16.0	0.8	0.1	0.2	0.3	0.3
37	Soil Site 75	89-SC-223	Dunitic Till	38	48	2	8	16.3	0.1	0.1	0.1	0.1	0.3
38	Soil Site 76	89-SC-226	Dunitic Till	55	5	2	3	6.5	0.1	0.1	0.3	0.1	0.4
39	Soil Site 47	88-SC-127	Dunitic Till (A-Zone)	85	2	2	8	7.6	0.5	0.2	0.2	0.2	0.3
40	Soil Site 51	88-SC-135	Dunitic Till (A-Zone)	205	36	2	10	14.4	0.2	0.1	0.2	0.2	0.3
41	Soil Site 53	88-SC-142	Dunitic Till (A-Zone)	42	4	2	4	15.0	0.5	0.2	0.2	0.2	0.3
42	Soil Site 54	88-SC-145	Dunitic Till (A-Zone)	42	2	2	1	30.3	0.1	0.4	0.4	0.2	0.3
43	Soil Site 55	88-SC-148	Dunitic Till (A-Zone)	93	2	2	4	16.1	0.1	0.3	0.2	0.2	0.3
44	Soil Site 56	88-SC-153	Dunitic Rubble(A-Zone)	455	2	2	1	7.4	0.5	0.2	0.2	0.2	0.3
45	Soil Site 57	88-SC-156	Dunitic Till (A-Zone)	266	3	2	3	30.5	0.2	0.1	0.2	0.2	0.3
46	Soil Site 59	88-SC-161	Dunitic Till (A-Zone)	77	5	6	10	26.4	0.8	0.1	0.2	0.2	0.3

Appendix 5.1
Overview Analytical Results: Till
Dunitic Till (Page 2)

	Site	Sample	Parent Material	SiO2 (%)	Al2O3 (%)	Fe2O3 (%)	MgO (%)	CaO (%)	Na2O (%)	K2O (%)	TiO2 (%)	P2O5 (%)	MnO (%)	Cr2O3 (%)	Ba (ppm)	LOI (%)	Total (%)
22	Soil Site 33	88-SC-079	Dunitic Till	47.62	7.20	12.68	17.81	3.36	0.85	0.57	0.60	0.08	0.13	0.26	198	8.8	99.99
23	Soil Site 34	88-SC-082	Dunitic Till	50.64	10.62	13.12	10.45	5.24	2.08	0.78	0.83	0.08	0.13	0.22	320	5.7	99.94
24	Soil Site 43	88-SC-112	Dunitic Till	46.27	6.90	9.95	28.73	2.10	1.12	0.68	0.41	0.10	0.17	0.25	242	3.3	100.02
25	Soil Site 63	89-SC-178	Dunitic Till	44.42	7.66	11.20	19.65	1.88	1.11	0.76	0.49	0.11	0.22	0.18	204	12.2	99.93
26	Soil Site 64	89-SC-182	Dunitic Till	48.23	9.29	9.94	15.52	3.60	1.39	0.94	0.63	0.10	0.14	0.25	278	9.9	100.00
27	Soil Site 65	89-SC-184	Dunitic Till	46.52	10.03	10.22	16.25	2.63	1.46	0.95	0.64	0.14	0.22	0.22	280	10.7	100.05
28	Soil Site 66	89-SC-189	Dunitic Till	47.28	8.25	10.82	17.03	3.95	1.02	0.79	0.60	0.15	0.16	0.16	200	9.7	99.96
29	Soil Site 67	89-SC-193	Dunitic Till	44.95	8.18	10.49	18.86	4.20	0.96	0.78	0.59	0.19	0.22	0.19	211	10.3	99.96
30	Soil Site 68	89-SC-197	Dunitic Till	45.25	9.92	11.00	16.35	2.80	1.14	1.07	0.59	0.10	0.19	0.19	282	11.2	99.87
31	Soil Site 69	89-SC-200	Dunitic Till	48.37	8.89	9.48	15.47	5.05	1.28	0.90	0.59	0.09	0.18	0.13	215	9.6	100.08
32	Soil Site 70	89-SC-203	Dunitic Till	44.23	8.71	11.27	15.99	3.17	1.10	0.69	0.56	0.11	0.18	0.24	228	13.7	100.01
33	Soil Site 71	89-SC-209	Dunitic Till	45.71	7.64	10.70	18.44	4.33	1.00	0.86	0.63	0.16	0.21	0.22	202	10.0	99.95
34	Soil Site 72	89-SC-213	Dunitic Till	47.34	9.95	9.67	15.22	3.68	1.24	1.04	0.63	0.14	0.18	0.12	252	10.7	99.97
35	Soil Site 73	89-SC-216	Dunitic Till	45.81	7.19	11.43	20.29	3.62	0.94	0.58	0.53	0.11	0.19	0.29	195	9.0	100.03
36	Soil Site 74	89-SC-219	Dunitic Till	44.95	12.44	8.82	10.73	2.89	1.65	0.96	0.62	0.15	0.15	0.18	352	16.4	100.02
37	Soil Site 75	89-SC-223	Dunitic Till	47.81	10.86	11.78	11.41	4.96	1.64	0.91	0.80	0.12	0.19	0.18	286	9.3	100.03
38	Soil Site 76	89-SC-226	Dunitic Till	48.05	10.38	12.27	12.51	5.58	1.63	0.87	0.90	0.09	0.18	0.17	272	7.5	100.19
39	Soil Site 47	88-SC-127	Dunitic Till (A-Zone)	49.81	11.26	11.96	11.66	3.65	2.09	0.79	0.74	0.09	0.15	0.23	332	7.6	100.09
40	Soil Site 51	88-SC-135	Dunitic Till (A-Zone)	46.12	9.57	14.96	14.17	3.27	1.50	0.72	0.68	0.06	0.22	0.29	263	8.6	100.20
41	Soil Site 53	88-SC-142	Dunitic Till (A-Zone)	50.27	11.68	10.86	10.64	4.48	1.88	0.73	0.79	0.08	0.15	0.12	273	8.4	100.13
42	Soil Site 54	88-SC-145	Dunitic Till (A-Zone)	51.01	12.08	9.53	11.50	2.75	2.29	0.73	0.61	0.08	0.13	0.23	334	9.1	100.10
43	Soil Site 55	88-SC-148	Dunitic Till (A-Zone)	50.19	10.23	11.20	12.72	4.01	1.77	0.65	0.70	0.06	0.12	0.31	253	8.1	100.10
44	Soil Site 56	88-SC-153	Dunitic Rubble(A-Zone)	42.96	8.20	10.97	19.06	1.24	1.26	0.56	0.37	0.15	0.29	0.51	260	14.4	100.01
45	Soil Site 57	88-SC-156	Dunitic Till (A-Zone)	44.63	7.86	14.05	17.25	2.80	1.06	0.35	0.53	0.07	0.23	0.36	182	10.8	100.02
46	Soil Site 59	88-SC-161	Dunitic Till (A-Zone)	50.21	10.30	10.69	13.69	4.07	1.92	0.73	0.71	0.07	0.15	0.16	266	7.2	99.95

Appendix 5.2
Overview Analytical Results: Colluvium (Page 1)

	Site	Sample	Parent Material	Pt (ppb)	Pd (ppb)	Rh (ppb)	Au (ppb)	As (ppm)	Sb (ppm)	Bi (ppm)	Ge (ppm)	Se (ppm)	Te (ppm)
1	Soil Site 7	88-SC-021	Colluvium	88	3	2	8	14.2	0.4	0.2	0.2	0.2	0.3
2	Soil Site 8	88-SC-022	Colluvium	108	3	2	17	28.5	0.6	0.3	0.2	0.2	0.3
3	Soil Site 9	88-SC-023	Colluvium	67	3	2	6	14.5	0.4	0.3	0.2	0.2	0.3
4	Soil Site 10	88-SC-025	Colluvium	66	2	2	12	22.2	0.2	0.2	0.2	0.2	0.3
5	Soil Site 11	88-SC-026	Colluvium	110	2	2	34	43.5	0.8	0.5	0.2	0.2	0.3
6	Soil Site 12	88-SC-027	Colluvium	88	2	2	25	28.1	0.9	0.4	0.2	0.2	0.3
7	Soil Site 13	88-SC-028	Colluvium	73	5	2	7	14.1	0.7	0.5	0.2	0.2	0.3
8	Soil Site 14	88-SC-029	Colluvium	68	5	2	20	24.1	0.8	0.4	0.2	0.2	0.3
9	Soil Site 15	88-SC-030	Colluvium	47	2	2	8	15.5	0.7	0.3	0.2	0.2	0.3
10	Soil Site 16	88-SC-031	Colluvium	885	2	3	2	38.1	0.5	0.3	0.2	0.2	0.3
11	Soil Site 17	88-SC-032	Colluvium	118	3	2	56	38.0	1.2	0.4	0.2	0.2	0.3
12	Soil Site 18	88-SC-033	Colluvium	32	2	2	9	10.9	0.5	0.3	0.2	0.2	0.3
13	Soil Site 24	88-SC-054	Colluvium	185	3	2	49	17.2	0.4	0.5	0.2	0.2	0.5
14	Soil Site 25	88-SC-056	Colluvium	56	2	2	33	22.6	1.0	0.3	0.2	0.2	0.3
15	Soil Site 26	88-SC-058	Colluvium	92	2	2	21	56.3	0.7	0.3	0.2	0.2	0.3
16	Soil Site 27	88-SC-061	Colluvium	173	2	2	39	17.9	0.5	0.3	0.3	0.2	0.3
17	Soil Site 28	88-SC-063	Colluvium	24	2	2	21	12.5	0.2	0.1	0.2	0.2	0.3
18	Soil Site 29	88-SC-066	Colluvium	47	3	2	54	21.5	0.7	0.1	0.2	0.2	0.3
19	Soil Site 30	88-SC-069	Colluvium	45	3	2	2	7.5	0.4	0.3	0.4	0.2	0.3
20	Soil Site 36	88-SC-090	Colluvium	97	3	2	27	15.0	0.5	0.3	0.3	0.2	0.3
21	Soil Site 37	88-SC-091	Colluvium	138	2	2	31	16.0	0.6	0.1	0.2	0.2	0.3
22	Soil Site 42	88-SC-105	Colluvium	112	2	2	28	14.2	0.3	0.2	0.2	0.2	0.3
23	Soil Site 60	88-SC-171	Colluvium	104	2	2	6	12.9	0.5	0.1	0.2	0.2	0.3
24	Soil Site 61	88-SC-173	Colluvium	99	2	2	8	13.9	0.2	0.2	0.2	0.2	0.3
25	Soil Site 62	88-SC-174	Colluvium	78	3	2	3	14.0	0.6	0.2	0.3	0.2	0.3
26	Soil Site 50	88-SC-132	Colluvium (A-Zone)	70	2	2	1	23.3	0.8	0.2	0.2	0.2	0.3
27	Soil Site 52	88-SC-139	Colluvium (A-Zone)	308	4	2	1	11.3	0.6	0.1	0.2	0.2	0.3

Appendix 5.2
Overview Analytical Results: Colluvium (Page 2)

	Site	Sample	Parent Material	SiO2 (%)	Al2O3 (%)	Fe2O3 (%)	MgO (%)	CaO (%)	Na2O (%)	K2O (%)	TiO2 (%)	P2O5 (%)	MnO (%)	Cr2O3 (%)	Ba (ppm)	LOI (%)	Total (%)
1	Soil Site 7	88-SC-021	Colluvium	39.50	5.23	12.57	22.91	1.87	0.95	0.51	0.34	0.10	0.26	0.37	143	15.6	100.23
2	Soil Site 8	88-SC-022	Colluvium	37.38	3.54	12.21	28.22	1.15	0.58	0.35	0.21	0.11	0.31	0.42	94	15.7	100.20
3	Soil Site 9	88-SC-023	Colluvium	42.17	6.34	12.10	22.67	2.02	1.03	0.57	0.38	0.08	0.22	0.32	186	11.9	99.83
4	Soil Site 10	88-SC-025	Colluvium	39.18	5.91	12.31	21.82	1.93	0.84	0.80	0.37	0.17	0.43	0.29	159	15.9	99.98
5	Soil Site 11	88-SC-026	Colluvium	34.60	4.09	11.13	23.38	1.49	0.57	0.46	0.26	0.22	0.57	0.39	141	22.8	99.98
6	Soil Site 12	88-SC-027	Colluvium	42.97	8.24	12.74	17.46	2.73	1.24	0.58	0.52	0.13	0.32	0.23	216	12.5	99.70
7	Soil Site 13	88-SC-028	Colluvium	43.56	9.73	13.72	14.29	3.29	1.30	0.65	0.62	0.12	0.27	0.26	206	12.0	99.85
8	Soil Site 14	88-SC-029	Colluvium	41.70	7.68	11.66	20.62	2.42	1.07	0.22	0.43	0.16	0.30	0.31	101	13.3	99.89
9	Soil Site 15	88-SC-030	Colluvium	44.15	8.27	11.64	19.95	2.24	1.30	0.29	0.46	0.11	0.23	0.25	136	11.1	100.01
10	Soil Site 16	88-SC-031	Colluvium	38.24	3.86	12.50	28.20	1.16	0.60	0.06	0.24	0.12	0.30	0.44	97	14.3	100.04
11	Soil Site 17	88-SC-032	Colluvium	35.25	2.14	11.97	30.83	0.76	0.22	0.06	0.14	0.15	0.42	0.35	96	17.8	100.11
12	Soil Site 18	88-SC-033	Colluvium	44.41	9.51	10.57	18.22	0.59	1.44	0.48	0.50	0.10	0.23	0.22	211	11.8	100.10
13	Soil Site 24	88-SC-054	Colluvium	36.93	5.57	12.43	20.94	2.51	0.75	0.13	0.40	0.17	0.29	0.32	112	19.7	100.16
14	Soil Site 25	88-SC-056	Colluvium	41.24	6.74	13.58	23.42	2.46	1.09	0.17	0.51	0.10	0.21	0.27	95	10.3	100.11
15	Soil Site 26	88-SC-058	Colluvium	40.64	1.21	11.51	32.78	0.35	0.08	0.06	0.08	0.08	0.25	0.32	39	12.7	100.07
16	Soil Site 27	88-SC-061	Colluvium	41.59	3.93	11.36	29.78	1.16	0.59	0.10	0.23	0.08	0.20	0.32	38	10.8	100.15
17	Soil Site 28	88-SC-063	Colluvium	43.31	8.44	10.20	21.68	2.27	1.41	0.19	0.47	0.08	0.15	0.24	133	11.6	100.06
18	Soil Site 29	88-SC-066	Colluvium	46.38	7.13	9.37	22.28	2.33	1.20	0.82	0.45	0.09	0.15	0.20	226	9.4	99.84
19	Soil Site 30	88-SC-069	Colluvium	35.26	1.87	9.65	30.49	0.65	0.26	0.05	0.12	0.13	0.23	0.46	78	20.8	99.98
20	Soil Site 36	88-SC-090	Colluvium	42.61	5.42	11.55	26.25	1.63	0.85	0.20	0.33	0.07	0.18	0.34	100	10.5	99.95
21	Soil Site 37	88-SC-091	Colluvium	40.65	3.48	12.29	28.61	1.27	0.53	0.21	0.25	0.09	0.24	0.38	95	12.1	100.12
22	Soil Site 42	88-SC-105	Colluvium	45.63	2.71	10.99	28.52	0.81	0.37	0.05	0.19	0.09	0.19	0.46	38	10.1	100.12
23	Soil Site 60	88-SC-171	Colluvium	40.05	5.69	13.58	23.75	2.07	0.87	0.09	0.38	0.10	0.32	0.50	95	12.7	100.12
24	Soil Site 61	88-SC-173	Colluvium	40.19	5.72	12.91	23.20	2.13	0.87	0.22	0.39	0.12	0.32	0.32	154	13.7	100.12
25	Soil Site 62	88-SC-174	Colluvium	39.25	5.33	12.74	23.84	2.06	0.81	0.26	0.36	0.14	0.24	0.34	132	14.8	100.19
26	Soil Site 50	88-SC-132	Colluvium (A-Zone)	45.04	9.51	13.28	14.29	2.79	1.52	0.82	0.60	0.10	0.27	0.17	312	11.8	100.24
27	Soil Site 52	88-SC-139	Colluvium (A-Zone)	43.67	8.45	11.84	16.33	1.99	1.55	0.68	0.45	0.09	0.21	0.54	270	14.3	100.15

Appendix 5.3
Overview Till Sites:
Sample Weight Data

Soil Site	Sample	Field Weight (g)	Weight Sieved (g)	+10 mesh (g)	-10+70 mesh (g)	-70 mesh (g)	Total Weight (g)	Total -10 mesh Weight (g)
Soil Site 1	88-SC-003	15009	2149	650.17	207.31	1082.13	1939.61	1289.44
Soil Site 2	88-SC-006	16530	2971	854.47	562.55	1104.09	2521.11	1666.64
Soil Site 3	88-SC-009	16242	1964	1077.57	381.68	396.59	1855.84	778.27
Soil Site 4	88-SC-012	12873	1817	786.07	323.37	568.78	1678.22	892.15
Soil Site 5	88-SC-016	17561	2489	1530.37	339.50	433.57	2303.44	773.07
Soil Site 6	88-SC-019	17065	2684	638.47	413.69	944.74	1996.90	1358.43
Soil Site 19	88-SC-036	13233	1966	1037.47	367.69	446.68	1851.84	814.37
Soil Site 20	88-SC-040	12897	1570	428.43	287.24	703.24	1418.91	990.48
Soil Site 21	88-SC-044	15383	2042	668.07	441.40	821.35	1930.82	1262.75
Soil Site 22	88-SC-048	9573	1826	611.30	393.42	668.45	1673.17	1061.87
Soil Site 23	88-SC-051	14626	2171	1030.47	537.08	442.96	2010.51	980.04
Soil Site 31	88-SC-072	14871	2217	846.17	529.86	715.72	2091.75	1245.58
Soil Site 32	88-SC-076	13833	1706	644.17	373.45	592.09	1609.71	965.54
Soil Site 33	88-SC-079	14514	1819	921.47	301.84	399.29	1622.60	701.13
Soil Site 34	88-SC-082	17839	1806	746.77	472.50	486.33	1705.60	958.83
Soil Site 35	88-SC-088	16991	1498	699.67	382.20	344.72	1426.59	726.92
Soil Site 38	88-SC-163	16350	2857	905.07	479.14	1211.58	2595.79	1690.72
Soil Site 39	88-SC-098	18542	1851	677.07	390.01	647.40	1714.48	1037.41
Soil Site 40	88-SC-102	18234	1803	701.97	464.76	578.16	1744.89	1042.92
Soil Site 41	88-SC-108	9935	1024	286.24	188.17	452.98	927.39	641.15
Soil Site 43	88-SC-112	14498	2128	512.11	641.66	888.78	2042.55	1530.44
Soil Site 44	88-SC-117	13889	2318	921.77	522.80	771.94	2216.51	1294.74
Soil Site 45	88-SC-120	12831	2081	703.67	483.35	783.07	1970.09	1266.42
Soil Site 46	88-SC-124	10134	1465	20.16	196.17	901.59	1117.92	1097.76
Soil Site 47	88-SC-127	11401	1669	664.77	294.49	440.02	1399.28	734.51
Soil Site 51	88-SC-135	14671	1652	528.50	296.85	632.37	1457.72	929.22
Soil Site 53	88-SC-142	13031	1781	735.47	305.09	548.10	1588.66	853.19
Soil Site 54	88-SC-145	16117	1965	1131.17	215.71	392.21	1739.09	607.92
Soil Site 55	88-SC-148	14778	1802	830.87	272.96	515.67	1619.50	788.63
Soil Site 56	88-SC-153	10695	1210	764.77	141.74	175.45	1081.96	317.19
Soil Site 57	88-SC-156	13462	1465	630.07	189.20	425.60	1244.87	614.80
Soil Site 59	88-SC-161	14970	1985	1020.47	334.05	510.80	1865.32	844.85
Soil Site 63	89-SC-178	14473	2471	939.86	363.00	737.03	2039.89	1100.03
Soil Site 64	89-SC-182	14741	2333	1219.91	364.58	490.80	2075.29	855.38
Soil Site 65	89-SC-184	14637	1830	568.82	282.30	685.96	1537.08	968.26
Soil Site 66	89-SC-189	17784	2371	783.26	406.51	865.25	2055.02	1271.76
Soil Site 67	89-SC-193	15915	2395	1161.96	528.98	448.90	2139.84	977.88
Soil Site 68	89-SC-197	15460	2382	755.76	288.18	919.12	1963.06	1207.30
Soil Site 69	89-SC-200	15572	2554	880.57	367.49	952.91	2200.97	1320.40
Soil Site 70	89-SC-203	18604	3248	1917.28	323.89	600.30	2841.47	924.19
Soil Site 71	89-SC-209	15466	2460	745.99	708.33	690.09	2144.41	1398.42
Soil Site 72	89-SC-213	19508	3057	1353.57	710.91	633.55	2698.03	1344.46
Soil Site 73	89-SC-216	14829	2315	1000.60	298.09	716.30	2014.99	1014.39
Soil Site 74	89-SC-219	14886	2046	976.36	155.49	528.12	1659.97	683.61
Soil Site 75	89-SC-223	15988	2084	760.70	311.28	701.18	1773.16	1012.46
Soil Site 76	89-SC-226	19412	2923	968.04	433.25	1162.29	2563.58	1595.54

Appendix 5.4
Overview Colluvium Sites:
Sample Weight Data

Soil Site	Sample	Field Weight (g)	Weight Sieved (g)	+10 mesh (g)	-10+70 mesh (g)	-70 mesh (g)	Total Weight (g)	Total -10 mesh Weight (g)
Soil Site 7	88-SC-021	11622	1979	1397.87	195.27	232.57	1825.71	427.84
Soil Site 8	88-SC-022	11399	1846	1455.97	138.96	164.49	1759.42	303.45
Soil Site 9	88-SC-023	12864	1960	1402.27	165.98	257.88	1826.13	423.86
Soil Site 10	88-SC-025	11175	1450	876.07	204.89	261.15	1342.11	466.04
Soil Site 11	88-SC-026	8164	949	555.31	137.51	165.97	858.79	303.48
Soil Site 12	88-SC-027	9267	1441	711.87	191.25	406.67	1309.79	597.92
Soil Site 13	88-SC-028	9123	1187	641.37	193.67	287.47	1122.51	481.14
Soil Site 14	88-SC-029	12590	1338	953.87	152.27	163.77	1269.91	316.04
Soil Site 15	88-SC-030	12684	1683	906.37	276.18	377.44	1559.99	653.62
Soil Site 16	88-SC-031	13885	2019	1506.27	242.76	166.18	1915.21	408.94
Soil Site 17	88-SC-032	10622	1498	944.87	302.29	194.85	1442.01	497.14
Soil Site 18	88-SC-033	11348	1348	851.27	168.39	250.12	1269.78	418.51
Soil Site 24	88-SC-054	9056	1267	626.77	371.71	175.51	1173.99	547.22
Soil Site 25	88-SC-056	14420	2103	1428.27	312.32	202.32	1942.91	514.64
Soil Site 26	88-SC-058	15623	2860	1827.37	399.80	308.63	2535.80	708.43
Soil Site 27	88-SC-061	13959	1946	1121.77	296.33	340.47	1758.57	636.80
Soil Site 28	88-SC-063	16119	2371	1734.17	265.84	180.85	2180.86	446.69
Soil Site 29	88-SC-066	13369	1885	1366.67	159.47	215.81	1741.95	375.28
Soil Site 30	88-SC-069	8894	1468	1299.27	53.12	30.75	1383.14	83.87
Soil Site 36	88-SC-090	17353	2018	1452.87	167.85	225.18	1845.90	393.03
Soil Site 37	88-SC-091	14894	2024	1405.57	230.34	291.40	1927.31	521.74
Soil Site 42	88-SC-105	13698	1923	1144.17	290.76	298.19	1733.12	588.95
Soil Site 50	88-SC-132	14522	1943	1308.07	224.09	219.22	1751.38	443.31
Soil Site 52	88-SC-139	14708	1684	1214.87	115.79	122.26	1452.92	238.05
Soil Site 60	88-SC-171	13740	1883	1132.27	333.73	318.40	1784.40	652.13
Soil Site 61	88-SC-173	16609	2105	1554.47	195.69	255.03	2005.19	450.72
Soil Site 62	88-SC-174	19926	2688	2073.47	263.05	221.73	2558.25	484.78

Appendix 5.5
Background Till Samples: Analytical Results

Site	Sample	Pt (ppb)	Pd (ppb)	Rh (ppb)	Au (ppb)	As (ppm)	Sb (ppm)	Bi (ppm)	Ge (ppm)	Se (ppm)	Te (ppm)
Background 1	89-SC-402	20	12	2	9	7.5	0.1	0.3	0.1	0.1	0.3
Background 2	89-SC-403	6	14	2	6	31.5	0.1	0.1	0.1	0.4	0.2
Background 3	89-SC-404	16	14	2	9	15.3	0.1	0.2	0.2	0.2	0.3
Background 4	89-SC-405	43	8	2	7	10.9	0.1	0.4	0.1	0.1	0.3
Background 5	89-SC-406	48	9	7	17	10.0	0.1	0.1	0.1	0.1	0.1

Site	Sample	SiO2 (%)	Al2O3 (%)	Fe2O3 (%)	MgO (%)	CaO (%)	Na2O (%)	K2O (%)	TiO2 (%)	P2O5 (%)	MnO (%)	Cr2O3 (%)	Ba (ppm)	LOI (%)	Total (%)
Background 1	89-SC-402	51.56	11.41	8.86	10.19	5.46	2.00	1.06	0.73	0.09	0.13	0.15	384	8.3	100.02
Background 2	89-SC-403	46.58	15.08	9.92	10.38	6.72	1.70	1.43	0.84	0.13	0.15	0.05	395	6.9	99.96
Background 3	89-SC-404	50.78	12.52	10.61	8.80	6.86	2.19	1.13	0.96	0.17	0.15	0.08	357	5.7	100.03
Background 4	89-SC-405	48.01	10.23	11.16	13.07	4.97	1.70	1.08	0.70	0.14	0.21	0.26	331	8.4	100.00
Background 5	89-SC-406	50.87	10.79	11.00	12.02	3.61	1.99	1.12	0.70	0.14	0.19	0.30	395	7.3	100.12

Appendix 5.6
Background Till Samples: Weight Data

Site	Sample	Field Weight (g)	Weight Sieved (g)	+10 mesh (g)	-10+70 mesh (g)	-70 mesh (g)	Total Weight (g)	Total -10 mesh Weight (g)
Background 1	89-SC-402	12223	1696	890.26	158.06	352.47	1400.79	510.53
Background 2	89-SC-403	15260	2681	1505.00	373.38	635.76	2514.14	1009.14
Background 3	89-SC-404	18334	3195	1446.00	602.05	901.75	2949.80	1503.80
Background 4	89-SC-405	15822	2246	536.87	343.92	1064.47	1945.26	1408.39
Background 5	89-SC-406	17685	2080	851.06	363.14	634.66	1848.86	997.80

Background Till Samples:
Particle Size Distribution Among Size Fractions
(Expressed as Weight Percent)

Site	Sample	-10+70 mesh as Wt. % of -10 mesh	-70 mesh as Wt. % of -10 mesh	+10 mesh as Wt. % of Total Sample	-10+70 mesh as Wt. % of Total Sample	-70 mesh as Wt. % of Total Sample
Background 1	89-SC-402	30.96	69.04	63.55	11.28	25.16
Background 2	89-SC-403	37.00	63.00	59.86	14.85	25.29
Background 3	89-SC-404	40.03	59.96	49.02	20.41	30.57
Background 4	89-SC-405	24.42	75.58	27.60	17.68	54.72
Background 5	89-SC-406	36.39	63.60	46.03	19.64	34.33

Appendix 5.7
Overview Till Sites:
Particle Size Distribution Among Size Fractions
(Expressed as Weight Percent)

Soil Site	Sample	-10+70 mesh as Wt. % of -10 mesh	-70 mesh as Wt. % of -10 mesh	+10 mesh as Wt. % of Total Sample	-10+70 mesh as Wt. % of Total Sample	-70 mesh as Wt. % of Total Sample
Soil Site 1	88-SC-003	16.08	83.92	33.52	10.69	55.79
Soil Site 2	88-SC-006	33.75	66.25	33.89	22.31	43.79
Soil Site 3	88-SC-009	49.04	50.96	58.06	20.57	21.37
Soil Site 4	88-SC-012	36.25	63.75	46.84	19.27	33.89
Soil Site 5	88-SC-016	43.91	56.08	66.44	14.74	18.82
Soil Site 6	88-SC-019	30.45	69.55	31.97	20.72	47.31
Soil Site 19	88-SC-036	45.15	54.85	56.02	19.86	24.12
Soil Site 20	88-SC-040	29.00	71.00	30.19	20.24	49.56
Soil Site 21	88-SC-044	34.95	65.04	34.60	22.86	42.54
Soil Site 22	88-SC-048	37.05	62.95	36.53	23.51	39.95
Soil Site 23	88-SC-051	54.80	45.20	51.25	26.71	22.03
Soil Site 31	88-SC-072	42.54	57.46	40.45	25.33	34.22
Soil Site 32	88-SC-076	38.68	61.32	40.02	23.20	36.78
Soil Site 33	88-SC-079	43.05	56.95	56.79	18.60	24.61
Soil Site 34	88-SC-082	49.28	50.72	43.78	27.70	28.51
Soil Site 35	88-SC-088	52.58	47.42	49.04	26.79	24.16
Soil Site 38	88-SC-163	28.34	71.66	34.87	18.46	46.67
Soil Site 39	88-SC-098	37.59	62.41	39.49	22.75	37.76
Soil Site 40	88-SC-102	44.56	55.44	40.23	26.64	33.13
Soil Site 41	88-SC-108	29.35	70.65	30.86	20.29	48.84
Soil Site 43	88-SC-112	41.93	58.07	25.07	31.41	43.51
Soil Site 44	88-SC-117	40.38	59.62	41.59	23.59	34.83
Soil Site 45	88-SC-120	38.17	61.83	35.72	24.53	39.75
Soil Site 46	88-SC-124	17.87	82.13	1.80	17.55	80.65
Soil Site 47	88-SC-127	40.09	59.91	47.51	21.05	31.45
Soil Site 51	88-SC-135	31.95	68.05	36.26	20.36	43.38
Soil Site 53	88-SC-142	35.76	64.24	46.29	19.20	34.50
Soil Site 54	88-SC-145	35.48	64.52	65.04	12.40	22.55
Soil Site 55	88-SC-148	34.61	65.39	51.30	16.85	31.84
Soil Site 56	88-SC-153	44.69	55.31	70.68	13.10	16.21
Soil Site 57	88-SC-156	30.77	69.22	50.61	15.20	34.19
Soil Site 59	88-SC-161	39.54	60.46	54.71	17.91	27.38
Soil Site 63	89-SC-178	33.00	67.00	46.07	17.80	36.13
Soil Site 64	89-SC-182	42.62	57.38	58.78	17.57	23.65
Soil Site 65	89-SC-184	29.16	70.84	37.01	18.36	44.63
Soil Site 66	89-SC-189	31.96	68.03	38.11	19.78	42.10
Soil Site 67	89-SC-193	54.09	45.91	54.30	24.72	20.98
Soil Site 68	89-SC-197	23.87	76.13	38.50	14.68	46.82
Soil Site 69	89-SC-200	27.83	72.17	40.01	16.70	43.30
Soil Site 70	89-SC-203	35.05	64.95	67.47	11.40	21.13
Soil Site 71	89-SC-209	50.65	49.35	34.79	33.03	32.18
Soil Site 72	89-SC-213	52.88	47.12	50.17	26.35	23.48
Soil Site 73	89-SC-216	29.39	70.61	49.66	14.79	35.55
Soil Site 74	89-SC-219	22.75	77.25	58.82	9.37	31.82
Soil Site 75	89-SC-223	30.74	69.25	42.90	17.55	39.54
Soil Site 76	89-SC-226	27.15	72.85	37.76	16.90	45.34

Appendix 5.8
Overview Colluvium Sites:
Particle Size Distribution Among Size Fractions
(Expressed as Weight Percent)

Soil Site	Sample	-10+70 mesh as Wt. % of -10 mesh	-70 mesh as Wt. % of -10 mesh	+10 mesh as Wt. % of Total Sample	-10+70 mesh as Wt. % of Total Sample	-70 mesh as Wt. % of Total Sample
Soil Site 7	88-SC-021	45.64	54.36	76.56	10.70	12.74
Soil Site 8	88-SC-022	45.79	54.21	82.75	7.90	9.35
Soil Site 9	88-SC-023	39.16	60.84	76.79	9.09	14.12
Soil Site 10	88-SC-025	43.96	56.03	65.28	15.27	19.46
Soil Site 11	88-SC-026	45.31	54.69	64.66	16.01	19.33
Soil Site 12	88-SC-027	31.98	68.01	54.35	14.60	31.05
Soil Site 13	88-SC-028	40.25	59.75	57.14	17.25	25.61
Soil Site 14	88-SC-029	48.18	51.82	75.11	11.99	12.90
Soil Site 15	88-SC-030	42.25	57.75	58.10	17.70	24.20
Soil Site 16	88-SC-031	59.36	40.64	78.65	12.68	8.68
Soil Site 17	88-SC-032	60.80	39.19	65.52	20.96	13.51
Soil Site 18	88-SC-033	40.23	59.76	67.04	13.26	19.70
Soil Site 24	88-SC-054	67.93	32.07	53.39	31.66	14.95
Soil Site 25	88-SC-056	60.69	39.31	73.51	16.07	10.41
Soil Site 26	88-SC-058	56.43	43.56	72.06	15.77	12.17
Soil Site 27	88-SC-061	46.53	53.47	63.79	16.85	19.36
Soil Site 28	88-SC-063	59.51	40.49	79.52	12.19	8.29
Soil Site 29	88-SC-066	42.49	57.51	78.46	9.15	12.39
Soil Site 30	88-SC-069	63.34	36.66	93.94	3.84	2.22
Soil Site 36	88-SC-090	42.71	57.29	78.71	9.09	12.20
Soil Site 37	88-SC-091	44.15	55.85	72.93	11.95	15.12
Soil Site 42	88-SC-105	49.37	50.63	66.02	16.78	17.20
Soil Site 50	88-SC-132	50.55	49.45	74.69	12.79	12.52
Soil Site 52	88-SC-139	48.64	51.36	83.61	7.97	8.41
Soil Site 60	88-SC-171	51.17	48.82	63.45	18.70	17.84
Soil Site 61	88-SC-173	43.42	56.58	77.52	9.76	12.72
Soil Site 62	88-SC-174	54.26	45.74	81.05	10.28	8.67

A

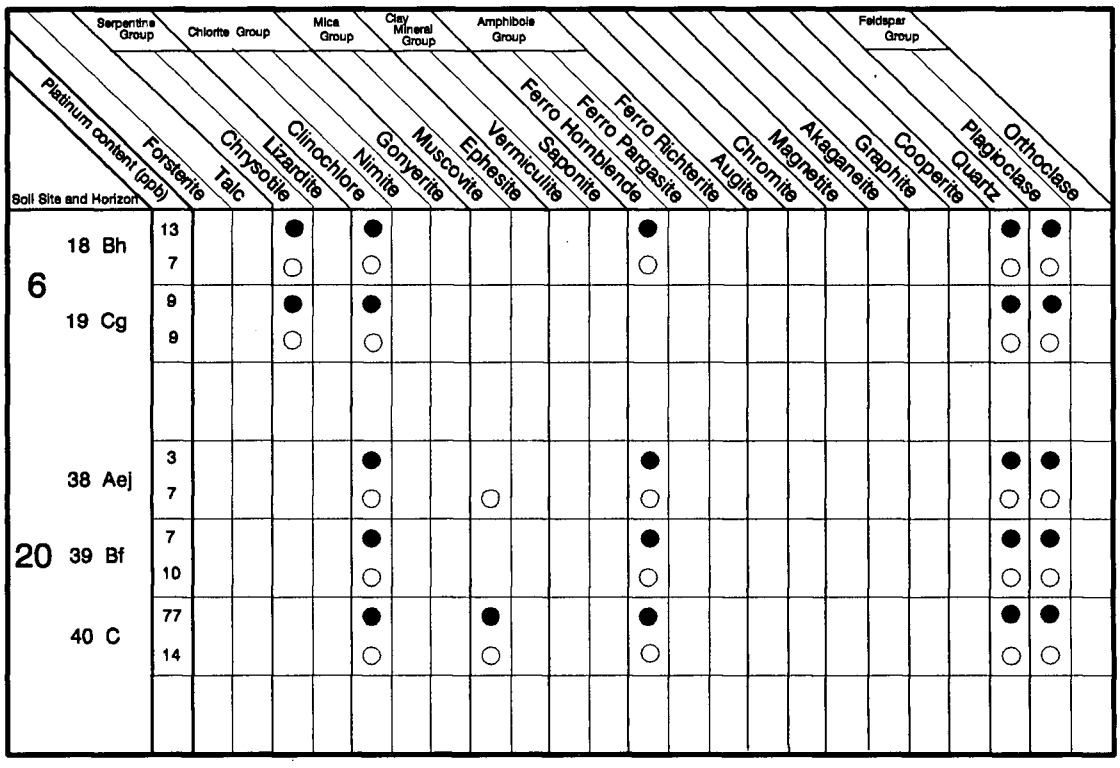

B

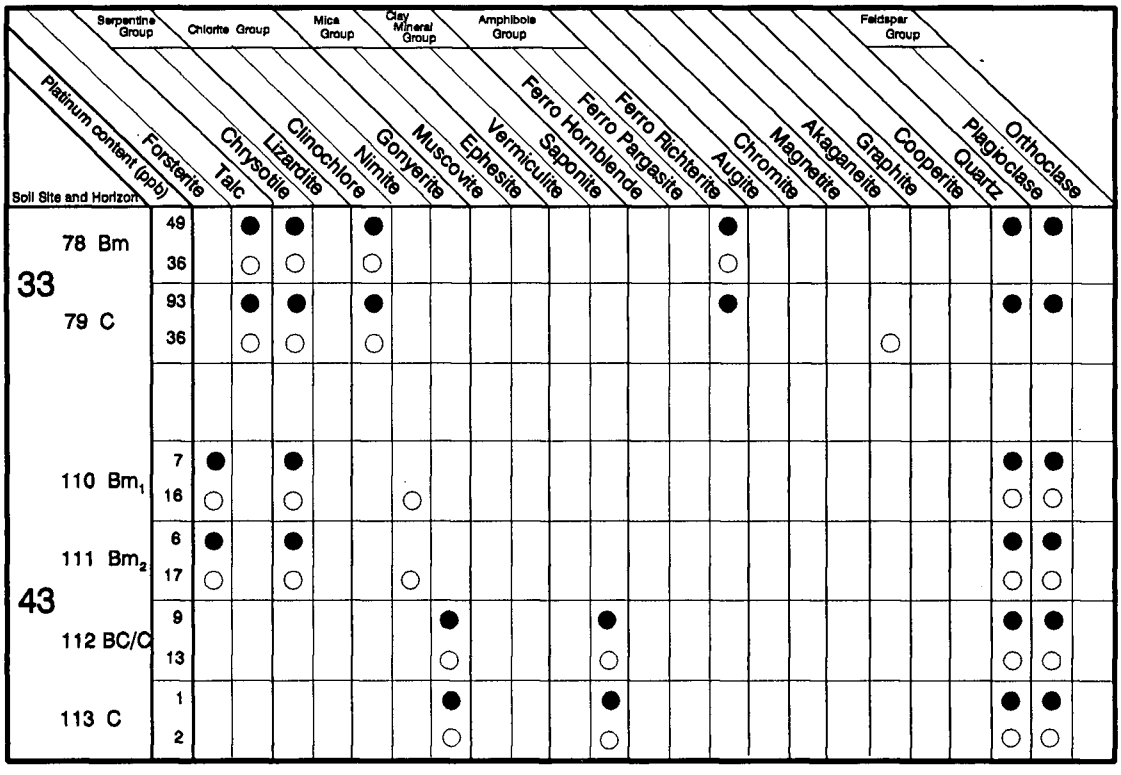

Appendix 6.1. XRD mineralogy of -10+40 mesh (black circles) and -270 mesh (open circles) fractions of soil horizons in A. Non-dunitic till; and B. dunitic till profiles.

A

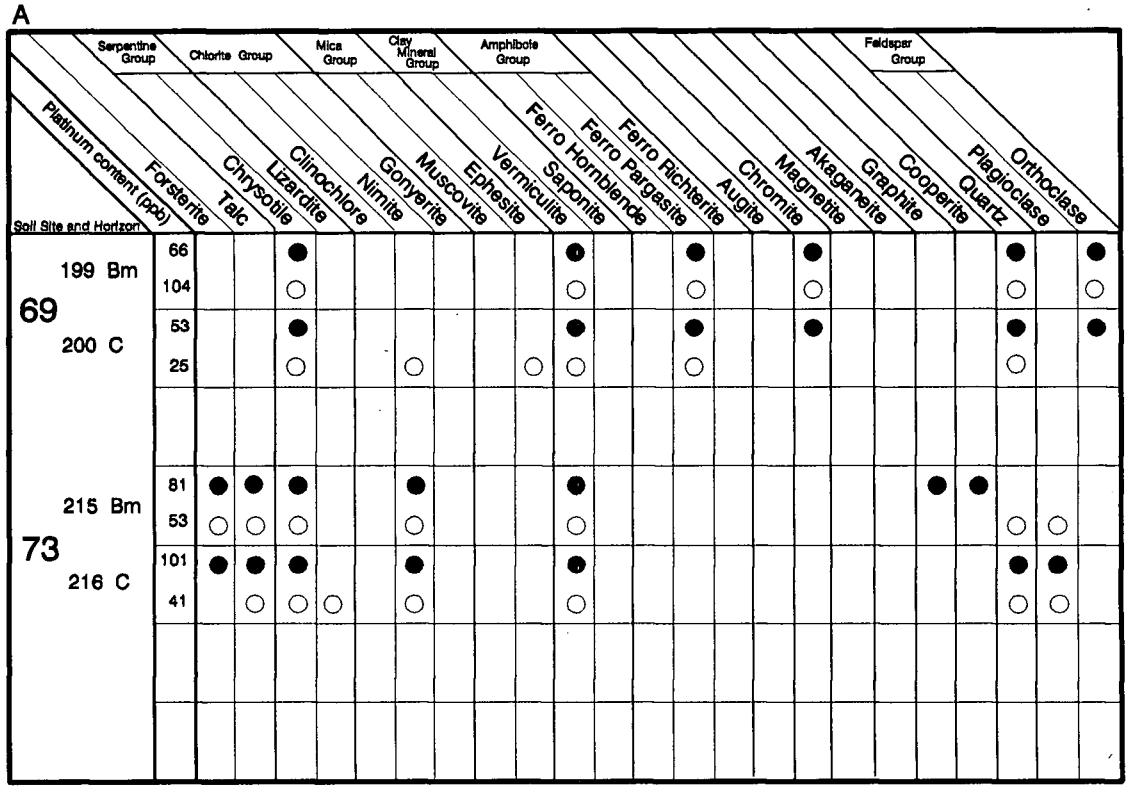

B

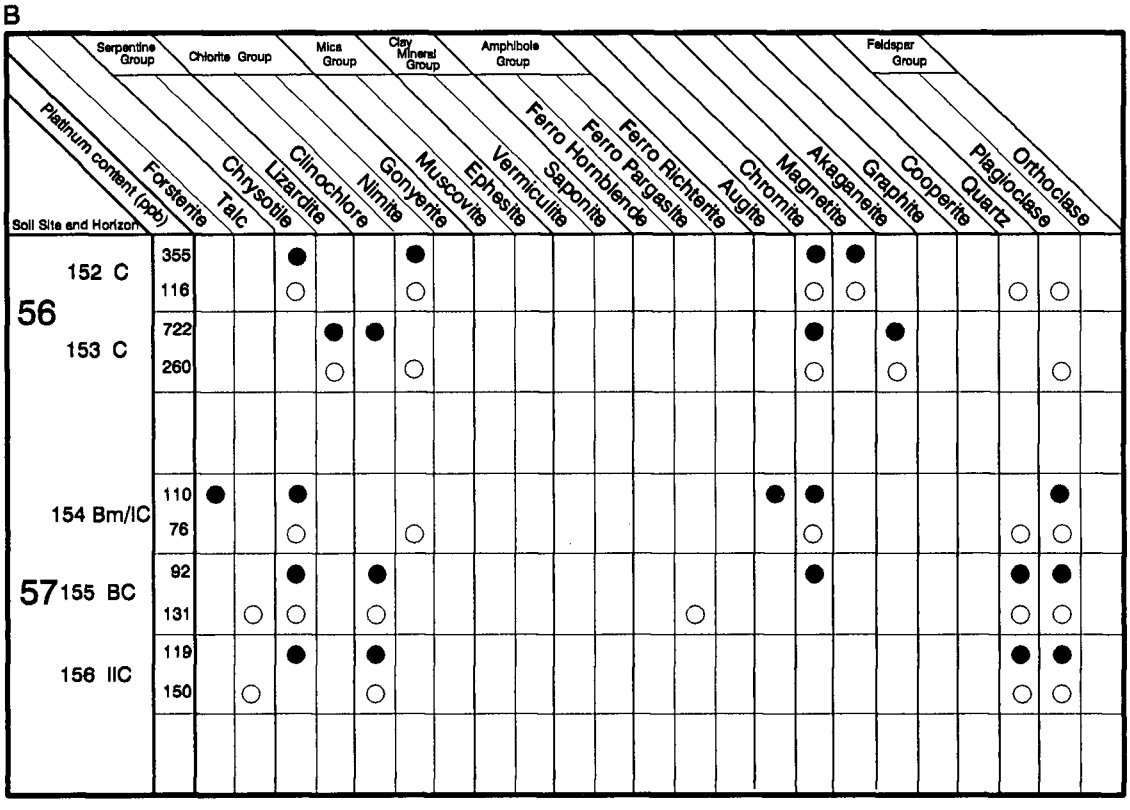

Appendix 6.2. XRD mineralogy of -10+40 mesh (black circles) and -270 mesh (open circles) fractions of soil horizons in dunitic till A. on the plateau of Grasshopper Mountain; and B. adjacent to the A-Zone PGE occurrence in the secondary study area (site 56 is dunitic rubble).

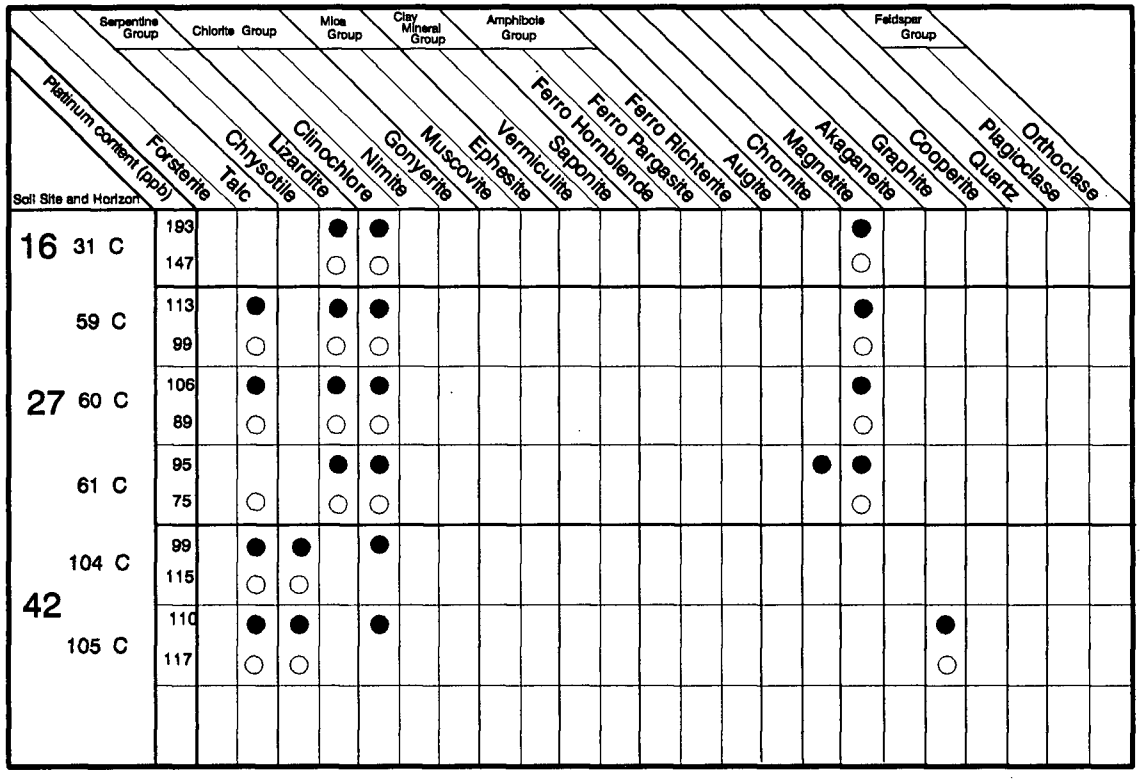

Appendix 6.3. XRD mineralogy of -10+40 mesh (black circles) and -270 mesh (open circles) fractions of soils developed on active colluvium.

Appendix 7.1
LFH Horizon Samples:
Analytical and Weight Data for Entire Suite
(n = 47)

Underlying Surficial Material	Site	Sample	Pt (ppb)	Pd (ppb)	Rh (ppb)	Au (ppb)	LFH/C Horizons Pt Ratio	Pre-ash Split Wt (g)	Ash Weight (g)	Weight Percent Ash (%)
Clay	1	88-SC-01	1	2	2	10	0.25	139.10	10.72	7.71
Clay	46	88-SC-121	7	7	2	10	1.00	144.71	11.81	8.16
Non-dunitic till	2	88-SC-04	16	19	2	46	1.78	123.30	9.88	8.01
Non-dunitic till	3	88-SC-07	8	7	2	4	0.57	101.65	13.03	12.82
Non-dunitic till	4	88-SC-10	7	6	2	4	1.17	99.72	18.95	19.00
Non-dunitic till	5	88-SC-13	2	3	2	12	0.11	205.33	12.00	5.84
Non-dunitic till	6	88-SC-17	6	8	2	5	2.00	138.31	25.21	18.23
Non-dunitic till	19	88-SC-34	18	2	2	8	2.25	92.30	12.92	14.00
Non-dunitic till	20	88-SC-37	4	5	2	5	0.20	103.09	10.16	9.86
Non-dunitic till	21	88-SC-42	5	3	2	8	1.67	99.31	9.06	9.12
Non-dunitic till	22	88-SC-45	4	2	2	6	0.80	116.13	21.86	18.82
Non-dunitic till	23	88-SC-49	3	7	2	13	0.60	56.95	8.03	14.10
Non-dunitic till	31	88-SC-70	10	2	3	7	1.25	97.64	8.34	8.54
Non-dunitic till	32	88-SC-74	6	4	2	4	0.50	130.75	49.25	37.67
Non-dunitic till	35	88-SC-83	9	2	2	8	0.64	98.92	11.58	11.71
Non-dunitic till	38	88-SC-92	12	4	2	7	0.80	88.29	12.27	13.90
Non-dunitic till	39	88-SC-95	4	2	2	7	2.00	107.54	17.36	16.14
Non-dunitic till	40	88-SC-100	7	2	2	9	3.50	112.92	11.15	9.87
Non-dunitic till	41	88-SC-103	6	3	2	6	1.20	97.34	8.50	8.73
Non-dunitic till	44	88-SC-114	10	2	2	3	0.56	108.28	18.41	17.00
Non-dunitic till	45	88-SC-118	8	3	2	5	0.62	100.94	19.90	19.71
Dunitic till	33	88-SC-77	8	2	2	9	0.29	93.76	10.87	11.59
Dunitic till	34	88-SC-80	10	2	2	4	0.28	120.80	26.08	21.59
Dunitic till	43	88-SC-109	6	2	2	4	0.38	75.62	11.45	15.14
Dunitic till	63	89-SC-176	15	2	2	4	0.34	177.26	15.03	8.48
Dunitic till	64	89-SC-179	7	2	2	1	0.39	164.71	33.92	20.59
Dunitic till	66	89-SC-186	16	2	2	1	0.47	179.11	38.51	21.50
Dunitic till	67	89-SC-190	7	2	2	2	0.22	132.16	11.90	9.00
Dunitic till	68	89-SC-194	7	2	2	1	0.16	168.37	19.05	11.31
Dunitic till	69	89-SC-198	20	2	2	4	0.41	193.61	21.72	11.22
Dunitic till	70	89-SC-201	15	2	2	4	0.44	138.28	13.99	10.12
Dunitic till	71	89-SC-204	10	2	2	2	0.28	122.53	12.85	10.49
Dunitic till	72	89-SC-210	20	2	4	1	0.71	99.23	8.56	8.63
Dunitic till	73	89-SC-214	18	2	2	1	0.06	96.99	13.15	13.56
Dunitic till	74	89-SC-217	32	2	2	7	0.64	152.51	10.79	7.07
Dunitic till	75	89-SC-220	23	2	2	1	0.61	135.85	24.49	18.03
Dunitic till	76	89-SC-227	10	2	2	3	0.18	137.53	25.18	18.31
Dunitic till (A-Zone)	47	88-SC-125	143	2	2	3	1.68	224.46	52.41	23.35
Colluvium (A-Zone)	52	88-SC-136	122	2	2	5	0.40	115.57	9.04	7.82
Dunitic till (A-Zone)	53	88-SC-137	96	2	2	6	2.29	277.08	15.34	5.54
Dunitic till (A-Zone)	54	88-SC-143	57	2	3	7	1.36	89.09	11.54	12.95
Dunitic till (A-Zone)	55	88-SC-146	167	4	3	6	1.80	91.88	14.82	16.13
Dunitic rubble (A-Zone)	56	88-SC-151	139	5	3	7	0.31	91.59	10.39	11.34
Dunitic till (A-Zone)	59	88-SC-159	9	2	2	9	0.12	101.67	9.35	9.20
Colluvium	7	88-SC-20	49	3	2	4	0.56	95.40	20.95	21.96
Colluvium	24	88-SC-53	141	2	3	17	0.76	134.87	49.95	37.03
Colluvium	62	88-SC-175	65	2	2	13	0.83	168.82	14.98	8.87

Appendix 7.2
LFH Horizon Samples:
Fe and Insoluble Residue Contents of Selected Samples
(n = 38)

Underlying Surficial Material	Site	Sample	Fe (%)	Ash Subsample Weight (g)	Insoluble Residue Weight (g)	Wt. Percent Insoluble Residue (%)
Clay	1	88-SC-01	1.62	0.50	0.05	10.0
Clay	46	88-SC-121	3.78	0.50	0.03	6.0
Non-dunitic till	2	88-SC-04	1.77	0.37	0.00	0.0
Non-dunitic till	3	88-SC-07	3.11	0.50	0.06	12.0
Non-dunitic till	4	88-SC-10	2.39	0.50	0.04	8.0
Non-dunitic till	5	88-SC-13	1.78	0.50	0.04	8.0
Non-dunitic till	6	88-SC-17	3.44	0.50	0.07	14.0
Non-dunitic till	19	88-SC-34	2.01	0.50	0.04	8.0
Non-dunitic till	22	88-SC-45	3.67	0.50	0.06	12.0
Non-dunitic till	32	88-SC-74	1.56	0.50	0.03	6.0
Non-dunitic till	35	88-SC-83	1.57	0.50	0.08	16.0
Non-dunitic till	38	88-SC-92	1.03	0.50	0.03	6.0
Non-dunitic till	39	88-SC-95	3.28	0.50	0.16	32.0
Non-dunitic till	40	88-SC-100	1.39	0.50	0.04	8.0
Non-dunitic till	44	88-SC-114	1.36	0.50	0.03	6.0
Non-dunitic till	45	88-SC-118	1.53	0.50	0.03	6.0
Dunitic till	33	88-SC-77	2.18	0.50	0.00	0.0
Dunitic till	34	88-SC-80	1.21	0.50	0.02	4.0
Dunitic till	43	88-SC-109	1.20	0.50	0.02	4.0
Dunitic till	63	89-SC-176	1.94	0.50	0.03	6.0
Dunitic till	64	89-SC-179	0.38	0.50	0.01	2.0
Dunitic till	67	89-SC-190	1.23	0.50	0.00	0.0
Dunitic till	68	89-SC-194	1.06	0.50	0.01	2.0
Dunitic till	69	89-SC-198	1.76	0.50	0.02	4.0
Dunitic till	70	89-SC-201	1.46	0.50	0.01	2.0
Dunitic till	71	89-SC-204	1.56	0.50	0.04	8.0
Dunitic till	72	89-SC-210	1.62	0.50	0.03	6.0
Dunitic till	73	89-SC-214	3.00	0.50	0.06	12.0
Dunitic till	74	89-SC-217	1.34	0.50	0.01	2.0
Dunitic till	75	89-SC-220	1.89	0.50	0.06	12.0
Dunitic till	76	89-SC-227	0.97	0.50	0.03	6.0
Dunitic till (A-Zone)	47	88-SC-125	4.06	0.50	0.18	36.0
Dunitic till (A-Zone)	53	88-SC-137	2.83	0.50	0.07	14.0
Dunitic till (A-Zone)	54	88-SC-143	3.56	0.50	0.04	8.0
Dunitic till (A-Zone)	55	88-SC-146	4.11	0.50	0.07	14.0
Dunitic rubble (A-Zone)	56	88-SC-151	3.62	0.43	0.03	7.0
Colluvium	7	88-SC-20	4.33	0.50	0.09	18.0
Colluvium	24	88-SC-53	4.83	0.50	0.09	18.0

Appendix 8.1
Pt, Pd, Rh and Au Analytical Data
for Stream Sediment and Moss Mat Sites,
Grasshopper Creek

Site	Sample	Stream Media	Pt (ppb)	Pd (ppb)	Rh (ppb)	Au (ppb)
1	88-SC-501	Sediment	18	2	4	2
1	88-SC-502	Moss mat	17	3	2	15
2	88-SC-503	Sediment	78	2	2	239
2	88-SC-504	Moss mat	8	2	2	29
3	88-SC-505	Sediment	11	2	2	3
4	88-SC-507A	Sediment	8	3	3	2
4	88-SC-507B	Moss mat	11	4	2	19
5	88-SC-509	Sediment	53	2	2	4
5	88-SC-510	Moss mat	47	41	2	3
6	88-SC-511	Sediment	20	7	4	6
7	88-SC-513	Sediment	91	2	2	5
8	89-SC-515	Sediment	32	5	2	6
8	89-SC-516	Moss mat	23	24	2	1

Appendix 8.2
Stream Sediments:
Sample Weight Data

Stream Site	Sample	Field Weight (g)	Weight Sieved (g)	+10 mesh (g)	-10+70 mesh (g)	-70 mesh (g)	Total Weight (g)	Total -10 mesh Weight (g)	-70 mesh as Wt.% of -10 (%)
1	88-SC-501	9103	1063	7.04	947.93	114.07	1062.00	1062.00	10.74
2	88-SC-503	9907	1071	14.58	950.70	99.54	1050.24	1050.24	9.48
3	88-SC-505	26177	2836	1888.67	694.10	234.15	928.25	928.25	25.22
4	88-SC-507	13970	1866	1560.07	245.56	62.01	307.57	307.57	20.16
5	88-SC-509	6527	750	7.86	603.32	133.62	736.94	736.94	18.13
6	88-SC-511	24357	2267	1608.87	341.83	124.78	466.61	466.61	26.74
7	88-SC-513	21250	2482	1845.87	317.41	160.51	477.92	477.92	33.59
8	89-SC-515	31127	3746	2157.16	474.62	505.36	979.98	979.98	51.57

Moss Mats:
Sample Weight Data

Stream Site	Sample	Original Dry Weight (g)	Weight Sieved (g)	+10 mesh (g)	-10+70 mesh (g)	-70 mesh (g)	Total Weight (g)	Total -10 mesh Weight (g)	-70 mesh as Wt. % of -10 (%)
1	88-SC-502	3547	1936	131.90	1063.34	729.97	1925.21	1793.31	40.70
2	88-SC-504	2699	1360	254.73	682.35	388.62	1325.70	1070.97	36.29
4	88-SC-507	8433	3748	2581.00	810.36	277.68	3669.04	1088.04	25.52
5	88-SC-510	2638	1511	350.17	673.52	483.61	1507.30	1157.13	41.79
8	89-SC-516	2171	1226	345.56	214.09	663.90	1223.55	877.99	75.61

Appendix 8.3
Bank Samples:
Pt, Pd, Rh and Au Analytical Data

Stream Site	Bank Location	Sample	Parent Material	Pt (ppb)	Pd (ppb)	Rh (ppb)	Au (ppb)
1	North	88-SC-601	Alluvium	9	2	2	3
1	South	88-SC-602	Alluvium	12	3	2	2
2	North	88-SC-603	Till	8	2	2	2
2	South	88-SC-604	Till	18	14	4	4
3	North	88-SC-605	Till	15	2	2	1
3	South	88-SC-606	Till	10	2	2	2
4	North	88-SC-607	Till	7	2	2	2
4	South	88-SC-608	Till	33	65	3	24
5	North	88-SC-609	Till	15	2	2	4
5	South	88-SC-610	Till	15	3	2	3

Bank Samples:
Sample Weight Data

Stream Site	Sample	Parent Material	Field Weight (g)	Weight Sieved (g)	+10 mesh (g)	-10+70 mesh (g)	-70 mesh (g)	Total Weight (g)	Total -10 mesh Weight (g)	-70 mesh as Wt. % of -10 (%)
1	88-SC-601	Alluvium	10505	1400	163.09	510.75	674.23	1348.07	1184.98	56.90
1	88-SC-602	Alluvium	14413	1472	966.37	294.46	104.82	1365.65	399.28	26.25
2	88-SC-603	Till	15373	2124	514.09	531.08	646.03	1691.20	1177.11	54.88
2	88-SC-604	Till	16792	2197	1229.57	605.87	249.41	2084.85	855.28	29.16
3	88-SC-605	Till	10334	1460	589.41	288.98	454.47	1332.86	743.45	61.13
3	88-SC-606	Till	7186	851	538.85	157.13	116.69	812.67	273.82	42.62
4	88-SC-607	Till	13723	1855	774.17	363.21	610.40	1747.78	973.61	62.69
4	88-SC-608	Till	10620	1380	620.77	263.50	406.54	1290.81	670.04	60.67
5	88-SC-609	Till	12407	1614	900.17	257.66	328.84	1486.67	586.50	56.07
5	88-SC-610	Till	9691	1310	714.97	147.03	316.70	1178.70	463.73	68.29

Appendix 9.1
Organic Bog Soils:
Pt, Pd, Rh and Au Analytical Data for
Pulverized versus Ashed Subsamples

Sample	Site	Pt Pulv. (ppb)	Pt Ashed (ppb)	Pd Pulv. (ppb)	Pd Ashed (ppb)	Rh Pulv. (ppb)	Rh Ashed (ppb)	Au Pulv. (ppb)	Au Ashed (ppb)
88-SC-701	Bog 1 (Centre)	4	67	3	13	5	2	1	14
88-SC-702	Bog 1 (Margin)	9	65	7	19	2	2	2	7
88-SC-703	Bog 2 (Centre)	1	8	9	2	2	2	4	1
88-SC-707	Bog 3 (Centre)	9	32	7	6	2	2	3	5
88-SC-708	Bog 3 (Margin)	21	55	7	3	2	2	3	4

Appendix 9.2
Organic Bog Soils:
Selected Analytical Data for Pulverized Subsamples

Sample	Site	As (ppm)	Sb (ppm)	MgO (%)	MnO (%)	Cr2O3 (%)	Fe2O3 (%)	LOI (%)
88-SC-701	Bog 1 (Centre)	2.3	3.9	2.94	0.03	0.01	0.51	93.1
88-SC-702	Bog 1 (Margin)	4.0	4.1	3.21	0.12	0.02	1.25	85.1
88-SC-703	Bog 2 (Centre)	3.2	0.8	2.02	0.02	0.01	2.52	66.0
88-SC-707	Bog 3 (Centre)	2.1	1.1	1.86	0.02	0.02	1.13	67.4
88-SC-708	Bog 3 (Margin)	1.0	1.5	2.92	0.02	0.06	1.49	66.2

Appendix 9.3
Organic Bog Soils:
Sample Weight and Comparative Loss on Ignition Data for
Pulverized versus Ashed Subsamples

Sample	Site	Original Dry Wt. (g)	Weight of Split for Pulverizing (g)	Weight of Split for Ashing (g)	Weight of Ash (g)	LOI Ashed (%)	LOI Pulv. (%)
88-SC-701	Bog 1 (Centre)	600.91	142.81	139.04	10.36	92.5	93.1
88-SC-702	Bog 1 (Margin)	903.24	237.37	240.35	38.10	84.1	85.1
88-SC-703	Bog 2 (Centre)	1545.25	225.06	227.14	80.96	64.4	66.0
88-SC-707	Bog 3 (Centre)	2902.39	163.97	168.85	56.66	66.4	67.4
88-SC-708	Bog 3 (Margin)	1518.22	191.95	209.07	71.32	65.9	66.2

Appendix 10

Pt Content and pH of Grasshopper Mountain Surface Waters
(n = 17)

Sample	Water Type	Location Relative to Other Media	Topography	Pt-1 (ppt)	Pt-2 (ppt)	pH	Colour
TU-01	Stream	Stream Site 1	Base of Slope	0.9	-	8.16	Clear
TU-02	Stream	Stream Site 2	Base of Slope	0.8	-	7.92	Clear
TU-03	Stream	Stream Site 3	Slope	0.8	1.3	8.06	Clear/Clear
TU-04	Stream	Stream Site 4	Slope	0.9	-	7.97	Clear
TU-05	Stream	Stream Site 5	Slope	0.9	-	7.99	Clear
TU-06	Stream	Stream Site 6	Slope	0.5	-	7.11	Clear
TU-07	Bog	-	Slope	1.0	-	6.30	Lt brown
TU-09	Bog	-	Plateau	1.3[a]	-	7.24	Clear
TU-10	Soil pit	Soil Site 6	Base of Slope	0.6	-	7.29	Lt brown
TU-11	Bog	Bog 2	Base of Slope	0.9	-	6.89	Lt brown
TU-12	Soil pit	Soil Site 2	Base of Slope	0.9	-	7.01	Clear
TU-13	Bog	Bog 1	Base of Slope	0.7	-	7.99	Lt brown
TU-14	Soil pit	Soil Site 46	Base of Slope	2.2	1.7	6.73	Lt brown/Lt brown
TU-15	Stream	-	Base of Slope	0.9	-	7.34	Lt brown
TU-16	Bog	Bog 3	Plateau/summit	3.2	-	7.42	Brown
TU-17	Pond	-	Plateau	1.8	-	7.59	Clear
TU-19	Bog	-	Plateau	3.5	1.8[b]	7.26	Lt brown/brown

[a] routine sample is unfiltered and unacidified

[b] duplicate sample is unfiltered and unacidified

Appendix 11.1
Detailed Soil Profiles:
Weight Data

Site	Sample	Field Weight (g)	Weight Sieved (g)	+10 mesh (g)	-10+40 mesh (g)	-40+70 mesh (g)	-70+140 mesh (g)	-140+270 mesh (g)	-270 mesh (g)	Total Dry Weight (g)	Total -10 mesh Dry Weight (g)
6	18	7506	6456	802.75	626.50	336.02	465.79	330.78	2031.99	4593.83	3791.08
6	19	16178	16178	3939.81	2156.56	889.48	1057.82	901.51	3879.01	12824.19	8884.38
20	38	9385	7846	2714.00	1145.95	398.13	421.67	390.69	2286.00	7356.44	4642.44
20	39	6020	5071	2055.00	694.67	224.97	260.44	225.94	1215.00	4676.02	2621.02
20	40	12897	9774	2607.00	1332.00	551.35	539.22	489.47	3340.00	8859.04	6252.04
33	78	5338	4580	1830.00	354.16	120.65	190.48	172.53	1076.43	3744.25	1914.25
33	79	14514	10815	6061.00	1187.75	389.87	337.60	259.35	1389.00	9624.57	3563.57
34	81	8969	8969	5826.00	504.19	156.75	357.00	243.32	1127.25	8214.51	2388.51
34	82	17839	13822	7234.00	2187.00	871.89	698.42	473.94	1586.00	13051.25	5817.25
43	110	10604	8931	1743.00	1121.51	1470.00	1698.00	835.74	1496.00	8364.25	6621.25
43	111	9277	7751	1441.00	989.11	1345.00	1569.00	767.05	1172.51	7283.67	5842.67
43	112	14498	10770	2860.00	2057.00	1516.00	1566.00	809.22	1414.00	10222.22	7362.22
43	113	7988	6565	2408.00	1044.11	385.58	348.21	285.79	1679.00	6150.69	3742.69
69	199	10998	9309	4734.20	765.60	266.90	423.81	358.81	1540.20	8089.52	3355.32
69	200	15564	10371	3939.50	1280.20	507.69	460.71	370.94	2476.30	9035.34	5095.84
73	215	13238	11082	4682.00	1002.39	697.00	1004.16	656.53	1835.50	9877.58	5195.58
73	216	14817	10381	4657.80	981.20	503.23	501.97	375.83	1961.20	8981.23	4323.43
51	133	11017	9593	5104.00	837.25	216.68	428.97	370.95	1731.00	8688.85	3584.85
51	134	9719	8196	3178.00	850.51	274.63	467.28	417.47	2008.00	7195.89	4017.89
51	135	14671	11481	4085.00	1514.00	574.30	569.61	490.06	2843.00	10075.97	5990.97
57	154	11575	9431	4995.00	601.78	176.52	359.10	296.10	1215.00	7643.50	2648.50
57	155	13766	11692	4816.00	1529.68	517.28	510.59	471.05	2553.00	10397.60	5581.60
57	156	13462	10274	4104.00	1161.34	387.86	391.34	330.00	2355.00	8729.54	4625.54
56	152	11419	9781	6308.00	756.88	136.30	345.90	263.15	1289.13	9099.36	2791.36
56	153	11038	11038	7154.33	1092.11	249.95	238.51	159.66	1183.30	10077.86	2923.53
27	59	16834	13824	10139.00	1330.00	349.38	324.85	237.13	898.16	13278.52	3139.52
27	60	17949	15006	9245.00	1921.00	478.08	472.14	323.89	1278.68	13718.79	4473.79
27	61	13959	9902	5862.00	1172.16	319.36	320.15	278.21	1048.19	9000.07	3138.07
42	104	13219	11308	7491.00	1557.00	363.71	273.12	201.32	1151.26	11037.41	3546.41
42	105	13698	10085	5930.00	1295.00	343.32	284.32	190.11	1111.14	9153.89	3223.89
9	24	9487	8133	5478.00	802.79	223.86	267.94	208.17	670.91	7651.67	2173.67
9	23	12864	9220	7093.00	560.36	150.95	217.25	155.59	586.88	8764.03	1671.03
16	31	12735	12735	8919.00	1648.00	377.30	326.88	192.42	684.70	12148.30	3229.30
02	503	9907	7746	78.79	5722.20	1008.50	395.94	161.96	361.58	7728.97	7650.18

Appendix 11.2
Grain Size Distribution Among Size Fractions
of Selected Soil Profiles
(Weight Percent of the < 2 mm Component)

Site	Sample	-10+40 mesh (%)	-40+70 mesh (%)	-70+140 mesh (%)	-140+270 mesh (%)	-270 mesh (%)
6	18	16.52	8.86	12.29	8.72	53.60
6	19	24.27	10.01	11.91	10.15	43.66
20	38	24.68	8.57	9.08	8.41	49.24
20	39	26.50	8.58	9.94	8.62	46.35
20	40	21.30	8.82	8.62	7.83	53.42
33	78	18.50	6.30	9.95	9.01	56.23
33	79	33.33	10.94	9.47	7.28	38.98
34	81	21.11	6.56	14.95	10.19	47.19
34	82	37.59	14.99	12.01	8.15	27.26
43	110	16.94	22.20	25.64	12.62	22.59
43	111	16.93	23.02	26.85	13.13	20.07
43	112	27.94	20.59	21.27	10.99	19.21
43	113	27.90	10.30	9.30	7.63	44.86
69	199	22.82	7.95	12.63	10.69	45.90
69	200	25.12	9.96	9.04	7.28	48.59
73	215	19.29	13.41	19.33	12.64	35.33
73	216	22.69	11.64	11.61	8.69	45.36
51	133	23.36	6.04	11.97	10.35	48.29
51	134	21.17	6.83	11.63	10.39	49.98
51	135	25.27	9.59	9.51	8.18	47.45
57	154	22.72	6.66	13.56	11.18	45.88
57	155	27.41	9.27	9.15	8.44	45.74
57	156	25.11	8.38	8.46	7.13	50.91
56	152	27.11	4.88	12.39	9.43	46.18
56	153	37.35	8.55	8.16	5.46	40.48
27	59	42.36	11.13	10.35	7.55	28.61
27	60	42.94	10.69	10.55	7.24	28.58
27	61	37.35	10.18	10.20	8.87	33.40
42	104	43.90	10.26	7.70	5.68	32.46
42	105	40.17	10.65	8.82	5.90	34.47
9	24	36.93	10.30	12.33	9.58	30.86
9	23	33.53	9.03	13.00	9.31	35.12
16	31	51.03	11.68	10.12	5.96	21.20
02	503	74.80	13.18	5.17	2.12	4.73

Appendix 11.3
Detailed Soil Profiles:
Weight Data for -70+140 mesh fraction
Heavy Mineral Concentrates

Site	Sample	Weight Sieved (g)	Original -70+140 Fraction Wt. (g)	Light Fraction Weight (g)	Heavy Fraction Weight (g)	Weight Percent Heavies (%)	Magnetic Fraction Weight (g)	Nonmagnetic Fraction Weight (g)
6	18	6456	219.92	211.05	7.82	3.57	4.60	3.21
6	19	16178	262.22	252.69	5.91	2.29	2.32	3.59
20	38	7846	421.67	367.00	50.83	12.16	8.04	42.59
20	39	5071	260.44	252.04	7.34	2.83	4.39	2.94
20	40	9774	539.22	480.58	53.38	10.00	12.77	40.54
33	78	4580	190.48	172.86	16.36	8.65	11.53	4.80
33	79	10815	337.60	291.02	44.13	13.17	27.45	16.61
34	81	8969	357.00	322.93	31.44	8.87	25.16	6.27
34	82	13822	345.46	292.09	53.04	15.37	31.06	21.90
43	110	8931	388.56	366.91	20.93	5.40	6.74	14.11
43	111	7751	483.58	415.71	67.52	13.97	7.80	59.66
43	112	10770	470.71	385.88	84.39	17.95	8.09	76.24
43	113	6565	348.21	327.22	19.97	5.75	5.24	14.71
69	199	9309	423.81	383.20	39.62	9.37	25.14	14.39
69	200	10371	460.71	410.05	50.23	10.91	20.08	30.03
73	215	11082	229.89	186.72	43.03	18.73	8.39	34.62
73	216	10381	501.97	389.32	111.85	22.32	39.65	72.11
51	133	9593	428.97	375.44	46.07	10.93	40.85	5.02
51	134	8196	467.28	414.93	48.34	10.43	38.65	9.53
51	135	11481	569.61	500.38	69.83	12.25	50.44	19.12
57	154	9431	359.10	334.31	21.33	6.00	19.13	2.09
57	155	11692	510.59	469.83	40.78	7.99	31.73	8.21
57	156	10274	391.34	341.46	48.74	12.49	32.32	16.29
56	152	9781	345.90	311.85	23.14	6.91	20.10	3.00
56	153	11038	238.51	215.76	19.49	8.28	18.16	1.31
27	59	13824	324.85	291.92	31.46	9.73	23.85	7.50
27	60	15006	472.14	431.18	40.89	8.66	33.90	6.89
27	61	9902	320.15	291.71	26.80	8.41	21.81	4.94
42	104	11308	273.12	246.59	23.40	8.67	19.54	3.80
42	105	10085	284.32	260.74	21.01	7.46	16.93	4.01
9	24	8133	267.94	243.65	19.70	7.48	16.21	3.43
9	23	9220	217.25	182.33	33.87	15.67	15.35	18.43
16	31	12735	326.88	299.40	27.50	8.41	22.96	4.48
02	503	7746	395.94	359.41	38.40	9.65	20.35	18.01

Appendix 11.4
Detailed Soil Profiles:
Weight Data for -140+270 mesh fraction
Heavy Mineral Concentrates

Site	Sample	Weight Sieved (g)	Original -140+270 Fraction Wt. (g)	Light Fraction Weight (g)	Heavy Fraction Weight (g)	Weight Percent Heavies (%)	Magnetic Fraction Weight (g)	Nonmagnetic Fraction Weight (g)
6	18	6456	330.78	314.13	15.57	4.72	10.00	5.57
6	19	16178	226.50	217.35	8.17	3.62	2.48	5.68
20	38	7846	390.69	363.15	26.63	6.83	8.39	18.14
20	39	5071	225.94	217.05	7.98	3.55	4.84	3.11
20	40	9774	489.47	463.45	18.53	3.84	8.21	10.27
33	78	4580	172.53	156.07	15.91	9.25	10.20	5.63
33	79	10815	259.35	232.41	25.49	9.88	15.79	9.60
34	81	8969	243.32	215.37	25.82	10.71	21.04	4.68
34	82	13822	473.94	395.05	78.08	16.50	41.98	35.92
43	110	8931	403.69	383.14	19.52	4.85	8.81	10.62
43	111	7751	436.43	421.13	15.07	3.45	7.12	7.90
43	112	10770	461.21	428.93	31.57	6.86	9.01	22.50
43	113	6565	285.79	271.42	10.62	3.77	5.32	5.28
69	199	9309	358.81	324.53	31.57	8.87	20.80	10.66
69	200	10371	370.94	349.64	20.59	5.56	12.72	7.81
73	215	11082	334.20	291.31	42.74	12.79	13.57	29.11
73	216	10381	375.83	333.42	42.06	11.20	23.85	18.14
51	133	9593	370.95	324.54	40.22	11.03	33.37	6.64
51	134	8196	417.47	370.64	37.93	9.28	29.22	8.57
51	135	11481	490.06	466.42	23.48	4.79	15.77	7.62
57	154	9431	296.10	269.60	25.80	8.73	18.22	7.37
57	155	11692	471.05	443.23	27.88	5.92	19.35	8.43
57	156	10274	330.00	286.57	39.31	12.06	21.44	17.73
56	152	9781	263.15	235.89	21.45	8.34	16.54	4.86
56	153	11038	159.66	147.78	10.00	6.34	8.69	1.29
27	59	13824	237.13	228.02	5.61	2.40	4.90	0.67
27	60	15006	323.89	309.50	13.57	4.20	11.82	1.71
27	61	9902	278.21	269.98	7.64	2.75	6.82	0.78
42	104	11308	201.32	191.00	7.93	3.99	6.04	1.84
42	105	10085	190.11	174.28	12.10	6.49	9.70	2.37
9	24	8133	208.17	191.74	11.53	5.67	9.48	1.99
9	23	9220	155.59	147.29	7.62	4.92	6.09	1.50
16	31	12735	192.42	179.92	12.25	6.37	10.17	2.05
02	503	7746	161.96	149.27	12.94	7.98	6.83	6.10

Appendix 11.5
Pt Concentrations in Five Standard Size Fractions
of Selected Soil Profiles

Site	Sample	Horizon	Surficial Material	-10+40 mesh (ppb)	-40+70 mesh (ppb)	-70+140 mesh (ppb)	-140+270 mesh (ppb)	-270 mesh (ppb)
6	18	Bh	Nondunitic Till	13	11	4	2	7
6	19	Cg	Nondunitic Till	9	8	6	5	9
20	38	Aej	Nondunitic Till	3	3	4	9	7
20	39	Bf	Nondunitic Till	7	5	8	2	10
20	40	C	Nondunitic Till	77	21	23	23	14
33	78	Bm	Dunitic Till	49	19	20	35	36
33	79	C	Dunitic Till	93	30	29	35	36
34	81	IC	Colluvium	16	53	42	41	53
34	82	IIC	Dunitic Till	14	21	19	25	21
43	110	Bm	Dunitic Till	7	1	5	8	16
43	111	Bm	Dunitic Till	6	1	3	6	17
43	112	BC/C	Dunitic Till	9	1	7	15	13
43	113	C	Dunitic Till	1	1	2	7	2
69	199	Bm	Dunitic Till	66	113	104	172	104
69	200	C	Dunitic Till	53	76	50	32	25
73	215	Bm	Dunitic Till	81	92	38	64	53
73	216	C	Dunitic Till	101	49	167	50	41
51	133	Bm	Dunitic Till	85	128	97	53	69
51	134	BC	Dunitic Till	74	103	74	55	53
51	135	C	Dunitic Till	96	632	157	141	89
57	154	Bm/IC	Colluvium	110	128	80	51	76
57	155	BC	Dunitic Till	92	128	149	90	131
57	156	IIC	Dunitic Till	119	152	155	164	150
56	152	C (upper)	Dunitic Till	355	402	83	38	116
56	153	C (lower)	Dunitic Till	722	588	278	257	260
27	59	C (upper)	Colluvium	113	104	78	149	99
27	60	C (middle)	Colluvium	106	88	67	83	89
27	61	C (lower)	Colluvium	95	388	74	90	75
42	104	C (upper)	Colluvium	99	128	78	152	115
42	105	C (lower)	Colluvium	110	139	64	91	117
9	24	C (upper)	Colluvium	248	178	53	42	61
9	23	C (lower)	Colluvium	85	121	225	53	71
16	31	C	Colluvium	193	176	277	167	147
2	503		Stream Sediment	1	12	21	18	23

Appendix 11.6
Pt Concentrations in Light (S.G. < 3.3) and
Heavy (S.G. > 3.3) Mineral Fractions
in Selected Soil Profiles

Site	Sample	Horizon	-70+140 Lights (ppb)	-70+140 Heavies (ppb)	-140+270 Lights (ppb)	-140+270 Heavies (ppb)
6	18	Bh	3	22	1	22
6	19	Cg	5	67	3	66
20	38	Aej	2	18	6	46
20	39	Bf	6	61	1	30
20	40	C	10	142	14	242
33	78	Bm	9	142	4	338
33	79	C	15	118	12	240
34	81	IC	4	428	2	362
34	82	IIC	11	62	11	98
43	110	Bm	1	71	4	95
43	111	Bm	1	18	3	78
43	112	BC/C	6	11	1	200
43	113	C	1	20	2	127
69	199	Bm	36	767	50	1429
69	200	C	31	201	20	237
73	215	Bm	13	145	15	400
73	216	C	23	669	15	329
51	133	Bm	25	682	18	331
51	134	BC	21	526	25	343
51	135	C	69	787	110	756
57	154	Bm/IC	30	868	23	340
57	155	BC	50	1292	57	607
57	156	IIC	70	754	74	817
56	152	C (upper)	34	744	24	193
56	153	C (lower)	160	1590	137	2027
27	59	C (upper)	40	426	128	1000
27	60	C (middle)	37	388	74	283
27	61	C (lower)	47	364	70	812
42	104	C (upper)	61	261	123	855
42	105	C (lower)	46	282	62	503
9	24	C (upper)	33	305	35	154
9	23	C (lower)	27	1288	42	273
16	31	C	69	2538	117	901
2	503	Sediment	1	207	7	148

Appendix 11.7
Pt Concentrations in Magnetic and Non-magnetic Heavy Fractions in Selected Soil Profiles

Site	Sample	Horizon	-70+140 Heavy Mags (ppb)	-70+140 Heavy NonMags (ppb)	-140+270 Heavy Mags (ppb)	-140+270 Heavy NonMags (ppb)
6	18	Bh	34	5	30	9
6	19	Cg	148	15	143	33
20	38	Aej	95	4	97	23
20	39	Bf	96	8	47	4
20	40	C	563	9	517	22
33	78	Bm	179	54	338	338
33	79	C	78	183	59	539
34	81	IC	400	541	297	655
34	82	IIC	96	13	128	64
43	110	Bm	158	30	95	95
43	111	Bm	51	14	108	51
43	112	BC/C	68	5	525	70
43	113	C	58	7	249	5
69	199	Bm	1142	112	1549	1195
69	200	C	490	7	273	179
73	215	Bm	704	10	1066	90
73	216	C	1732	85	474	139
51	133	Bm	759	57	358	193
51	134	BC	653	12	367	261
51	135	C	1075	28	987	278
57	154	Bm/IC	962	8	299	442
57	155	BC	792	3225	413	1053
57	156	IIC	695	870	359	1371
56	152	C (upper)	755	669	185	219
56	153	C (lower)	1671	466	1857	3172
27	59	C (upper)	393	530	738	2916
27	60	C (middle)	348	587	85	1655
27	61	C (lower)	317	569	339	4950
42	104	C (upper)	253	305	284	2730
42	105	C (lower)	288	257	199	1749
9	24	C (upper)	331	180	168	86
9	23	C (lower)	2782	43	170	691
16	31	C	2721	1601	855	1128
2	503	Sediment	361	34	149	146

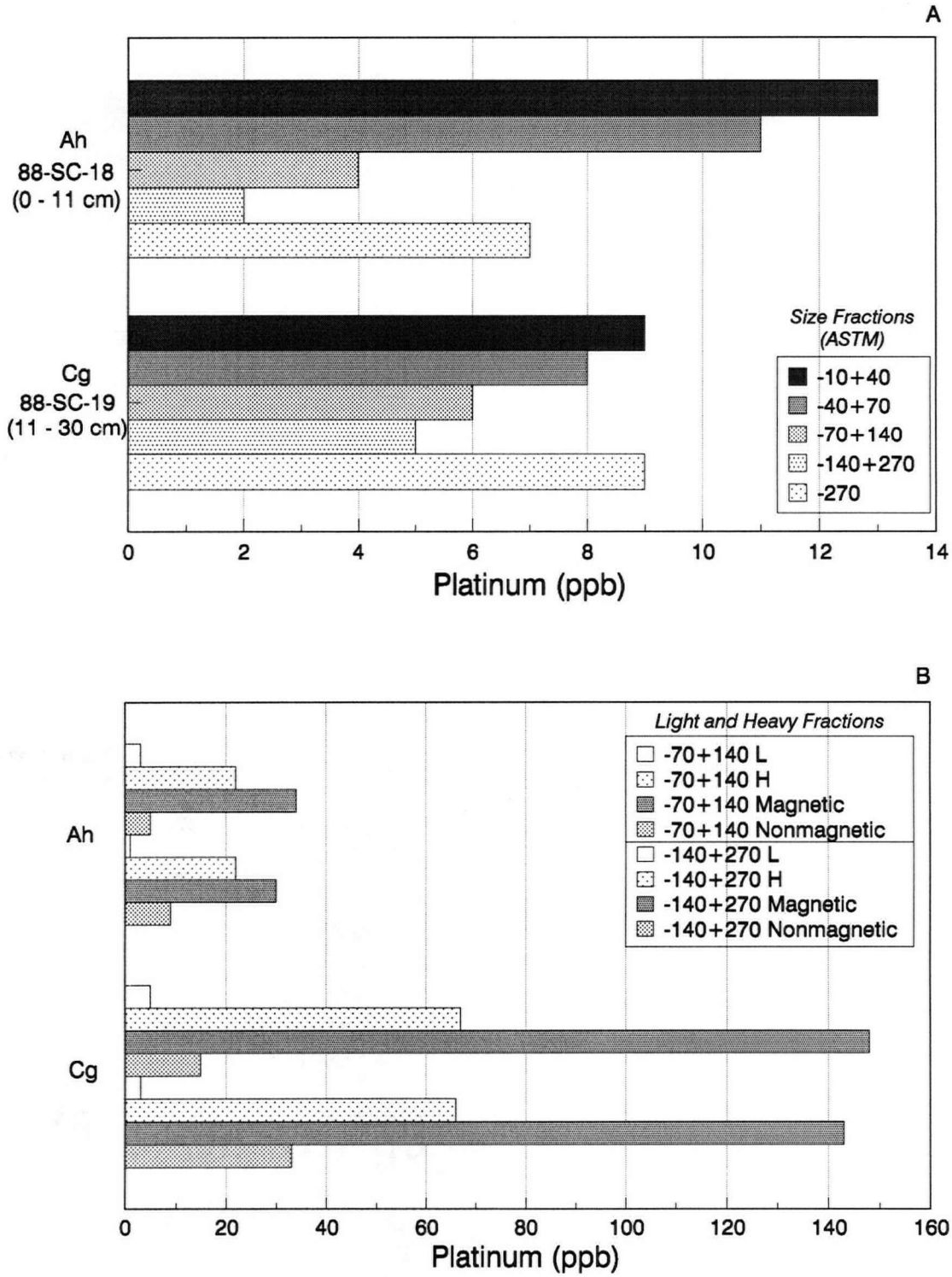

Appendix 12.1. Pt distribution (ppb) in melanic brunisol (soil site 6) on non-dunitic till, showing A. Pt content of five size fractions and B. Pt content of light, heavy, heavy magnetic and heavy non-magnetic mineral fractions of the -70+140 (bars 1-4) and -140+270 (bars 5-8) mesh size fractions

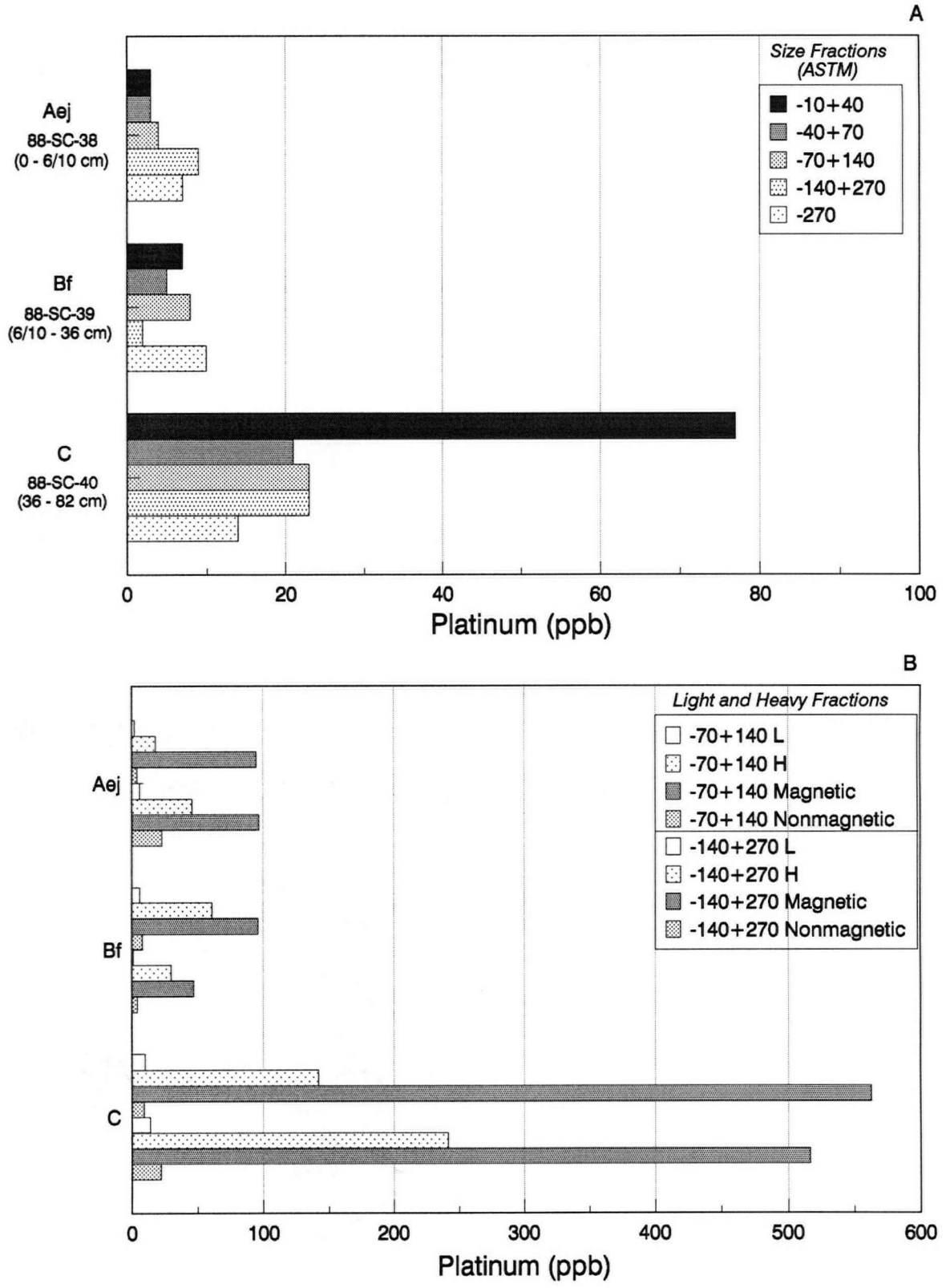

Appendix 12.2. Pt distribution (ppb) in humo-ferric podzol (soil site 20) on non-dunitic till, showing A. Pt content of five size fractions and B. Pt content of light, heavy, heavy magnetic and heavy non-magnetic mineral fractions of the -70+140 (bars 1-4) and -140+270 (bars 5-8) mesh size fractions.

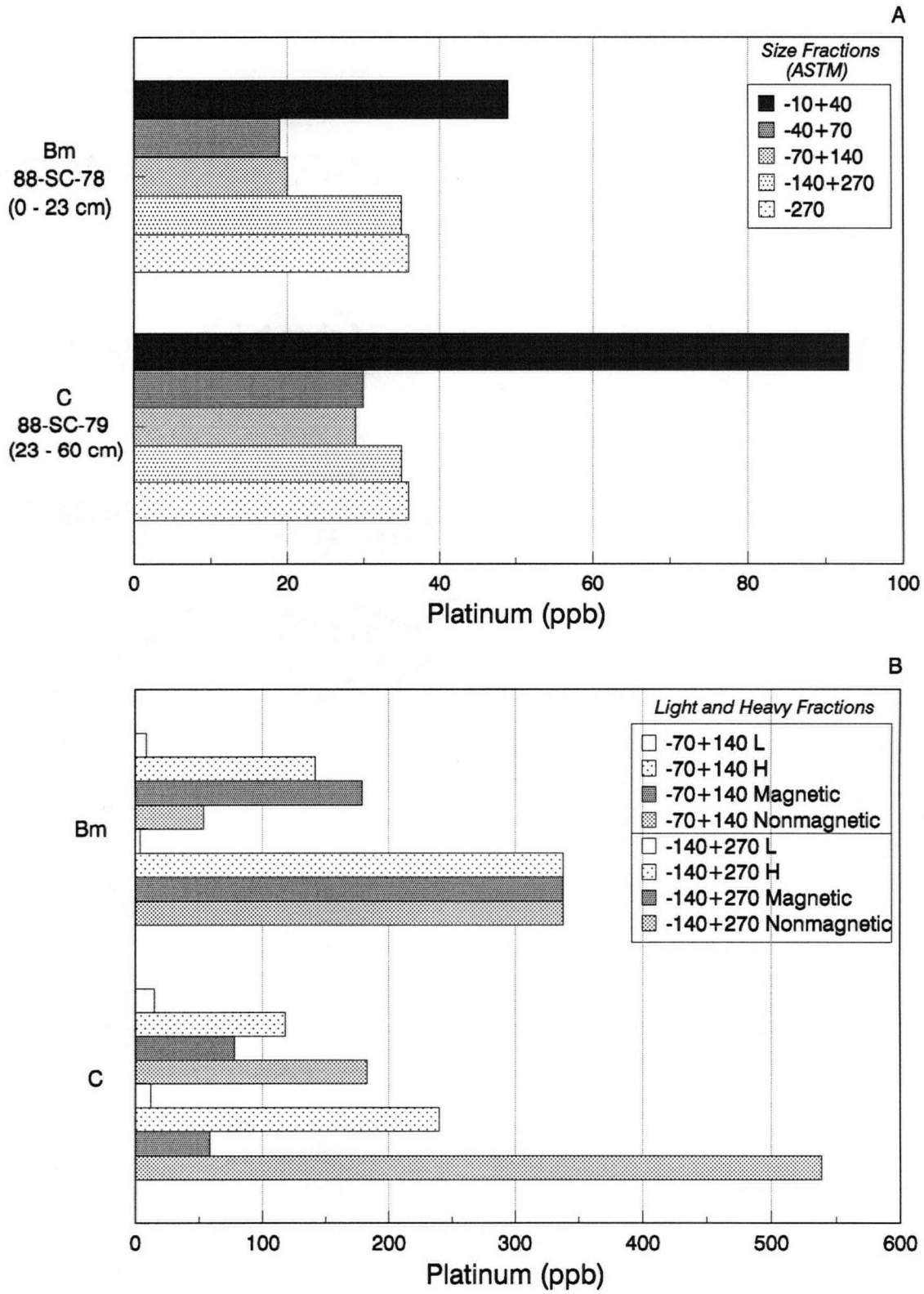

Appendix 12.3. Pt distribution (ppb) in eutric brunisol (soil site 33) on dunitic till, showing A. Pt content of five size fractions and B. Pt content of light, heavy, heavy magnetic and heavy non-magnetic mineral fractions of the -70+140 (bars 1-4) and -140+270 (bars 5-8) mesh size fractions.

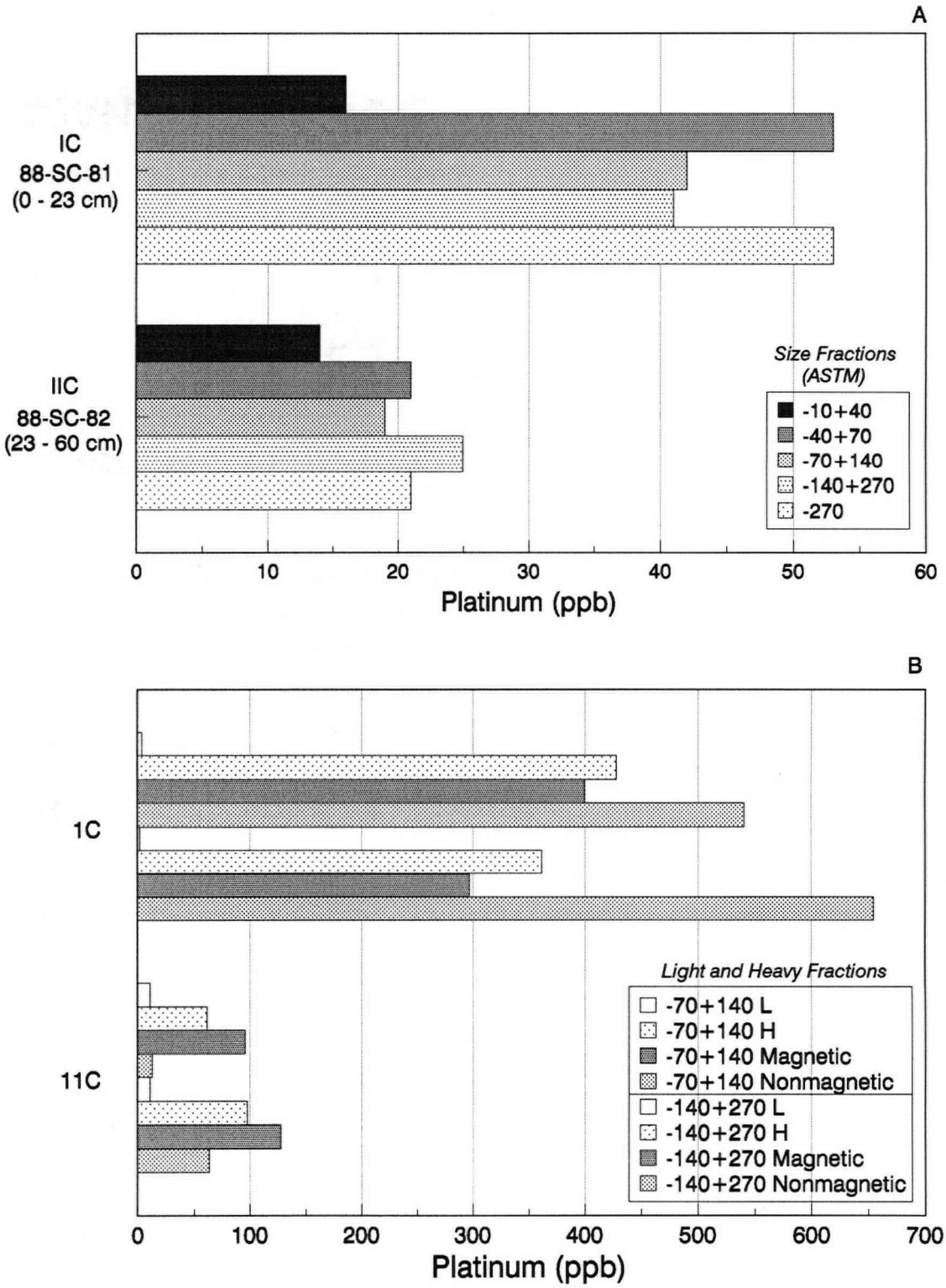

Appendix 12.4. Pt distribution (ppb) in composite soil profile (soil site 34) of dunitic colluvium (IC) overlying dunitic till (IIC), showing A. Pt content of five size fractions and B. Pt content of light, heavy, heavy magnetic and heavy non-magnetic mineral fractions of the -70+140 (bars 1-4) and -140+270 (bars 5-8) mesh size fractions.

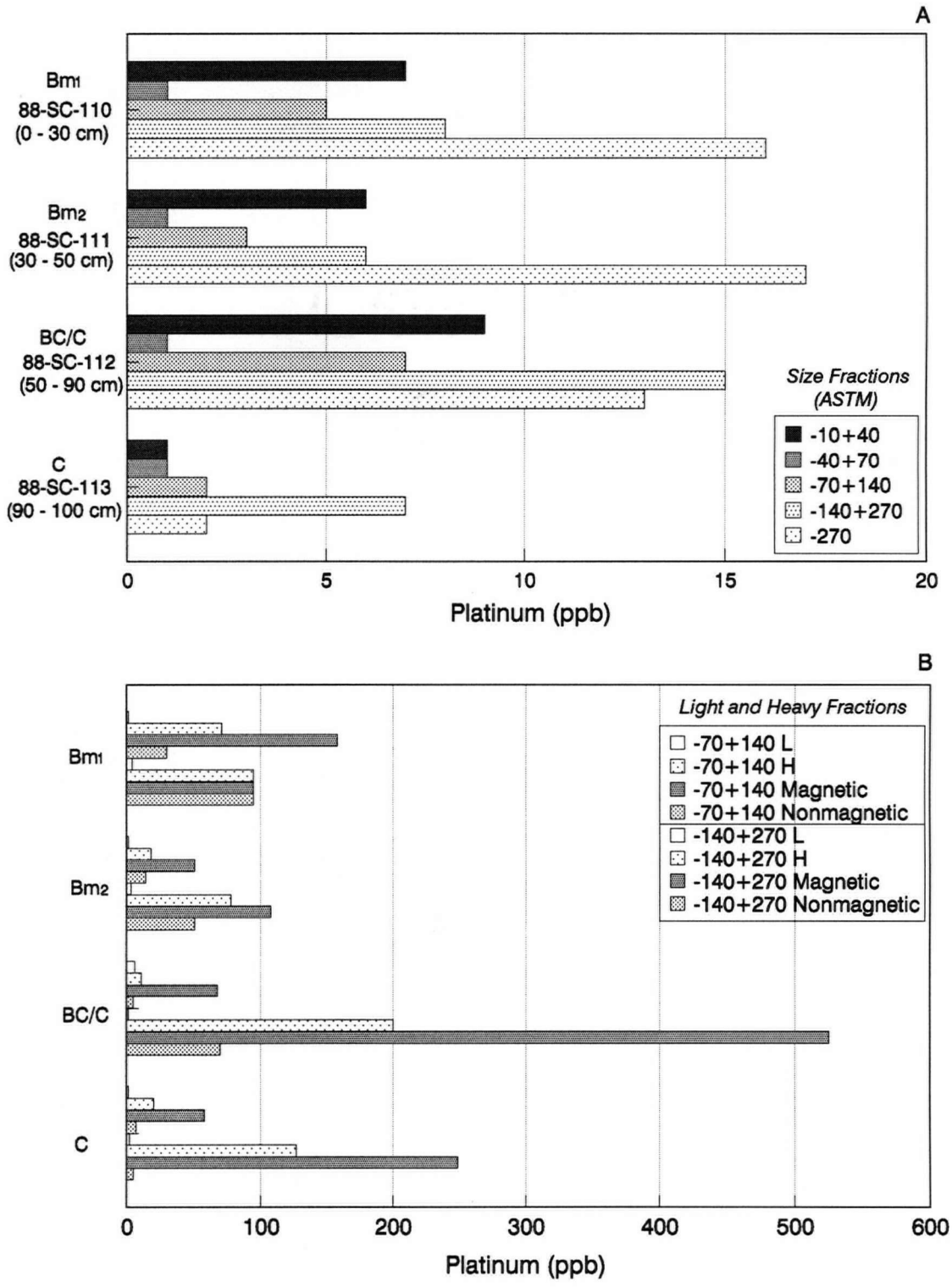

Appendix 12.5. Pt distribution (ppb) in composite soil profile (soil site 43) of possibly glaciofluvially-reworked dunitic till (Bm horizons) above dunitic till (BC/C, C), showing A. Pt content of five size fractions and B. Pt content of light, heavy, heavy magnetic and heavy non-magnetic mineral fractions of the -70+140 (bars 1-4) and -140+270 (bars 5-8) mesh size fractions.

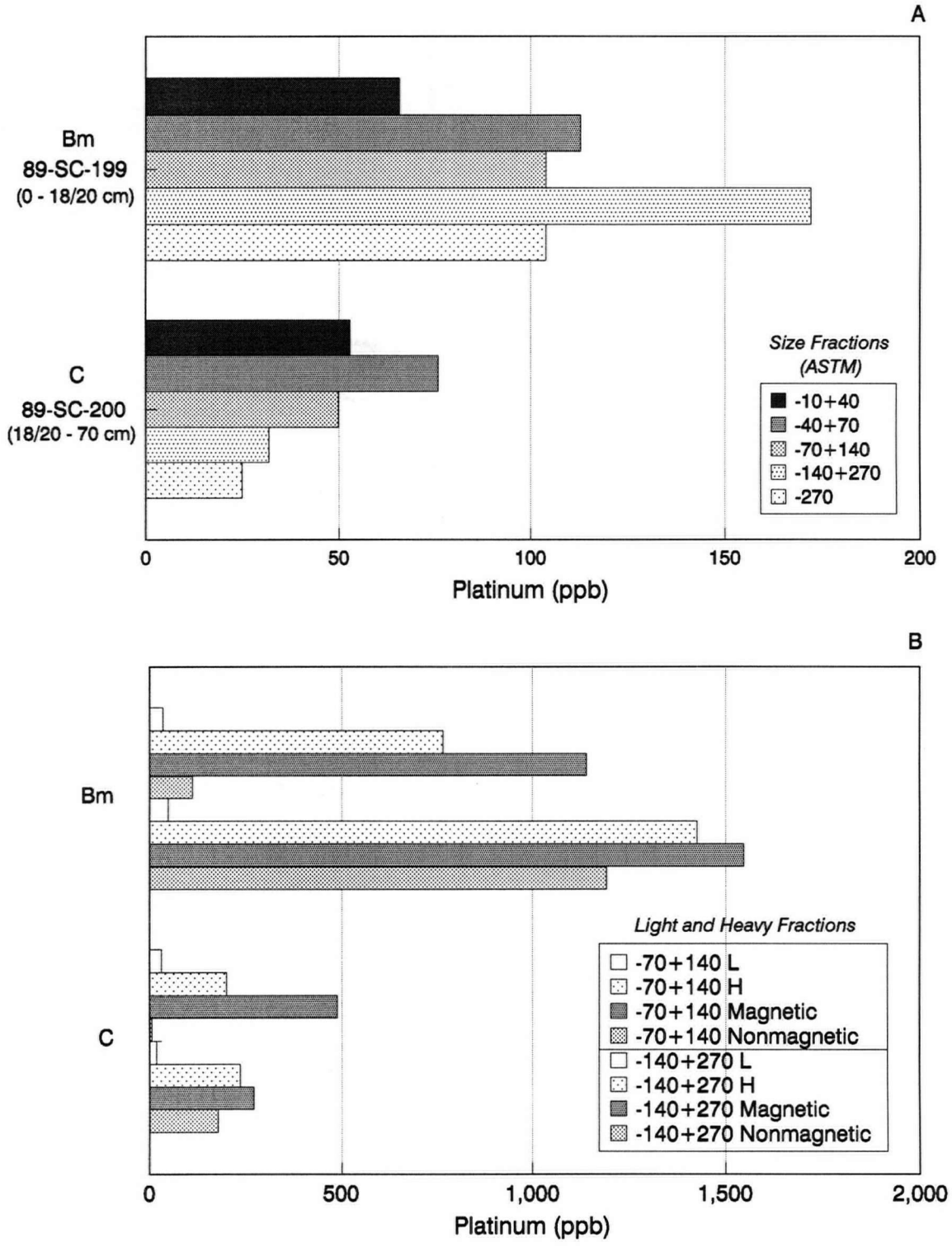

Appendix 12.6. Pt distribution (ppb) in eutric brunisol (soil site 69) on dunitic till, showing A. Pt content of five size fractions and B. Pt content of light, heavy, heavy magnetic and heavy non-magnetic mineral fractions of the -70+140 (bars 1-4) and -140+270 (bars 5-8) mesh size fractions.

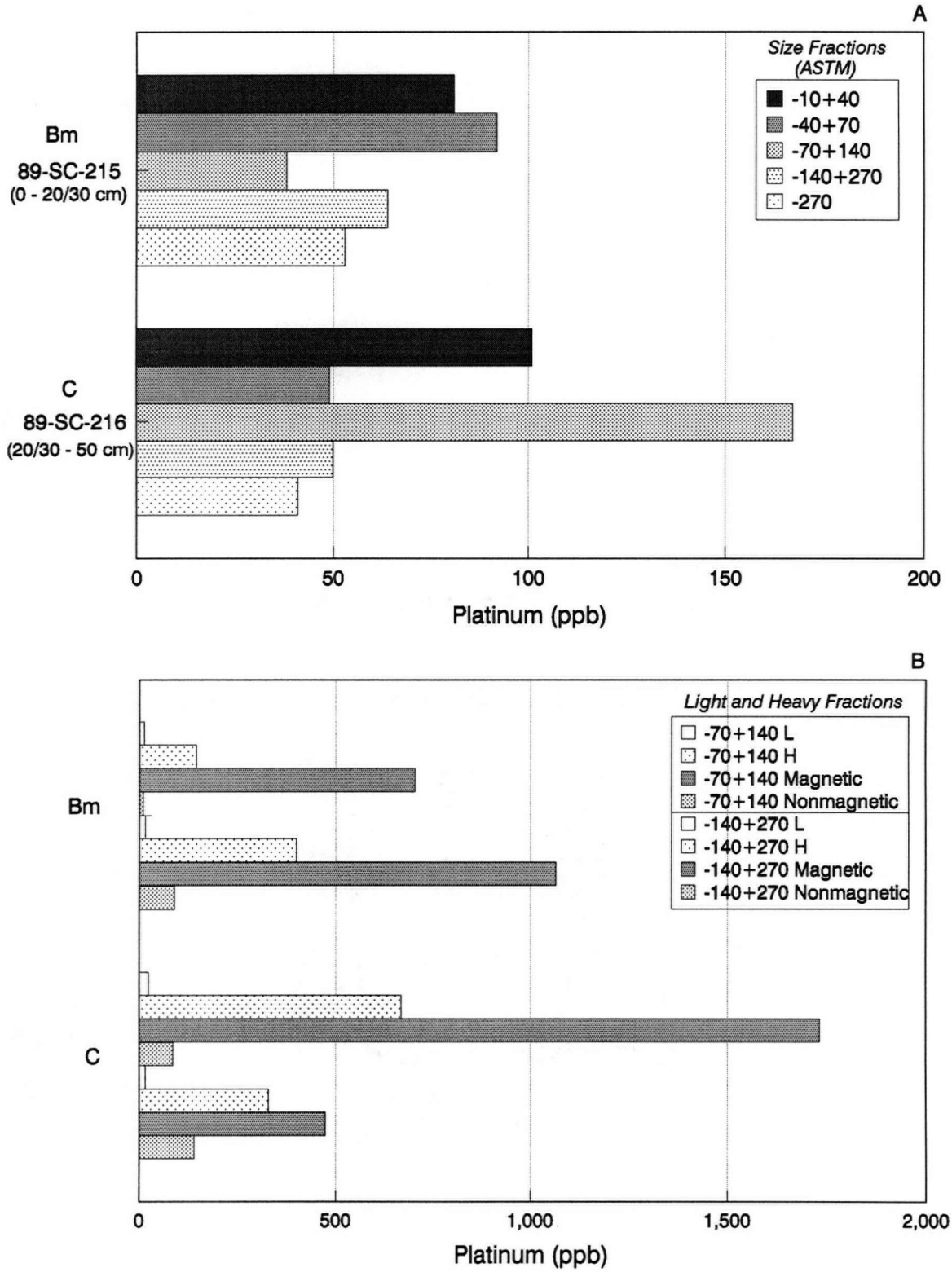

Appendix 12.7. Pt distribution (ppb) in eutric brunisol (soil site 73) on dunitic till, showing A. Pt content of five size fractions and B. Pt content of light, heavy, heavy magnetic and heavy non-magnetic mineral fractions of the -70+140 (bars 1-4) and -140+270 (bars 5-8) mesh size fractions.

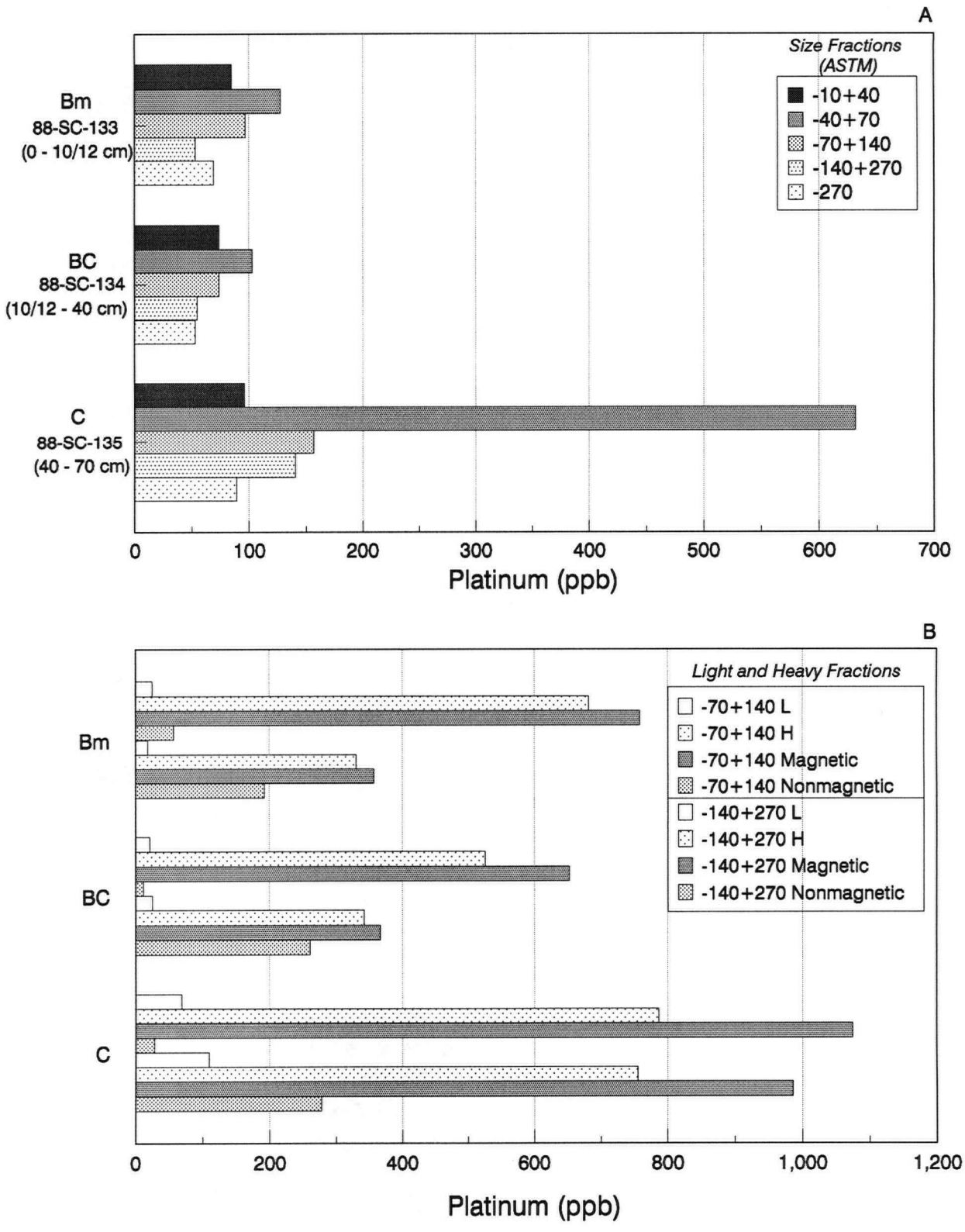

Appendix 12.8. Pt distribution (ppb) in eutric brunisol (soil site 51) on dunitic till near A-Zone PGE occurrence, secondary study area, showing A. Pt content of five size fractions and B. Pt content of light, heavy, heavy magnetic and heavy non-magnetic mineral fractions of the -70+140 (bars 1-4) and -140+270 (bars 5-8) mesh size fractions.

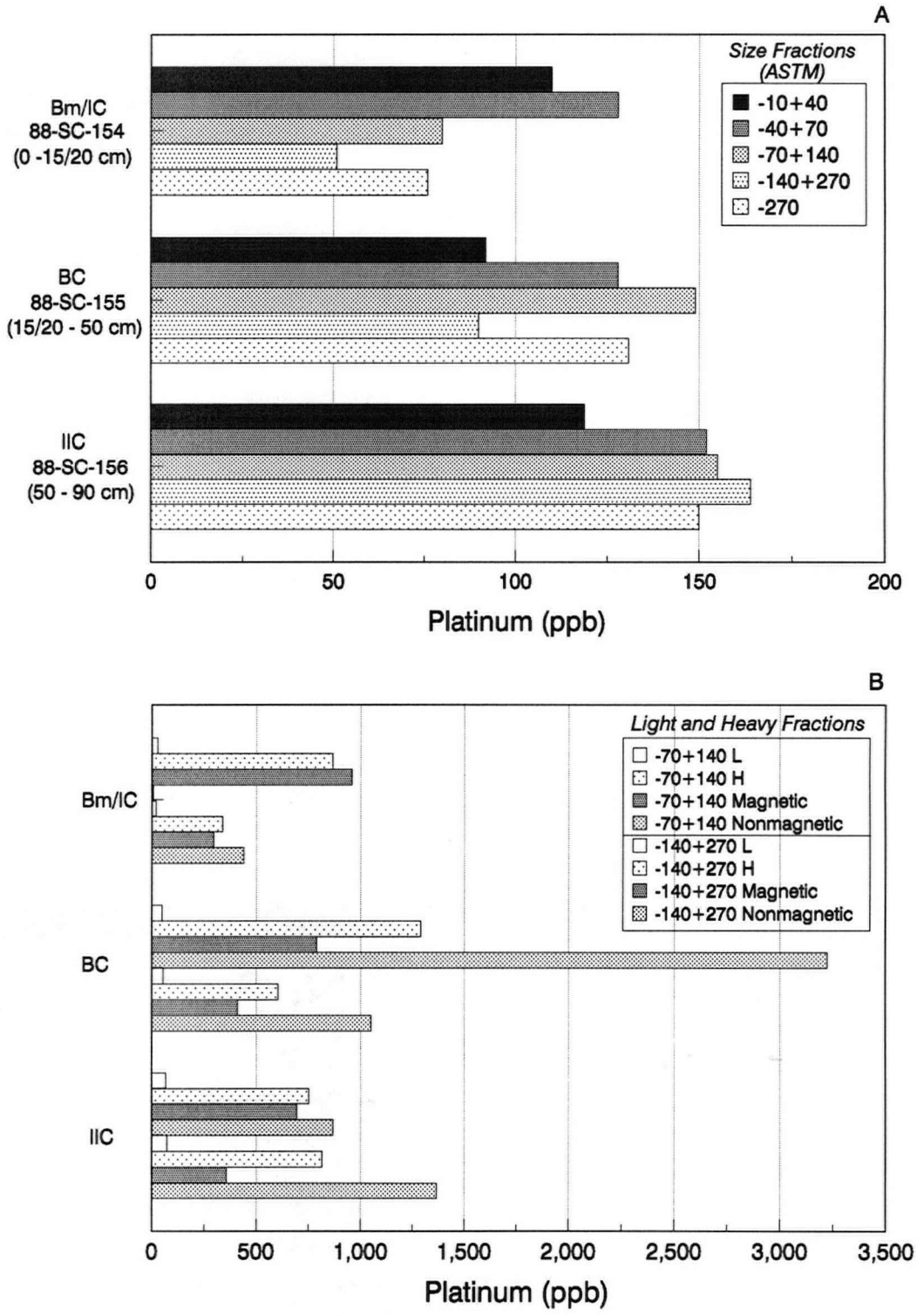

Appendix 12.9. Pt distribution (ppb) in eutric brunisol (soil site 57), with colluvial Bm horizon, on dunitic till near A-Zone PGE occurrence, secondary study area, showing A. Pt content of five size fractions and B. Pt content of light, heavy, heavy magnetic and heavy non-magnetic mineral fractions of the -70+140 (bars 1-4) and -140+270 (bars 5-8) mesh size fractions.

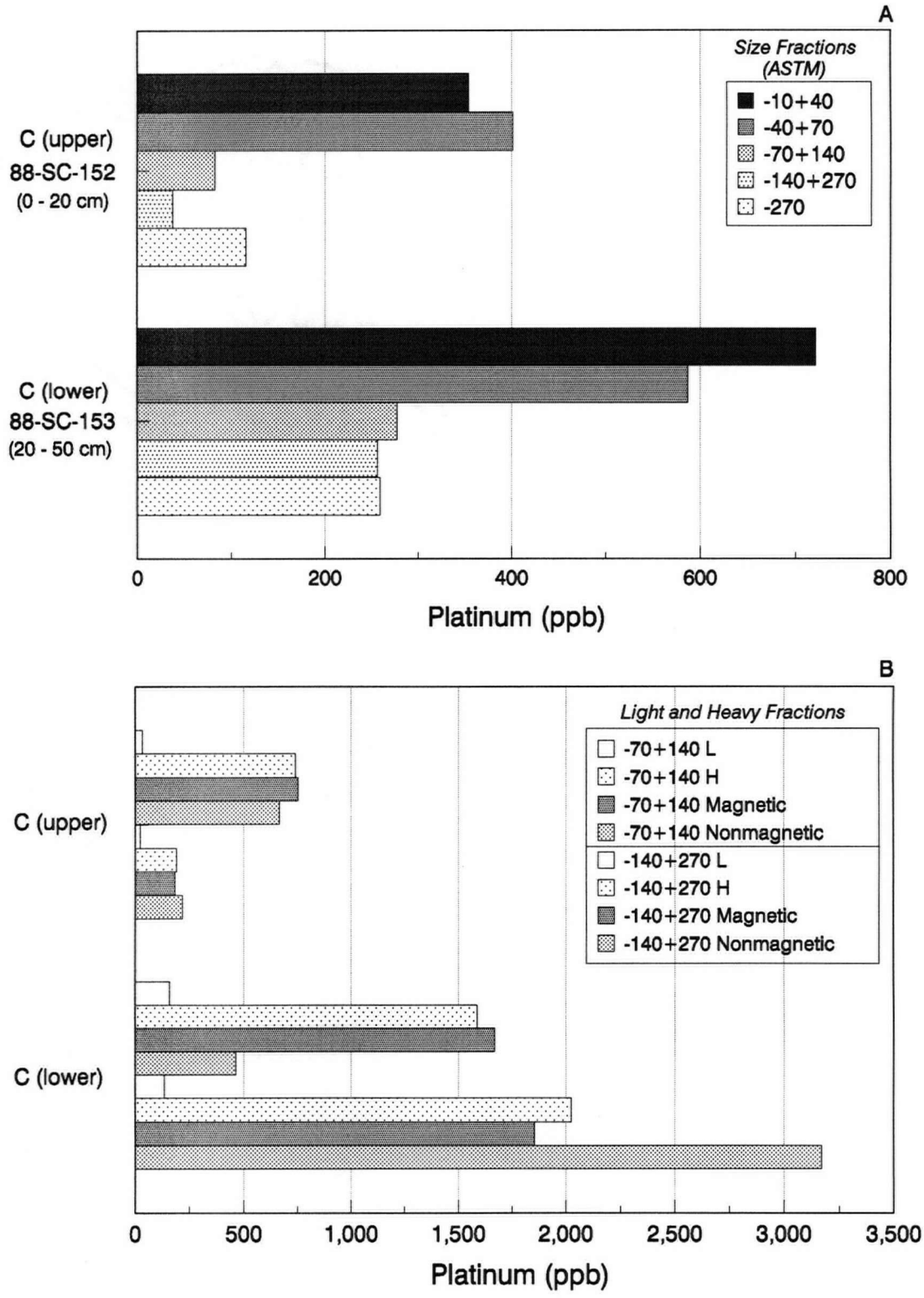

Appendix 12.10. Pt distribution (ppb) in orthic regosol (soil site 56) on dunitic rubble immediately above A-Zone PGE occurrence, secondary study area, showing A. Pt content of five size fractions and B. Pt content of light, heavy, heavy magnetic and heavy non-magnetic mineral fractions of the -70+140 (bars 1-4) and -140+270 (bars 5-8) mesh size fractions.

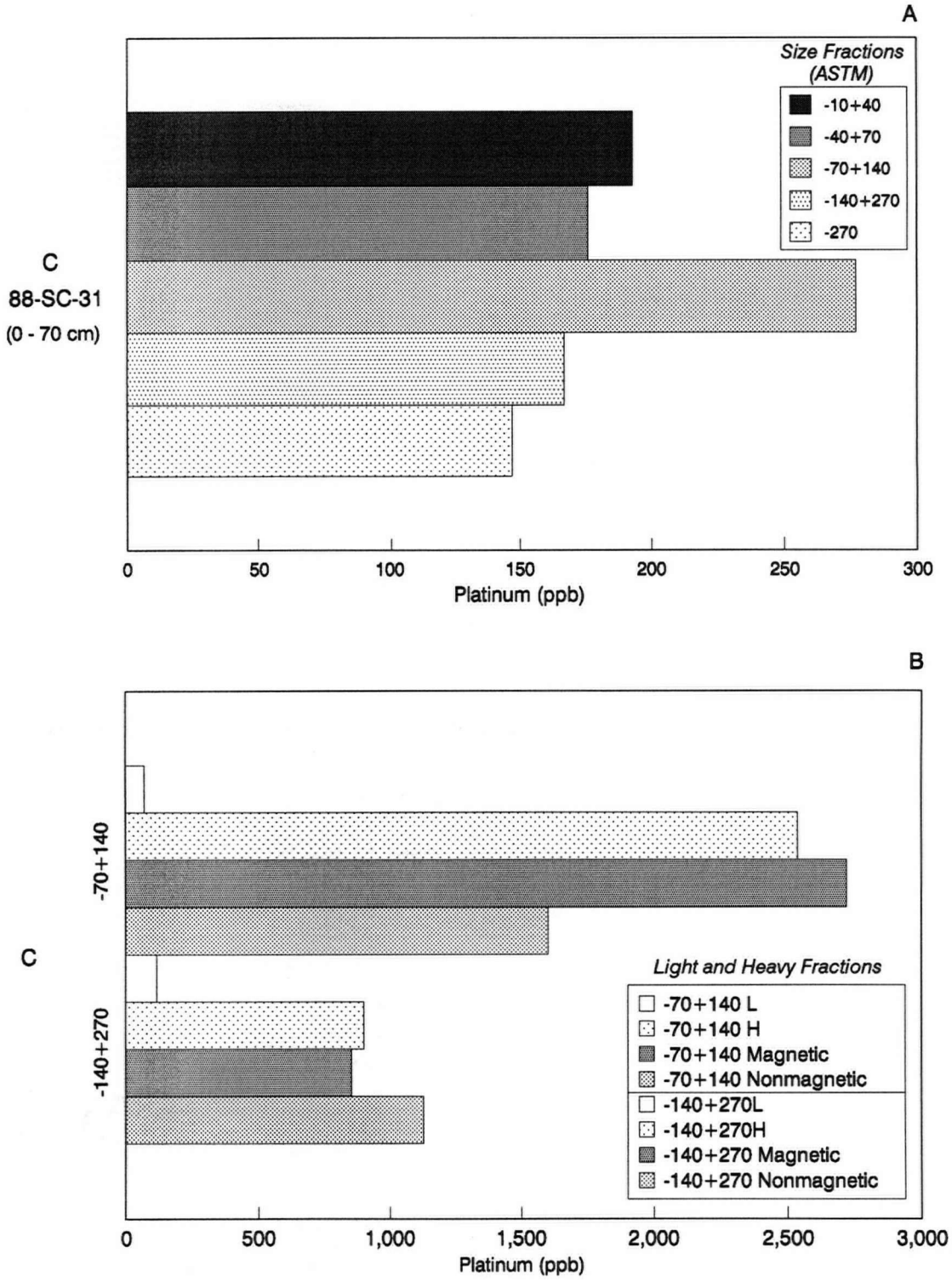

Appendix 12.11. Pt distribution (ppb) in orthic regosol (soil site 16) on dunite colluvium below Cliff Zone PGE occurrences, showing A. Pt content of five size fractions and B. Pt content of light, heavy, heavy magnetic and heavy non-magnetic mineral fractions of the -70+140 (bars 1-4) and -140+270 (bars 5-8) mesh size fractions.

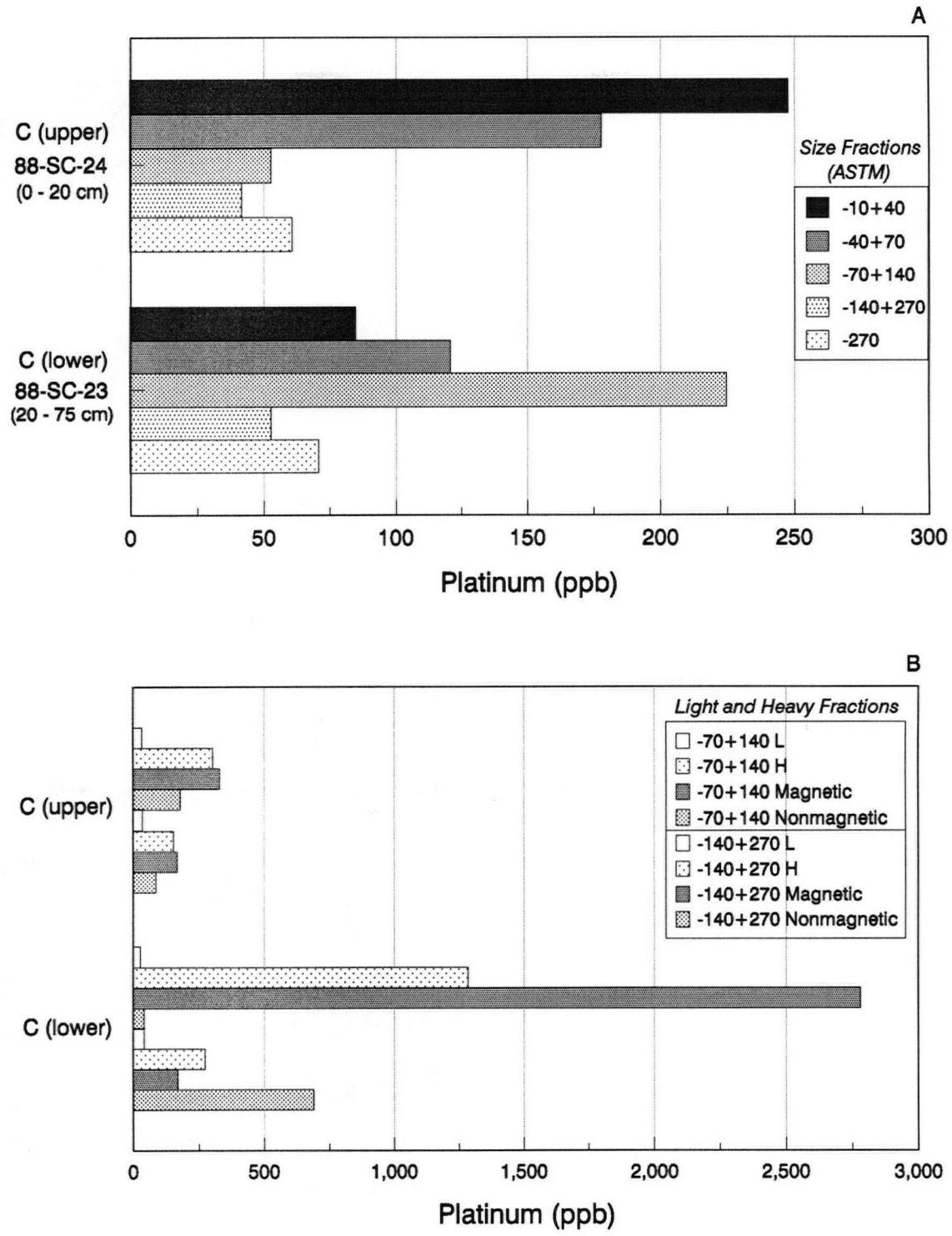

Appendix 12.12. Pt distribution (ppb) in orthic regosol (soil site 9) on dunite colluvium below Cliff Zone PGE occurrences, showing A. Pt content of five size fractions and B. Pt content of light, heavy, heavy magnetic and heavy non-magnetic mineral fractions of the -70+140 (bars 1-4) and -140+270 (bars 5-8) mesh size fractions.

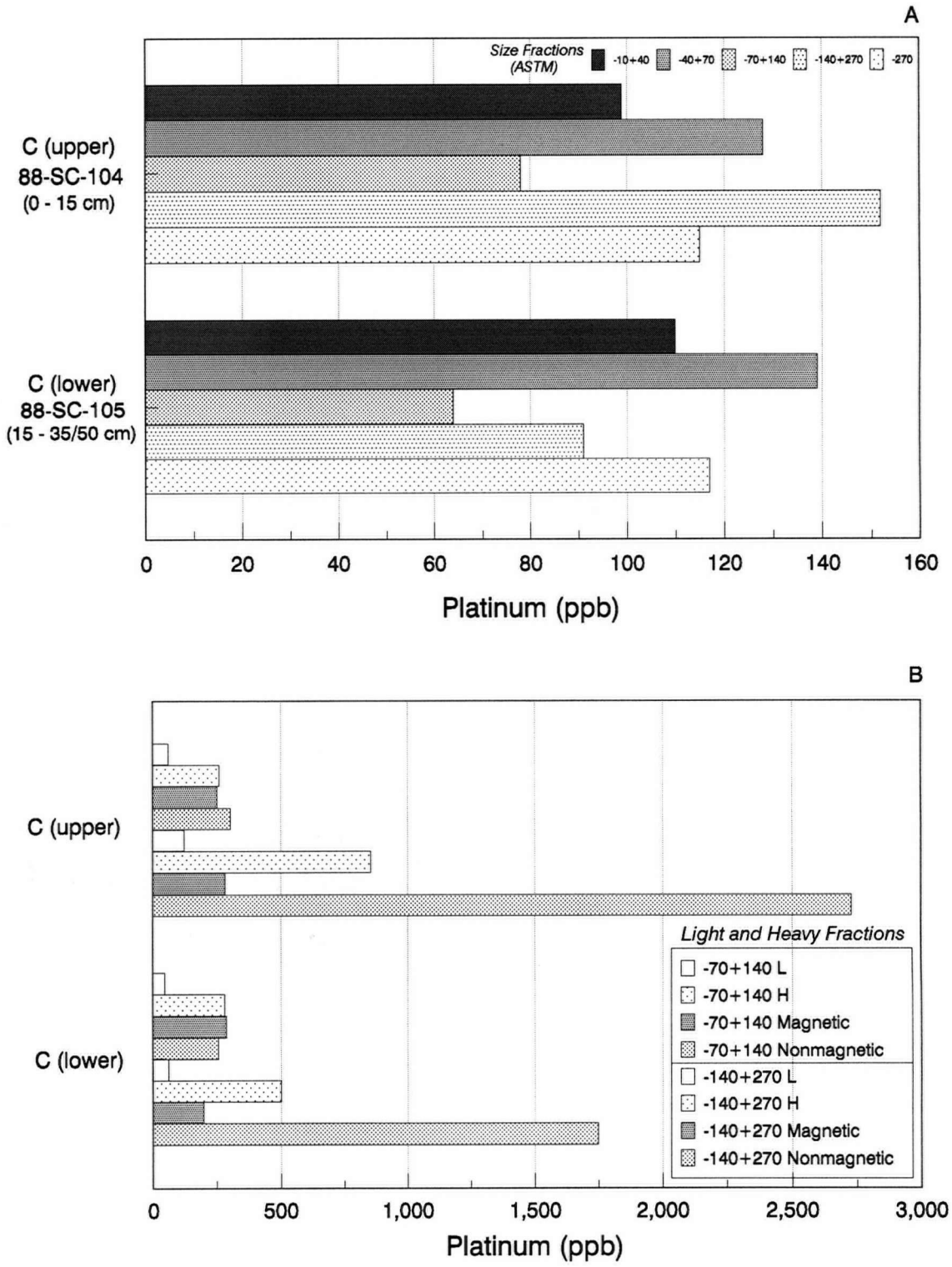

Appendix 12.13. Pt distribution (ppb) in orthic regosol (soil site 42) on serpentine colluvium, showing A. Pt content of five size fractions and B. Pt content of light, heavy, heavy magnetic and heavy non-magnetic mineral fractions of the -70+140 (bars 1-4) and -140+270 (bars 5-8) mesh size fractions.

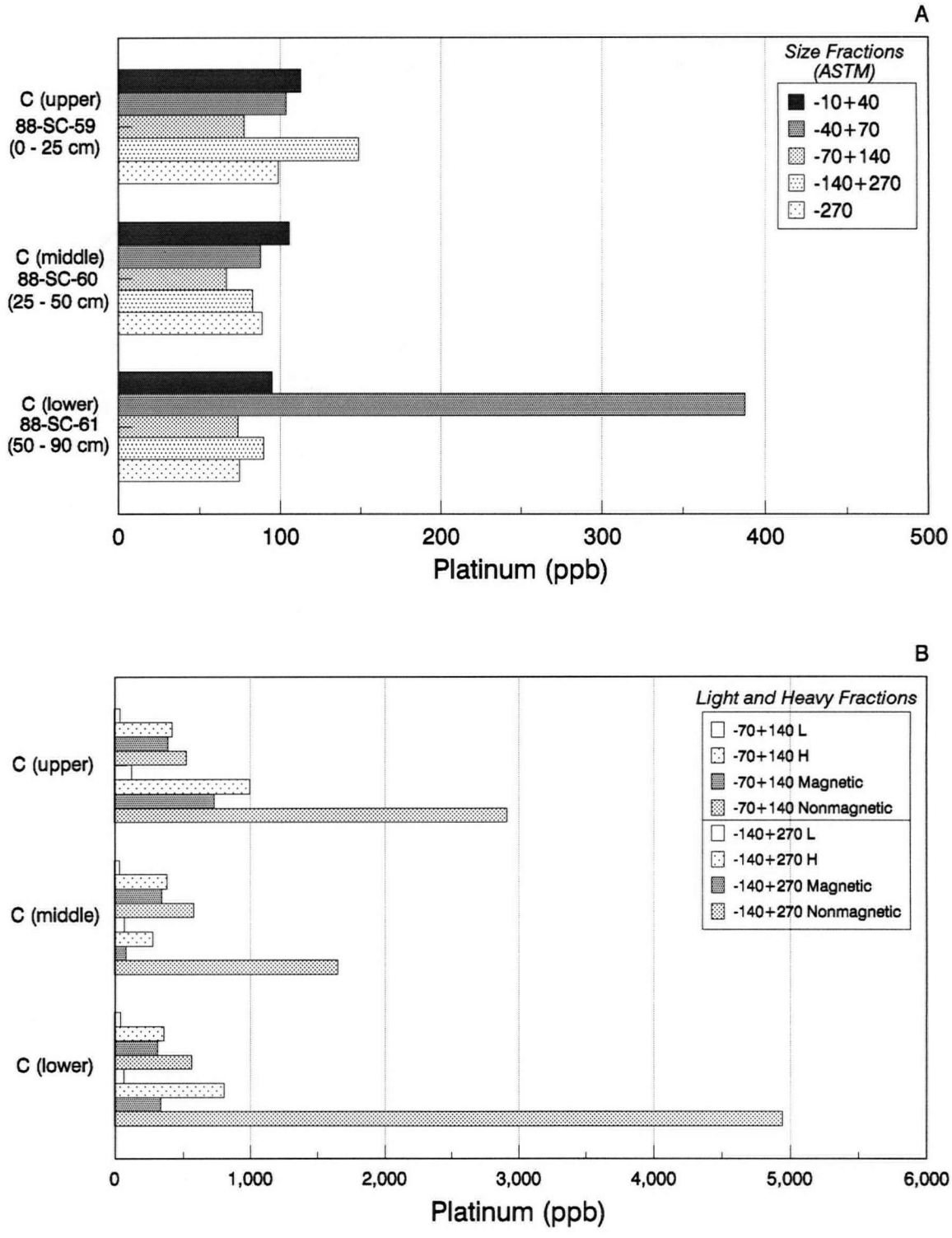

Appendix 12.14. Pt distribution (ppb) in orthic regosol (soil site 27) on serpentine colluvium, showing A. Pt content of five size fractions and B. Pt content of light, heavy, heavy magnetic and heavy non-magnetic mineral fractions of the -70+140 (bars 1-4) and -140+270 (bars 5-8) mesh size fractions.